Regulation of cell cycle transitions and CHK1 inhibitor sensitivity by MMB-FOXM1 feedback loops

HARVARD UNIVERSITY
Graduate School of Arts and Sciences

DISSERTATION ACCEPTANCE CERTIFICATE

The undersigned, appointed by the

Division of Medical Sciences Committee on

Virology have examined a dissertation

entitled

Regulation of cell cycle transitions and CHK1 inhibitor sensitivity by MMB-FOXM1 feedback loops

presented by Timothy Bruce Branigan

candidate for the degree of Doctor of Philosophy and hereby certify that it is worthy of acceptance.

Nick Dyson

Signature: _____ Nick Dyson (Apr 29, 2021 14:12 EDT)

Typed Name: Dr. Nicholas Dyson

Peter Sicinski

Signature: _____ Peter Sicinski (May 6, 2021 12:29 EDT)

Typed Name: Dr. Piotr Sicinski

Wei, Wenyi

Signature: _____ Wei, Wenyi (Apr 29, 2021 10:39 EDT)

Typed Name: Dr. Wenyi Wei Karlene Cimprich

Signature: _____ Karlene Cimprich (Apr 30, 2021 10:06 PDT)

Typed Name: Dr. Karlene Cimprich

Date: April 28, 2021

Regulation of cell cycle transitions and CHK1 inhibitor sensitivity by MMB-FOXM1 feedback loops

A dissertation presented

by

Timothy Bruce Branigan

to

The Division of Medical Sciences

in partial fulfillment of the requirements

for the degree of

Doctor of Philosophy

in the subject of

Virology

Harvard University

Cambridge, Massachusetts

April 2021

Dissertation Advisor: James A. DeCaprio Timothy Bruce Branigan

Regulation of cell cycle transitions and CHK1 inhibitor sensitivity by MMB-FOXM1 feedback loops

Abstract

The cell division cycle requires duplication of the genome and segregation of the replicated genomes into daughter cells. Failure to keep these two processes distinct can compromise genomic integrity, causing oncogenic mutations or cell death. The interaction of transcriptional and post-translational pathways coordinates genome duplication and genomes segregation. Post-translationally, cyclin/CDK complexes generate distinct cellular states, while protein degradation erase these states to enable transition to the next. The ATR-CHK1 kinases modulate CDK activity to separate the two cellular states. Transcriptionally, two waves of gene expression facilitate these states: a G1/S wave controlled by E2F to enable DNA replication and a G2/M wave to enable mitosis driven by the MYBL2/MuvB(MMB)-FOXM1 complex.

We identified a MYBL2-cyclin F feedback loop controlled by CDK phosphorylation. The E3 ubiquitin ligase complex SKP1-CUL1-F-BOX(SCF)$^{cyclin\ F}$ specifically degrades MYBL2 in G2/M. Loss of cyclin F led to persistence of the MMB-FOXM1 complex, G2/M gene expression, and cyclin B1 levels through mitosis. A genome-wide CRISPR screen identified the MMB-FOXM1 complex as required for sensitivity to CHK1 inhibitors that induced replication catastrophe. We demonstrated that CHK1i derepressed an MMB-FOXM1-CDK1 positive feedback loop that induced premature mitosis leading to replication stress and cell death.

Prolonged CHK1 inhibition led to APC/C dysregulation and CHK1i-induced replication catastrophe. CHK1i induced the APC/C-dependent degradation of origin licensing factors impairing DNA replication. The MMB-FOXM1 complex also was required for impaired DNA replication and loss of origin licensing factors after CHK1 inhibition implicating the mitotic transcriptional program in managing DNA replication. Consequently, the APC/C regulators,

Aurora B and FBXO5, were identified as potential biomarkers for CHK1i sensitivity. This work demonstrated how MMB-FOXM1feedback loops facilitated cell cycle transitions that could be dysregulated by CHK1 inhibition.

Acknowledgements

I would first like to acknowledge my advisor, Dr. James A. DeCaprio, for his efforts in guiding me in the completion of this work. Jim has been fundamental to my development as a scientist. From his emphasis on conducting rigorous, well-controlled experiments to his willingness to share his approach to science, I have grown by leaps and bounds as a scientist in his lab. Additionally, Jim's patience and willingness to communicate to find solutions have helped me grow as a person and for that I thank him.

Next, I would like to thank my Dissertation Advisory Committee, Dr. Nicholas J. Dyson, Dr. Randal W. King, and Dr. Jarrod A. Marto. The key insights and support that I received from them over the course of this Ph.D. will serve me well long into the future, both inside and outside of science.

I would also like to thank my collaborators who efforts helped bring these projects to fruition. For the cyclin F-mediated degradation of MYBL2 project, I need to thank Dr. Luo Guo-Burren for getting the project off the ground and Drs. Mega Padhi and Christian Berrios for being willing to contribute work and thoughts. For the work on the MMB-FOXM1 complex and CHK1 inhibition, I need to thank Dr. David Kozono and Peter Deraska for conducting the original screen and for being great colleagues as we sought to make sense of what was confusing data at times. I need to thank Larissa Sambel, Dr. Amy E. Schade, and Hembly G. Rivas for helping to keep the project going and getting it across the finish line. I also need to thank Drs. Alan D'Andrea, Geoffrey Shapiro and other members of the Center for DNA Damage and Repair at DFCI for their feedback and support as we made sense of how the MMB-FOXM1 complex was influencing CHK1 sensitivity.

Additionally, I want to thank the fellow members of the DeCaprio Lab and colleagues on the 4th floor of Mayer that I have had the pleasure to work with over the years. From Happy Hours in the conference room to our conversations in the hallway, our conversations at all hours

of the day have helped me grow as a scientist and as a person for which I will always be grateful.

Outside of lab, my friends and family have been a strong foundation of support during my doctoral studies. Thank you for adding some fun to my journey through Graduate School and being there to share in my successes and my tribulations. In particular I want to thank my parents for their constant support from listening politely as I ramble on about my work to offering perspective when I encountered road blocks in my experiments.

Table of Contents

Table of Figures

Chapter 2

Chapter 3

Chapter 4

Chapter 1. Introduction

Duplication of the genome followed by separation into two cells is the fundamental task of the cell division cycle to propagate eukaryotic life. Within the cell division cycle, genomes are duplicated during S phase and separated during mitosis. Reflecting the need to temporally separate genome duplication from division, there are two gap phases, G1, between mitosis and S phase, and G2, between S phase and mitosis. Failure to separate these two fundamental tasks can lead to mutations that result in cancer or cell death. Faced with this challenge, the cell needs to reliably create two distinct cellular states for DNA replication and mitosis from a single genome.

The cell contains a variety of protein complexes that can read the genome and create or erase distinct cellular states to distinguish DNA replication from cytokinesis. Cyclin/cyclin-dependent kinase (CDK) complexes can post translationally modify a wide range of substrates to write distinct cellular states for DNA replication and mitosis (Malumbres, 2011, 2014). They regulate a series of transcriptional complexes that transactivate two distinct transcriptional programs required for DNA replication and mitosis (Fischer et al., 2016; Sadasivam and DeCaprio, 2013). Signals generated during DNA replication and mitosis subsequently activate the E3 ubiquitin ligases SKP1-CUL1-F-BOX (SCF) and the Anaphase Promoting Complex/Cyclosome (APC/C) respectively to erase these different cell cycle identities upon their completion and prior to the next phase (Jang et al., 2020; Zhou et al., 2016). Consequently, the cell cycle transcription factors, the cyclin/CDK complexes, and the proteolytic regulatory complexes interact at cell cycle checkpoints to manage these cell cycle transitions. Cells with oncogenic mutations that accelerate cell division are particularly dependent on these regulatory pathways to manage these transitions creating potential therapeutic opportunities for treating cancer (Kotsantis et al., 2018; Qiu et al., 2018). Understanding how the cell cycle readers, writers, and erasers interact will provide insights into cell division as well as the targeting of these pathway for cancer treatment.

Cyclin/CDK complexes write distinct cell cycle identities for DNA replication and mitosis through post translational modification of proteins

Cyclin/CDK complexes establish temporally distinct cell cycle identities or states for DNA replication and mitosis through phosphorylation of a multitude of substrates. The CDK serine/threonine kinases typically phosphorylate S/T-P sites although other serine and threonine sites can be phosphorylated as well (Errico et al., 2010; Malumbres, 2014; Suzuki et al., 2015). Binding of the regulatory cyclins to the PSTAIRE helix of CDK catalytic subunit triggers a conformation change thereby enabling kinase activation (Jeffery et al., 1995). While there are over 20 members of the CDK kinase family, four CDK have major roles in the cell cycle: CDK1, CDK2, CDK4, and CDK6, with CDK4 and CDK6 showing tissue specific expression and largely overlapping roles (Malumbres, 2011, 2014). Phosphorylation of substrates at different times of the cell cycle is achieved by pairings of the individual CDKs with specific cyclins. CDK4 and CDK6 are paired with D-type cyclins, CDK2 is paired with cyclins E and A, and CDK1 with cyclins A and B (Bates et al., 1994; Devoto et al., 1992; Draetta et al., 1989; Elledge et al., 1992; Malumbres, 2011; Meyerson and Harlow, 1994; Rosenblatt et al., 1992). There is some redundancy in these pairings as CDK1 can also pair with cyclin E in the absence of CDK2 and cyclin E compensating for cyclin A in cyclin A knockout (KO) fibroblasts (Kalaszczynska et al., 2009; Santamaria et al., 2007).

A hydrophobic MRAILXXWXXE motif, conserved in cyclins A, B, and E but not D, interacts with RxL(F) motifs on substrates (Adams et al., 1999; Brown et al., 1999; Schulman et al., 1998; Takeda et al., 2001). Subtle variations in how the cyclin/CDKs interact and within the cyclin folds of cyclin A and cyclin B allow for further discrimination of substrates (Brown et al., 2007). Similarly, the cyclin-binding preference of a substrate can be shifted from cyclin A to cyclin B with a point substitution of the arginine in the RxL(F) motif to glutamic acid, resulting in a charge reversal, to make it an ExL(F) motif (Ord et al., 2020). Cyclin D1 contains a less conserved cyclin fold, with multiple motifs influencing binding to substrates. Perturbation of the

RxL, LxCxE and the N-terminal helix motifs on the canonical cyclin D/CDK4 substrate RB, encoded by the retinoblastoma tumor suppressor gene *RB1*, all lead to reduced cyclin D binding by differing extents (Dowdy et al., 1993; Topacio et al., 2019).

During the G1 phase of the cell cycle, cyclin D/CDK4/6 facilitates cell cycle reentry. Phosphorylation of the pocket proteins, RB and RBL2, by cyclin D/CDK4 derepresses cell cycle gene expression (Dowdy et al., 1993; Ewen et al., 1993; Johnson, 1995; Matsushime et al., 1992; Schade et al., 2019b; Schulze et al., 1994). In addition to RB, cyclin D1/CDK4/6 phosphorylation of GCN5 also promotes gene expression (Lee et al., 2014). While the phosphorylation GCN5 by cyclin D/CDK4/6 complexes has been only examined in post-mitotic cells, GCN5 participates in TRRAP-containing complexes that promote E2F- and MYC-dependent gene expression (Lang et al., 2001; Liu et al., 2003) suggesting that cyclin D/CDK4/6 may mobilize additional complexes and pathways to facilitate cell cycle entry.

CDK2 is activated by cyclins E1 and E2 as cells progress through G1 and initiates DNA replication. Cyclin E/CDK2 hyperphosphorylates (multi-phosphorylates) the pocket protein RB to inactivate it and fully derepress E2F-dependent expression of genes involved in DNA replication (Akiyama et al., 1992; Dick and Rubin, 2013; Harbour et al., 1999; Hinds et al., 1992). In addition, cyclin E/CDK2 phosphorylation of CDC45, Treslin, and TopBP1 triggers the initiation of DNA replication (Bell and Dutta, 2002; Jeon et al., 2007; Kumagai et al., 2011). As cyclin E levels increase, autocatalytic phosphorylation by CDK2 leads to the degradation of cyclin E (Clurman et al., 1996; Welcker et al., 2003) making way for the formation of cyclin A/CDK2 complexes. As cyclin E is degraded, cyclin A/CDK complexes form and contribute to the completion of DNA replication (Katsuno et al., 2009).

Cyclin A activates CDK1 to facilitate the transition from DNA replication to mitosis, starting preparations for chromosome segregation. Cyclin A/CDK1/2 complexes phosphorylate the transcription factors MYBL2 and FOXM1 to activate the G2/M transcriptional program (Lane et al., 1997; Laoukili et al., 2008b; Saldivar et al., 2018). As the levels of cyclin A exceed the

levels of unbound CDK2, cyclin A/CDK1 complexes will form (Merrick et al., 2008). Upon completion of DNA replication, cyclin A/CDK1 complexes initiate positive feedback loops with PLK1 and CDC25B to activate cyclin B1/CDK1 complexes that triggers a rapid increase in CDK1 activity (Lemmens et al., 2018; Van Horn et al., 2010; Vigneron et al., 2018). This increase in CDK1 activity promotes replication fork disassembly and prevents further initiation of DNA replication (Deng et al., 2019). Cyclin/CDK1 complexes phosphorylate BORA to activate and sustain the activity of the PLK1 and Aurora kinases (Feine et al., 2014; Hutterer et al., 2006; Van Horn et al., 2010; Vigneron et al., 2018), and thereby facilitating the transition into mitosis.

Cyclin B1/CDK1 complexes promote cytokinesis by activating a number of mitotic processes. Chromatin condensation is promoted by the cyclin B1/CDK1-dependent phosphorylation of factors such as condensin II and KIF4A (Abe et al., 2011; Takata et al., 2018). Hyperphosphorylation of Nup98 and Nup53 by cyclin B1/CDK1, PLK1, and the mitotic kinase NIMA facilitates nuclear pore complex disassembly (Laurell et al., 2011; Linder et al., 2017), leading to permeabilization of the nuclear envelope. Cyclin B1/CDK1 phosphorylation of spindle associated factors including RanGAP1, RCC1, and importin-α1 leads to activation and nucleation of the mitotic spindles, microtubule filaments used to separate the duplicated chromosomes (Guo et al., 2019; Hutchins et al., 2004; Li and Zheng, 2004; Swaminathan et al., 2004). Further, cyclin/CDK1 complexes promote the assembly of the core APC/C complex, the ubiquitin ligases that triggers the metaphase to anaphase transition, while preventing the association of co-activating proteins (Fujimitsu et al., 2016; Kramer et al., 2000; Yudkovsky et al., 2000; Zhang et al., 2016), providing additional time for the mitotic spindles to form. Thus, cyclin B1/CDK1 complexes establish and maintain a mitotic cellular identity or state until the cell is ready for cytokinesis and can trigger the metaphase to anaphase transition.

Limiting the activity of cyclin/CDK complexes to the appropriate phase of the cell cycle is achieved through multiple mechanisms including post-translation modification of the CDK subunit and regulation of cyclin levels. CDK activating kinases (CAKs), in particular cyclin

H/CDK7, phosphorylate CDKs on the T-loop (T172 on CDK4, T160 on CDK2, and T161 on CDK1) to stabilize the cyclin-CDK interaction (Desai et al., 1995; Ducommun et al., 1991; Fesquet et al., 1993; Fisher and Morgan, 1994; Mäkelä et al., 1994; Matsuoka et al., 1994; Merrick et al., 2008). CDK7 can phosphorylate monomeric CDK2 while CDK1 must be bound by a cyclin to be phosphorylated by CDK7 (Merrick et al., 2008). This difference in CDK7 specificity could explain the initial preference of cyclin A for CDK2 over CDK1. Phosphorylation of T161 on CDK1 is coupled with MYT1-dependent inhibitory phosphorylation of T14 (Coulonval et al., 2011). Linking T161 and T14 phosphorylation prevents aberrant CDK1 activation during cyclin/CDK1 complex assembly. WEE1 kinase phosphorylates CDK1/2 on Y15 to repress CDK activity (McGowan and Russell, 1993b; O'Connell et al., 1997). Phosphorylation of T14 and Y15 restricts CDK activity by blocking ATP-hydrolysis (Bartova et al., 2004). The inhibitory phosphorylation of T14 and Y15 are removed by the CDC25 family of phosphatases (Gu et al., 1992; Sur and Agrawal, 2016). Regulation of CDK activity by these post-translational modifications allows for the fine tuning of CDK activity in response to cell cycle stimuli independent of cyclin levels.

While CDK protein levels remain relative stable during the cell cycle, protein levels of the cyclin regulatory subunits can fluctuate, limiting the activity of a particular cyclin/CDK complex to the relevant phase of the cell cycle. Cyclin D expression is driven by a wide variety of mitogenic signals and undergoes degradation in the absence of mitogenic signaling to prevent aberrant cell cycle entry (Diehl et al., 1998; Yao et al., 2008). To limit cyclin E/CDK2 activity to DNA replication, cyclin E is expressed as part of the DNA replication transcriptional program while its degradation is promoted by autocatalytic phosphorylation (Fischer et al., 2016; Welcker et al., 2003). Cyclins A and B are expressed as part of the mitotic transcriptional program and degraded by the APC/C complex, a ubiquitin ligase that drives the transition out of mitosis (King et al., 1995; Muller et al., 2012; Sudakin et al., 1995; Zhou et al., 2016). This results in the protein levels of the mitotic A and B cyclins peaking late in the cell cycle and decreasing during

the transition to the next round of cell division. Thus, temporally distinct cellular identities for DNA replication and mitosis are achieved by using distinct transcriptional “reader” complexes and E3 ubiquitin ligase “erasers” to modulate levels of specific cyclin/CDK complexes at distinct points in the cell cycle.

E2F and MMB-FOXM1 transcriptional complexes read the genome to create two distinct transcriptional programs in a motif and cyclin/CDK dependent manner

A series of interconnected transcriptional complexes contribute to the creation of separate cellular states for DNA replication and mitosis. There are two distinct waves of gene expression during the cell cycle: an early (G1/S) wave that enables DNA replication and a late (G2/M) wave that facilitates mitotic progression. The activating E2F1-3 transcription factors drive expression of the early cell cycle genes during the G1/S transition while a complex of MYBL2 (B-MYB)/MuvB (MMB) and FOXM1 forms during the S/G2 transition to promote late cell cycle gene expression (Dimova and Dyson, 2005; Fischer et al., 2016; Sadasivam and DeCaprio, 2013). The early and late cell cycle genes can be distinguished at the sequence level with early cell gene promoters enriched for E2F binding sites and late cell cycle gene promoters enriched for CHR motifs, to which the MuvB complex binds (Fischer et al., 2016; Muller et al., 2017).

In quiescent G0 cells, both the early and late cell cycle genes are repressed by the DREAM (DP, RB-like, E2F and MuvB) complex. The pocket protein RBL2 (p130) bridges dimers of DP proteins and repressive E2F4 or E2F5 with the MuvB complex to bind to early (E2F) and late (CHR) cell cycle promoters (Litovchick et al., 2007a). MuvB is a 5-protein complex containing LIN37, LIN52, LIN9, RBBP4 and LIN54 and remains intact throughout the cell division cycle. The CXC domains of LIN54 binds specifically to the CHR motif in phosphorylation-dependent manner (Marceau et al., 2016; Schmit et al., 2009a). Phosphorylation of LIN52 at S28 promotes DREAM assembly by creating a LxpSxE motif, which

resembles the LxCxE motif on cyclin D (Guiley et al., 2015; Litovchick et al., 2011). The DREAM complex interacts with the SIN3B/HDAC complex to repress cell cycle gene expression (Bainor et al., 2018). In G1, cyclin D/CDK4/6 complexes phosphorylate RBL2 to promote DREAM disassembly (Schade et al., 2019b).

Upon dissociation from the DREAM complex, early cell cycle promoters are subsequently occupied by activating E2F1/DP dimers to express G1/S genes and read the DNA replication cellular identity from the genome (Takahashi et al., 2000; Trimarchi and Lees, 2002; Wells et al., 2000). E2F1 recruits Tip60 containing complexes to promote H3 and H4 acetylation (Taubert et al., 2004). In addition, E2F family members E2F2 and E2F3 can also transactivate E2F target genes (Dimova and Dyson, 2005). RB will bind these activating E2Fs and repress early cell cycle gene expression (Kato et al., 1993). While cyclin D/CDK4/6 phosphorylation of RB may partially relieve E2F inhibition, some evidence suggests that cyclin D/CDK4/6 phosphorylation of RB may also prime RB to interact with E2F1 creating a barrier to G1/S progression. This leaky inhibition may allow for expression of certain E2F target genes including CCNE1 and CCNE2 (Fischer et al., 2016; Ohtani et al., 1995; Yao et al., 2008). Once sufficient levels of cyclin E are achieved, cyclin E/CDK2 complexes hyperphosphorylate and fully inactivate RB to facilitate E2F-dependent gene expression that enables entry into S phase (Akiyama et al., 1992; Harbour et al., 1999; Hinds et al., 1992; Rubin et al., 2005).

During S phase, the MMB-FOXM1 complex assembles on the promoters of late cell cycle genes, such as cyclins A2 (*CCNA2*) and B1 (*CCNB1*) (Chen et al., 2013b; Down et al., 2012b; Knight et al., 2009; Sadasivam et al., 2012a; Schmit et al., 2007). The MMB-FOXM1 complex therefore functions as the transcriptional “on” signal or reader for the mitotic cellular identity. MYBL2 and the MuvB complex cooperatively bind late cell cycle promoters and subsequently recruit FOXM1 (Down et al., 2012b; Sadasivam et al., 2012a). The MMB-FOXM1 complex likely activates cell cycle gene expression by recruiting the CBP/p300 acetyl-transferases to deposit activating acetylations on promoter histones. While MYBL2 has been

reported to interact with p300/CBP in a phosphorylation-independent manner, cyclin/CDK1/2 phosphorylation of FOXM1 is required for FOXM1 to interact with CBP (Major et al., 2004). PLK1 phosphorylates FOXM1 in a CDK1-dependent manner to disrupt an intramolecular interaction between the N-terminus of FOXM1 and the TAD to facilitate the CBP/p300 interaction and promote gene transactivation (Fu et al., 2008; Marceau et al., 2019). Thus, in a phosphorylation dependent manner, MYBL2, MuvB, and FOXM1 transcriptionally create the mitotic identity by driving G2/M gene expression in a step-wise fashion.

MYBL2 and FOXM1 are two unrelated transcription factors with distinct regions that function similarly: a MuvB binding domain, a transcription activation domain (TAD), and DNA binding domain. Both MYBL2 and FOXM1 have sequence specific DNA binding domains with binding affinities that are considered weak for their respective families (Bergholtz et al., 2001; Littler et al., 2010). The low affinity of the MYBL2 and FOXM1 DNA binding domains potentially provides the rational for the CHR motif being the common feature of G2/M promoters (Muller et al., 2012; Muller et al., 2014). Cooperative binding by MuvB to the late cell cycle promoters can increase the binding affinity of MYBL2 and FOXM1. However, the MYB sites in the BIRC5 promoter were required for FOXM1 recruitment (Down et al., 2012b) suggesting that, while the CHR is the dominant feature of late cell cycle promoters, MYB and Forkhead binding sequence may also contribute to the complex formation at particular late cell cycle genes. p300 interacts with the central TAD of MYBL2 (Bessa et al., 2001; Oka et al., 2012). The C-terminal TAD of FOXM1 also serves as p300/CBP binding region given the requirement for phospho-T611 on FOXM1 for the interaction (Major et al., 2004; Marceau et al., 2019). A conserved region on the C-terminus of MYBL2 interacts with MuvB components LIN52 and LIN9 (Guiley et al., 2018) while the N-terminus of FOXM1 interacts with LIN9 (Wiseman et al., 2015) implicating LIN9 as the scaffold of the MMB-FOXM1 complex.

The stepwise activation of G2/M genes by the MMB-FOXM1 is likely regulated by cyclin/CDK phosphorylation. Both MYBL2 and FOXM1 are phosphorylated by cyclin/CDK

complexes at multiple sites(Anders et al., 2011; Johnson et al., 2002; Johnson et al., 1999; Lane et al., 1997; Laoukili et al., 2008b; Major et al., 2004; Robinson et al., 1996; Ziebold et al., 1997). These phosphorylation events are reported to be pro-transcriptional but mutagenic studies that underlie this assessment used reporter constructs based on MYB and Forkhead sites and not on CHR motifs. Therefore, it is unclear what role phosphorylation plays for MYBL2 and FOXM1 in MMB-FOXM1-driven gene expression.

Cyclin/CDK1 phosphorylation of MYBL2 is required for MYBL2 to interact with the prolyl isomerase, PIN1, that reduces the inhibiting intramolecular interactions between the C-terminus and DNA-binding domain of MYBL2 and facilitates additional phosphorylation events (Werwein et al., 2019). While mutation of the PLK1 phosphorylation sites in MYBL2 led to decreased expression of cyclin B1 and PLK1 in asynchronous populations, the mitotic phospho-Histone H3 (pH3) population in these asynchronous samples also increased reflecting activation of the mitotic transcriptional program. Further study is required to understand how CDK-phosphorylation of MYBL2 contributes to the MMB-FOXM1 paradigm of G2/M gene expression.

Cyclin A/CDK2 phosphorylation of FOXM1 reduces intramolecular interactions between the N-terminus, which interacts with MuvB, and the TAD domain of FOXM1 (Chen et al., 2013b; Laoukili et al., 2008b). The use of Forkhead-based reporters in this study again means that it is unclear what the significance of the CDK-dependent conformational change in FOXM1 implies for MMB-FOXM1 activity. Thus, the recruitment of p300/CBP and conformational changes promoted by cyclin/CDK phosphorylation of MYBL2 and FOXM1 have yet to be integrated into the MMB-FOXM1 mechanism of action.

The differential preferences of MYBL2 and FOXM1 for cyclin/CDK complexes may provide some clues for how cyclin/CDK phosphorylation regulates the MMB-FOXM1 complex. FOXM1 is promiscuously phosphorylated by cyclin/CDK complexes as all major cyclin/CDK complexes have been implicated in FOXM1 phosphorylation (Anders et al., 2011; Laoukili et al., 2008a; Major et al., 2004). In contrast, MYBL2 has a strong preference for cyclin A/CDK

complexes (Johnson et al., 2002; Johnson et al., 1999; Robinson et al., 1996; Sala et al., 1997; Ziebold et al., 1997). This difference in cyclin/CDK complex usage would indicate that FOXM1 could be phosphorylated earlier in the cell cycle than MYBL2. Additionally, the preference of MYBL2 for cyclin A/CDK complexes would suggest that MYBL2 functions at a later step of MMB-FOXM1 activation as cyclin A expression is largely driven by the MMB-FOXM1 complex. Together, it suggests a model of MMB-FOXM1 activation in which CDK phosphorylation of FOXM1 triggers a confirmation change that allows recruitment of FOXM1, p300/CBP, or both to the MMB complex. This is followed by MYBL2 phosphorylation as cyclin A and cyclin B levels increase leading to activation of MMB-FOXM1. However, whether MYBL2 phosphorylation promotes G2/M gene expression remains unclear.

Anaphase promoting complex/Cyclosome (APC/C) and SKP1-CUL1-F-BOX (SCF) complexes erase cell cycle identity through degradation of cyclins and cell cycle transcription factors

While cyclin/CDK complexes and cell cycle transcription factors write the different cell cycle identities during S phase and mitosis, these cell cycle identities need to be erased when DNA replication and genome segregation is completed to facilitate progress to the next step of cell division. The erasure of early and late cell identities is carried out by the E3 ubiquitin ligases SCF and the APC/C. These E3 ubiquitin ligases recruit E2 ubiquitin ligases to attach polyubiquitin chains to protein substrates and mark them for degradation. The APC/C is multi-subunit E3 ubiquitin ligase that has two co-activators, FZR1 and CDC20, that recruit substrates through their WD40 domains (Alfieri et al., 2017; Zhou et al., 2016). SCF complexes contain the E2-recruiting cullin 1, the adaptor protein SKP1 and substrate receptor F-box proteins (Bai et al., 1996; Jang et al., 2020). Similar to the APC/C, several co-activating F-box proteins have been implicated in cell cycle regulation allowing for degradation of specific cyclins and transcription factors at temporally distinct points in the cell cycle.

SCF complexes degrade early cell cycle cyclins to regulate cell cycle transitions or in response to DNA damage. During the G1 phase of the cell cycle, GSK3 and DYRK1A phosphorylates cyclin D at threonine 286 to generate a binding site, or phospho-degron site, for SCF complexes (Chen et al., 2013a; Diehl et al., 1998; Diehl et al., 1997; Lin et al., 2006; Santra et al., 2009). An FBXO31-containing SCF complex (SCF^{FBXO31}) promotes cyclin D degradation in response to DNA damage (Santra et al., 2009) while an SCF^{FBXO4} complex will degrade cyclin D during G1 (Lin et al., 2006). Perturbation of these degradation events promotes cell cycle progression (Lin et al., 2006; Santra et al., 2009; Thompson et al., 2015) suggesting that cyclin D1 degradation serves as a barrier to cell cycle entry. DYRK1A activity also promotes DREAM formation (Litovchick et al., 2011) while GSK3 activity is suppressed by mitogenic signaling (Diehl et al., 1998). GSK3 phosphorylation promotes the dimerization of FBXO4 that is necessary for the SCF^{FBXO4} complex to interact with cyclin D (Barbash et al., 2008) suggesting that GSK3 activity may serve as a general check on cell cycle entry. Thus, in the absence of mitogenic signaling or presence of DNA damage, cyclin D1 accumulation is suppressed and the cell remains quiescent.

Cyclin E is degraded by a phospho-degron that is generated by autocatalytic phosphorylation. Cyclin E/CDK2 activity can directly phosphorylate the T380 residue or phosphorylate S384 on cyclin E to enable GSK3 binding and subsequent phosphorylation of T380 (Welcker et al., 2003). This phospho-degron (pS380-x-x-x-pS384) is recognized by SCF^{FBXW7} and SCF^{SKP2} complexes (Koepp et al., 2001; Yeh et al., 2001). FBXW7 is a p53-dependent gene and will promote degradation of cyclin E in response to p53 signaling (Fischer et al., 2016; Kimura et al., 2003; Mandal et al., 2010). SKP2 is a G1/S gene that will accumulate during S phase (Fischer et al., 2016; Zhang and Wang, 2006) suggesting that SKP2-mediated degradation of cyclin E functions to turn off cyclin E/CDK2 complexes as the cell progresses through S phase, allowing cyclin A/CDK2 complexes to form. Mutation of the S384 phosphorylation site results in the accumulation of S phase cells (Welcker et al., 2003)

indicating that cyclin E degradation functions to limit S phase identity in response to DNA damage or in preparation for the transition to G2/M.

The late cell cycle cyclins, cyclin A and cyclin B are predominantly degraded by the APC/C in mitosis facilitating the transition back to G1 once cytokinesis is complete. CDK1 phosphorylation of APC1 and APC3 promotes assembly of the core APC/C complex (Fujimitsu et al., 2016; Zhang et al., 2016) while phosphorylation of the coactivators FZR1 and, to a lesser extent, CDC20 prevents their association with the APC/C core complex (Hein and Nilsson, 2016; Jaspersen et al., 1999; Kramer et al., 2000; Yudkovsky et al., 2000; Zachariae et al., 1998). APC/C^{CDC20} complexes are inhibited by the mitotic checkpoint complex (MCC). The MCC, comprised of several proteins including MAD2, BUBR1 and BUB3, blocks APC/C activation by preventing substrate binding to the APC/C-CDC20 complex and sequesters an additional CDC20 subunit away from the core APC/C complex (Izawa and Pines, 2015; Sudakin et al., 2001). This MCC-inhibited APC/C complex is still capable of degrading cyclin A2. Cyclin A binds to the CDC20 monomer bound to the MCC through non-canonical APC/C substrate recognition motifs that allow for ubiquitination by the core APC/C complex (Zhang et al., 2019). MCC disassembly coincides with the metaphase to anaphase transition as the APC/C is activated to facilitate the release of sister chromosomes for segregation (Alfieri et al., 2017; Irniger et al., 1995; Kim et al., 2018). Consequently, APC/C^{CDC20} activity triggers a cascade of phosphatase activation resulting in FZR1 dephosphorylation and its association with the core APC/C complex (Hein et al., 2017; Jaspersen et al., 1999; Sanidas et al., 2019). The APC/C^{FZR1} complexes proceed to degrade cyclin B1 via its D-box APC/C recognition motif when the cell transitions from mitosis into the next G1 phase (King et al., 1996; Zur and Brandeis, 2002). Cell expressing a non-degradable cyclin B1 will delay or arrest mitotic progression (Chang et al., 2003; Clijsters et al., 2014) indicating that cyclin B1 degradation is required for the M/G1 transition. In the absence of APC/C activity during a prolonged mitosis, cyclin B1 can also be degraded by $CUL2^{ZYG11}$ (Balachandran et al., 2016). This alternative degradation pathway

functions as a timer for mitosis as cyclin B1 loss will trigger APC/C^{FZR1} activation and a premature G1 state in the absence of chromosome segregation. The resulting tetraploid state can activate p53 and induce either apoptosis or senescence (Andreassen et al., 2001 ; Ganem et al., 2014).

Similar to cyclins, cell cycle transcription factors can be degraded by SCF and APC/C complexes to limit cell cycle identities. The activating E2Fs are degraded by SCF$^{cyclin\ F}$ during G2 to prevent genome re-replication while FOXM1 is degraded by APC/C^{FZR1} in G1 to prevent premature expression of the G2/M genes (Laoukili et al., 2008a; Park et al., 2008). The KEN box on FOXM1 that is recognized by APC/C overlaps with the required region for MuvB binding (Chen et al., 2013b; Laoukili et al., 2008a; Park et al., 2008) suggesting that FOXM1 bound to MuvB cannot be degraded by the APC/C. Thus, it is unclear if FOXM1 degradation functions as an “off” switch for transcription of G2/M genes or as a reset button for cell cycle gene expression as the cell enters a new round of division. In contrast to FOXM1, MYBL2 is degraded during G2/M by an unknown factor (Sadasivam et al., 2012a) and its role in regulating MMB-FOXM1 activity remains to be elucidated. Degradation of MYBL2 coincides with peak G2/M gene expression (Sadasivam et al., 2012a) suggesting that it could be necessary for maximal G2/M gene expression or maximal G2/M gene expression triggers MYBL2 degradation.

To prevent premature activation of these erasers, the activities of SCF and APC/C complexes oppose one another in negative feedback loops. During G1, the F-box protein cyclin F and SKP2 are degraded by the APC/C (Bashir et al., 2004; Choudhury et al., 2016) allowing for the accumulation of cyclin E and E2F1. The APC/C inhibitor FBXO5 is expressed as part of the E2F G1/S phase transcription program and antagonizes APC/C activity (Hsu et al., 2002), facilitating the subsequent accumulation of cyclin F and SKP2. As cyclin F is incorporated into SCF complexes it degrades FZR1 to facilitate entry into S phase (Choudhury et al., 2016). As the cell progresses through S phase, degradation of the G1/S cyclin E and E2F1 by SCF complexes curtails DNA replication and facilitates the transition to G2/M (Clijsters et al., 2019;

Welcker et al., 2003; Yeh et al., 2001), when the APC/C becomes activated. Notably, both FZR1 and cyclin F can be degraded by the $SCF^{\beta\text{-}TRCP}$ complex in response to differing phosphorylation signals (Mavrommati et al., 2018; Pal et al., 2020). Cells remain in S phase when degradation resistant FZR1 mutants are expressed and in mitosis when β-TRCP-mediated degradation of cyclin F is perturbed (Mavrommati et al., 2018; Pal et al., 2020). Thus, the effect of this β-TRCP-mediated degradation is to create a barrier that reduces aberrant activation of cyclin F and FZR1 complexes that would antagonize cyclin/CDK activity and cell cycle progression.

The ATR-CHK1 pathway separates DNA replication and mitosis during the cell cycle by modulating cyclin/CDK1 and APC/C activity

The ATR-CHK1 pathway functions to keep the activity of the writers and readers for DNA replication (E2F and cyclin E/CDK2) separate from the activity of the readers and writers for mitosis (MMB-FOXM1 and cyclin/CDK1) to allow for the completion of DNA replication before initiation of mitosis. It achieves this feat by limiting mitotic CDK1 activity during DNA replication thereby preventing premature activation of the mitotic program and by coordinating APC/C activation with chromosome segregation to eliminate the mitotic complexes as the cell exits mitosis and enter G1. Ataxia telangiectasia and Rad3-related (ATR) is a phosphoinositide 3-kinase related protein kinase that phosphorylates a wide range of proteins with SQ motifs and is essential for cell viability (Brown and Baltimore, 2000; Cimprich et al., 1996; Kim et al., 1999; Klein et al., 2000; Saldivar et al., 2017). ATR is recruited to RPA-bound, ssDNA-containing, structures and activated by ETAA1 or interactions with ATRIP and TopBP1 (Dart et al., 2004; Haahr et al., 2016; Kumagai et al., 2006; Lee et al., 2016). Once activated, ATR will proceed to phosphorylate the checkpoint kinase 1 (CHK1) on S317 and S345, derepressing the kinase (Emptage et al., 2017; Liu et al., 2000; Walker et al., 2009; Zhao and Piwnica-Worms, 2001). Activated CHK1 phosphorylates the CDC25 phosphatases and WEE1 kinase to promote their

interactions with the scaffolding protein 14-3-3 (Dalal et al., 1999; Lee et al., 2001; Lopez-Girona et al., 1999). CDC25 family members are sequestered and degraded in the cytoplasm by 14-3-3 (Chen et al., 2003; Dalal et al., 1999; Kasahara et al., 2010; Lopez-Girona et al., 1999) while the WEE1 interaction with 14-3-3 promotes WEE1 activity (Lee et al., 2001). The increase in WEE1 activity and sequestration of CDC25 family members results in increased phosphorylation of the inhibitory Y15 on CDK1 (de Gooijer et al., 2017; O'Connell et al., 1997). Recently, CHK1 was also shown to oppose CDK1 activity by phosphorylating the PP2A phosphatase inhibitor FAM122A/PIBAR1. CHK1-dependent phosphorylation of FAM122A increases PP2A-B55α activity by creating a 14-3-3 binding motif that sequesters FAM122A from the PP2A holoenzyme (Li et al., 2020). The increased PP2A-B55α activity stabilizes WEE1 as well as opposes CDK phosphorylation events in general (Godfrey et al., 2017; Li et al., 2020).

Activation of the ATR-CHK1 pathway during S phase limits CDK1 activity to coordinate the completion of DNA replication prior to progression into mitosis. Activation of ATR during S phase occurs in an RPA-dependent manner (Dart et al., 2004), leading to the CHK1 signaling cascades described above. ETAA1 appears to be the preferred activator ATR during an unperturbed S phase although there is evidence supporting a role for TopBP1, particularly in the case of impaired replication (Rainey et al., 2020; Saldivar et al., 2018; Sokka et al., 2018). The ATR-CHK1 pathway subsequently limits the cyclin A/CDK1 activity that drives MMB-FOXM1-dependent transcription of the G2/M wave of transcription (Saldivar et al., 2018). However, cyclin A/CDK1 also promotes late origin firing (Katsuno et al., 2009) so complete suppression of CDK1 activity will hinder DNA replication. Furthermore, phosphorylation of RIF1 by CDK1 disrupts the RIF1-PP1 interaction that limits replication fork assembly (Moiseeva et al., 2019). Inhibition of ATR and CHK1 activity can accelerate progression through S phase as CDK1 activity increases, leading to DNA replication in condensed chromatin (Eykelenboom et al., 2013). This DNA replication in condensed chromatin highlights the role that the ATR-CHK1

pathway plays in separating DNA replication from mitosis. Thus, by modulating CDK1 activity on the post-translation level in response to DNA replication, the ATR-CHK1 pathways ensures orderly DNA replication and prevents premature reading and writing of the mitotic program until DNA replication is complete.

More recently, a CDK-independent role for the ATR-CHK1 pathway has emerged as ATR and CHK1 activity have been shown to have a role in limiting APC/C activation prior to cytokinesis. Late in the cell cycle, ATR relocalizes to centromeres in an Aurora A-dependent manner (Kabeche et al., 2018). At the centromere, ATR is activated by R-loops and proceeds to upregulate CHK1 activity. CHK1 phosphorylates the kinase Aurora B on S331 to promote formation of the chromosome passenger complex (CPC), a complex of Aurora B, INCEP, BORA, and Survivin that fully activates Aurora B in mitosis (Carmena et al., 2012; Petsalaki et al., 2011). Activated Aurora B will phosphorylate BUBR1, facilitating its recruitment to the kinetochore (Carmena et al., 2012; Morrow et al., 2005; Petsalaki et al., 2011). At the kinetochore, BUBR1, as part of the mitotic checkpoint complex (MCC), will limit APC/C activity until the mitotic spindles are ready for cytokinesis (Liu and Zhang, 2016; Morrow et al., 2005; Sudakin et al., 2001). Similar to its role during S phase where it limits entry into mitosis, the ATR-CHK1 pathway functions during mitosis to preserve the mitotic cellular identity by limiting APC/C activity until the cell is ready for cytokinesis.

Readers, writers, erasers, and separators of cell cycle identities interact in feedback loops at cell cycle checkpoints to coordinate cell cycle transitions

The transition between DNA replication and mitosis is managed by cell cycle checkpoints where the readers, writers, erasers, and separates interact to switch from the DNA replication cellular identity to the mitotic cellular identity and back again. Crosstalk between these complexes and pathways can cause the cell to pause cell division at checkpoints if the cell is not ready to proceed. The G1/S checkpoint occurs late in G1 at which point the DNA

replication cellular identity is read and written as the cell begins genome duplication. In S phase, the intra S phase checkpoint can be activated, pausing the reading and writing of the mitotic cellular identity to allow for the completion of DNA replication. Finally, the Spindle Assembly Checkpoint (SAC) is activated to prevent erasure of the mitotic cellular identity before cytokinesis can occur.

During G1, the E2F transcription factors, APC/C, and cyclin E/CDK2 interact to form the G1/S checkpoint at which the DNA replication cellular identity is read and written by E2F transcription factors and cyclin E/CDK2 complexes respectively. The APC/C along with PP1 and PP2A phosphatases is activated as the cell exits mitosis to erase the mitotic cellular identity (Alfieri et al., 2017; Kernan et al., 2018; Wurzenberger and Gerlich, 2011). In addition to mitotic cyclins and regulators, APC/C^{CDC20} complexes also degrade geminin, an inhibitor of DNA replication that binds CDT1 (Clijsters et al., 2013; McGarry and Kirshcner, 1998). With geminin degraded, CDT1 interacts with CDC6 and the origin of replication complex to load MCM helicases onto chromatin, a process that licenses sites on the genome for the initiation of DNA replication (Clijsters et al., 2013; Coleman et al., 1996; Cook et al., 2004; Nishitani et al., 2000). However, there is limited time to license the genome in the absence of E2F activity, as E2F-target gene CDC6 is degraded in G1 as APC/C^{FZR1} complexes form (Clijsters et al., 2013; Peterson et al., 2000). PP2A and PP1 phosphatases activated during the exit from mitosis help to establish the new G1 state by dephosphorylating CDK1 substrates such as RB1 (Grallert et al., 2015; Nelson et al., 1997). This dephosphorylated RB can then proceed to bind and inhibit the activating E2F family members from reading the DNA replication program from the genome as part of the G1/S wave of cell cycle gene expression (Chellappan et al., 1991; Helin et al., 1993). Thus, at the G1/S checkpoint, the cells need to relieve RB repression of the E2F-dependent cell cycle gene expression and inhibit the APC/C to allow the accumulation of DNA replication regulators such as CDC6 and geminin.

Cyclin D/CDK4 phosphorylates RB during G1 which primes RB to interact with the activating E2F-DP1 dimers but also weakens the association between RB and these dimers (Ewen et al., 1993; Kato et al., 1993; Narasimha et al., 2014; Yao et al., 2008), resulting in leaky inhibition of E2F activity. This trickle of E2F gene expression allows for the expression of *CCNE1* and *CCNE2* (Ohtani et al., 1995; Yao et al., 2008), which form cyclin E/CDK2 complexes. The accumulation of cyclin E/CDK2 complexes that occurs with sustained mitogenic signal results in the hyperphosphorylation of RB by cyclin E/CDK2, relieving the inhibition of E2F activity by triggering a conformational change in RB (Burke et al., 2010; Lundberg and Weinberg, 1998; Rubin et al., 2005; Yao et al., 2008). With G1/S cell cycle gene expression activated, FBXO5, an inhibitor of the APC/C, accumulates and inhibits APC/C activity by binding the core APC/C complex in addition to FZR1 to prevent the APC/C from interacting with poly-ubiquitin-containing E2 enzymes (Cappell et al., 2016; Cappell et al., 2018; Hsu et al., 2002). At low levels, FBXO5 can be degraded by the APC/C due to it interaction with FZR1 (Cappell et al., 2018), so robust E2F activity is needed for inactivation of the APC/C, further linking the expression and accumulation of DNA replication factors as the cell transitions into DNA replication.

During S phase, the ATR-CHK1 pathway controls cyclin A/CDK1 writer complexes and MMB-FOXM1 reader complexes to prevent the onset of the mitotic cellular identity prior to the completion of DNA replication. As an E2F-dependent gene, MYBL2 accumulates as the cell enters S phase forming the MMB complex to recruit FOXM1 and initiate mitotic gene expression (Down et al., 2012b; Knight et al., 2009; Lam and Watson, 1993; Robinson et al., 1996; Sadasivam et al., 2012a). Expression of mitotic cyclins and regulators leads to events that impede DNA replication such as degradation of RRM2 and E2F1 (Clijsters et al., 2019; D'Angiolella et al., 2012), disassembly of the replication forks (Deng et al., 2019), and repurposing of the DNA damage response machinery for chromosome segregation (Bakhoum et al., 2014; Kabeche et al., 2018; Palazzo et al., 2014). The cell could prevent this premature

activation of the mitotic program by targeting mitotic transcription factor or cyclins for degradation however cyclin A/CDK1 activity promotes late origin firing (Katsuno et al., 2009), as cyclin E get degraded due to autocatalytic activity (Clurman et al., 1996; Welcker et al., 2003) and cyclin A accumulates (Akopyan et al., 2014; Erlandsson et al., 2000). Consequently, degradation of cyclin A would impair the completion of DNA replication. Thus, the cell needs away to limit mitotic CDK1 activity and mitotic gene expression on the post-translational level until DNA replication is complete.

The cell causes this delay by using DNA replication as a negative signal against reading and writing the mitotic cellular program. DNA replication blocks the activation of the mitotic kinases such as cyclin B1/CDK1 via the ATR-CHK1 pathway and when DNA replication is blocked by degrading CDC6 and inhibiting CDC7, mitotic CDK1 and PLK1 activity is rapidly induced (Lemmens et al., 2018). The ATR-CHK1 pathway limits CDK1 activity by promoting the accumulation of inhibitory phosphorylations on CDK1 as previously discussed. This ATR-CHK1-dependent block prevents reading of the mitotic programs via CDK1-dependent FOXM1 activation and expression of G2/M genes (Saldivar et al., 2018). The restriction of MMB-FOXM1 activity prevents cyclin F expression (Chen et al., 2013b; Fischer et al., 2016; Musa et al., 2019), limiting the degradation of E2F1 during S phase (Clijsters et al., 2019) and allowing for the continued reading of the DNA replication identity by E2F-dependent gene expression. The intra S phase checkpoint also has implications for APC/C activity as FBXO5 levels needs to be sustained to prevent premature activation of APC/C which would trigger the reestablishment of G1 in S phase and rereplication (Machida and Dutta, 2007). FBXO5 is part of a small subset of genes with both an E2F site and a CHR site at its promoter (Fischer et al., 2016) so its expression can start with E2F activation and continue into G2/M with MMB-FOXM1 activation but MMB-FOXM1 activity coincides with activation and expression of PLK1, which degrades FBXO5 (Hansen et al., 2004; Moshe et al., 2004). This means that, as MMB-FOXM1 and CDK1 activity increase, FBXO5 will be degraded with the establishment of the mitotic cellular identity.

Consequently, sustained E2F activity and suppressed MMB-FOXM1 activity allows for the continued accumulation of FBXO5 while limiting FBXO5 degradation. Once DNA replication is completed as reflected by the reduced levels of ssDNA-RPA, ATR-CHK1 activity decreases and the restriction on cyclin/CDK1 activity is released (Eykelenboom et al., 2013; Saldivar et al., 2018), allowing for the cell to establish the mitotic cellular identity.

In mitosis, the ATR-CHK1 pathway intersects with the APC/C at the SAC to prevent the erasing of the mitotic reader FOXM1 and mitotic writer cyclin B/CDK1 complexes prior to genome segregation. As the mitotic cellular identity is established through MMB-FOXM1-dependent gene expression and cyclin/CDK1 activity, CDC20 and FZR1 expression increases via MMB-FOXM1-dependent gene expression (Chen et al., 2013b; Fischer et al., 2016) and CDK1 activity promotes assembly of the core APC/C complex (Fujimitsu et al., 2016; Zhang et al., 2016). CDK1 phosphorylation of FZR1 however disfavors its association with the core APC/C complex (Jaspersen et al., 1999; Kramer et al., 2000; Zachariae et al., 1998), so establishment of the mitotic cellular identity results in the assembly and activation of the APC/C^{CDC20} complexes, which will proceed to degrade a variety of mitotic substrates (Zhou et al., 2016). It is important to note that this activation of the APC/C can occur independently of genome segregation (Yang and Ferrell, 2013) so the cell needs a checkpoint to coordinate APC/C activation, and subsequent erasure of mitotic identity, with genome segregation.

The ATR-CHK1 pathway also prevents the premature erasing of mitotic cellular identity by activating the mitotic kinases Aurora B and PLK1 to promote MCC formation, which will coordinate APC/C activation with genome segregation. Aurora A kinase activity causes ATR to associate with R-loops at centromeres leading to CHK1 activation (Kabeche et al., 2018). Activated CHK1 phosphorylates Aurora B on S331 and PLK1 on T210 to promote activation of these kinases (Adam et al., 2018; Petsalaki et al., 2011). The activation of PLK1 by CHK1 is notable as under low CDK activity conditions, such as DNA damage, CHK1 will antagonize PLK1 in a PP2A-dependent process (Lee et al., 2010; Wang et al., 2015). Phosphorylation of

CHK1 by PIM2 and CDK1 shifts CHK1 away from promoting CDK1 repression. CDK1 phosphorylation promotes the nuclear export of CHK1 (Enomoto et al., 2009; Shiromizu et al., 2006). This allows for the CDK1 positive feedback loops to promote the degradation of WEE1 and prevent the inhibitory phosphorylation of CDC25C (Peng et al., 1997). PIM2 phosphorylation of CHK1 at S280 retargets CHK1 specificity to phosphorylation of PLK1 T210 (Adam et al., 2018) through a mechanism that remains to be fully elucidated. It is also unclear whether CDK1 or PIM2-dependent phosphorylation of CHK1 are required for Aurora B activation. Activated Aurora B phosphorylates BUBR1 to facilitate its recruitment to kinetochores and inhibition or loss of CHK1 impairs Aurora B activity resulting in decreased BUBR1 recruitment to kinetochores (Ditchfield et al., 2003; Morrow et al., 2005; Petsalaki et al., 2011). In addition, Aurora B phosphorylate outer components of the kinetochore to prevent aberrant microtubule attachments, linking regulation of mitotic spindle attachment with MCC formation (Ditchfield et al., 2003; Tien et al., 2010).

The cell coordinates the activation of the APC/C with chromosome segregation through the MCC. The core MCC, consisting of BUBR1, BUB1, BUB3, MAD1, MAD2, and MPS, binds APC/C^{CDC20} complexes to block substrate binding and sequesters an additional CDC20 subunit preventing its association with the core APC/C complex (Fraschini et al., 2001; Izawa and Pines, 2015; Liu and Zhang, 2016; Sudakin et al., 2001). Phosphorylated BUBR1 at the kinetochores interacts with BUB3 and MAD2 to repress APC/C^{CDC20} activity. MAD1 and MPS1 along with unattached kinetochores catalyze the conversion of MAD2 from the inactivate, open confirmation (o-MAD2) to a closed confirmation (c-MAD2) that can interact with BUBR1 and CDC20 (Chen et al., 1996; De Antoni et al., 2005; Hewitt et al., 2010; Luo and Yu, 2008; Tipton et al., 2013). Recruitment of active PLK1 by BUB1 to kinetochores promotes Aurora B activity to help enforce the SAC (O'Connor et al., 2015; Wei et al., 2006) through a mechanism yet to be fully understood. c-MAD2 interacts with BUBR1, which functions as a pseudosubstrate, to bind APC/C-bound CDC20 and block APC/C activity while BUBR1 sequesters an additional CDC20

subunit (Fang, 2002; Fang et al., 1998; Izawa and Pines, 2015; Malureanu et al., 2009; Sudakin et al., 2001; Tang et al., 2001; Tipton et al., 2011). The attachment of mitotic spindles to kinetochores slows the generation of c-MAD2 while ubiquitination of APC/C-bound CDC20 by APC15 leads to disassembly of the MCC during mitosis. The slowing of c-MAD2 generation allows TRIP13 and its adaptor p31 comet to convert the remaining c-MAD2 into the inactive o-MAD2 thereby fully inactivating the MCC and triggering APC/C^{CDC20} activity and chromosome segregation (Collin et al., 2013; Eytan et al., 2014; Kim et al., 2018; Wang et al., 2014a; Ye et al., 2015) With the activation of the APC/C and chromosome segregation as the cell undergoes the metaphase to anaphase transition, the mitotic cellular identity is erased as the cell exits from mitosis.

The ATR-CHK1 pathway resolves oncogene-induced replication stress

Replication stress or the slowing of replication forks and subsequent accumulation of incomplete DNA replication products can be caused by oncogenic perturbations that dysregulate the licensing and firing of DNA origins of replications and impede the ability of the cell to duplicate it genome. Oncogenic perturbations such as cyclin E or c-MYC overexpression, the presence of HPV E7, or mutant RAS, directly and indirectly promote the inactivation of RB leading to increased accumulation of cyclin E/CDK2 activity and G1/S gene expression (Gray-Bablin et al., 1996; Hinds et al., 1992; Hwang et al., 2002; Leone et al., 1997; Munger et al., 1989; Nass and Dickson, 1998), circumventing a barrier in G1 that limits expression of DNA replication cellular identity and accumulation of cyclin/CDK2 activity to write that identity. The elevated CDK2 activity results in the increased firing of more origins, decoupling the replication program from progress through genome duplication (Thomson et al., 2010). Replication fork progression slows as the number of origins fired increases likely due to the levels of rate limiting replication factors (Zhong et al., 2013). The MCM helicase continues to unwind DNA and, while

MCM4 limits excessive unwinding, ssDNA accumulates due to the slowed replications forks (Nitani et al., 2008).

This dysregulation of E2F gene expression can also lead to origin refiring as elevated levels of origin licensing factors CDC6 and CDT1, expressed as part of the G1/S wave of gene expression, continue to relicense fired origins during S phase (Vaziri et al., 2003). Cyclin E overexpression, mutant Ras, and HPV E7 upregulate CDC6 expression while MYC will directly promote CDT1 expression (Di Micco et al., 2006; Fan et al., 2016; Mailand and Diffley, 2005; Valovka et al., 2013). Additionally, mutant cyclin D will prevent the CUL4-mediated degradation of CDT1 in S phase (Aggarwal et al., 2007), leading to increased licensing, while decreased geminin and cyclin A stability from FBXO5 loss can result in DNA rereplication (Machida and Dutta, 2007). Refiring of the origin results in head-to-tail collision, where replication machinery from the leading strand of refired origin collides with adjacent, unligated Okazaki fragments, resulting in double stranded DNA breaks (DSBs) (Davidson et al., 2006).

Another consequence of this deregulated G1/S checkpoint can be the under-licensing of DNA origins. Under licensing caused by CDC6 depletion prevents CDK2 activation during G1 due to abrogation of the G1/S checkpoint and p53 activity, leading to impaired DNA replication and apoptosis (Nevis et al., 2009). It seemingly is difficult to reconcile how the under-licensing of origins could trigger replication stress when increased origin firing induce replication stress. However, the extra, dormant origins that get licensed in G1 are fired in response to replication stress, allowing DNA replication to continue (Ge et al., 2007). Many of the oncogenic stresses that alter cyclin E/CDK2 activity and origin licensing also induce increased transcription leading to conflicts with the DNA replication machinery (Jones et al., 2013; Kotsantis et al., 2016). Thus, the under-licensing of origins caused by these oncogenic drivers may leave the cell ill-disposed to remedy stress induced by transcription. The end result of the dysregulation of origin firing and licensing is under-replicated DNA which must be addressed prior to the initiation of mitosis.

As mentioned, oncogenes, such as MYC and HRAS, promote global increased transcription, which can result in collisions between the transcription and replication machinery during S phase (Kotsantis et al., 2016; Valovka et al., 2013). Similarly, the increased origin firing from cyclin E also leads to transcription-replication collisions (Jones et al., 2013). Inhibition of transcription reduced the replication stress induced by HRAS or cyclin E overexpression highlighting these conflicts as a source of replication stress (Jones et al., 2013; Kotsantis et al., 2016). Collisions between the transcription and replication machinery can either be co-directional, where the replication and transcription fork are headed in the same direction, or head-on, where the replication and transcriptional machinery are traveling in opposing directions. Head-on collisions result in the accumulation of R-loops while R-loops are resolved in the co-directional collisions (Hamperl et al., 2017). The accumulation of R-loops contributes to replication stress during cyclin E and Ras overexpression as expression of RNaseH1, an RNAse that can process R-loops, improved fork progression and DNA replication in these cells (Hamperl et al., 2017; Jones et al., 2013; Kotsantis et al., 2016). The accumulation of R-loops that occurs with head-on collisions impairs transcription and DNA replication and results in ATR-CHK1 activation (Hamperl et al., 2017).

The ATR-CHK1 pathway resolves oncogene-induced replication stress through multiple approaches: (i) delaying the reading and writing of the mitotic cellular program, as discussed earlier, to provide time to resolve the structures, (ii) limiting DNA replication, (iii) stabilizing the replication fork, and (iv) mobilizing the DNA damage response to resolve these structures and facilitate the completion of DNA replication. ATR and CHK1 preserve replication forks by limiting CDK1 activity as cyclin B/CDK1 activity leads to replication fork disassembly (Deng et al., 2019). Both ATR and CHK1 phosphorylate proteins to prevent CDC45 loading onto chromatin and block origin firing. CHK1 phosphorylates Treslin to block CDC45 loading while ATR phosphorylates the methyltransferase MLL to promote H3K4 methylation that blocks CDC45 loading (Guo et al., 2015; Liu et al., 2010). Both ATR and CHK1 stabilize forks by slowing origin

firing, which limits the accumulation of ssDNA species. Further, ATR phosphorylates the DNA translocase SMARCAL1 to limit fork reversal and prevent fork collapse (Couch et al., 2013). FANCI and FANCD2 are both phosphorylated by ATR to activate the Fanconi Anemia repair pathway to stabilize and help resolve stalled replication forks (Ho et al., 2006; Schlacher et al., 2012; Tan et al., 2020). Phosphorylation of RPA32, a subunit of the ssDNA-binding RPA complex, on S33 by ATR facilitates DNA synthesis under stressed conditions and recovery from replication stress (Vassin et al., 2009). Activation of the ATR-CHK1 pathway in response to replication stress will prevent formation of new DNA replication factors, or clusters of replicating forks, but will allow the firing of dormant origins to complete replication in existing replication factories (Ge and Blow, 2010). ATR phosphorylates MCM2 in response to genotoxic stress including at S92 (Cortez et al., 2004; Yoo et al., 2004). Phosphorylation of MCM2 at S92 recruits PLK1 leading to CDC45 loading and origin firing. Firing of dormant origins allows for the completion of ongoing DNA replication and prevents the generation of DSBs (Trenz et al., 2008).

Inhibition of the ATR-CHK1 pathway triggers replication and mitotic catastrophe in cancer cells

ATR-CHK1 inhibition selectively kills cancers cells by inducing replication catastrophe. DNA replication is induced after ATR or CHK1 inhibition due to the increased origin firing resulting from elevated CDK1 activity but replication fork progress slows with the increased origin firing (Moiseeva et al., 2017; Petermann et al., 2010; Syljuåsen et al., 2005; Zhong et al., 2013). This could be due to nucleotide pools being depleted from the increased active forks as well as increased RRM2 degradation (Buisson et al., 2015), which would further disrupt the nucleotide pools. As fork progression slows, RPA binds to the accumulating ssDNA species to protect them from cleavage by nucleases while recruiting ATR to initiate ATR-CHK1 signaling (Buisson et al., 2015; Toledo et al., 2013). As such, it is important to note that inhibition of CHK1

by CHK1 inhibitors causes ATR activation as part of a feedback loop from increased DNA replication (Syljuåsen et al., 2005). This explains the increased pCHK1 levels after CHK1 inhibition but also complicates the interpretation of DNA damage markers, such as γ-H2AX or RPA, which are also ATR substrates (Vassin et al., 2009; Ward and Chen, 2001). Similarly, in the presence of ATR inhibition and replication stress, CHK1 can be activated by DNA-PK (Buisson et al., 2015) leading to pCHK1 and cell cycle arrest. DNA-PK will get activated as the unresolved ssDNA replication structures accumulate, due to inhibition of the ATR-CHK1 pathway, and are converted into DSBs by the MUS81 or SLX4 nucleases (Couch et al., 2013; Forment et al., 2011; Matos et al., 2020; Ragland et al., 2013). Consequently, the DSB DNA damage response (DDR) is mobilized, resulting in the phosphorylation of the DDR machinery as the cell tries to resolve the DSBs generated by the replication stress. ATM as well as DNA-PK or ATR can phosphorylate KAP1 on S824 to promote chromatin relaxation and facilitate repair of the DSB break (White et al., 2006; Ziv et al., 2006). Phosphorylation of RPA at S4/S8 by DNA-PK limits DNA replication and cell cycle progression (Ashley et al., 2014), creating a window of time for the cell to recover from the stress.

Failure to adequately resolve the DNA replication stress can lead to DNA replication or mitotic catastrophe. The ssDNA generated from the excess of stalled replication forks consumes the free RPA in the cell. Eventually, the cell exhausts its supply of RPA leading to widespread fork breakage and irreparable DNA damage (Dunlop et al., 2020; Toledo et al., 2013). Either ATR or CHK1 inhibition can induce DNA replication catastrophe while co-treatment with hydroxyurea rapidly triggers DNA replication catastrophe (Dunlop et al., 2020; King et al., 2015; Toledo et al., 2013). What remains unclear is how the threshold for RPA exhaustion is determined and what makes widespread fork breakage unrepairable. Additionally, replication catastrophe was largely defined in the presence of a DNA replication stress agent or RPA perturbation rather than just ATR or CHK1 inhibition alone potentially biasing replication catastrophe phenotypes observed towards DNA replication associated factors and pathways.

Mitotic catastrophe has also been observed with ATR or CHK1 inhibition (King et al., 2015; Mak et al., 2015; Ruiz et al., 2016). Mitotic catastrophe, broadly speaking, is when mitotic processes are dysregulated such that genome segregation is prematurely initiated or fails to be triggered resulting subsequently in tetraploidy and senescence or cell death by apoptosis (Castedo et al., 2004). While the precise mechanism of mitotic catastrophe after ATR/CHK1 inhibition is still unclear, it thought that the under-replicated DNA and replication stress generated from increased origin firing persist into mitosis (King et al., 2015; Ruiz et al., 2016), since unable to be resolved, and DNA damage leading to apoptosis is triggered when the partially replicated genome undergoes genome segregation. In line with this, fragmented mitotic chromosomes have been observed with CHK1 inhibitor treatment (King et al., 2015).

Currently, ATR and CHK1 inhibitors are being developed and tested for use as cancer therapeutics either as monotherapy or in combination with replication stress inducing agents such as gemcitabine or WEE1 inhibitors (Cleary et al., 2020; Qiu et al., 2018). Preclinical work in cellular and xenograft models has shown increased efficacy with combinations of these compounds and ATR/CHK1 inhibitors (Chaudhuri et al., 2014; Chung et al., 2019; Dunlop et al., 2020; Fordham et al., 2018; Jin et al., 2018; Liu et al., 2017; Nair et al., 2020; Qiu et al., 2018; Wallez et al., 2018). In addition, preclinical studies have found ATR or CHK1 inhibition to be synthetically lethal with MYC or cyclin E amplifications and deficiencies in the DDR such as ATM or BRCA1 loss, offering some potential biomarkers that could help target ATR and CHK1 in the clinics (Cleary et al., 2020; Cole et al., 2011; Murga et al., 2011; Paculova et al., 2017). In fact, one trial with the CHK1 inhibitor, prexasertib, (NCT02873975) has used these markers of replication stress or DDR deficiency as inclusion criteria. Prexasertib is a potent CHK1 inhibitor that exhibits anti-proliferative activity in multiple cancer types but not in non-transformed cells such as RPE-TERT cells or BJ-hTERT fibroblast (Blosser et al., 2020; King et al., 2015; Koppenhafer et al., 2018). Like other ATR/CHK1 inhibitors, prexasertib can synergize with WEE1 inhibition and gemcitabine but resistance was observed after prolonged treatment of

xenografts with prexasertib in combination with a WEE1i (Chung et al., 2019). This underscores the need to identify and examine factors that confer resistance or sensitivity to ATR and CHK1 inhibitors. Understanding how these factors regulate the ability of ATR/CHK1 inhibitors, like prexasertib, to trigger replication and mitotic catastrophe will provide insights that will help guide the use of these compounds in the clinic.

MMB-FOXM1 components are frequently overexpressed in tumors providing potential therapeutic opportunities

MMB-FOXM1 components, MYBL2 and FOXM1, are frequently overexpressed in proliferating tumors. High levels of MYBL2 or FOXM1 have been reported across multiple cancer types including breast and ovarian (Barger et al., 2019; Calvisi et al., 2011; Gentles et al., 2015; Hibi et al., 1998; Inoue and Fry, 2016; Qin et al., 2019; Raschellà et al., 1999). Given the requirement for cyclin/CDK activity for MMB-FOXM1 activity, it is likely that this high levels of MYBL2 and FOXM1 are a consequence of the increased proliferation rate in these tumors rather than a driving oncogene. However, MYBL2 and FOXM1 contribute to genomic instability in tumors as overexpression of FOXM1 and MYBL2 as well as E2F1 were implicated as drivers of aneuploidy in breast cancer (Pfister et al., 2018). This is supported by observations that MYBL2 and FOXM1 levels are particularly high in p53-deficient backgrounds (Barsotti and Prives, 2009; Pandit et al., 2009; Parikh et al., 2014). FOXM1 and MYBL2 also have prognostic value. High FOXM1 levels correlate with lower overall survival across a range of cancer types (Gentles et al., 2015; Li et al., 2017) while MYBL2 was incorporated into the proliferation section of OncotypeDX (Sparano and Paik, 2008), a 21-gene RT-qPCR assay used to determine if a patient would benefit from adjuvant chemotherapy in estrogen receptor-positive, node-negative breast cancer.

Several lines of evidence demonstrate that the increase levels of MMB-FOXM1 component support this oncogenic proliferation and can influence drug sensitivity. Knockdown

of MYBL2 or FOXM1 in cancer cells of various origins impedes cell cycle and cellular viability (Calvisi et al., 2011; Consolaro et al., 2015; Li et al., 2021; Musa et al., 2019; Yang et al., 2013; Zhao et al., 2014). High FOXM1 levels have been implicated in resistance to anti-mitotic and DNA agents damaging like cisplatin (Carr et al., 2010; Nestal de Moraes et al., 2015; Zhao et al., 2014). Similarly, increased levels of MYBL2 have been found to confer resistance to DNA damaging agents like Doxorubicin and the estrogen receptor inhibitor, tamoxifen (Calvisi et al., 2011; Li et al., 2021; Thorner et al., 2009). Notably in hepatocellular carcinoma cells, depletion of MYBL2 or MuvB-component LIN9 increased sensitivity to doxorubicin (Calvisi et al., 2011), implicating MMB-FOXM1 activity in doxorubicin sensitivity. A limiting factor however in examining MYBL2 or FOXM1 in the clinic is the limited understanding of the mechanism of MMB-FOXM1 activity in G2/M gene expression that impairs our ability to ask informed questions and effectively interpret clinical data. Understanding the underlying mechanism of the MMB-FOXM1 complex will enable us to ask profound clinical question about these frequently overexpressed factors as well as provide basic insights into cell division.

Chapter 2. A cyclin F-MYBL2 degradation feedback loop turns off mitotic gene expression

Author Contributions

The immunoblotting of cyclin A-depleted lysates in Figure 1, the immunoblotting of cyclin F KO MEFs in Figure 3, and immunoprecipitations of endogenous cyclin F lysates and FLAG-cyclin F lysates in Figure 7 were performed by Dr. Luxuan Guo-Burren. The analysis of published synchronized HeLa microarray data in Figure 3 was a collaboration of Drs. Megha Padi and Luxuan Guo-Burren. The in vivo ubiquitination assay in Figure 6 was performed by Dr. Thomas Bonacci in the Laboratory of Dr. Michael Emmanuelle. Dr. Luxuan Guo-Burren also provided writing describing the technical details of the experiments she performed. Otherwise, all other experiments were conceived and performed by myself. I would like to thank Dr. Liam Cromwell for the sgCTRL sequence, the laboratory of Dr. Michele Pagano for cyclin F expression constructs and the laboratory of Dr. Stephen Elledge for *Ccnf* KO MEFs.

This research was supported by the US Public Health Service grants F31CA189328 to T.B. and R35CA232128, R01CA63113, R01CA173023 and P01CA203655 to J.A.D.

Abstract

While cyclin B1-CDK1 is required for entry into mitosis, the levels of cyclin B must be restrained for the cell to exit mitosis and enter G1. The MMB-FOXM1 transcriptional complex activates cyclin B expression, but it is no known how it is regulated to ensure that cyclin B1 levels are limited as the cell exits mitosis. Here, we describe a CDK-dependent, negative feedback loop between $SCF^{cyclin\ F}$ complexes and MYBL2 that limits mitotic gene expression. $SCF^{cyclin\ F}$ complexes are required for the degradation of MYBL2 in G2/M. MYBL2 interacts with cyclin F through an atypical RxH cyclin binding motif that is modulated by CDK phosphorylation on MYBL2. Loss of cyclin F leads to increased pFOXM1 levels in G2 and persistent expression of MMB-FOXM1 target genes, including cyclin B1 and cyclin F. Accumulation of cyclin F protein levels in G2 were dependent on MMB-FOXM1 indicative of a negative feedback loop. Cyclin B1 levels and CDK1 phosphorylation events persisted through the M/G1 transition in cyclin F KOs indicating that the MYBL2-cyclin F feedback loop limits cyclin B1 expression by turning off G2/M gene expression through the degradation of MYBL2.

Introduction

Cyclin A and cyclin B/CDK1 complexes promote entry into mitosis by activating mitotic kinases such as PLK1 and Aurora A as well as by delaying activation of the APC/C that terminates mitosis through inhibitory phosphorylation of the APC coactivators, FZR1 and CDC20 (Abrieu et al., 1998; Gheghiani et al., 2017; Hein and Nilsson, 2016; Hutterer et al., 2006; Vigneron et al., 2018). However, if the activity of the cyclin A and cyclin B/CDK1 complexes persist too long during mitosis, they can impair the metaphase to anaphase transition and subsequent G1 checkpoint (Clijsters et al., 2014; Geley et al., 2001; Sorensen et al., 2001; Yudkovsky et al., 2000). As such, the levels of cyclin A and B complexes must be regulated to ensure orderly progression through the cell cycle. Cyclins A and B are regulated on the posttranslational level by APC/C-mediated degradation as the cell exits mitosis (Geley et al., 2001; King et al., 1995). Transcriptionally, the MYBL2(B-MYB)/MuvB (MMB)-FOMX1 complex upregulates the expression of cyclin A and cyclin B as part of the mitotic program (Fischer et al., 2016). However, whether the MMB-FOXM1 complex is regulated to ensure the proper expression levels of cyclins late in the cell cycle remains unclear.

MYBL2 and FOXM1 are both phosphorylated by cyclin A/CDK2 complexes as the cell progresses through S-phase and G2 (Laoukili et al., 2008b; Robinson et al., 1996). CDK-dependent phosphorylation of MYBL2 facilitates an interaction with prolyl-isomerase PIN1 resulting in a conformational change in MYBL2 that leads to phosphorylation by PLK1 (Werwein et al., 2019). Similarly, cyclin/CDK2 phosphorylation of FOXM1 relieves an interaction between the N-terminus and domain-terminal activation domain (Laoukili et al., 2008b). Phosphorylation of T600 and T611 in the central transactivation domain of FOXM1 by cyclin/CDK complexes is associated with target gene expression (Lane et al., 1997; Laoukili et al., 2008b; Saldivar et al., 2018). Indeed, phosphorylation of MYBL2 and FOXM1 by CDKs is reported to activate transcription (Laoukili et al., 2008b; Major et al., 2004) but the mechanism by which CDK phosphorylation facilitates MMB-FOXM1 complex activation is not known. During S phase,

MYBL2 and MuvB, a 5-protein complex comprised of LIN9, LIN37, LIN52, LIN54 and RBBP4, interact and bind to G2/M cell cycle promoters (Knight et al., 2009; Litovchick et al., 2007a; Pilkinton et al., 2007; Schmit et al., 2009a). FOXM1 is subsequently recruited to these promoters in a MYBL2 and MuvB-dependent fashion (Chen et al., 2013b; Down et al., 2012b; Sadasivam et al., 2012a). FOXM1 recruitment to the MMB complex coincides with an increase in G2/M cell cycle gene expression.

In G0/G1 phase of the cell cycle, MYBL2 is degraded by CUL2-pVHL complexes in the absence of growth signaling (Okumura et al., 2017). MYBL2 is also degraded in G2 during the peak of G2/M cell cycle gene expression (Sadasivam et al., 2012a). However, factors required for the loss of MYBL2 during G2/M remain to be identified. Cyclin/CDK activity is potentially involved in MYBL2 degradation as phosphorylation at several CDK consensus sites on MYBL2 coincides with its degradation. Overexpression of cyclin A leads to reduced MYBL2 protein half-life and promotes MYBL2 ubiquitination (Charrasse et al., 2000) while MYBL2 phospho-mutants are not affected by cyclin A overexpression implicating CDK activity in MYBL2 degradation (Charrasse et al., 2000; Saville and Watson, 1998).

In contrast to other cyclins, cyclin F functions as part of an E3 ubiquitin ligase with CUL1 and SKP1 to form an SCF complex to regulate cell cycle progression (Bai et al., 1996; D'Angiolella et al., 2010; Fung et al., 2002). Cyclin F plays an important role in regulating cell cycle progression by degrading several cell cycle factors including E2F1, CDC6, RRM2, CP110, and CDH1 (Choudhury et al., 2016; Clijsters et al., 2019; D'Angiolella et al., 2012; D'Angiolella et al., 2010; Walter et al., 2016). Cyclin F is a negative regulator of MYBL2 that has been reported to limit activating MYBL2 phosphorylation by competing with cyclin A for MYBL2 binding (Klein et al., 2015; Mavrommati et al., 2018). However, there has been no evidence that cyclin F promotes MYBL2 degradation (Klein et al., 2015). Furthermore, it is unclear how the negative regulation of MYBL2 by cyclin F fits into the mechanism of MMB-FOXM1 complex activation.

Here we report that MYBL2 is degraded in a cyclin A-dependent manner by an $SCF^{cyclin\ F}$ complex upon MMB-FOXM1 activation. MYBL2 binds to cyclin F through an atypical RxH motif in a phosphorylation dependent manner. The degradation of MYBL2 by cyclin F functions as an off switch for MMB-FOXM1 activity while the accumulation of cyclin F in S/G2 is dependent on the MMB-FOXM1 complex. Thus, we describe a negative feedback loop within the mitotic transcriptional program that not only limits cyclin/CDK activity but is also activated by cyclin/CDK activity, tightly regulating levels of cyclin A and B expression during the G2 and M phases of the cell cycle.

Results

MYBL2 is degraded during the S/G2 transition when the MMB-FOXM1 complex is activated

To examine the relationship between cyclin/CDK phosphorylation of the MMB-FOXM1 complex and cyclin expression, MMB-FOXM1 components and cyclin levels were assessed in lysates of synchronized HeLa cells by immunoblot (**Fig. 2.1A**). Slower migrating, phospho-FOXM1 protein species, consistent with activation of the MMB-FOXM1 complex and increased levels of the MMB-FOXM1 target genes, cyclins A and B1, appeared as HeLa cells progressed through S phase into a 4N state at 6-8 hours after a thymidine block and release. Phosphorylation of T487 on MYBL2 was detected at 6 hours post release just prior to the loss of total MYBL2 at 8 hours post release, and coinciding with peak *CCNB1* transcript levels (**Fig. 2.1B**). The appearance MYBL2 phospho-species (pT487) just prior to the decrease in MYBL2 protein levels raises the possibility that MYBL2 loss in G2 is dependent on CDK phosphorylation when cyclin A and cyclin B1 levels increased. Depletion of cyclin A2 by siRNA reduced MYBL2 loss at 8 hours post release (**Fig. 2.1C**). Since cyclin A/CDK complexes have been reported to phosphorylate both MYBL2 and FOXM1 and contribute to the transactivation of target genes this raises the possibility that MYBL2 loss was linked to MMB-FOXM1 activation.

To determine if MYBL2 loss in G2 was associated with MMB-FOXM1 activation, levels of MYBL2 and pT600 FOXM1 (pFOXM1), a CDK-dependent marker for MMB-FOXM1 activity (reference), were assessed during the cell cycle by flow cytometry. Three MYBL2 populations, a 2N MYBL2-negative, a MYBL2-positive, and a 4N MYBL2-negative population, that roughly corresponded to the G1, S, and G2/M phases of the cell cycle respectively were observed in asynchronous HeLa cells (**Fig. 2.1D**). These three MYBL2 populations could also be separated based on pFOXM1 levels with the 4N-negative MYBL2 population having the highest pFOXM1 levels followed by the MYBL2-positive and the 2N- negative populations respectively (**Fig. 2.1E**). Levels of pFOXM1 were significantly higher in 4N-negative than MYBL2-positive cells in

Figure 2.1. MYBL2 is degraded in G2 when MMB-FOXM1 is active in a cyclin A-dependent manner

A) Immunoblot showing MYBL2 loss in G2. HeLa cells were synchronized by double thymidine block and collected at the denoted time point after releases. Samples were then immunoblotted for the denoted protein or were assessed for DNA content by Propidium Iodide staining and flow cytometry.

B) RT-qPCR of *CCNB1* transcript levels in HeLa cells synchronized as in A.

C) Immunoblot of MYBL2 levels in CCNA2 KD synchronized samples. HeLa cells were reverse transfected with siCTRL and siCCNA2 and synchronize and collected as in A.

D-F) Flow cytometric analysis of MYBL2 and pFOXM1 levels during the cell cycle. HeLa cells were pulsed with BrdU for 1 hour and stained with antibodies to BrdU, MYBL2, pFOXM1, as well stained with DAPI. A) Dot plot of MYBL2 levels vs DAPI with cell cycle populations overlaid and color as denoted in the legend. B) Dot plot of MYBL2 levels vs pFOXM1 levels with MYBL2 population as denoted in the legend overlaid. C) pFOXM1 MFI in MYBL2 populations during S phase and G2. N=3; Two-way ANOVA with Tukey correction; **, $p<0.01$; ***, $p<0.001$; ****, $p<0.0001$.

G) RT-qPCR of *MYBL2* transcript levels in HeLa cells synchronized as in A.

H) Immunoblot of HeLa cells synchronized as in A that were treated with the proteasome inhibitor bortezomib 4 hours post release for the denoted time periods.

Figure 2.1. (cont.)

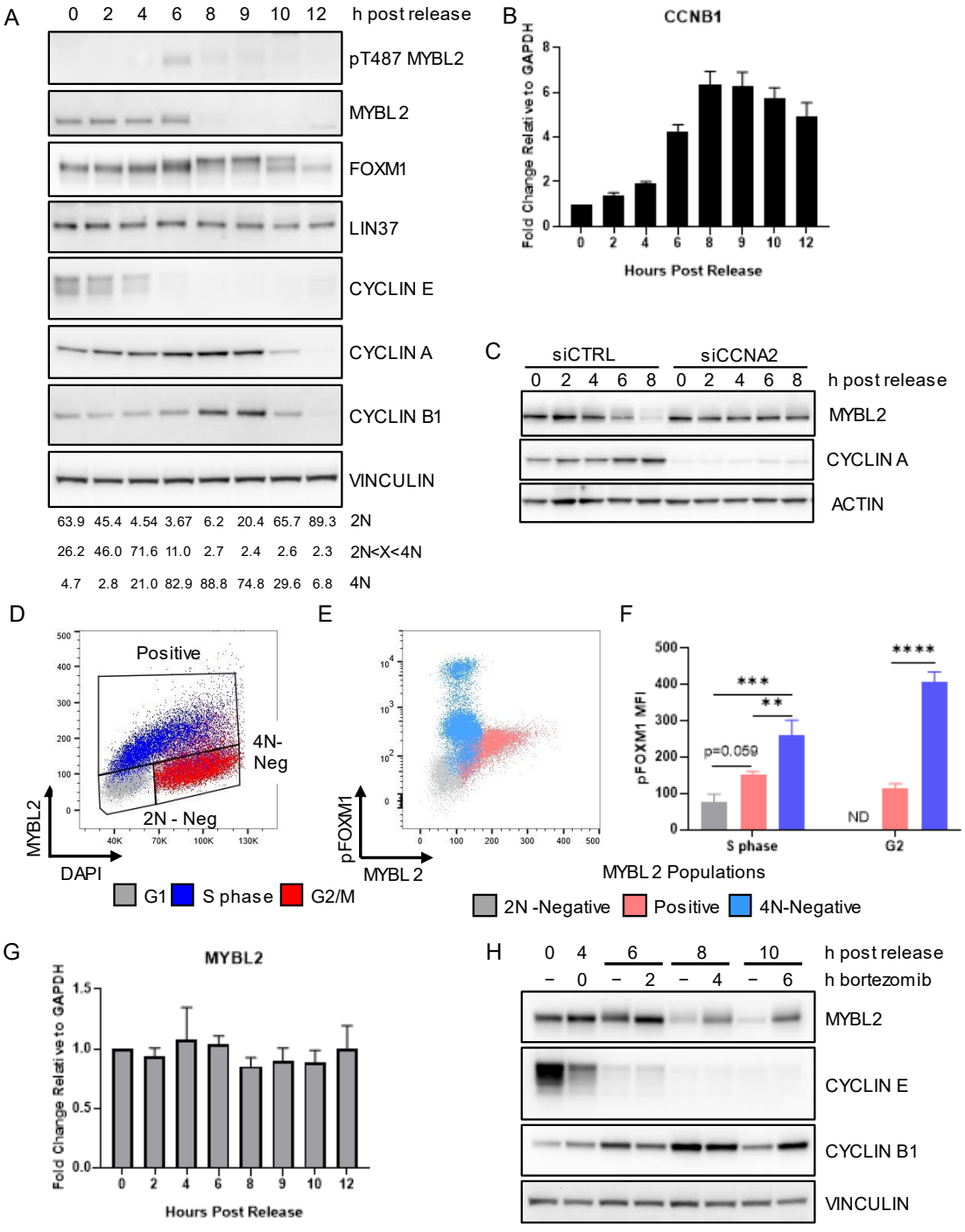

both S phase and G2 (**Fig. 2.1E and 2.1F**) suggesting that MMB-FOXM1 activity is linked to decreased levels of MYBL2 in 4N cells. *MYBL2* transcript levels did not change during the time course (**Fig 2.1G**) and MYBL2 loss could be blocked by the proteosome inhibitor bortezomib (**Fig. 2.1H**) indicating that the loss of MYBL2 in G2 is likely due to proteasome-dependent protein degradation. Together this data suggests that MYBL2 is degraded in a cyclin A-dependent manner during the S/G2 transition as the MMB-FOXM1 is being activated.

An $SCF^{cyclin\ F}$ complex is required for MYBL2 degradation in G2

We next asked what factors were required for MYBL2 degradation in G2. The NEDDylation inhibitor MLN4924 blocked MYBL2 degradation in G2 (**Fig. 2.2A**) implicating the Cullin family of E3 ubiquitin ligases in MYBL2 degradation. Cullin 1 (CUL1) was required for MYBL2 loss in G2/M but not CUL2, CUL3, CUL4, CUL5, or CUL7 when Cullin family members were depleted by siRNA (**Fig. 2.2B and 2.2C**). CUL1 interacts with SKP1 and a family of adaptor proteins known as F-box proteins to form SKP1-CUL1- F-Box (SCF) complexes (Bai et al., 1996; Wang et al., 2014b). Cyclin E is degraded by an SCF^{SKP2} complex in S phase (Nakayama et al., 2000). Depletion of SKP1 resulted in MYBL2 and cyclin E levels persisting after release from a double thymidine block (**Fig. 2.2D**) indicating that an SCF complex is required for MYBL2 degradation in G2.

Transcriptional analysis of SCF complex components in synchronized HeLa cells identified two F-box proteins of interest (**Fig. 2.3A**). As shown in the heatmap, levels of Cyclin F mRNA (*CCNF*) peaked at 8 hours when MYBL2 is typically degraded while *SKP2* levels were similar to MYBL2. Both F-box proteins have been previously reported to interact with MYBL2 (Charrasse et al., 2000; Klein et al., 2015). *SKP2* and *CCNF* were knocked down in synchronized HeLa cells and MYBL2 protein levels were assessed (**Fig. 2.3B**). Cyclin E levels persisted during the S phase and G2 in SKP2-depleted samples consistent with previous

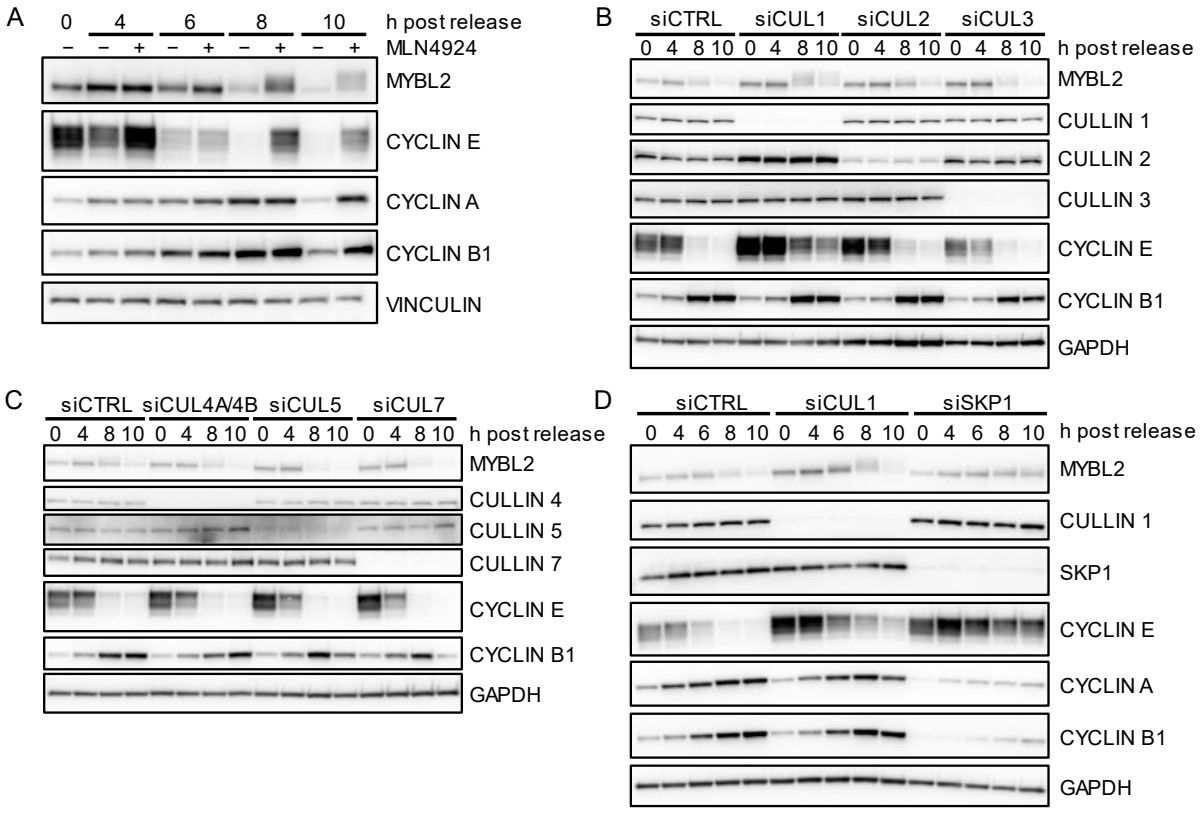

Figure 2.2. A SKP1-CUL1-F-BOX (SCF) complex promotes MYBL2 loss in G2/M

A) Immunoblot with the indicated antibodies of HeLa whole cell extracts synchronized by a double thymidine block, treated with 0.5 μM MLN4924 4 hours post release, and collected at the denoted time points.

B and C) Immunoblot of HeLa whole cell extracts synchronized as in A) after depletion for cullin family members. Samples depleted for B) CUL1-3 or C) CUL3-7 were probed with indicated antibodies.

D) Immunoblot of synchronized HeLa cell lysates after depletion of SCF complex components CUL1 or SKP1 with the indicated antibodies.

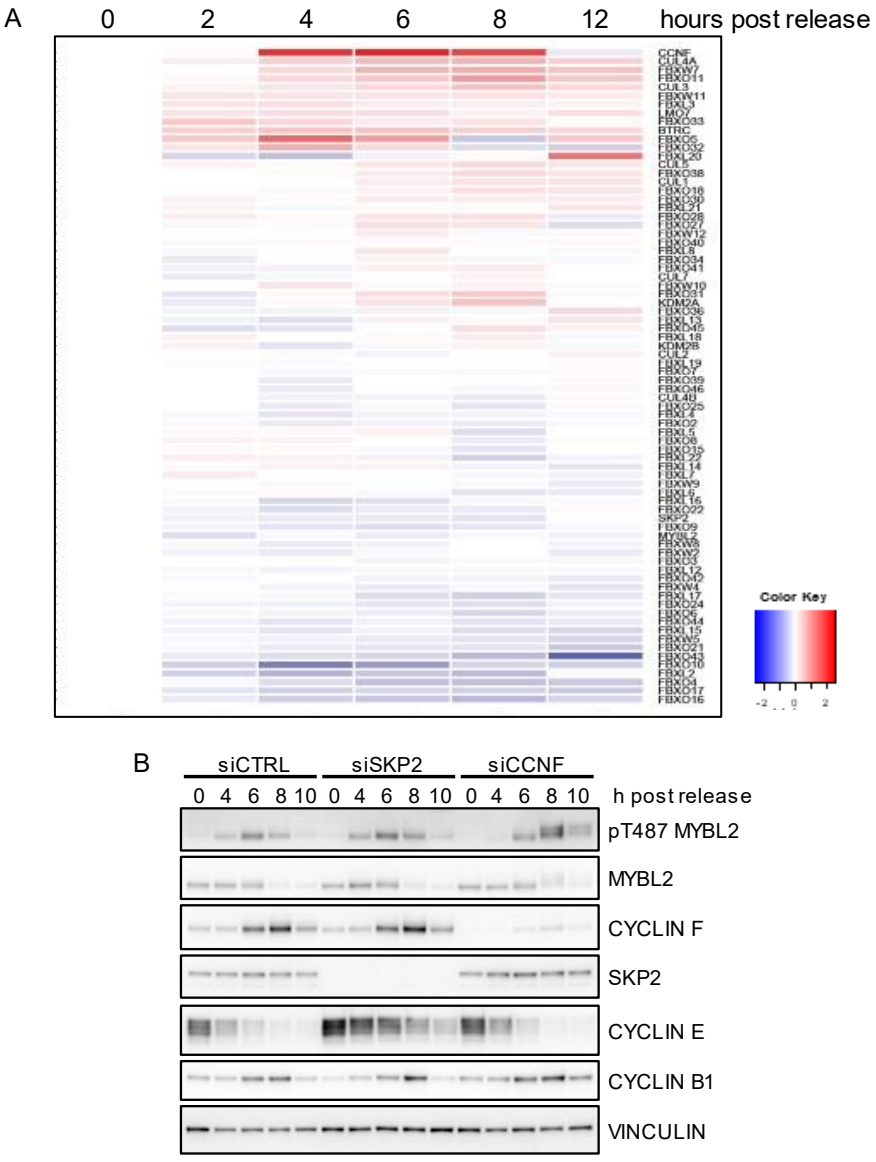

Figure 2.3. The F-box protein cyclin F is required for MYBL2 loss in G2/M

A) Heat map depicting the changes in mRNA expression of F-box containing proteins, cullins and MYBL2 in HeLa cells, as assayed by Affymetrix Human Genome U133 Plus 2.0 Array, after double thymidine block and release. Expression values of the target genes derived from microarray analysis of the 0, 2, 4, 6, 8 and 12-hr time points were normalized to 0 hour.

B) Immunoblot of synchronized HeLa cell lysates depleted for the F-box protein SKP2 and cyclin F.

studies. In contrast, MYBL2 levels persisted into later time points after knockdown of *CCNF*, but not *SKP2*, suggesting that an $SCF^{cyclin\ F}$ complex is required for MYBL2 degradation in G2.

To confirm that cyclin F was required for MYBL2 degradation in G2/M, MYBL2 levels were examined in CCNF KO MEFs and HeLa cells. The levels of MYBL2 as well as other cyclin F substrates, CP110 and RRM2, were elevated in the CCNF KO MEF (**Fig. 2.4A**). In HeLa CCNF KOs, MYBL2 levels were significantly increased in G2/M but not G1 or S phase in cyclin F KO cells (**Fig. 2.4B and 2.4C**) suggesting that the degradation of MYBL2 by cyclin F is limited to G2/M. Phospho-MYBL2 species robustly persisted into late cell cycle time points in the CCNF KO cells consistent with the siRNA studies (**Fig. 2.5A and 2.5B**). Knockout of cyclin F allowed the persistence of phospho-MYBL2 species into mitosis in nocodazole-synchronized HeLa and HCT116 cells (**Fig. 2.5C and 2.5D**) indicating cyclin F is necessary to limit MYBL2 protein levels during the G2/M transition.

Cyclin F promotes MYBL2 degradation in G2

The requirement of cyclin F for MYBL2 degradation during G2/M suggested the possibility that MYBL2 was a direct substrate of the $SCF^{cyclin\ F}$ complex. Cyclin F interacts with substrates through its cyclin fold and binds to SKP1 through its F-box domain (**Fig. 2.6A**). Alternatively, it has been proposed that cyclin F limits MYBL2 phosphorylation by competing with cyclin A for MYBL2 binding, rather than promoting MYBL2 degradation (Klein et al., 2015). This alternative model would predict that an F-box mutant of cyclin F would suppress phospho-MYBL2 species as the cyclin F fold should be sufficient. Expression of an F-box domain mutant of cyclin F however failed to increase the migration speed of MYBL2 or reduce MYBL2 protein levels in three independent CCNF KO cell lines tested (**Fig. 2.6B**) indicating that the E3 ubiquitin ligase activity of cyclin F is required for the suppression of phospho-MYBL2 species.

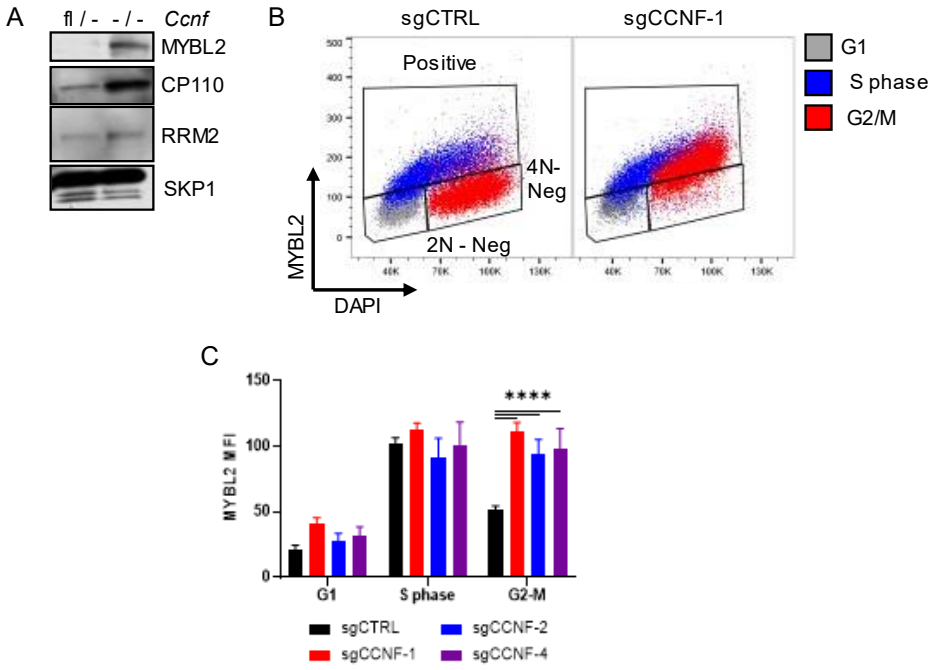

Figure 2.4. Increased levels of MYBL2 in CCNF KOs

A) Immunoblot of parental cyclin F flox/- and cyclin F KO MEFs whole cell lysates with the indicated antibodies.

B and C) Flow cytometric analysis of MYBL2 levels in CCNF KO cells. C) Dot plot of MYBL2 levels vs DAPI levels in sgCTRL and sgCCNF-1 cells. Cell cycle populations were overlaid as denoted and determined by BrdU vs DAPI staining. D) MYBL2 MFI for cell cycle populations in CTRL and CCNF KO cell lines. N=3; Two-way ANOVA with Tukey correction; ****, $p<0.0001$.

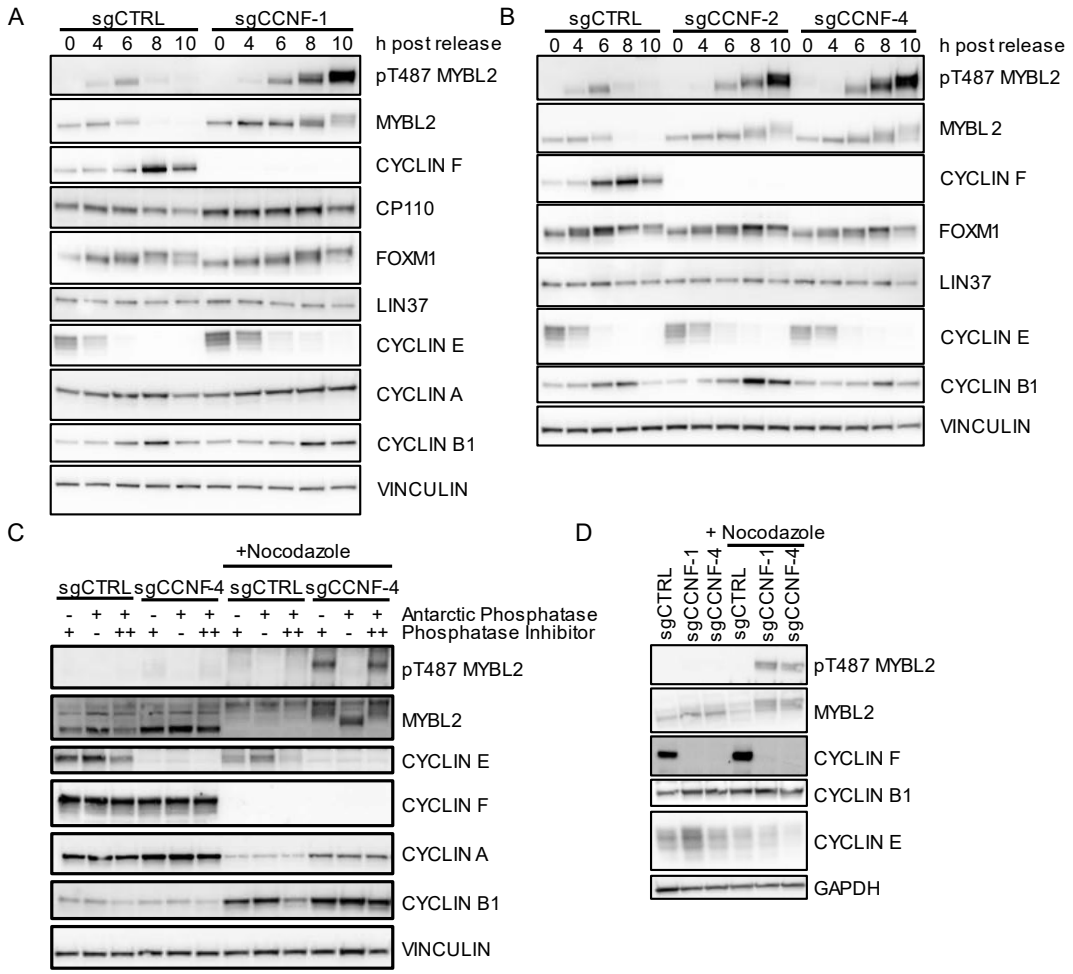

Figure 2.5. Phosphorylated MYBL2 persists into mitosis in CCNF KO cells

A and B) Immunoblot of MYBL2 levels in synchronized CCNF KO cells. CTRL or CCNF KO HeLa were synchronized by double thymidine block, released and collected as denoted time points. Lysates for A) sgCTRL and sgCCNF-1 or B) sgCTRL and sgCCNF-2 and -4 were analyzed by immunoblot using the antibodies indicated.

C) Immunoblot of phospho-MYBL2 levels in HeLa CTRL and CCNF KO synchronized to mitosis by nocodazole treatment. Whole cell extracts were treated with Alkaline Phosphatase in the presence or absence of phosphatase inhibitor to confirm the presence of phospho-MYBL2 species.

D) Immunoblot of phospho-MYBL2 levels in HCT116 CTRL and CCNF KO synchronized to mitosis by nocodazole treatment and blotted with indicated antibodies.

Figure 2.6. F-box domain of cyclin F is required for MYBL2 loss in mitosis

A) Schematic of cyclin F denoting functional domains and approximate location of point mutations used in this figure.

B) Immunoblot showing rescue of the cyclin F KO lines with cyclin F WT or cyclin F LP/AA constructs. CCNF KOs cells were transduced with cyclin F WT or LP/AA F-box mutant constructs, selected with blasticidin, and treated with 100 ng/ml for 18 hours to enrich for mitotic cells. Samples were collected, whole cell extracts generated and blotted with the denoted antibodies.

C and D) Coimmunoprecipitation of MYBL2 with cyclin F constructs. A) FLAG-cyclin F WT, F-box domain mutant or cyclin fold mutant constructs were expressed in 293Ts. Whole cell extracts were generated, FLAG-protein species were immunoprecipitated and interrogated by immunoblot with the indicated antibodies. B) Same as in A except with FLAG-cyclin F constructs containing the ALS-associated R392T mutation or the Burkitt lymphoma-associated R451C mutation.

Figure 2.6. (cont.)

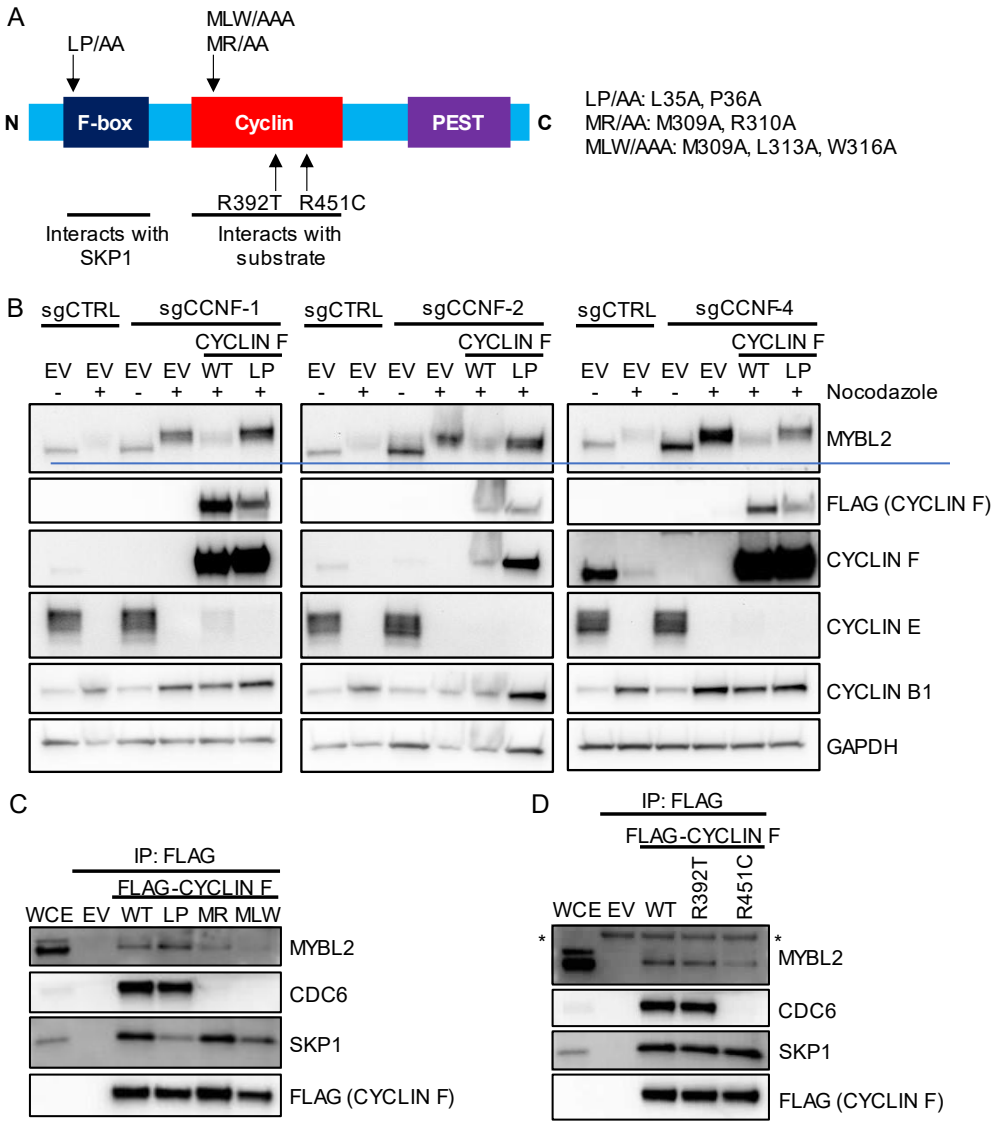

MYBL2 was able to interact with an F-box cyclin F mutant (**Fig 2.6C**) similar to CDC6, a reported substrate of cyclin F. The cyclin fold of cyclin F was mutated in the MRXXLXXW hydrophobic patch, conserved between cyclin A and cyclin F (**Fig. 2.9D**), or by point substitution of the ALS-associated R392T or Burkitt Lymphoma-associated R451C mutations in the cyclin fold (Abate et al., 2015; Williams et al., 2016). The MLW mutant failed to interact with either MYBL2 or CDC6 while the MR mutation reduced the MYBL2-cyclin F interaction while abrogating the CDC6-cyclin F interaction (**Fig. 2.6C**). For the disease-associated variants, the R451C cyclin F mutation had impaired interactions with MYBL2 and CDC6 in contrast to R392T that retained binding to both (**Fig. 2.6D**). Thus, MYBL2 interacts with the cyclin fold of cyclin F similar to other cyclin F substrates.

Recently, cyclin F has been reported to degrade the activating E2F transcription factors that promote MYBL2 expression (Clijsters et al., 2019). MYBL2 transcripts levels however weren't elevated during S/G2 in the CCNF KO HeLa cells (**Fig. 2.7A**), likely due to E2F deregulation by HPV E7, meaning that the increased levels MYBL2 observed in the absence of cyclin F were not due to increased E2F activity. Using Azidohomoalaninine (AHA) labeling to examine protein turnover, AHA-labeled MYBL2 protein species persisted through S/G2 in the CCNF KO cells indicating that MYBL2 protein turnover was impaired in the CCNF KO cells. Furthermore, MYBL2 ubiquitination increased with cyclin F overexpression suggesting that cyclin F promotes MYBL2 ubiquitination (**Fig. 2.7**). The promotion of MYBL2 ubiquitination and requirement of E3 ubiquitin ligase activity to reduce MYBL2 protein levels in G2/M indicate that cyclin F acts in an SCF complex as an E3 ubiquitin ligase to promote MYBL2 degradation in G2/M.

Figure 2.7. Cyclin F promotes MYBL2 ubiquitination

A) RT-qPCR of *MYBL2* transcript levels in sgCTRL, sgCCNF-1, and sgCCNF-4 HeLa cells synchronized as in Fig. 1A.

B) Immunoblot of AHA-labeled species and inputs from sgCTRL, sgCCNF-1, and sgCCNF-4 Hela cells synchronized as in Fig. 1A. Samples were labeled with 1 mM AHA during the second thymidine block in methionine-free growth media, were released into regular growth media containing 200 μM methionine and collected at the denoted timepoints post release.

C) Immunoblot of in vivo ubiquitination of MYBL2 by cyclin F. Ubiquitin conjugates from 293T cells expression Myc-cyclin F, V5-MYBL2 and 6xHis-FLAG-ubiquitin were recovered on nickel agarose under denaturing conditions.

Figure 2.7. (cont.)

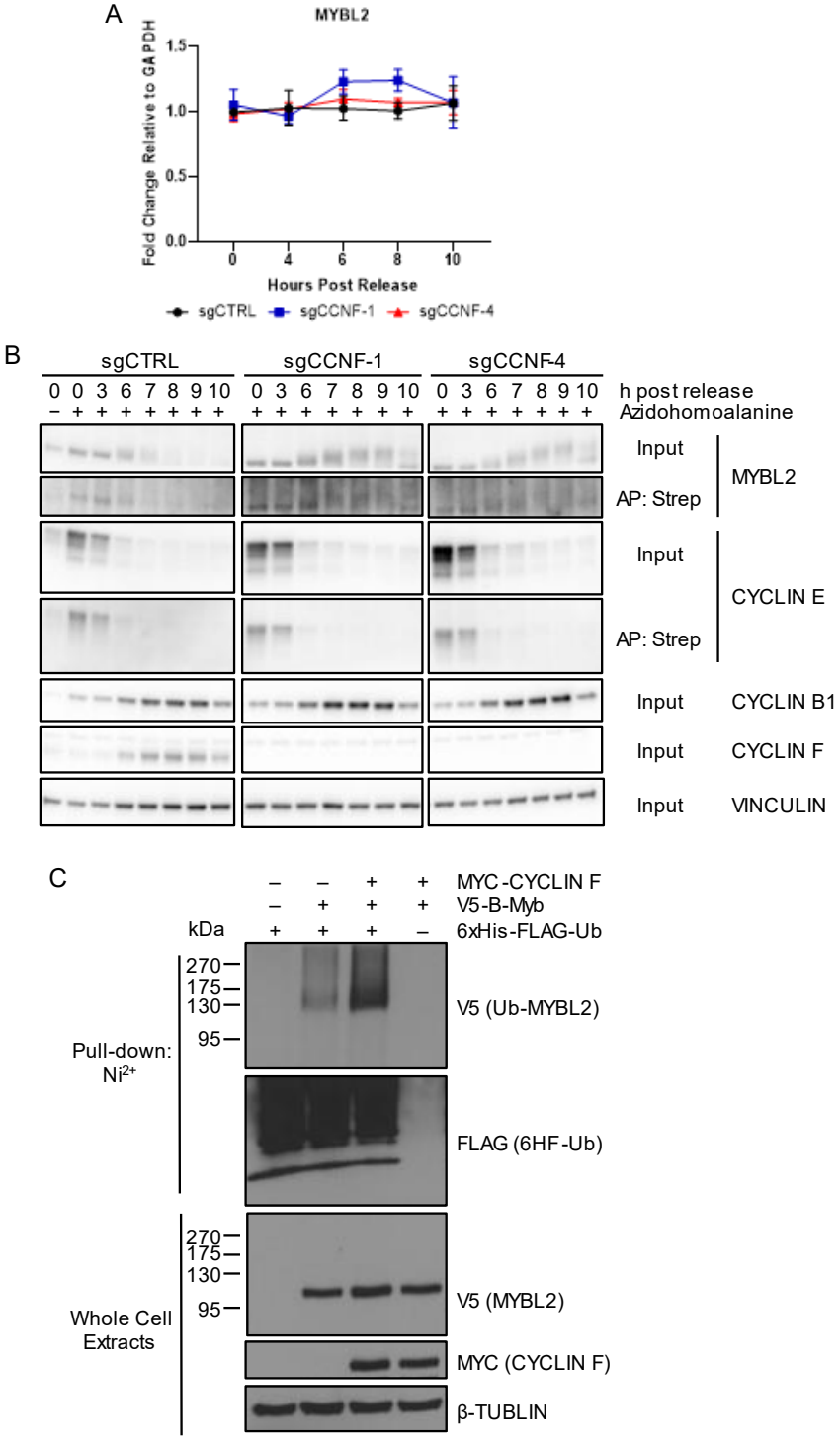

MYBL2 interacts with cyclin F through an atypical cyclin motif in a CDK phosphorylation-dependent manner

Phospho-MYBL2 species were co-immunoprecipitated with the FLAG-cyclin F constructs (**Fig 2.8A**) and endogenously expressed cyclin F interacted with phospho-MYBL2 in HeLa cells during G2/M (**Fig. 2.8B**) raising the possibility that cyclin/CDK phosphorylation of MYBL2 could be potentially regulating the MYBL2-cyclin F interaction. To identify the regions of MYBL2 required for the cyclin F interaction, the necessary and sufficient regions of MYBL2 for the cyclin F interaction were mapped using truncation mutants (**Fig. 2.8C**). The C-terminus of MYBL2 was sufficient for the cyclin F interaction as the 500-700 fragment of MYBL2 co-immunoprecipitated cyclin F as well MuvB complex (**Fig. 2.8D**). While the interaction with the MuvB complex and cyclin F was retained in the 1-685 construct, the MuvB components LIN9 and LIN37 failed to bind to MYBL2 when MYBL2 was truncated prior to residue 685 consistent with previous studies (Guiley et al., 2018). The 1-660 construct retained the interaction with cyclin F (**Fig. 2.8E**). The cyclin F interaction however was lost when MYBL2 was further C-terminally truncated implicating the 620-660 region of MYBL2 as required to interact with cyclin F. The 620-660 region of MYBL2 was further narrowed to the 643-660 as the 1-643 MYBL2 truncation mutant failed to interact with cyclin F (**Fig. 2.9A and 2.9B**).

The 643-660 region of MYBL2 contains a highly conserved RxH motif, which resembles the RxL cyclin binding motif (**Fig. 2.9C**). Mutation of this RxH motif on MYBL2 abolished the cyclin F interaction without abrogating the MuvB interaction indicating the MYBL2 requires the RxH motif to interact with cyclin F. Compared to a typical RxL cyclin binding motif, the histidine of the RxH motif would be in position to have Van der Waals interaction with the cyclin fold (**Fig. 2.9D**) potentially explaining why MYBL2 but not CDC6, which interacts through typical RxL motifs, could still interact with the cyclin F MR mutant (**Fig. 2.8C**).

Figure 2.8. The C-terminus of MYBL2 is required to interact with cyclin F

A) Co-immunoprecipitation of phospho-MYBL2 species FLAG cyclin F constructs from transfected 293T lysates.

B) Co-immunoprecipitation of MYBL2 with cyclin F containing complexes in G2/M. Cyclin F was immunoprecipitated from synchronized HeLa treated with 10 M MG-132 starting at hour 4 and immunoprecipitated complexes were subject to immunoblot with listed antibodies.

C) Schematic of MYBL2 depicting the MYBL2 truncation mutants used in this figure and their observed ability to interact with the MuvB complex or cyclin F.

D and E) Co-immunoprecipitation studies with MYBL2 truncation mutants. 293T cells were transfected with empty vector, WT, C-terminal (D), or N-terminal (E) V5-MYBL2 truncation mutant constructs and cellular lysates were immunoprecipitated with a V5 antibody. The resulting immunoprecipitates were analyzed by immunoblot as indicated.

Figure 2.8. (cont.)

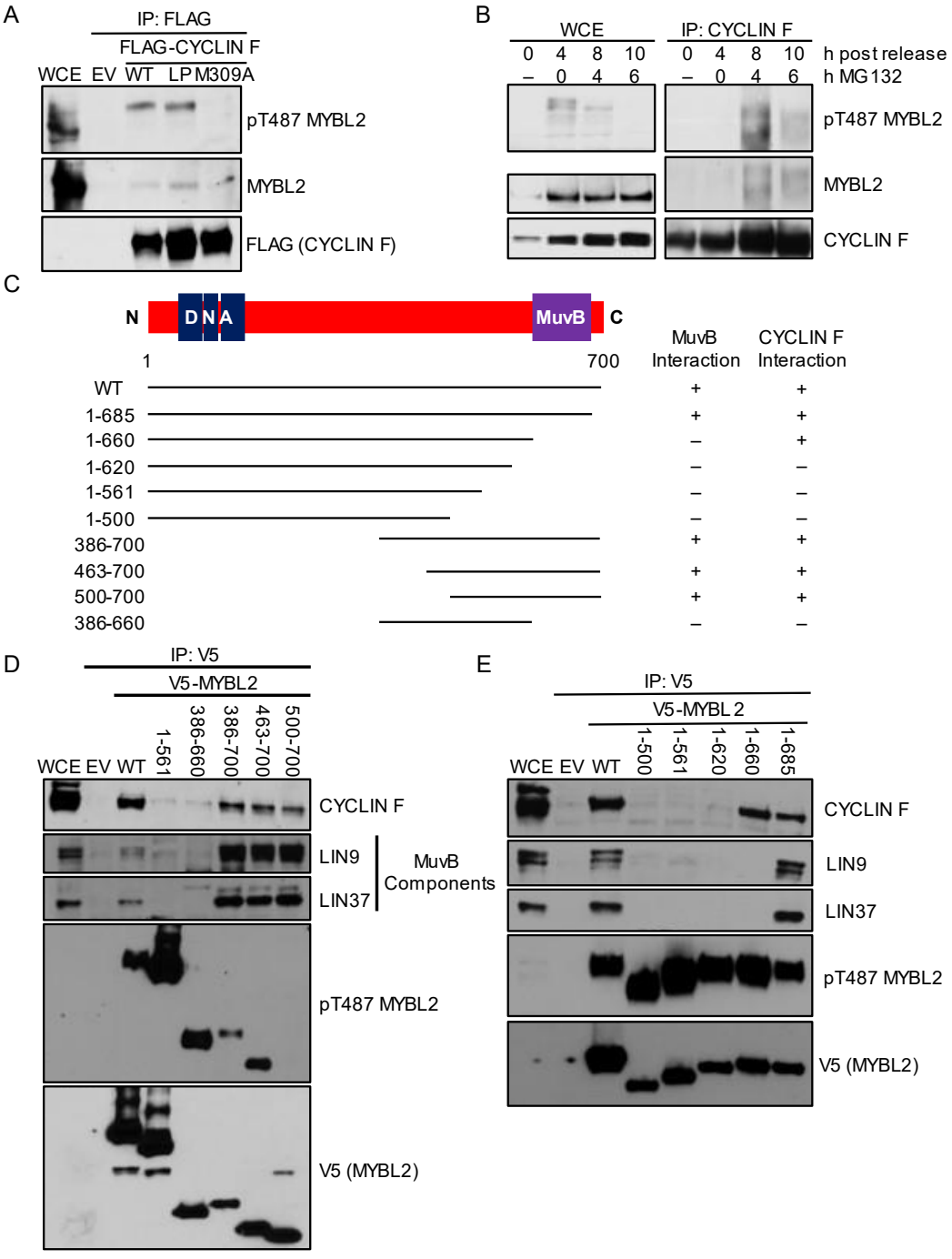

The MYBL2 386-660 truncation mutant, which contains the RxH motif, failed to bind to cyclin F (**Fig. 2.8D**) indicating that the cyclin F-MYBL2 interaction is regulated by additional variables. The canonical cyclin binding RxL motifs, located near the N- and C-termini of MYBL2, have been truncated from this mutant. One of these RxL motifs have been previously implicated in cyclin A binding raising the possibility that CDK phosphorylation could regulate the cyclin F-MYBL2 interaction. Two additional MYBL2 phosphorylation mutants were generated: (i) a T405A mutant was generated as this site resembles a CDK1 phosphorylation site on RRM2 that was previously implicated in the RRM2-cyclin F interaction (D'Angiolella et al., 2012) and (ii) a ΔCDK mutant in which five CDK phosphorylation sites, previously implicated in the literature (Johnson et al., 2002; Johnson et al., 1999), were mutated to alanine (**Fig 2.9A**). The cyclin F interaction was impaired for the MYBL2ΔCDK mutant to greater extent than the T405A mutant while both phospho-MYBL2 mutants interacted with MuvB (**Fig. 2.9E**) implicating CDK phosphorylation in facilitating the MYBL2 interaction. This data suggests that MYBL2 interacts with cyclin F through a non-canonical RxH cyclin binding motif that also requires CDK phosphorylation for the interaction.

Cyclin F-mediated degradation of MYBL2 is a CDK dependent off-switch for G2/M gene expression

Previous studies had proposed that cyclin F antagonizes MYBL2 activation but G2/M expression was assessed in asynchronous and/or DNA-damaged samples (Klein et al., 2015; Mavrommati et al., 2018). MMB-FOXM1 activity was assessed in cyclin F KO by probing for levels of pFOXM1. pFOXM1 for mitotic cells were separated from G2 cells, as in previous studies (Saldivar et al., 2018), since these have an MFI roughly a log higher than the G2 population (**Fig. 2.10A**). Surprisingly, pFOXM1 levels were similar in CCNF KO and CTRL cells (**Fig. 2.10B**) indicating that cyclin F does not limit basal activation of the MMB-FOXM1 activity. When MMB-FOXM1 target gene expression was examined in synchronized samples, *CCNB1*

Figure 2.9. MYBL2 interacts with cyclin F through an atypical cyclin binding motif in a phosphorylation-dependent manner

A) Schematic of MYBL2 depicting the MYBL2 point mutants used in this figure and their observed ability to interact with the MuvB complex or cyclin F.

B) Co-immunoprecipitation studies with MYBL2 RxH mutant to assess cyclin F interaction. Experiment same as described in **Fig. 2.8D**.

C) Alignment denoting degree of conservation of the 640-663 region of MYBL2.

D) Schematic showing the residues involved in cyclin-substrate interactions. Based upon aligning cyclin F sequences with cyclin A and comparing cyclin A-RxL interactions from the cyclin A3 – p107 structure (Brown et al., 1999).

E) Co-immunoprecipitation studies with MYBL2 phospho-mutant to assess cyclin F interaction. Experiment same as described in **Fig. 2.8**.

Figure 2.9. (cont.)

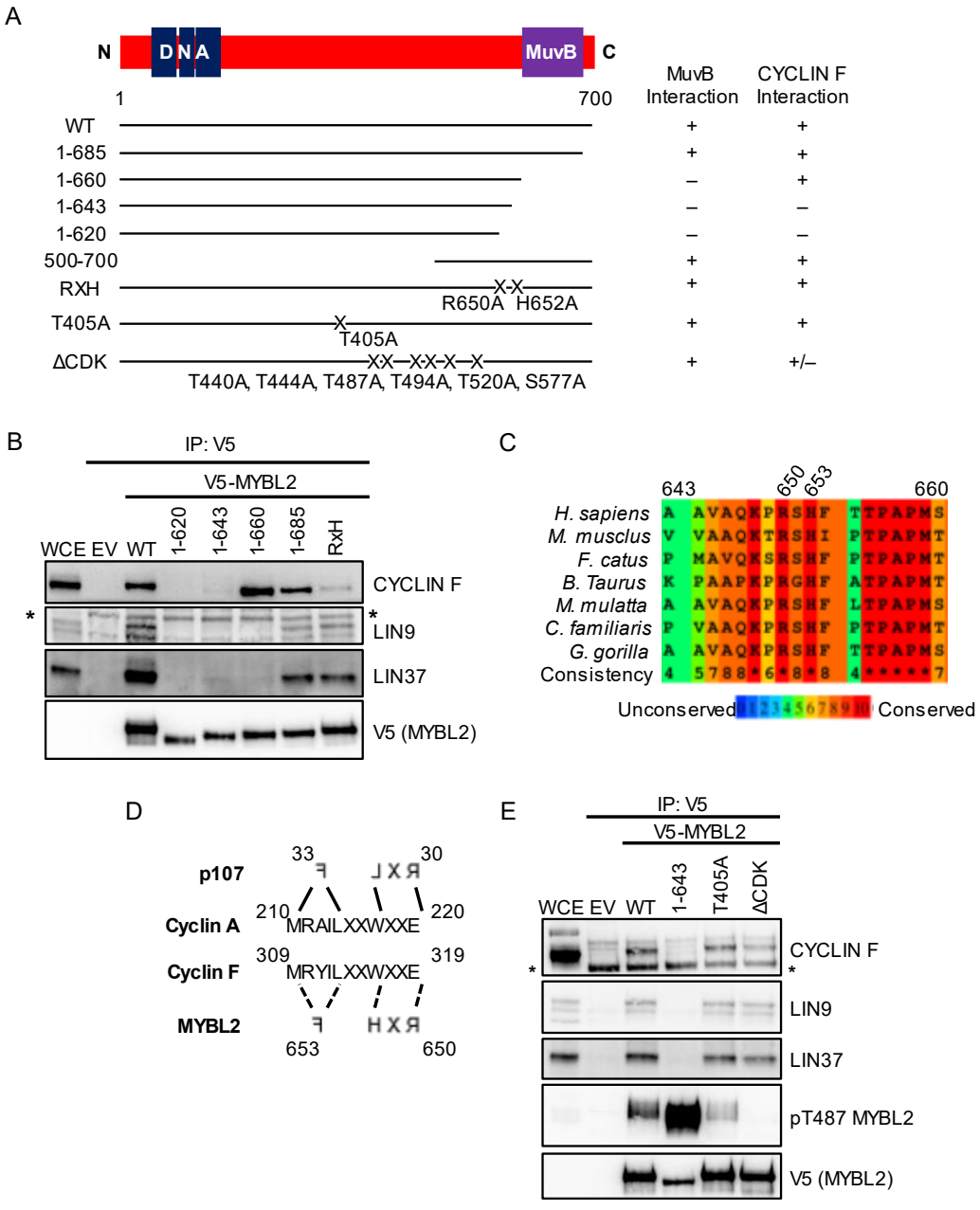

Figure 2.10. Cyclin F turns off MMB-FOXM1 target gene expression by limiting MMB complex formation

A and B) pFOXM1 levels in sgCTRL and sgCCNF KO cells. A) Schematic of the different pFOXM1 populations. B) pFOXM1 levels in cell cycle populations in sgCTRL and sgCCNF HeLa cells. G2/M was split base on the gating in A). N=3. Mean SEM. ANOVA with Tukey correction.

C and D) RT-qPCR of MMB-FOXM1 target genes C) *CCNB1* and D) *CCNA2* in synchronized Parental and sgCCNF-2 HeLa Cells synchronized as in Fig 1A.

E) Coimmunoprecipitation of the MMB-FOXM1 complex during mitosis in CCNF KO cells. sgCTRL and sgCCNF HeLa cells were synchronized with nocodazole and whole cell extracts were generated for the coimmunoprecipitations with antibodies for the denoted proteins.

Figure 2.10. (cont.)

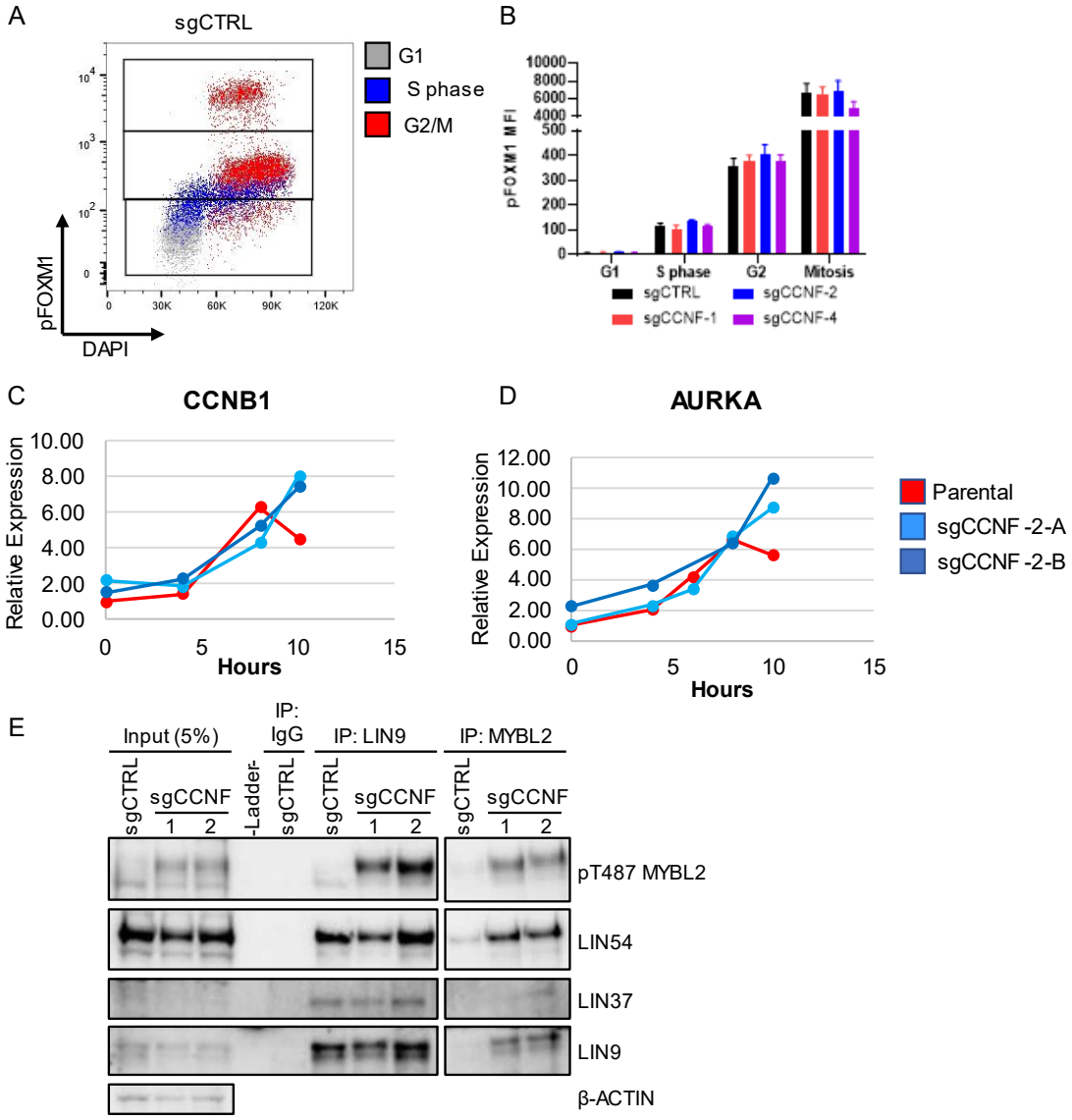

and *AURKA*, were expressed at similar levels during S phase, and at 4h and 8 hours post release, in CTRL and cyclin F KOs cells (**Fig. 2.10C and 2.10D**). However, cyclin F KO cells had increased levels of both G2/M genes at the 10h time point when there was a high fraction of mitotic cells. MYBL2 and MuvB components could co-precipitate each other in mitotic lysates of cyclin F KOs but not CTRL cells (**Fig. 2.10E**). This data indicates that the MYBL2 degradation by cyclin F is not the rate limiting step of MMB-FOXM1 complex activity during activation but functions as an off signal for MMB-FOXM1 complex activity as the cell progresses into mitosis by limiting MMB complex formation.

MYBL2 and cyclin F are in a negative feedback loop that limits CDK activity in mitosis

Based on meta-analysis of genome wide data sets, cyclin F is predicted to be an MMB-FOXM1 target gene (Fischer et al., 2016). Depletion of MYBL2, FOXM1, or the MuvB component LIN54, reduced cyclin F transcript and protein expression in G2/M (**Fig. 2.11A and 2.11B**) indicating cyclin F expression is MMB-FOXM1 complex dependent late in the cell cycle. Notably, cyclin F protein species were less stable with a faster turnover rate than MYBL2 during S phase and mitosis (**Fig. 2.11C and 2.11E**). Cyclin F levels decreased faster than other APC/C substrates in cycloheximide-treated cells during the M/G1 transition as the $SCF^{\beta\text{-}TRCP}$ complex is reported to limit cyclin F accumulation in mitosis (Mavrommati et al., 2018). MYBL2 protein species were more stable than cyclin F protein species when translation and cell cycle progression were blocked with cycloheximide at every timepoint tested during the S/G2 transition (**Fig 2.11D**). The cyclin F instability in S phase maybe due to degradation by B-TRCP, which this data suggests may actually function earlier in the cell cycle. The instability of cyclin F compared to MYBL2 after CHX treatments indicates that the activation of negative feedback loop is dependent on cell cycle progression and MMB-FOXM1.

Figure 2.11. The MMB-FOXM1 complex drives cyclin F accumulation in S/G2

A and B) RT-qPCR of *CCNF* transcript and immunoblot of whole extracts from HeLa cells depleted for MMB-FOXM1 components. Cells were transfected with the denoted siRNAs, synchronized as in Fig 1A, and samples collected at the listed time points.

C and D) Immunoblots of MYBL2 and CCNF protein levels after cycloheximide treatment in synchronized HeLa cells. Cells were synchronized as Fig. 1A and treated with cycloheximide for the denoted times. In D), DNA content was also determined in samples using PI stain.

E) Immunoblot of cyclin F and cyclin F substrates after cycloheximide treatment in nocodazole-synchronized sgCTRL or sgCCNF-4 cells. Nocodazole-synchronized cells were released into growth media or growth media containing cycloheximide for the denoted periods of time.

Figure 2.11. (cont.)

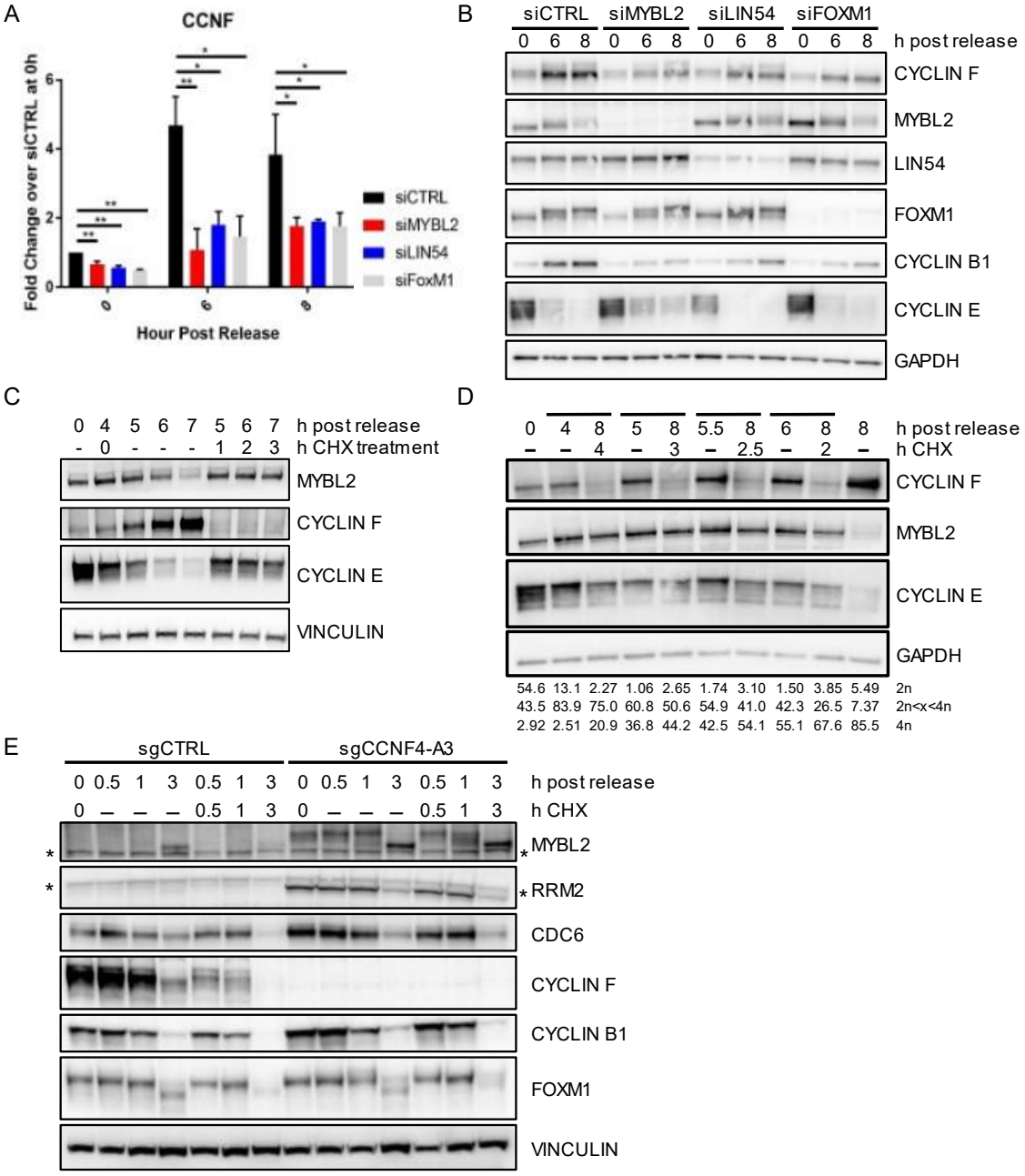

Disruption of this cyclin F-MYBL2 “off” switch could impair the M/G1 progression as expression of mitotic cyclins and the mitotic program persists. Consistent with this hypothesis, the 4N population persisted in CCNF KO cells at 11 and 12 hours post release from a double thymidine block, when cells typically have entered the next G1 (**Fig. 2.12A**). Cyclin B1 protein levels and slower-migrating FOXM1 phospho-species persisted into G1 in the cyclin F KOs (**Fig. 2.11E and 2.12B**). Further, mitotic pH3 was higher in cyclin F KO cells after an extend incubation of synchronized cells with nocodazole (**Fig. 2.12C**) suggesting that disruption of this off switch prevents slippage through the spindle assembly checkpoint likely due to the continued expression of the mitotic program.

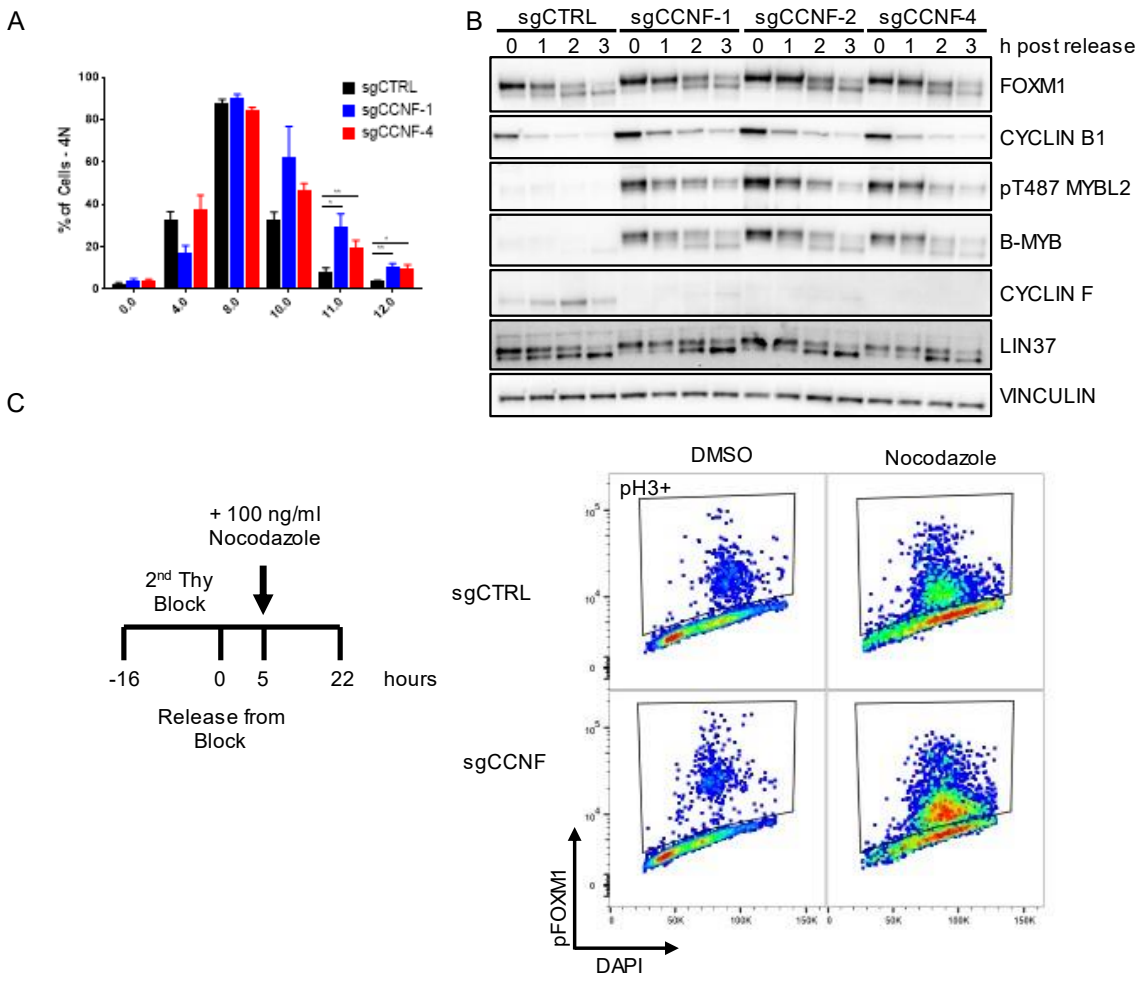

Figure 2.12. Mitotic cellular identity persists in the absence of cyclin F

A) 4N population in synchronized HeLa CTRL and CCNF KO cells. Cell were synchronized as Fig. 1A and 4N population was assessed using PI staining.

B) Immunoblot of HeLa sgCTRL and sgCCNF lysates after release from nocodazole synchronization and collected at the denoted times.

C) pH3 levels in synchronized sgCTRL and sgCCNF-2 HeLa cells trapped in mitosis with nocodazole. Samples were synchronized and treated as describe in the schematic on the left and, on the right, dot plots of pH3 populations pseudocolored for density.

Discussion

Here, we describe a cyclin F “off” switch that contributes to terminating G2/M gene expression (**Fig. 2.13**). During the S/G2 transition, cyclin F accumulation is driven by the MMB-FOXM1 complex. MYBL2 is subsequently degraded by an $SCF^{cyclin\ F}$ complex in G2/M to disrupt the MMB complex and reduce G2/M gene expression during mitosis. MYBL2 contains an atypical cyclin binding motif that requires phosphorylation at CDK sites to optimally interact with cyclin F linking activation of this negative feedback loop to CDK activity.

Multiple studies have implicated CDK-dependent phosphorylation of MYBL2 as pro-transcriptional but it remains unclear how CDK phosphorylation facilitates MMB-FOXM1 target gene expression as MYBL2 phospho-mutants can still interact with p300/CBP (Bartsch et al., 1999; Bessa et al., 2001; Johnson et al., 2002; Johnson et al., 1999; Lane et al., 1997; Muller-Tidow et al., 2001; Robinson et al., 1996; Saville and Watson, 1998; Ziebold et al., 1997). Recently, CDK-dependent phosphorylation of MYBL2 was implicated in facilitating an interaction with PIN1 that triggered a conformational change in MYBL2 leading to reportedly pro-transcriptionally PLK1 phosphorylation (Werwein et al., 2019). The most compelling evidence for cyclin/CDK phosphorylation being pro-transcriptional is impaired transactivation of reporters by MYBL2 phospho-mutants and increased reporter expression with cyclin A overexpression (Bartsch et al., 1999; Johnson et al., 2002; Johnson et al., 1999; Lane et al., 1997; Sala et al., 1997; Saville and Watson, 1998; Ziebold et al., 1997) but the reporters used to study the mutants were built around MYB or GAL4 binding sites rather than the CHR motif found at G2/M promoters and activation of the endogenously expressed MYBL2 cannot be separated from FOXM1 activation by cyclin A overexpression.

We observed that cyclin A/CDK phosphorylation was required for MYBL2 degradation which limited G2/M gene expression indicating that CDK phosphorylation of MYBL2 is actually a negative regulatory event in the context of the MMB-FOXM1 complex and G2/M gene expression. Loss of MYBL2 in G2/M coincided with increased levels of pFOXM1, a marker for

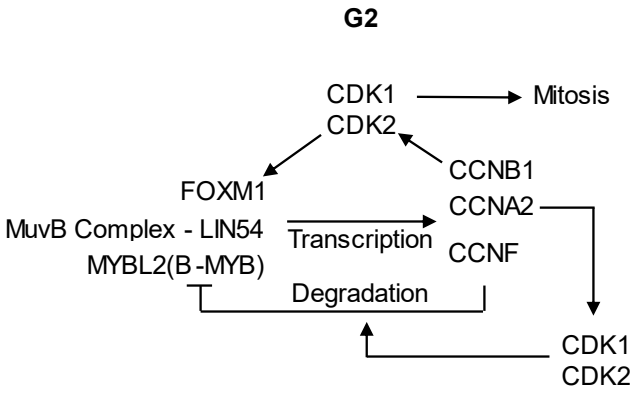

Figure 2.13. Model of MYBL2-cyclin F switch that turns off G2/M gene expression

In G2, CDK activity drives expression of G2/M genes including the mitotic cyclins and cyclin F. MYBL2 subsequently is degraded by cyclin F in a phosphorylation-dependent manner, which limits G2/M gene expression as the cell progresses to mitosis.

MMB-FOXM1 activity. While MYBL2 is predominantly phosphorylated by cyclin A/CDK complexes, FOXM1 can interact and be activated by cyclin D, cyclin E, cyclin A, and cyclin B containing CDK complexes (Anders et al., 2011; Fu et al., 2008; Laoukili et al., 2008b; Major et al., 2004). Although cyclin A/CDK1 phosphorylation appears to be rate limiting for FOXM1 phosphorylation during the S/G2 transition (Laoukili et al., 2008b; Saldivar et al., 2018), this difference in cyclin interactors suggests a model in which promiscuous CDK phosphorylation of FOXM1 activates the complex while cyclin A/CDK phosphorylation of MYBL2 in G2 specifically turns off the complex leading to MYBL2 degradation and preventing further recruitment of FOXM1.

In an earlier study, cyclin F was reported to not degrade MYBL2 as depletion of cyclin F didn't alter MYBL2 protein stability after cycloheximide treatment (Klein et al., 2015). Since cycloheximide blocks all protein translation, a key assumption when examining protein turnover with cycloheximide is that the protein promoting the degradation event is more stable than the protein being degraded. This is not the case with cyclin F and MYBL2 as MYBL2 was more stable than cyclin F in the presence of cycloheximide at each time point tested during S/G2 test in this study and the previous study (Klein et al., 2015). The rapid turnover of cyclin F implies that the MYBL2-cyclin F feedback loop can't be activated until there is persistent MMB-FOXM1 activity as cyclin F will be rapidly turnover and preventing premature activation of this negative feedback loop. Consistent with this model, expression of a cyclin F mutant that cannot be degraded by an SCF results in impaired G2/M gene expression and progression through mitosis (Mavrommati et al., 2018).

The dependency of cyclin F accumulation on MMB-FOXM1 complex activity during S/G2 also highlights that there are opposing signals within the G2/M transcriptional program that constitute a transcriptional switch involved in mitotic progression. Similar to how cyclin A and cyclin B/CDK1 complexes promote their own degradation by driving mitotic progression via positive feedback loops that activate the APC/C (Yang and Ferrell, 2013), *CCNA2* and *CCNB1*

eventually limit their own expression as cyclin/CDK complexes drive MMB-FOXM1-dependent *CCNF* expression and promote the MYBL2 and cyclin F interaction. The presence of the “on” and “off” feedback loops within the G2/M transcriptional program suggests that a finite amount of mitotic gene expression is hardwired into G2/M transcription. Loss of cyclin F abrogates this switch leading to the persistence of mitotic gene expression and allowing the cell to maintain the mitotic phosphorylated histone H3 (pH3) for an extended period of time.

Recently, cyclin F was recently implicated in CHK1 inhibitor sensitivity as CCNF F KO cells has increased sensitivity to CHK1 inhibitors (Burdova et al., 2019) which is notable given the regulation of FOXM1 activity by the ATR-CHK1 pathway. Similar to CHK1 inhibition or depletion, depletion of cyclin F led to increased mitotic entry as well as increased G2/M gene expression after irradiation (Klein et al., 2015). Unfortunately, viability assays were not conducted to determine if this increase in mitotic entry reflected abrogation of the G2 DNA damage checkpoint or recovery from G2/M DNA damage in cyclin F-depleted cells. The increased MMB-FOXM1 activity that results from depleting cyclin F can promote DNA damage recovery as cyclin B1 levels correlate with the ability to recover from G2/M DNA damage (Lindqvist et al., 2009).

While the increase in CHK1i sensitivity observed in CCNF KOs was attributed to increased E2F gene expression due to an absence of cyclin F-dependent degradation (Burdova et al., 2019), CHK1 limits CDK1 activity similar to the MYBL2-cyclin F negative feedback loops. In contrast to CHK1 inhibition, the receptor tyrosine kinase inhibitor sorafenib synergizes with CDK1 inhibition in hepatocellular carcinoma (Wu et al., 2018) highlighting how levels of CDK1 activity during the late cell cycle can modulate sensitivity to targeted therapeutics. Further investigation of the MYBL2-cyclin F switch and MMB-FOXM1 activity in response to CHK1 or RTK inhibition may yield further insights into cell division and the targeting to cancer therapeutics.

Materials and Methods

Cell Culture

HeLa, HCT116, and 293T cells were propagated in DMEM medium (Life Technologies, Grand Island, NY) supplemented with 10% fetal bovine serum (Sigma-Aldrich, St. Louis, MO) and 1% Pen/Strep (Gibco) at 37ºC in 5% CO_2. CCNF KO MEF were kindly provided by Dr. Steve Elledge (Harvard Medical School, Boston, MA). CRISPR CCNF KO cell lines were generated by transducing the cells with the appropriate lentiCRISPRv.2 lentivirus, selecting with puromycin, and generating clonal populations using serial dilution. Loss of cyclin F was confirmed in clonal populations by immunoblot. Inhibitors and chemicals used in tissue culture experiments are listed in **Table 2.1**.

For thymidine synchronizations, samples were synchronized by two sequential 16 hours incubations with 2 mM Thymidine Media. Cells were released into prewarmed for 8 hours between incubations with 2 washes with prewarmed PBS. 2 washes with prewarmed PBS was also used to release sample into prewarmed media for collection.

For siRNA experiments in synchronized samples, ~3 x 10^6 HeLa cells were reverse transfected at a final concentration of 20 nM or 50 nM (for siCCNF and siSKP2) with the siRNAs list in **Table 2.2** using Lipofectamine RNAiMAX (Invitrogen, 13778030) in 100 mm dish. The next day, samples were split into smaller 60 mm dishes (~5 x 10^5 cells) and double thymidine blocks were initiated as described above.

For nocodazole synchronizations, media on the samples were replaced after triturating the plates with 100 ng/ml nocodazole containing media and incubated for ~16-18 hours. To release cell from synchronization, mitotic cells were triturated into nocodazole containing media and washed twice with prewarmed PBS. Cells were then resuspended into prewarmed media and divided into sample for collection.

Table 2.1. Inhibitors and Chemicals

Thymidine	Sigma-Aldrich	T1985
Nocodazole	Sigma-Aldrich	M1404
Bortezomib	Cell Signaling Technologies	2204S
MLN4924	Active Biochem	A1139
Cycloheximide	VWR	97064-724
Polyethylenimine (PEI)	Polysciences	23966-1

Table 2.2**. siRNA oligonucleotides**

siCTRL	Dharmacon	D-001810-10
siCCNA2	Dharmacon	L-003205-00
siCUL1	Dharmacon	L-004086-00
siCUL2	Dharmacon	L-007277-00
siCUL3	Dharmacon	L-010224-00
siCUL4A	Dharmacon	L-012610-00
siCUL4B	Dharmacon	L-017965-00
siCUL5	Dharmacon	L-019553-00
siCUL7	Dharmacon	L-017673-00
siSKP1	Dharmacon	L-003323-00
siSKP2	Dharmacon	L-003324-00
siCCNF	Dharmacon	L-009762-00
siMYBL2	Dharmacon	L-010444-01
siLIN54	Dharmacon	L-019325-01
siFOXM1	Dharmacon	L-009762-00

Immunoblots

Whole-cell extracts were generated by incubating cell pellets in EBC buffer (50 mM Tris pH 8.0, 150 mM NaCl, 0.5 mM EDTA, 10% Glycerol, 0.5% NP-40, Protease Cocktail Set I and Phosphatase Cocktail Set I) and cleared by centrifugation. Relative protein levels in lysates were normalized by Bradford assay and samples were boiled in 6x SDS buffer. Samples were then loaded on 4-20% TGX gels (Bio-Rad) for electrophoresis which were then transferred to a nitrocellulose membrane (Bio-Rad) by wet transfer. Membranes were blocked in 5% nonfat milk (Boston Biochem) for 1 h at room temperature and incubated in primary antibody overnight at 4°C. Primary antibodies (listed in **Table 2.3**) were diluted as follows: FBXO5 was diluted 1:50 in 3% nonfat milk in TBST; cyclin F (sc-515207) and cyclin E were diluted 1:200 in 3% nonfat milk in TBST; CULLIN 1, CULLIN 2, CULLIN 3, CULLIN 4, CULLIN 5, CULLIN 7, and SKP1 were diluted 1:500 in 3% milk in TBST; FLAG, LIN9 and MYBL2 were diluted 1:1000 in 3% nonfat milk in TBST; cyclin F (Bethyl and sc-952), cyclin A, SKP2, cyclin B1, and GAPDH were diluted 1:2000 in 3% nonfat milk TBST; LIN54, Actin, V5 and CP110 (Bethyl) was diluted 1:1000 in 5% nonfat milk in TBST; FOXM1 was diluted 1:2000 in 5% nonfat milk TBST; pT487 MYBL2 was diluted 1:5000 in 3% nonfat milk in TBST; vinculin was diluted 1:30000 in 5% nonfat milk in TBST; LIN37, CP110 (CST), and CDC6 were diluted 1:1000 in 5% BSA in TBST; Membranes were incubated in secondary antibodies, diluted 1:5000 in 5% nonfat milk, for 1 h at room temperature. Bands were visualized using Super Signal West Pico (Thermo Scientific) or Immobilon Western Chemiluminescent (Millipore) HRP substrate on the G-box imaging system (Syngene).

For the phosphatase assay, sample pellets were split and lysed in EBC buffer or EBC buffer without phosphatase inhibitor. To 50 µg of samples lysed with EBC buffer without phosphatase inhibitor, 2 µl (10 U) of Antarctic Phosphatase (NEB, M0289S) was added. Phosphatase inhibitor was added to a final concentration of 2X to a set of Antarctic phosphatase

Table 2.3. Antibodies

Cyclin E	Santa Cruz Biotechnology	sc-247
Cyclin B1	Santa Cruz Biotechnology	sc-752
FOXM1	Santa Cruz Biotechnology	sc-520
pT487 MYBL2	Abcam	Ab76009
MYBL2	Millipore	MABE866
MYBL2	Santa Cruz Biotechnology	sc-724
pT600 FOXM1	Cell Signaling Technologies	14655S
LIN37	Bethyl Laboratories	A300-BL2983
LIN9	Bethyl Laboratories	A300-BL2981
LIN54	Bethyl Laboratories	A300-799A-M
CYCLIN F	Bethyl Laboratories	A303-406A-M
CYCLIN F	Santa Cruz Biotechnology	sc-952
CYCLIN F	Santa Cruz Biotechnology	sc-515207
CYCLIN A	Santa Cruz Biotechnology	sc-751
CULLIN 1	Santa Cruz Biotechnology	sc-17775
CULLIN 2	Zymed Laboratories	51-1800
CULLIN 3	Santa Cruz Biotechnology	sc-166110
CULLIN 4A/4B	Santa Cruz Biotechnology	sc-377188
CULLIN 5	Santa Cruz Biotechnology	sc-373822
CULLIN 7	Santa Cruz Biotechnology	sc-53810
SKP1	Santa Cruz Biotechnology	sc-7163
SKP2	Santa Cruz Biotechnology	sc-7164
CP110	Bethyl Laboratories	A301-343
CP110	Cell Signaling Technologies	12140S

Table 2.3. Antibodies (cont.)

RRM2	Santa Cruz Biotechnology	sc-10846
CDC6	Cell Signaling Technologies	3387S
FLAG	Sigma-Aldrich	F1804
FLAG-HRP	Sigma-Aldrich	A8592
MYC	Santa Cruz Biotechnology	sc-40
V5	GenScript	A01724
Actin	Santa Cruz Biotechnology	sc-47778
GAPDH	Santa Cruz Biotechnology	sc-47724
VINCULIN	Sigma-Aldrich	V9131
FLAG magnetic beads	Sigma-Aldrich	M8823-1ML
FLAG affinity matrix	Sigma-Aldrich	A2220
anti-V5 goat agarose beads	Bethyl Laboratories	S190-199
pS10 histone H3 - Alexa 488 conjugate	Cell Signaling Technologies	3465S
anti-mouse IgG - HRP	Bethyl Laboratories	A90-116P
anti-rabbit IgG - HRP	Bethyl Laboratories	A120-101P
Rabbit Trueblot: Anti-Rabbit IgG HRP	Rockland Immunochemicals	18-8816-33
anti-mouse IgG - Alexa 488 conjugate	Cell Signaling Technologies	4408S
anti-Rabbit IgG - PE conjugate	Cell Signaling Technologies	4340S
Rabbit IgG Alexa 488 isotype control	Cell Signaling Technologies	4340S

Table 2.3. Antibodies (cont.)

anti-BrdU-APC conjugate	Biolegend	339808
APC Mouse IgG1, k isotype control	Biolegend	400120

samples as a negative control. All samples were incubated at 37°C for 1 hour and 6X SDS buffer was added to each sample, followed by heating at ~95°C to stop the reaction and prepare the sample for SDS-PAGE and immunoblotting.

Immunoprecipitation

For co-immunoprecipitation studies with expression constructs in 293Ts, constructs were transfected into sub confluent 293T cells using 2 ug/ml PEI. Whole cell extracts were generated using EBC on ice and cleared twice sequentially by centrifugation (16,100 rcf, 5 min 4°C). FLAG-cyclin F and V5-MYBL2 containing complexes were then immunoprecipitated using FLAG M2 magnetic beads or FLAG M2 affinity matrix and anti-V5-goat agarose beads respectively. Immunoprecipitations were incubated at 4°C for 4 hours and washed three times with EBC. Captured protein were then eluted from the beads by heating the samples at 70C in 1X SDS buffer.

For immunoprecipitation of the endogenous MMB complex, lysates were generated as described above and 1mg of lysate was incubated with 1 ug of either MYBL2 antibody or LIN9 antibody and magnetic protein A/G beads overnight at 4°C. Samples were then washed as above. During immunoblotting, TrueBlot anti-rabbit IgG was used at 1:2000 for the secondary to prevent detection of eluted rabbit IgG used for the immunoprecipitation.

For the co-immunoprecipitation studies with endogenous cyclin F, Cells were lysed in EBC lysis buffer. Cell extracts were cleared at 14,000 rpm for 10 minutes and then mixed with antibody for 12 hours at 4°C. Immune complex were captured with Protein A agarose beads (Roche) for 1 hour at 4°C and washed 3 times with EBC buffer and 2 times with EBC buffer containing 300 mM NaCl.

Azidohomoalanine labeling

The CLICK reaction for biotin conjugation to AHA-labeled species was based on previous studies (Presolski et al., 2011) and used reagents listed in **Table 2.4**. Briefly, HeLa cells were pulsed with 1 mM AHA in methionine-free growth media for 16 hours during the second thymidine block of a double thymidine block. Samples were then released into regular growth media containing 200 µM L-methionine. Samples were collected and cell pellets stored at -80°C. Lysates were generated from cell pellets by resuspending pellets in 100 mM PBS + 1% NP-40 lysis buffer on ice for 15 min and were then cleared by centrifugation (16,100 rcf, 10 min, 4°C). Input samples were generated at this point. Biotin was conjugated to AHA-labeled protein species using CLICK chemistry in a reaction comprised of the following final concentrations/amounts: 400 µg of sample, 20 µM biotin-PEG4-Alkyne, premixed 0.1 mM CuSO4 + 0.5 mM THPTA, 5 mM aminoguanidine, 5 mM sodium ascorbate, 100 mM PBS to 500 ul). Reactions were rotated at room temperature for 1 hour. Excess biotin was removed by from the reactions using Amicon 10 kDa ultracentrifuge filters (10000 rpm, 15 min, room temp) with 450 µl of 100 mM PBS being adding to ~30 µl concentrate and spun for a second time. The resulting concentrate was resuspended 900 µl of 100 mM PBS to which 100 µl of Magnetic Streptavidin beads was added. Beads and lysates were incubated rotating at room temperature for 90 min and washed 3 times with 100 mM PBS. AHA-labeled proteins were then eluted from the beads by heating for 5 min at 75°C in 1x SDS-PAGE buffer. Elutes and inputs were then assessed by immunoblot.

Flow cytometry

Trypsinized cells were washed with PBS and fixed in 4% formalin in PBS for 15 min at room temperature. Cells were then washed three times with 1% BSA in PBS and permeabilized in 70% ethanol at -20ºC for 30 min to overnight. After three washes with 1% BSA in PBS, incorporated BrdU was exposed by incubating samples in 200 ug/ml DNaseI in DPBS for 1 hour at 37ºC, using the reagents listed in **Table 2.4**. Samples were then washed thrice with 1% BSA

Table 2.4**. Reagents for AHA labeling and flow cytometry**

Azidohomoalainine	Click Chemistry Tools	1066
THPTA	Click Chemistry Tools	1010
Biotin-PEG4-Alkyne	Click Chemistry Tools	TA105
Streptavidin Magnetic Beads	New England Biolabs	S1420S
Amicon Ultra-0.5 Centrifugal Filter Unit -10 KDa	Millipore-Sigma	UFC501024
5-bromo-2'-deoxyuridine (BrdU)	Sigma-Aldrich	B5002
DNaseI	Sigma-Aldrich	D4513-1VL
4′,6-diamidino-2-phenylindole (DAPI)	Invitrogen	D3571

in PBS and incubated with the primary antibody in 1% BSA in PBS overnight at 4ºC. Primary antibodies were diluted as follows: 1:200, MYBL2, 1:250, pT600 FOXM1. After 3 washes with 1% BSA in PBS, samples were incubated with secondary antibodies, which were diluted 1:250 in 1% BSA in PBS, for 1 h at room temperature in darkness. An anti-mouse Alexa 488 conjugate and anti-rabbit PE conjugate were used to detect MYBL2 and pFOXM1 respectively. Following three 1% BSA in PBS washes, samples were incubated with anti-BrdU-APC (1:50 in 1% BSA in PBS) for 1 hour at room temperature. After three more 1% BSA in PBS washes, DNA staining was then conducted by incubating samples in darkness and at room temperature for 1 h in a 1 μg/ml DAPI, 100 ng/ml RNase A staining solution. A negative control where an BrdU pulse and primary antibodies were omitted but otherwise normally processed was used to establish negative populations and perform background subtraction on MFIs. For the negative control, an APC isotype was used in place of the BrdU-APC conjugate. Single fluorophore and fluorescence minus one control for the Alexa 488 channel were used to set any compensation parameters to address spillover of the fluorophores into other filters. Samples were analyzed on a Fortessa analyzer (BD Biosciences) and 50,000 total events were captured for each sample.

For DNA staining with PI, cells were harvested by trypsinization and fixed in ice cold 70% ethanol for 30 min to overnight after a PBS wash. Fixed samples were washed three times in PBS-Tween and resuspended in 10X PI stain diluted in PBS. Samples were then analyzed on a FACSCanto.

For pH3, samples were harvested by trypsinization, fixed in 4% formaldehyde for 30 min at room temp, and fixed in ice cold 70% ethanol for 30 min to overnight after a PBS wash. Fixed samples were washed three times in PBS-Tween, incubated with pH3 Alexa Fluor 488 conjugate diluted 1:50 in 5% BSA in PBS-T overnight at 4C. After 3 more PBS-T washes, samples were resuspended in 10X PI stain diluted in PBS. Samples were then analyzed on a FACSCanto.

RNA Expression

For RT-qPCR, Total RNA was extracted from cell pellets using the RNeasy Plus kit (Qiagen). cDNA was generated from total RNA isolated using the High-Capacity cDNA Reverse Transcription Kit (Applied Biosystems). qPCR was performed on the cDNA using the primers listed in **Table 2.5** and Brilliant III Ultra-Fast qPCR Master Mix (Agilent) using a MxAria (Agilent).

Relative expression was determine using the ΔΔCq method with GAPDH as reference gene. The microarray analysis was previously described (Sadasivam et al., 2012a). The HeLa microarray data were downloaded from GEO (GSE26922). The HeLa data were generated using Affymetrix Gene 1.0 ST arrays. Fluorescence intensities were normalized using RMA normalization and subsequently log-transformed. For each gene in our panel, we identified the corresponding probesets on the array and computed a summarized vector of expression levels by taking the average. We then subtracted the time zero value for each gene from each expression level for that gene. These were the final values that were visualized on the heatmap and the genes were clustered using hierarchical clustering using complete linkage and Euclidean distance.

Ubiquitination Assay

Ubiquitin Assays were conducted as previously described. Briefly, 20% of each sample harvested was used to analyze inputs by immunoblot and 80% for His-pulldowns to detect ubiquitinated proteins. For the His-pulldowns, samples were lysed in buffer 1 (6 M Guanidine-HCl, 0.1 M Na_2HPO_4/NaH_2PO_4, 0.01 M Tris/HCl [pH 8.0], 15 mM imidazole, and 10 mM β-mercaptoethanol [βME]) and used for pull-down of His-ubiquitin-conjugated proteins. The lysates used for pull-down were sonicated to reduce viscosity and loaded onto 50 µl of Ni^{2+}-NTA

Table 2.5**. Oligonucleotides: qPCR Primers**

CCNB1-qPCR-Forward Primer:	5’-GATGGAGCTGATCCAAACC-3’
CCNB1-qPCR-Reverse Primer:	5’-GGATGGCTCTCATGTTTCC-3’
MYBL2-qPCR-Forward Primer:	5’-CATCTCGGACCCTCATCTT-3’
MYBL2-qPCR-Reverse Primer:	5’-AGGTCACCTGAAGACTCTC-3’
AURKA-qPCR-Forward Primer:	5’-CTGCATTTCAGGACCTGTTAAGG-3’
AURKA-qPCR-Reverse Primer:	5’-AATGCGCTGGGAAGAATTT-3’
CCNF-qPCR-Forward Primer:	5’-TGCTCTTGAACCGGAAAC-3’
CCNF-qPCR-Reverse Primer:	5’-GTGGCCAGAATTCCCTTATAG-3’
GAPDH-qPCR-Forward Primer:	5'-CGCCCAATACGACCAAAT-3'
GAPDH-qPCR-Reverse Primer:	5'-CGCCCAATACGACCAAAT-3'

resin pre-washed with buffer 1. Binding was performed at room temperature for 4 hr. The beads were successively washed with 750 µl of each of the following buffers: buffer 1; buffer 2 (8 M urea, 0.1 M Na_2HPO_4/NaH_2PO_4, 0.01 M Tris/HCl [pH 8.0], 10 mM βME); buffer 3 (8 M urea, 0.1 M Na_2HPO_4/NaH_2PO_4, 0.01 M Tris/HCl [pH 6.3], 10 mM βME) plus 0.2% Triton X-100; buffer 3 and then buffer 3 plus 0.1% Triton X-100. After the last wash, beads were eluted by incubating in 50 µl of buffer 4 (200 mM imidazole, 0.15 M Tris/HCl [pH 6.7], 30% glycerol, 0.72 M βME, 5% SDS) for 20 min

Constructs

The lentiCRISPRv.2 constructs used in this study were generated by cloning the oligonucleotides listed in Table 2.6 as previously described (Choudhury et al., 2016; Sanjana et al., 2014; Shalem et al., 2014).

To rescue the CCNF KO cell lines, the pHAGE-3xFLAG-HA-gateway-SV40promoter-blastocidin was generated by excising the ApaI-SV40promoter-blasticidin-ClaI fragment from pwlz backbone and ligating into the pHAGE-3xFLAG-HA-Gateway linearized with ApaI and ClaI (NEB) digestion backbone using T4 DNA ligase. pcDNA3-FLAG-Cyclin F WT, LP/AA mutant and M309A mutant were kind gifts from Michele Pagano (New York University, NY). The cyclin F WT and LP/AA mutant ORFs were amplified by PCR and recombined into the pDONR221 and then pHAGE-3xFLAG-HA-gateway-SV40promoter-BSD backbones using BP and LR recombinases (Invitrogen) respectively. Silent mutations were introduced into cyclin F ORF to disrupt the NGG site for sgCCNF-4 by site directed mutagenesis using the Quikchange Mutagenesis kits (Agilent) ; no silent mutations were needed for sgCCNF-1 or sgCCNF-2 due to overlap of the sgRNA and 5’ UTR. Additional cyclin F point mutants used in co-immunoprecipitation studies were also generated in the pcDNA3 backbone by site directed mutagenesis.

The MYBL2 truncation mutants were generated by PCR amplifying the MYBL2 ORF and recombing the PCR fragments in the pDONR221 backbone using BP clonase. MYBL2 point mutants were generated by site directed mutagenesis in the pDON221 backbone. MYBL2 ORFs were moved from the pDON221 vector to the pcDNA3.1-nV5-DEST (Invitrogen) using LR clonase to express the MYBL2 constructs in cells.

Data Analysis

Praline multiple sequence alignment program (https://www.ibi.vu.nl/programs/pralinewww/) was used to align the MYBL2 sequences from the following species from UniProt database (www.uniprot.org): H. sapiens (P10244), M. musculus (P48972), F. catus (M3WEJ8), B. taurus (Q17QY0), M. mullatta (G7NT2), C. familiaris (F1PQ73), and G. gorilla (G3REHS).

Flow cytometry data was analyzed using FlowJo. GraphPad Prism was used to generate graphs and conduct statistical analyses for DepMap data, flow cytometry, viability, growth curves and RT-qPCR.

Chapter 3. MMB-FOXM1-driven premature mitosis is required for CHK1i sensitivity

Author Contributions

Dr. David Kozono, Peter Deraska, and Hunter D. Reavis performed the A549 and H460 sensitivity curves and CRISPR screen in Figure 3.1 and generated the sgEV and sgLIN54-1 cell lines used in this study. The sgLIN54-2 and sgFOXM1 KO cell lines used in this study were generated in collaboration with Larissa Sambel. The proliferation assay in Figure 3.2 and analysis of the RNA-seq in Figures 3.10 and 3.16 was a collaboration with Dr. Amy E. Schade. Hembly Rivas performed the CHK1i and ATRi sensitivity curves in Figure 3.2. All other assays and experiment were conceived and performed by me. I collaborated with Dr. David Kozono to write the manuscript that serves as the basis of this chapter which was edited by Dr. James A. DeCaprio. Dr. Amy E. Schade also provided assistance in writing the sections of the paper pertaining to the RNA-seq analysis. Dr. Geoffrey I. Shapiro and Dr. Alan D. D'Andrea also helped conceptualize of the initial aims of this study. I would like to thank Huy Nguyen for assistance with bioinformatics analysis and visualization for Figures 1E and 1F as well as Mona Ahmed for technical assistance regarding the pATM staining and DNA-PKcs reagents in Figure 3.

This research was supported by the US Public Health Service grants F31CA189328 to T.B.; R35CA232128, R01CA63113, R01CA173023 and P01CA203655 to J.A.D.; and K08CA172354 to D.K. This work was also supported by the Joint Center for Radiation Therapy (to D.K.) and in part by a Sponsored Research Agreement from Eli Lilly to G.I.S. and A.D.D.

The published version of this work can be found under the following citation:

Branigan, T. B., Kozono, D., Schade, A. E., Deraska, P., Rivas, H. G., Sambel, L., Reavis, H. D., Shapiro, G. I., D'Andrea, A. D., and DeCaprio, J. A. (2021). MMB-FOXM1-driven premature mitosis is required for CHK1 inhibitor sensitivity. Cell Rep *34*, 108808

Abstract

The ATR-CHK1 pathway coordinates DNA replication with cell cycle progression providing a potential therapeutic opportunity in cancer cells where oncogenic perturbations leaded to accelerated cell division. The critical downstream events after perturbation of the ATR-CHK1 pathway remain unclear potentially limiting the clinical use of inhibitors of pathway components such as CHK1. To identify genes whose loss confers resistance to CHK1 inhibitors, a genome-wide CRISPR-Cas9 screen was performed in NSCLC cell lines treated with the CHK1 inhibitor prexasertib (CHK1i). Five of the top six hits of the screen, MYBL2 (B-MYB), LIN54, FOXM1, cyclin A2 (CCNA2), and CDC25B, are cell cycle regulated genes that contribute to entry into mitosis. Knockout of MMB-FOXM1 complex components, LIN54 and FOXM1, conferred resistance to inhibition of either ATR or CHK1 as well as reduced CHK1i-induced DNA replication stress markers. Mechanistic experiments into the contribution of the MMB-FOXM1 complex to CHK1i-induced DNA replication stress revealed that premature activation of the mitotic program was required for CHK1i-induced replication catastrophe. Activation of a feedback loop between the MMB-FOXM1 complex and CDK1 was required for CHK1i-induced premature mitosis in Late S phase and subsequent replication catastrophe indicating that dysregulation of the S/G2 to M transition is necessary for CHK1 inhibitor sensitivity. Cells resistant to CHK1i however remained sensitive to inhibition of WEE1. These findings provide mechanistic insights into small molecule inhibitors currently studied in clinical trials and provide rationale for combination therapies.

Introduction

Duplication of the eukaryotic cellular genome occurs in an orderly process during S phase of cell division. Replication of the genome must be completed prior to mitosis to avoid events that result in genomic instability. DNA replication stress can occur when oncogenes, genotoxic agents, or inhibitors of DNA replication cause stalled replication forks leading to activation of DNA Damage Response (DDR) pathways. CHK1 is activated by ATR phosphorylation of the SQ sites S317 and S345 (Kim et al., 1999; Zhao and Piwnica-Worms, 2001), to resolve incomplete DNA replication structures consisting at least partly of single-strand DNA (Lupardus et al., 2002; Saldivar et al., 2017; Zou and Elledge, 2003). Replication stress also leads to the phosphorylation of the replication fork component RPA32 on S4, S8, and S33, and the regulator of heterochromatin KAP1 (also known as TRIM28 or TIF1B) on S824 to remedy this altered DNA replication (Ashley et al., 2014; Liu et al., 2012; Olson et al., 2006; Yajima et al., 2009). Unresolved replication stress can lead to cell death via replication catastrophe, where exhaustion of replication factors, such as RPA, triggers widespread DNA double-strand breaks (DSBs) marked by γ-H2AX (Furuta et al., 2003; Toledo et al., 2013). Understanding how the ATR-CHK1 pathway prevents replication catastrophe is critical as inhibitors of ATR or CHK1 are considered for clinical use.

The ATR-CHK1 pathway limits DNA replication stress during S phase by coordinating origin firing with CDK activity. ATR-activated CHK1 antagonizes CDK1 activity by activating the CDK1-inhibitory WEE1 kinase and suppressing the CDK1-activating CDC25 phosphatases (Furnari et al., 1997; O'Connell et al., 1997). Suppression of CDK1 activity during S phase by ATR and CHK1 prevents premature activation of the transcription factor FOXM1 and expression of mitotic genes (Saldivar et al., 2018). Cyclin A (CCNA2)/CDK1 activity however also is required for late origin firing (Katsuno et al., 2009). Therefore, complete suppression of CDK activity would decrease origin firing and subsequent activation of ATR. During S phase, the

ATR-CHK1 pathway maintains a careful balance of sufficient CDK1 activity to complete DNA replication but not enough to trigger mitosis.

Transcriptional regulation also plays a key role in managing cell cycle progression. When cells enter the cell cycle, an E2F-dependent wave of gene expression facilitates DNA replication during the G1/S transition, while the MYBL2/MuvB (MMB)-FOXM1 complex drives a second wave of gene expression during G2/M that promotes mitosis. During S phase, the MuvB complex, comprised of LIN54, LIN9, LIN37, LIN52, and RBBP4, together with MYBL2 binds to cell cycle genes homology region (CHR) DNA motifs, which are LIN54 binding sites, at promoters of genes whose expression is required for mitosis (Knight et al., 2009; Litovchick et al., 2007b; Muller et al., 2012; Pilkinton et al., 2007; Schmit et al., 2009b). FOXM1 is subsequently recruited to these promoters in an MMB-dependent fashion. This recruitment coincides with an increase in the levels of several hundred G2/M cell cycle genes, including CCNA2, CCNB1, PLK1, and CDC25B (Chen et al., 2013b; Down et al., 2012a; Fischer et al., 2016; Sadasivam et al., 2012b).

Due to oncogene-driven acceleration of cell division, cancer cells may become hyper-dependent on the ATR-CHK1 pathway to manage replication stress and maintain sufficient genomic integrity for continued survival. Inhibitors of ATR and CHK1 have been developed as anti-cancer agents to exploit this vulnerability. Monotherapy with the CHK1 inhibitor prexasertib (CHK1i) has shown safety and tolerability (Hong et al., 2016; Hong et al., 2018). Prexasertib treatment or CHK1 depletion have little to no effect on non-transformed cells such as RPE-1, while CHK1i monotherapy has exhibited activity in multiple cancer cell lines (Blosser et al., 2020; Cole et al., 2011; King et al., 2015; Koppenhafer et al., 2018). However, intrinsic or acquired resistance to CHK1i may limit clinical efficacy. Given the myriad roles of CHK1, such resistance could potentially emerge by a wide range of possible mechanisms. CRISPR-Cas9 pooled whole-genome sgRNA knockout screens have emerged as particularly useful tools for unbiased discovery of gene losses that confer a phenotype of interest (Hanna and Doench,

2020). Prior CRISPR screens with ATR inhibitors (ATRi) have implicated both the cell cycle and DDR regulatory roles of the ATR-CHK1 pathway in modulating inhibitor sensitivity. Loss of CDC25 family members conferred resistance to ATR inhibition while the loss of RNaseH2 increased sensitivity (Ruiz et al., 2016; Wang et al., 2019). Mechanistic efforts to understand how different roles of the ATR-CHK1 pathway mediate drug sensitivity can increase understanding of the underlying biology of these inhibitors, identify potential markers and improve strategies to overcome drug resistance.

Results

MMB-FOXM1 complex components are required for CHK1 inhibitor sensitivity in NSCLC cells

To identify genes whose monogenic loss confers resistance to the CHK1 inhibitor prexasertib (CHK1i), genome-wide CRISPR-Cas9 knockout screens were performed in two non-small cell lung cancer (NSCLC) cell lines A549 and NCI-H460. Both lines showed comparable CHK1i sensitivity with IC50 values in the 50-100 nM range (**Fig. 3.1B**). When treated at these concentrations, cells showed increased levels of markers of replication stress including phosphorylation of RPA32 on residues S4/S8 and S33 and KAP1 on S824 (pKAP1) (**Fig. 3.1A**). There was also a concomitant increase in the DNA DSB marker γ-H2AX. CHK1 phosphorylation reached maximum levels near the CHK1i IC50 dose, while overall levels of CHK1 decreased at higher doses (**Fig. 3.1A**). The decrease in total CHK1 is consistent with the induction of specific degradation by ubiquitin-proteasome in response to genotoxic stress (Zhang et al., 2005). The decreased viability, appearance of replication stress markers pRPA and pKAP1 and indication of DSB reflected by γ-H2AX indicate that CHK1 inhibition in A549 and H460 NSCLC cells leads to replication stress-induced catastrophe.

Screens to identify genes required for CHK1i sensitivity were performed in A549 and H460 cells using the Brunello human genome-wide lentiviral gRNA pooled library. The library consists of 76,441 sgRNAs targeting 19,114 unique genes (Doench et al., 2016). A549 and NCI-H460 cells were grown for nearly three weeks in the continuous presence of 100 nM and 50 nM CHK1i respectively, leading to equal amounts of cell proliferation and cytotoxicity. DNA sequencing was performed to identify sgRNAs that were substantially enriched compared to the input levels, reflecting genes whose losses conferred CHK1i resistance. The STARS algorithm (Doench et al., 2016) identified hits at the gene level with false discovery rates below 10% in both cell lines. Loss of CCNA2, CDC25B, FOXM1, LIN54, and MYBL2 emerged as the top hits

Figure 3.1. MMB-FOXM1 complex components are required for CHK1i sensitivity in NSCLC cells

A) Immunoblot of replication stress markers in A549 and NCI-H460 cells after treatment with increasing CHK1i concentrations for 24 h.

B) Sensitivity curves comparing the viability of A549 and H460 cells in the presence of increasing CHK1i concentrations for 72 h. Mean ± SD.

C) Table of genes identified by the STARS algorithm as having multiple sgRNAs significantly enriched after CHK1i treatment.

D) Heat map of individual genes enriched in STARS program either A549 or H460 cells.

E and F) Volcano plots of sgRNA enrichment in CHK1i positive selection screen in A549 (E) and NCI-H460 (F) cells.

Figure 3.1. (cont.)

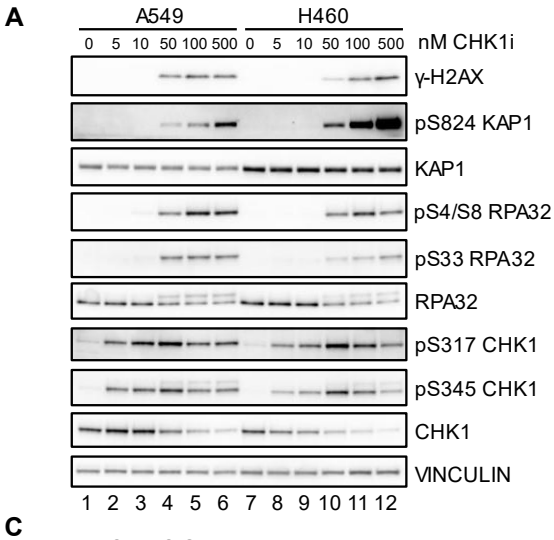

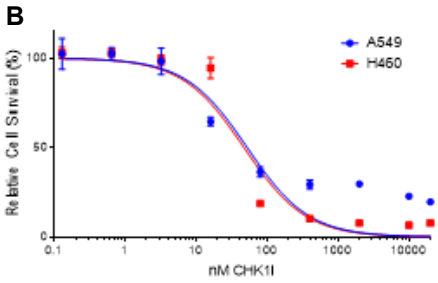

C

STARS Gene Ranking Algorithm

Gene	FDR A549	FDR H460
CCNA2	< 0.01%	1.33%
MYBL2 (B-MYB)	< 0.01%	< 0.01%
LIN54	< 0.01%	< 0.01%
CDC25B	< 0.01%	< 0.01%
FOXM1	5.34%	< 0.01%

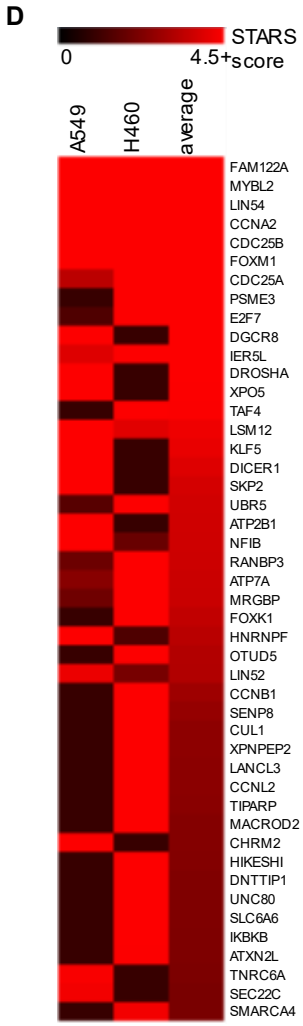

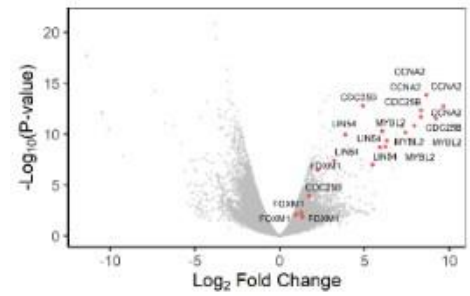

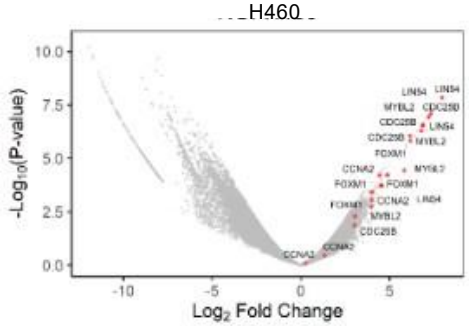

in both cell lines (**Fig. 3.1C and 3.1D**). All four of the individual sgRNAs targeting each of these genes showed substantial enrichment in both cell lines (**Fig. 3.1E and 3.1F**). The presence of a CDC25 family member and CCNA2 is consistent with previous studies (King et al., 2015; Ruiz et al., 2016; Wang et al., 2019) but having multiple MMB-FOXM1 complex components as hits, including LIN52 in A549 cells (**Fig. 3.1D**), stood out as this implicated mitotic gene expression in CHK1i sensitivity.

To determine how the loss of mitosis-promoting genes would confer CHK1i resistance, clonal A549 cell lines with two independent sgRNAs targeting FOXM1 and LIN54 were generated (**Fig. 3.2A**). There were no apparent differences in the growth rate of the LIN54 and FOXM1 KO vs. EV cells over 10 days (**Fig. 3.2B**). LIN54 and FOXM1 KO cells showed increased viability in the presence of CHK1i and two different ATR inhibitors (ATRi) (**Fig. 3.2C-E**).

Perturbation of LIN54 and FOXM1 reduces replication stress markers during Late S phase

To determine if LIN54 and FOXM1 were required for replication stress induced by CHK1i, LIN54 and FOXM1 KO cells were treated with CHK1i for up to 24 h (**Fig. 3.3**). Phosphorylated CHK1 (pS317 and pS345) appeared within 2 h of treatment in EV as well as in LIN54 and FOXM1 KO cells. In EV cells, phosphorylated RPA (pS4/S8) appeared within 2 h of treatment (**Fig. 3.3, Lanes 2 and 17**), followed by pKAP1 at 4 and 8 h (**Fig. 3.3, Lanes 3-4 and 18-19**). Eventually, γ-H2AX accumulated after 8 and 24 h of treatment (**Fig. 3.3, Lanes 4-5 and 19-20**). In contrast, LIN54 and FOXM1 KO cells showed greatly reduced levels and delayed appearance of the replication stress markers in response to CHK1i. Detectable levels of pS4/S8-RPA were delayed until 8 and 24 h after CHK1i and were diminished in both LIN54 and FOXM1 KO cells compared to EV (**Fig. 3.3, Lanes 9-10, 14-15, 24-25, and 29-30**). Levels of

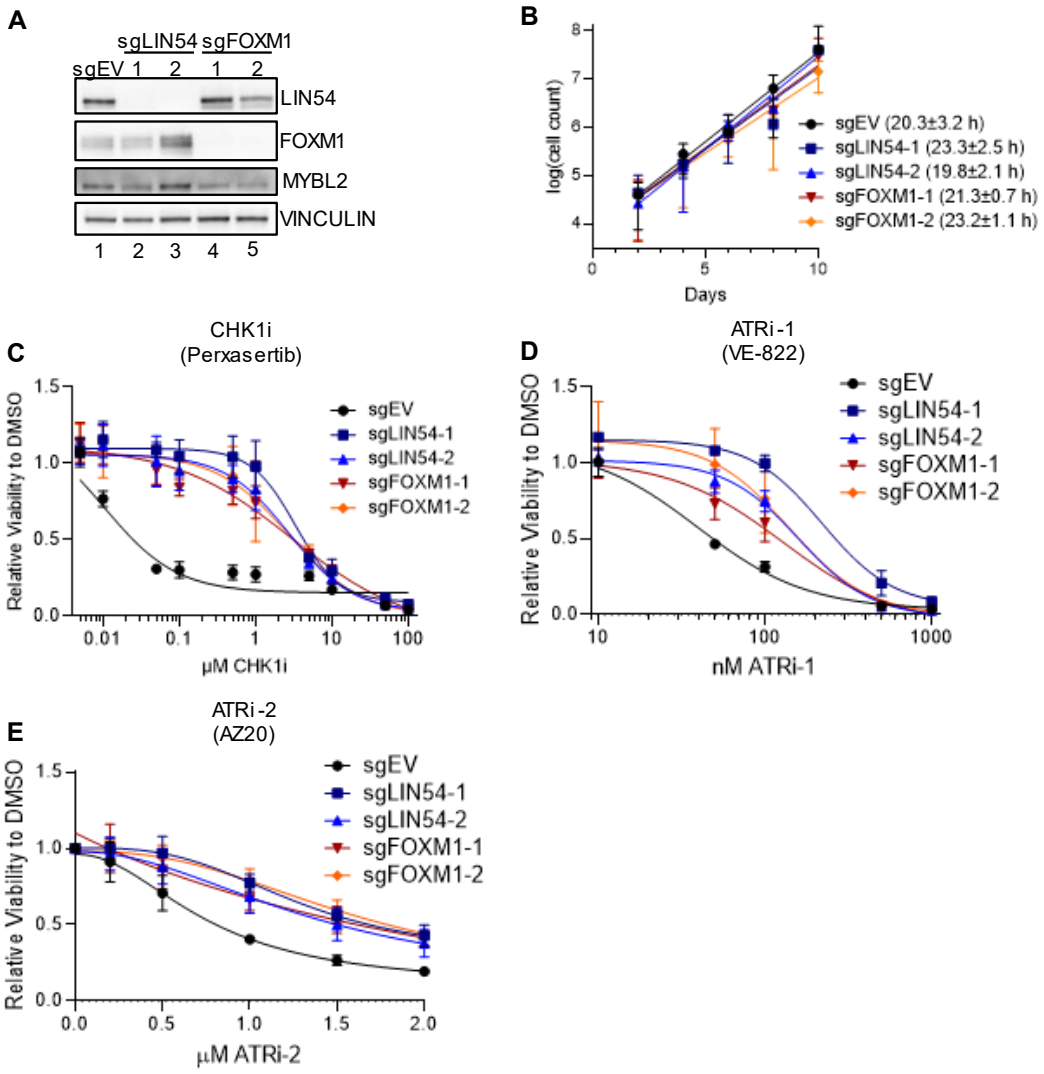

Figure 3.2. Perturbation of MMB-FOXM1 components confers resistance to CHK1 and ATR inhibitors

A) Immunoblot of MMB-FOXM1 components in A549 LIN54 KO, and FOXM1 KO cells lines.

B) 10-day growth curve and doubling time of A549 EV, LIN54 KO, and FOXM1 KO cells. N=3.

C-E) Viability curves of A549 EV, LIN54 KO, and FOXM1 KO cells in the presence of increasing concentrations of CHK1i or ATR inhibitors (ATRi) for 72 h. CHK1i (C), ATRi-1 (VE-822) (D), and ATR-2 (AZ20) (E). Viability was assessed using Cell-Titer Glo and normalized to 0 μM/nM concentration of drug for each cell line. N=3.

Mean ± SD.

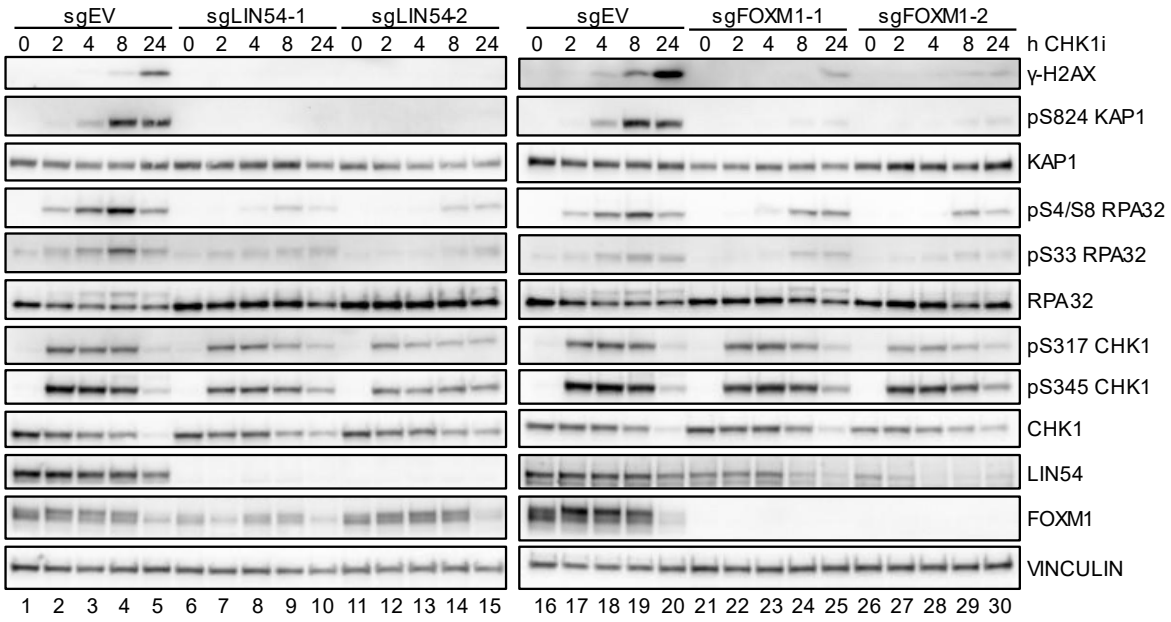

Figure 3.3. Loss of LIN54 or FOXM1 reduces induction of replication stress markers

Immunoblot of replication stress markers in EV, LIN54 KO and FOXM1 KO A549 cells treated with 100 nM CHK1i over a 24 h time course.

pKAP1 and γ-H2AX were also decreased in LIN54 and FOXM1 KO cells (**Fig. 3.3, Lanes 10, 15, 25, and 30**). These results indicate that, while the LIN54 and FOXM1 KO cells respond in a similar manner as EV cells to CHK1i as indicated by phosphorylation of CHK1 at ATR target sites, they showed greatly reduced DNA replication stress and DNA damage responses.

To determine if CHK1i-induced replication stress was induced in a specific phase of the cell cycle, pKAP1 levels during the cell cycle were assessed in four NSCLC cell lines by flow cytometry. Of note, both A549 and NCI-H460 harbor KRAS mutations and are p53 wild-type, while NCI-H23 has both KRAS and p53 mutations, and NCI-H1299 contains wild-type KRAS and is p53 null. CHK1i treatment of the NSCLC cell lines did not lead to substantial changes in cell cycle distribution regardless of KRAS or p53 status except for a slight but significant decrease in the G2/M phase of H460 cells (**Fig. 3.4A and 3.4B**). pKAP1 was induced by CHK1i during Late S phase and, to a lesser extent, Early S phase but not during G1 or G2/M in NSCLC cells regardless of their KRAS or p53 status (**Fig. 3.4C and 3.4D**) indicating that CHK1i-induced replication stress mostly occurs during late DNA synthesis.

Next, pKAP1 levels and cell cycle distribution were interrogated in LIN54 and FOXM1 KO cells or cells depleted for CCNA2, MYBL2, or LIN54 to determine if perturbation of these genes prevented the induction of pKAP1 in Late S phase. MYBL2 and cyclin A have been previously implicated in DNA synthesis (García and Frampton, 2006; Katsuno et al., 2009) raising the possibility that altered S phase progression could explain why perturbation of these loci conferred CHK1i resistance. CHK1 inhibition did not alter the cell cycle distribution of the LIN54 or FOXM1 KO cells, although both showed increased G2/M populations consistent with impaired G2/M progression (**Fig. 3.5A**). Similar to the LIN54 and FOXM1 KO cells, depletion of LIN54, CCNA2, or MYBL2 led to diverging changes in S phase populations and increased G2/M populations consistent with impaired G2/M progression (**Fig. 3.5B and 3.5C**).

Figure 3.4. CHK1 inhibition induces pKAP1 in late S phase in NSCLC cell lines

Assessing pKAP1 staining during the cell cycle by flow cytometry. Asynchronous cells were treated with 100 nM CHK1i for 2 h and pulsed with 10 μM EdU for the last hour. Samples were stained for pKAP1, EdU incorporation and with DAPI and analyzed by flow cytometry.

A and B) Analysis of cell cycle populations. A) Representative EdU vs DAPI and pKAP1 vs DAPI plots denoting the cell cycle gates used in the study described in Fig. 2B. Gates were based on no staining negative controls shown. B) Cell cycle populations in A549, H460, H23, H1299 NSCLC cells , including breakdown of Early and Late S phase populations. N=4.

C and D) Flow cytometry to assess pKAP1 levels in different cell cycle phases. C) NSCLC cells were treated with DMSO or 100 nM CHK1i for 2 h and pulsed with 10 μM EdU for the last hour. Samples were then stained for pKAP1 while DAPI staining and EdU labeling were used to determine the cell cycle phase. pKAP1 vs DNA content with cell cycle populations denoted by the colors in the legend. Box denotes the gate for pKAP1-positive cells. D) Quantification of (B), with replicates. N=3.

Mean ± SEM. ANOVA with Tukey correction; *, $p<0.05$; **, $p<0.01$; ***, $p<0.001$; ****, $p<0.0001$.

Figure 3.4. (cont.)

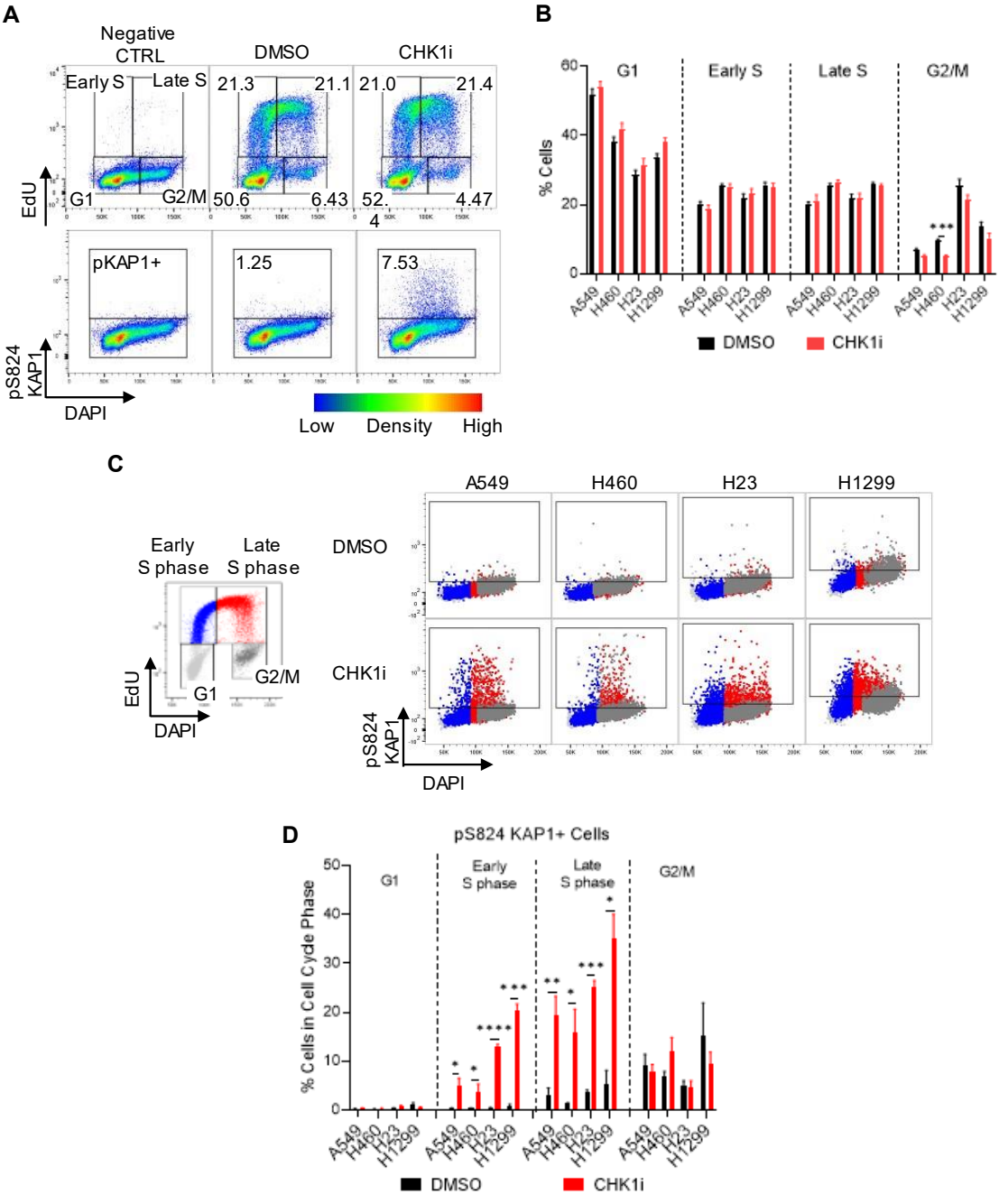

Figure 3.5. Perturbation of LIN54 or FOXM1 prevents induction of pKAP1 in late S phase

Asynchronous EV, sgLIN54-2, sgFOXM1 or A549 cells transfected with denoted siRNA cells were treated with 100 nM CHK1i for 2 h and pulsed with 10 μM EdU for the last hour. Samples were stained for pKAP1, EdU incorporation and with DAPI and analyzed by flow cytometry.

A) Cell cycle populations in EV, LIN54 KO, and FOXM1 KO cells , including breakdown of Early and Late S phase populations. N=4.

B) Immunoblot showing siRNA knockdown of LIN54, CCNA2, and MYBL2 in A549 cells.

C) Cell cycle distribution of A549 cells following LIN54, CCNA2, or MYBL2 siRNA knockdown and treated as in **Fig. 4**. N=3.

D) EV, LIN54 KO, and FOXM1 KO cells were treated and labeled as in B. pKAP1-positive cells in each cell cycle phase. N=3.

E) pKAP1 staining of A549 cells following LIN54, CCNA2, or MYBL2 siRNA knockdown and treated as above. N=3.

Mean ± SEM. ANOVA with Tukey correction; *, $p<0.05$; **, $p<0.01$; ***, $p<0.001$; ****, $p<0.0001$.

Figure 3.5. (cont.)

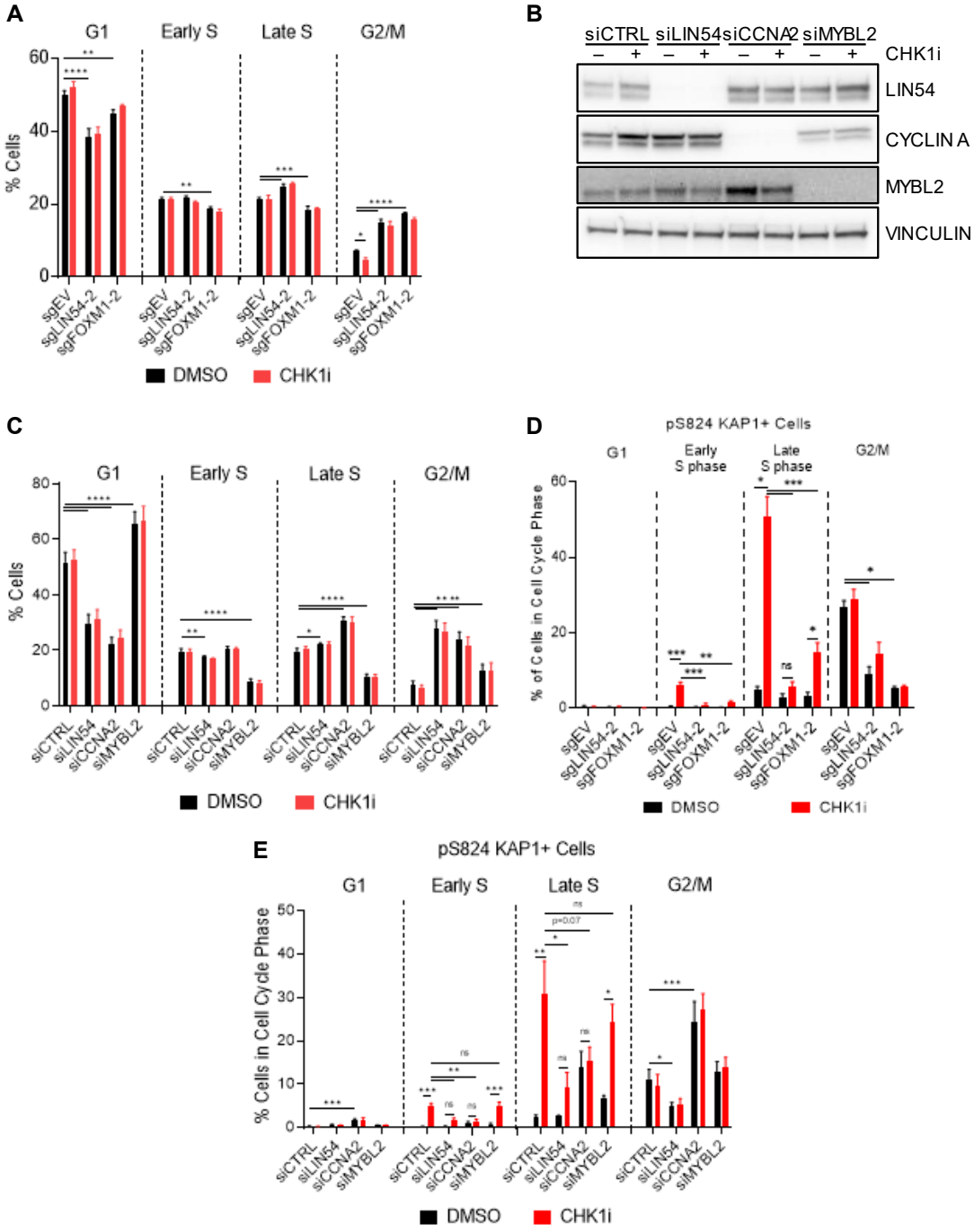

Loss of either LIN54 or FOXM1 significantly reduced the induction of pKAP1 in Late S phase cells as well as a small but significant population in Early S phase (**Fig. 3.5D**). pKAP1 levels in G2/M were similar in CHK1i compared to vehicle-treated cells but the overall levels of pKAP1 in G2/M were lower in the LIN54 and FOXM1 KO cells compared to EV cells. Depletion of LIN54 reduced the appearance of pKAP1 in Late S phase similar to the LIN54 KO cells while perturbation of CCNA2 resulted in increased pKAP1 levels that were insensitive to CHK1i (**Fig. 3.5E**). In contrast, pKAP1 was significantly induced by CHK1i in siMYBL2 samples in both Early and Late S phase. These results suggest that induction of replication stress may not be sufficient for CHK1i sensitivity.

Induction of pKAP1 by CHK1i during Late S phase is ATR-dependent

To understand the role of replication stress in CHK1i sensitivity, the requirements for the induction of phosphorylated KAP1 were assessed. ATM, ATR, and DNA-PK activities have been linked to KAP1 phosphorylation at S824 (White et al., 2006). Subsequent studies predominantly focused on ATM-dependent KAP1 phosphorylation in response to DNA DSBs (White et al., 2012; Ziv et al., 2006) or, more recently, DNA-PK-dependent KAP1 phosphorylation in response to ATR inhibition (Buisson et al., 2015; Dunlop et al., 2020). To assess the contribution of ATM and DNA-PK activity to KAP1 phosphorylation after treatment with CHK1i or agents that induce DNA damage, i.e., hydroxyurea (HU) or doxorubicin (DOXO), ATM and DNA-PK autophosphorylation was assessed in relation to pKAP1 levels by immunoblot and by flow cytometry in the case of ATM. Auto-phosphorylation of pDNA-PK was induced to a similar extent by all three treatments while pATM was preferentially induced by DOXO (**Fig. 3.6A and 3.6B**). HU led to reduced DNA synthesis, while CHK1i or DOXO did not alter DNA synthesis appreciably (**Fig. 3.6C**). pKAP1-positive cells were induced modestly after CHK1i or HU and to a greater extent after DOXO treatment (**Fig. 3.6A and 3.6D**). Similarly,

pATM levels in pKAP1-positive cells were elevated to a lesser extent in CHK1i or HU treated cells than DOXO treated cells (**Fig. 3.6E, and 3.7F**), raising the possibility that another kinase led to CHK1i-induced activation of pKAP1 during Late S phase.

Given that increased pCHK1 after CHK1i treatment is a marker of ATR activity, it was possible that ATR could phosphorylate KAP1 instead of ATM. To determine the relative contribution of ATM, ATR, and DNA-PK to KAP1 phosphorylation, cells were treated with specific ATR, ATM, or DNA-PK inhibitors alone or in combination with CHK1i. Similar to CHK1i, ATRi treatment led to a modest decrease in the G2/M population, while ATMi or DNA-PKi treatment did not perturb the relative cell cycle distribution (**Fig. 3.7A**). In contrast to CHK1i, ATRi alone did not increase levels of pKAP1 during S phase, indicating that the induction pKAP1 at early time points was specific to CHK1i (**Fig. 3.7B and 3.7C**). ATRi, but not ATMi or DNA-PKi, when combined with CHK1i, led to a significant reduction in pKAP1-positive cells during Late S phase. The requirement of ATR activity for CHK1i-induced pKAP1 suggested that DNA replication was deregulated.

CHK1i increases DNA replication regardless of loss of LIN54 or FOXM1

CHK1 inhibition can lead to increased origin firing in a CDK-dependent manner (Petermann et al., 2010). To assess the levels of DNA synthesis after CHK1 inhibition, EdU incorporation was quantified in EV, LIN54 KO, and FOXM1 KO cells (**Fig. 3.8A**). The levels of DNA synthesis in both Early and Late S phase increased significantly in response to CHK1i compared to DMSO in EV, LIN54 KO, and FOXM1 KO cells. Although the increased levels of DNA synthesis after CHK1i treatment were similar in EV, LIN54 KO, and FOXM1 KO cells during Early S phase, DNA synthesis during Late S phase was significantly reduced in the CHK1i-treated LIN54 KO and FOXM1 KO cells compared to EV cells.

Figure 3.6. A pATM low pKAP1 positive cell population is induced by CHK1 inhibition

A) Immunoblot of replication stress markers in A549 cells treated with 100 nM CHK1i, 2 mM HU, or 500 nM DOXO for 2 h.

B-F) Flow cytometry to assess ATM activity and pKAP1 levels after replication stress or DNA damage as in (A) and pulsed with 10 μM EdU for the last hour. B) Density dot plot of EdU vs DAPI with cell cycle populations gated C) pKAP1 vs DAPI levels. Box denotes the pKAP1+ positive population drawn using negative control, with the % of single cells in the box shown. D) Density dot plot of pS1981 ATM levels vs DAPI stain with the gate denoting pS1981 ATM high cells, based on the 98th percentile of the DMSO sample, and the % of single cells in the gate shown. E) Density dot plot of pS1981 ATM levels vs DAPI stain of pKAP1-positive cells. The gate denotes pS1981 ATM high based on the 98th percentile of the DMSO sample. F) pS1981 ATM mean fluorescence intensity (MFI) in pKAP1-positive cells identified in Fig. S3B. N=4.

Figure 3.6. (cont.)

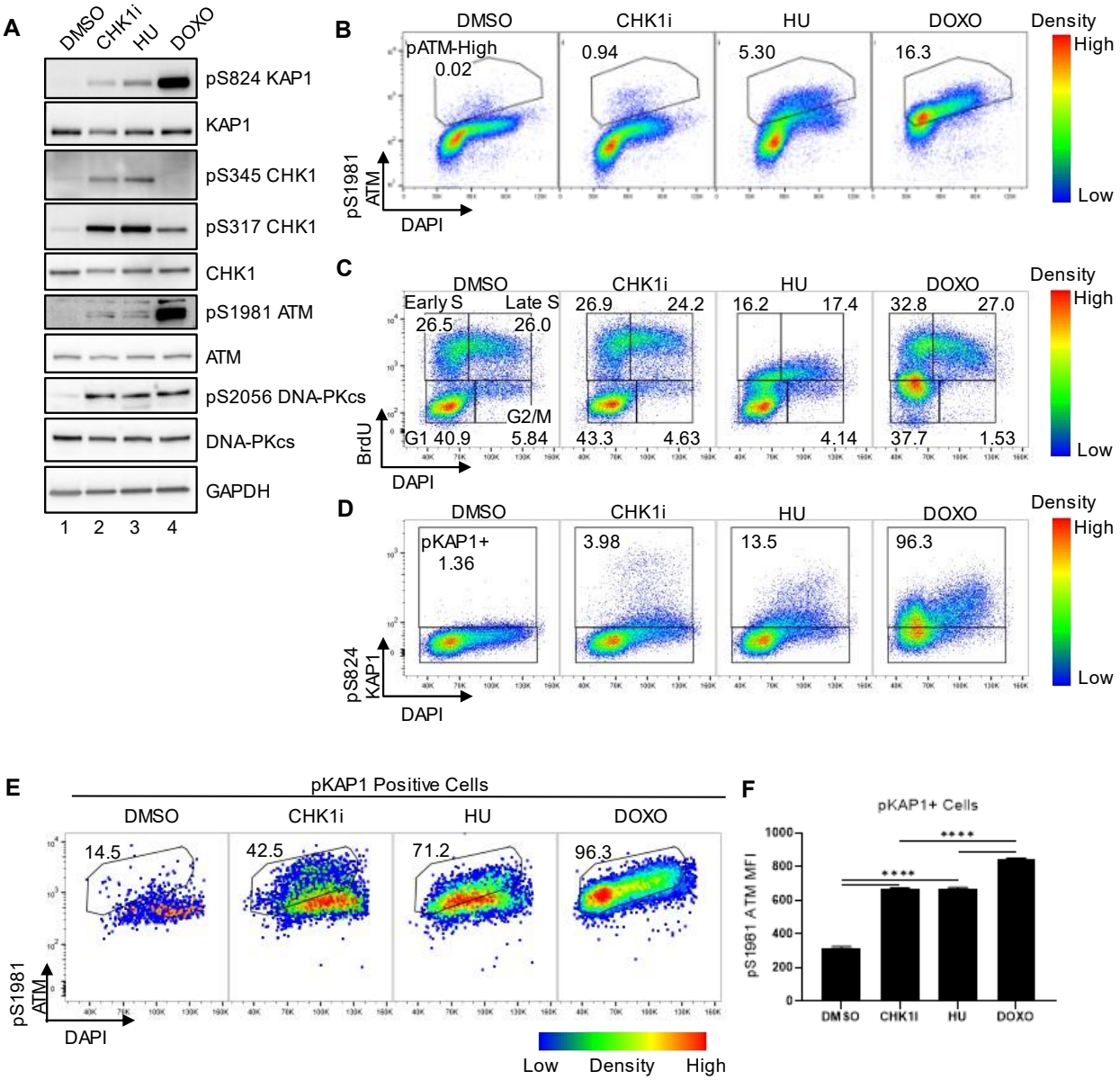

Figure 3.7. Induction of pKAP1 by CHK1i during Late S phase is ATR-dependent

Flow cytometry to determine if KAP1 T824 phosphorylation after CHK1i is ATR, ATM or DNA-PK-dependent after 2 hour co-treatment in A549 cells.

A) Flow cytometry of cell cycle states for cells treated with CHK1i, ATRi, ATMi, or DNA-PKi. Density dot plot for EdU vs DAPI with cell cycle populations gated.

B) pKAP1 vs DAPI levels with cell cycle phases overlaid in the colors denoted in the legend. Box denotes the pKAP1-positive population. C) pKAP1-positive cells in each cell cycle phase shown in (B). N=5. ANOVA-mixed effects analysis with Tukey correction

Mean ± SEM; ANOVA with Tukey correction; *, $p<0.05$; **, $p<0.01$; ***, $p<0.001$.

Figure 3.7. (cont.)

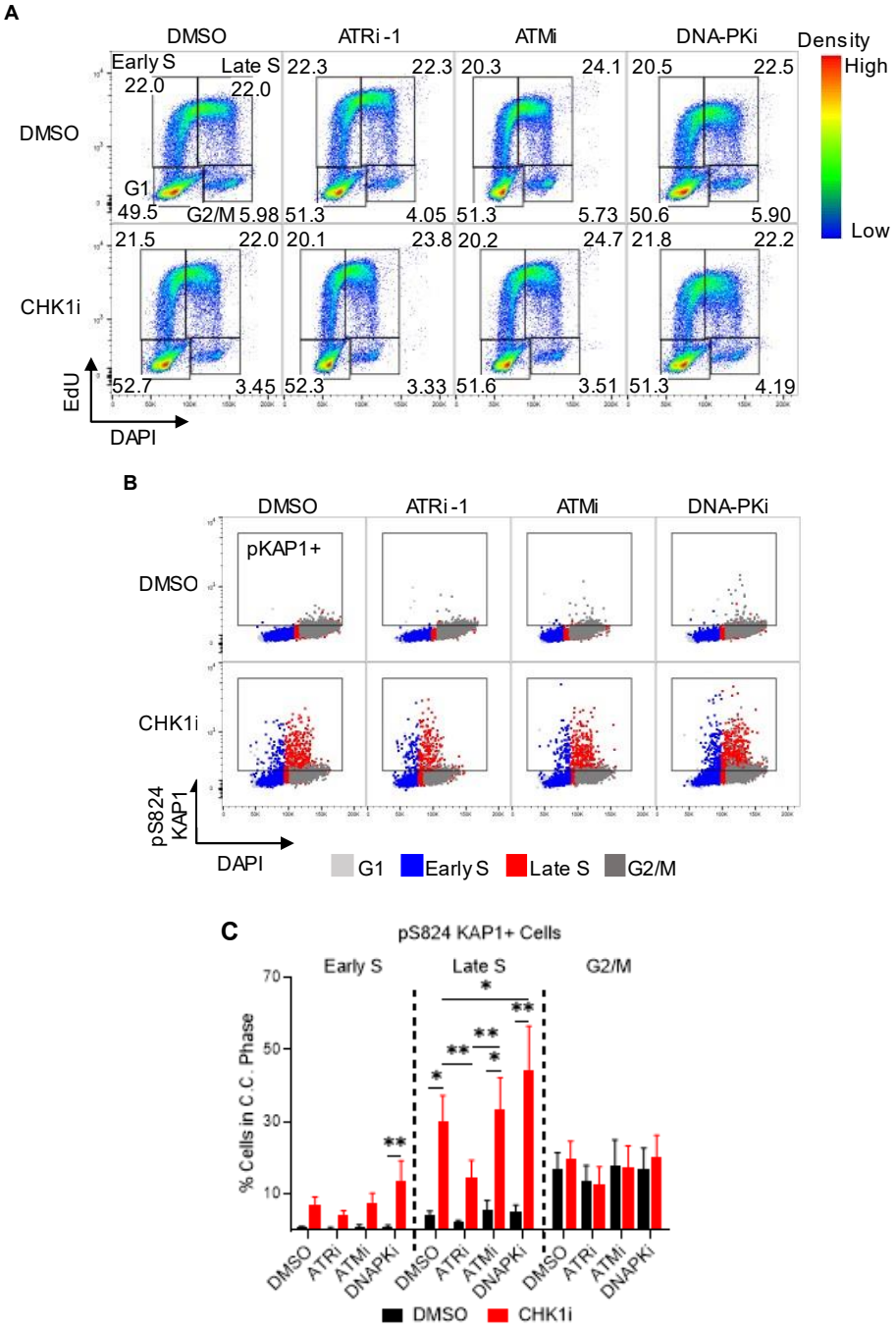

Figure 3.8. CHK1i increases DNA replication regardless of loss of LIN54 or FOXM1

A) Relative EdU incorporation in Early S and Late S phase in LIN54 or FOXM1 KO cells after CHK1 inhibition. MFI of S phase populations per gates in Fig. S2A were normalized to EV DMSO Early S populations for each replicate. N=3.

B and C) Chromatin flow cytometry for chromatin-bound CDC45. B) Chromatin bound CDC45 vs DAPI levels with cell cycle phases overlaid in the colors denoted. Box denotes the CDC45 High gate drawn at the 98th percentile of the sgEV-DMSO sample. C) MFI of chromatin-bound CDC45 in Early and Late S phase. N=3.

D and E) Chromatin flow cytometry for chromatin-bound PCNA. D) Chromatin bound PCNA vs DAPI levels with cell cycle phases overlaid in the colors denoted. Box denotes the PCNA High gate drawn at the 98th percentile of the sgEV-DMSO sample. E) MFI of chromatin-bound PCNA in Early and Late S phase. N=3.

Mean ± SEM; ANOVA with Tukey correction; *, $p<0.05$; **, $p<0.01$; ***, $p<0.001$.

Figure 3.8. (cont.)

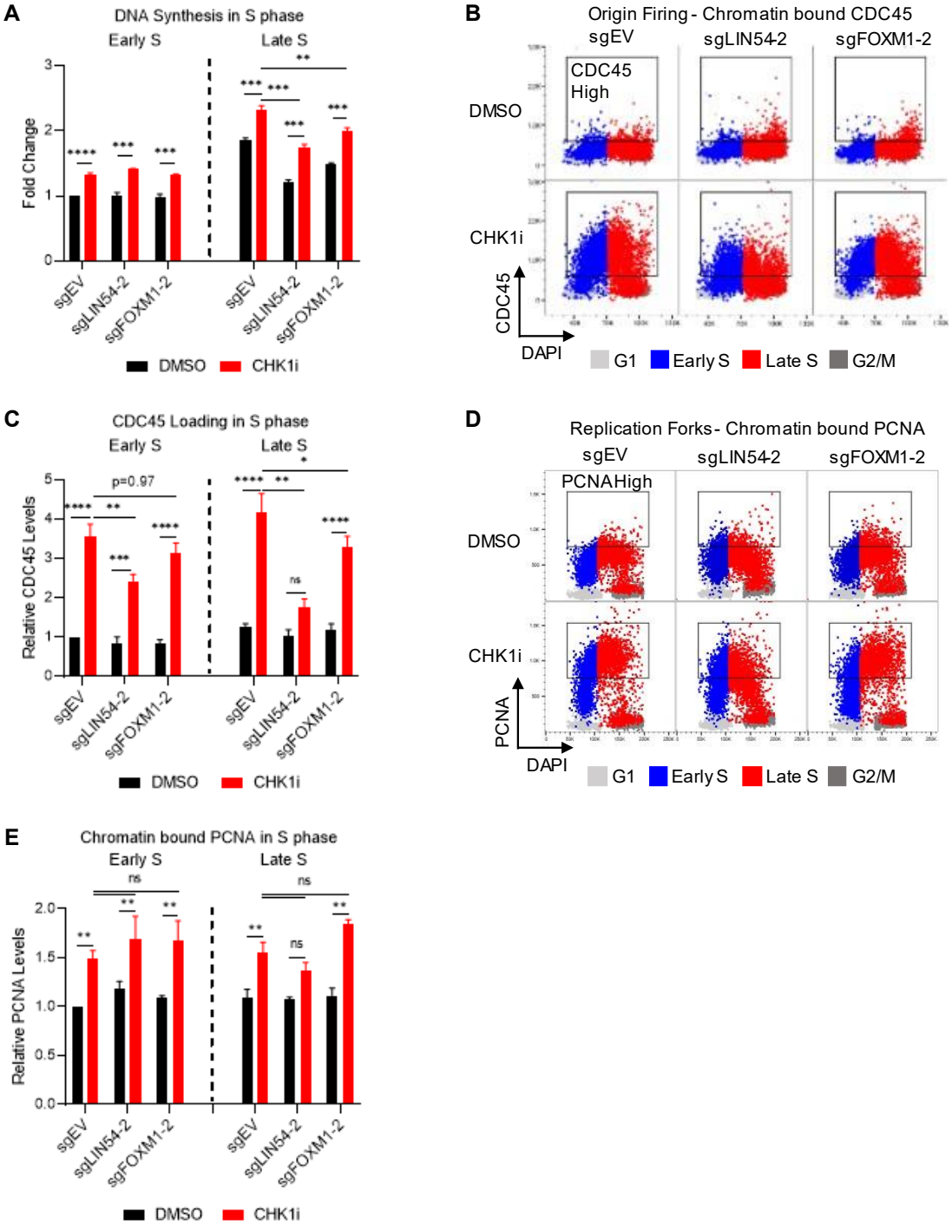

To understand the impact of CHK1 inhibition on DNA replication, levels of chromatin-bound CDC45 and PCNA were assessed by chromatin flow cytometry. CDC45 loading on DNA can provide a measure of origin firing (Kohler et al., 2016), while chromain-bound PCNA can be used to assess active DNA replication (Janke et al., 2018; Sirbu et al., 2013). Chromatin-bound CDC45 and PCNA increased significantly in response to CHK1i in EV cells as well as LIN54 and FOXM1 KO cells during Early S phase, and in EV and FOXM1 KO cells during Late S phase (**Fig. 3.8B-E**) consistent with increased origin firing throughout S phase. Chromatin-bound CDC45 and PCNA increased less in LIN54 KO cells compared to EV cells while the increase in FOXM1 KO cells was not significantly different than in EV cells except for reduced chromatin-bound CDC45 in Late S phase. Given that CHK1i-induced increases in DNA replication and origin-firing were not blunted by loss of LIN54 or FOXM1, particularly in Early S phase, suggested that another function of the MMB-FOXM1 complex was required for CHK1i sensitivity.

Activation of G2/M genes after CHK1i is MMB-FOXM1 dependent

Phosphorylation of the MMB-FOXM1 components MYBL2 and FOXM1 by cyclin-CDK complexes promotes their transcriptional activity in an ATR-CHK1-dependent manner (Laoukili et al., 2008b; Saldivar et al., 2018; Ziebold et al., 1997). The induction of phosphorylation on T600 of FOXM1 (pFOXM1) was assessed in synchronized A549 cells and asynchronous A549 by flow cytometry. pFOXM1 appeared within 2 h post-release from a thymidine block after 1 h of CHK1i treatment compared to 9 h after release in untreated cells (**Fig. 3.9A**). Similarly, the restriction of high levels of pFOXM1, as denoted by the pFOXM1-High gate, to the G2/M population was abrogated by CHK1i in asynchronous A549 cells (**Fig. 3.9B**). pFOXM1 was induced by CHK1i in Late S phase in four NSCLC cell lines regardless of their KRAS or p53

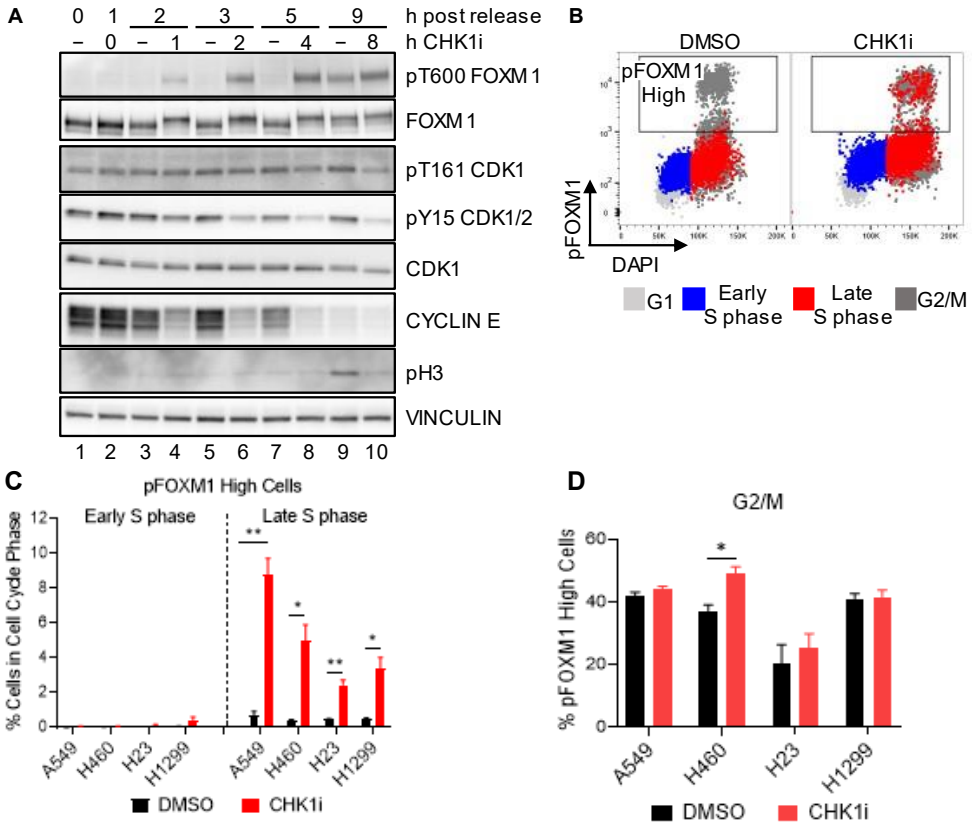

Figure 3.9. MMB-FOXM1 activity is induced in Late S phase after CHK1 inhibition in NSCLC cell lines

A) Immunoblot of FOXM1 phosphorylation in A549 cells synchronized by a single thymidine block to S phase. Cells were released for 1 h and then treated with DMSO or 100 nM CHK1i for the indicated times.

B-D) pFOXM1 levels in NSCLC cell lines after CHK1i. Cells were treated with 100 nM CHK1i for 2 h with an EdU pulse for the last hour. Samples were stained for pFOXM1, EdU, and DAPI. B) pFOXM1 vs DAPI levels with cell cycle phase overlaid in the colors denoted. The gate drawn is for high pT600 FOXM1 levels found in G2/M cells of the DMSO sample. Percent of pFOXM1-high cells in C) Early and Late S phase and D) G2/M. N=4.

Mean ± SEM; ANOVA with Tukey correction; *, p<0.05; **, p<0.01; ***, p<0.001; ****, p<0.0001.

status (**Fig. 3.9C and 3.9D**) indicating premature activation of the MMB-FOXM1 complex in the absence of CHK1 activity.

To determine if disruption of the MMB-FOXM1 complex alters gene expression in response to CHK1 inhibition, RNA-seq profiling was performed in EV, LIN54 KO, and FOXM1 KO cells synchronized in S phase and treated with CHK1i for 2 h. GSEA analysis revealed that DNA repair genes were not significantly perturbed by CHK1 inhibition (**Fig. 3.10A**). In contrast, G1/S genes, comprised of genes involved in DNA replication, were significantly decreased (**Fig. 3.10B**) while G2/M genes, many of which encode mitotic regulators, were significantly increased following CHK1 inhibition (**Fig. 3.10C**). G1/S and G2/M genes were well represented in the top 350 most differentially expressed genes in the EV cells after CHK1 inhibition (**Fig. 3.10D**). G1/S genes comprised the downregulated genes (**Fig. 3.10E**), while G2/M genes were among the upregulated genes (**Fig. 3.10F**), consistent with the GSEA analysis. Compared to EV cells, loss of LIN54 restored expression of downregulated genes to a greater extent than the loss of FOXM1 (**Fig. 3.10G**). The induction of upregulated genes, however, was impaired to a similar extent in both LIN54 and FOXM1 KO cells (**Fig. 3.10H**).The induction of MMB-FOXM1 target genes by CHK1i was significantly reduced in both the LIN54 and FOXM1 KO cells (**Fig. 3.10I-K**). Of note, CCNA2, a top screen hit, and CCNB1, a significant hit in H460 cells (**Fig. 3.1D**), were both present in group of highly expressed MMB-FOXM1 target genes not induced by CHK1i in either LIN54 or FOXM1 KO cells. Levels of these genes, as well as top hit CDC25B, were significantly increased in S phase by CHK1 inhibition in EV but not LIN54 and FOXM1 KO cells (**Fig. 3.10L-P**). Cyclin B1 protein levels were reduced and not induced by CHK1i in S-phase LIN54 KO cells (**Fig. 3.11A**). Thus, perturbing the MMB-FOXM1 complex impairs the induction of CDK1 activators during S phase after CHK1 inhibition.

The decrease in CDK1 activators with MMB-FOXM1 complex perturbation suggested a positive feedback between the MMB-FOXM1 complex and cyclin/CDK1 complexes. Consistent

Figure 3.10. CHK1i induces the G2/M transcriptional program in a MMB-FOXM1 dependent manner

Changes in gene expression after CHKi in S phase. EV, LIN54 KO, and FOXM1 KO cells were synchronized by a single thymidine block. Samples were treated with DMSO or 100 nM at 1 h post-release and samples were collected at 3 h post-release. Total RNA was extracted and sequenced.

A-C) Gene set enrichment was performed on the EV samples for B) DNA repair genes, C) G1/S genes and D) G2/M genes.

D-H) Analysis of changes in cell cycle gene expression in EV cells. D) Heat map showing the 350 most differentially expressed genes in EV cells between the DMSO and CHK1 treated samples. Gene annotations for G1/S and G2/M are from Schade et al. (Schade et al., 2019a). Percentage of annotated gene categories in genes E) down- and F) upregulated by CHK1 inhibition. Fold change in G) down- and H) upregulated genes between DMSO and CHK1i-treated samples in EV, LIN54 KO, and FOXM1 KO A549 cells.

I-J) Analysis of MMB-FOXM1 Target genes in LIN54 and FOXM1 KOs. I) Expression of MMB-FOXM1 target genes in relation to EV cells. Log_2 fold change calculated using DESeq2. J and K) Expression of MMB-FOXM1 target genes upregulated in EV cells after CHK1i by ≥ 1.5-fold change (51 genes), depicted as J) log_2 fold change determined in relation to EV DMSO treated cells, with % of genes upregulated above 1.5-fold change in each sample reported, and K) as a heat map.

L-N) Mean counts of MMB-FOXM1 target genes L) CDC25B, M) CCNA2, and N) CCNB1. N=2.

O and P) RT-qPCR of MMB-FOXM1 target genes O) CCNA2 and P) CCNB1 during S phase in EV, LIN54 KO, and FOXM1 KO cells after CHK1 inhibition as above. N=3.

Figure 3.10. (cont.)

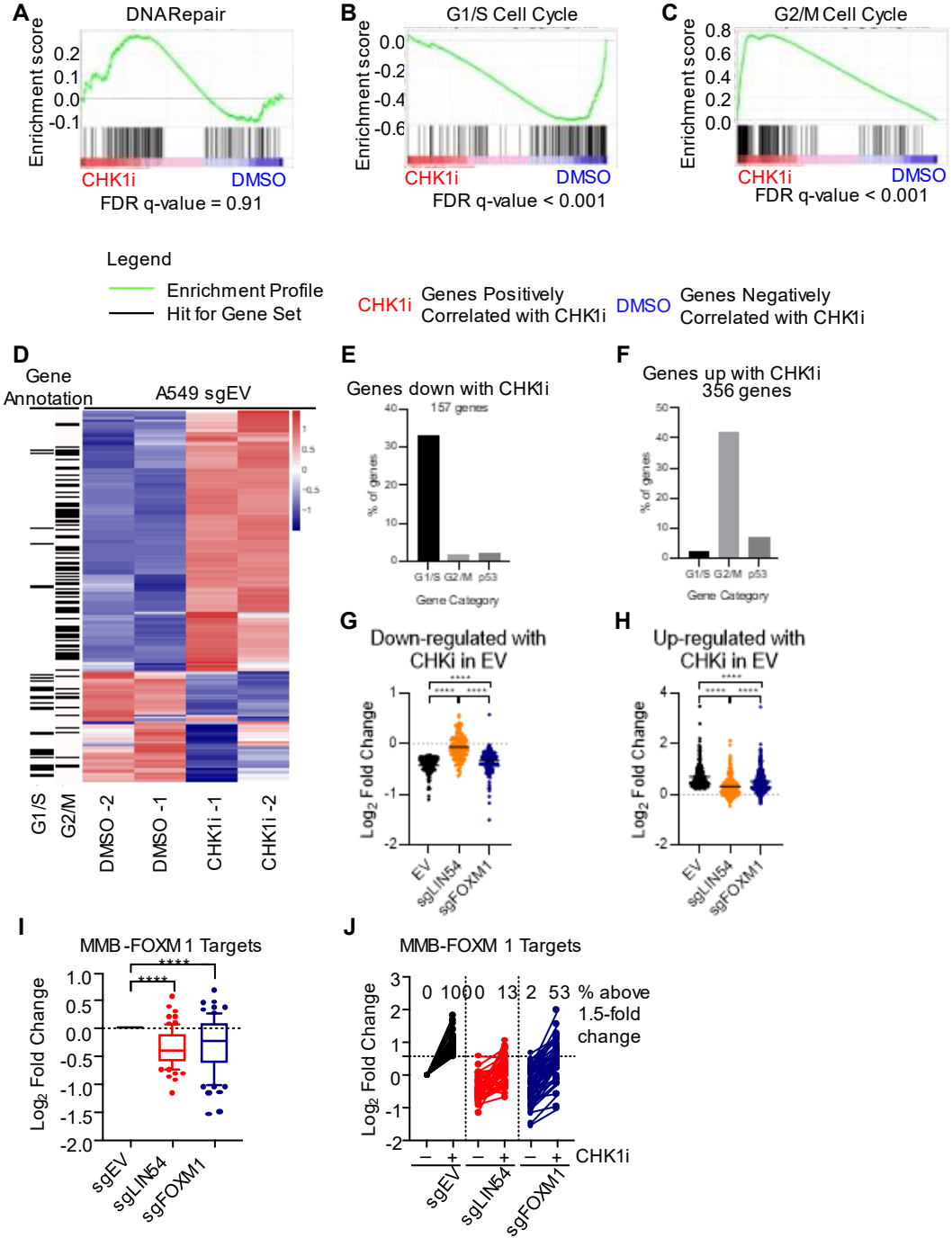

Figure 3.10. (cont.)

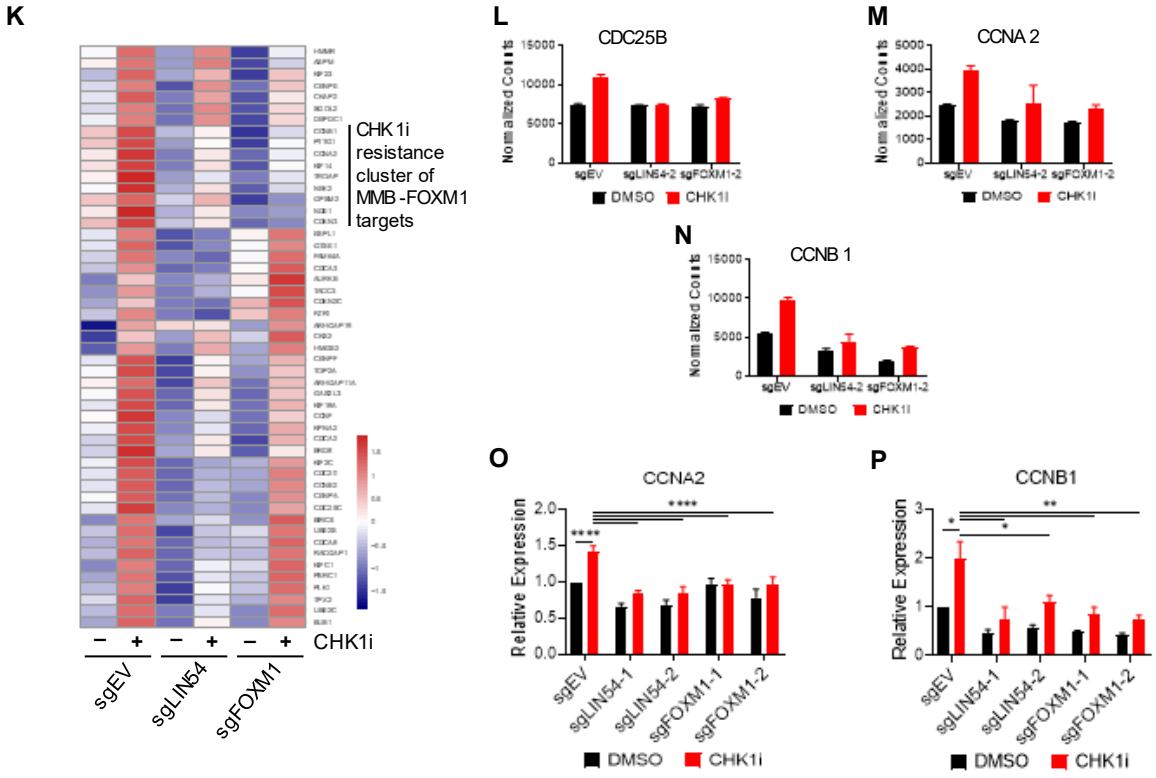

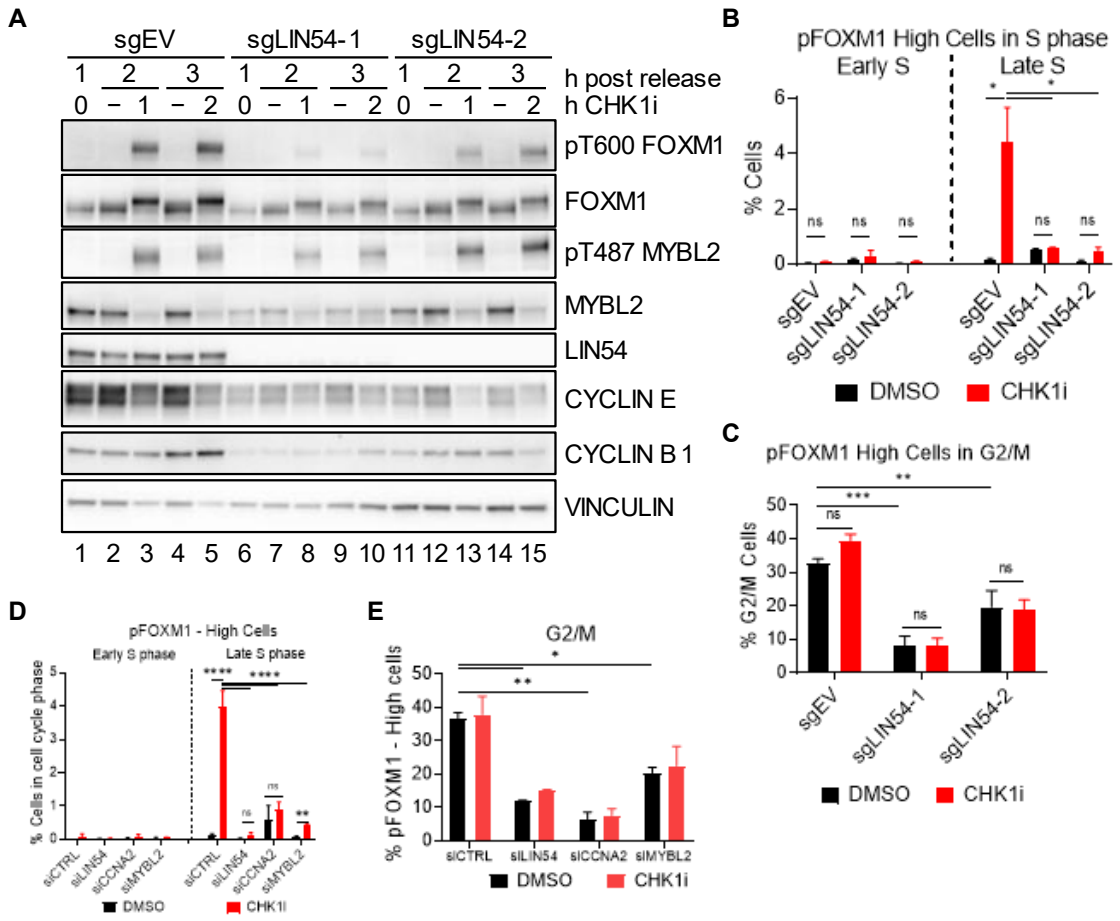

Figure 3.11. CHK1i induces the G2/M transcriptional program in an MMB-FOXM1 dependent manner

A) Immunoblot for MMB-FOXM1 complex phosphorylation. A549 sgEV, sgLIN54-1, and sgLIN54-2 cells were by a single thymidine block to S phase. Cells were released for 1 h and then treated with DMSO or 100 nM CHK1i for the indicated times.

B and C) pFOXM1 levels in LIN54 KO cells. EV or LIN54 KO cells were treated with 100 nM CHK1i for 2 h with an EdU pulse for the last hour. Samples were stained for pFOXM1, EdU and DAPI. Percent of pFOXM1-high cells in B) Early and Late S phase and C) G2/M. N=4.

D and E) Percentages of A549 cells with high levels of pFOXM1 after siRNA knockdown of LIN54, CCNA2, or MYBL2, and CHK1i treatment as in B) and C) during D) Early and Late S phase and E) G2/M. N=3.

Mean ± SEM; ANOVA with Tukey correction; *, p<0.05; **, p<0.01; ***, p<0.001; ****, p<0.0001.

with this, CCNA2 siRNA knockdown substantially decreased the percentages of high pFOXM1 cells in Late S and G2/M (**Fig. 3.11D and 3.11E**).The fraction of G2/M cells with high levels of pFOXM1 was not significantly affected by CHK1i but was significantly decreased in LIN54 KO and siMYBL2 cells (**Fig. 3.11C and 3.11E**). Perturbation of LIN54 or MYBL2 also prevented the induction of pFOXM1 in Late S phase by CHK1i (**Fig. 3.11A, 3.11B, and 3.11D**) indicating that full activation of MMB-FOXM1 complex requires an intact MMB complex. Taken together, these results indicate that an MMB-FOXM1-CDK1 feedback loop drives the CHK1i-dependent induction of the G2/M transcription program during S phase.

MMB-FOXM1 complex components are required for CHK1i-induced premature mitosis in Late S phase

The premature activation of the mitotic program in response to CHK1i raised the possibility that essential S-phase and mitotic processes were occurring simultaneously. Increased or premature histone H3 S10 phosphorylation (pH3), a mitotic marker, has been previously observed following perturbation of the ATR-CHK1 pathway (Ruiz et al., 2016; Zuazua-Villar et al., 2014). A limitation of these studies is that the cell cycle phase was assessed by DNA content leaving it unclear whether pH3 induced by these inhibitors coincided with active DNA synthesis. Simultaneous pH3 and BrdU staining, however, was observed in CHK1 haploinsufficient mice (Lam et al., 2004). If DNA synthesis and mitosis were occurring simultaneously, mitotic events could sufficiently disrupt DNA synthesis to trigger replication catastrophe.

To determine if ATR or CHK1 inhibition led to a breakdown in the separation of DNA synthesis from mitosis, levels of pH3 were assessed by flow cytometry during each cell cycle phase in four NSCLC cell lines representing various combinations of KRAS and p53 mutations (**Fig. 3.12A**). Levels of pH3 were increased particularly in Late S phase in all four lines (**Fig.**

3.12B and 3.12C). An increase in pH3 positive cells was observed during Late S phase following inhibition of ATR or CHK1 but not ATM (**Fig. 3.12D**). Similarly, inhibition of ATR or CHK1 but not ATM led to some increase in pH3 in G2/M cells (**Fig. 3.12E**). Dual inhibition of ATR and CHK1 led to a significant increase, relative to either alone, in pH3 positive cells during Late S phase but not G2/M (**Fig. 3.12D and 3.12E**). These results indicate that inhibition of the ATR-CHK1 pathway leads to DNA replication and mitotic events occurring simultaneously particularly during Late S phase.

Next, we assessed the role of the MMB-FOXM1 complex in regulating CHK1i-induced pH3 during S phase (**Fig. 3.12F**). While CHK1 inhibition led to increased levels of pH3 during Late S phase in EV cells, the loss of LIN54 or FOXM1 abolished this effect (**Fig. 3.12F and 3.12G**). LIN54 and FOXM1 KO cells also showed a significantly smaller fraction of G2/M cells positive for pH3 independent of CHK1i treatment (**Fig. 3.12H**). This was similarly observed following siRNA knockdown of LIN54, CCNA2, or MYBL2 compared to siCTRL (**Fig. 3.12I and 3.12 J**). This indicates that a functional MMB-FOXM1 complex is required for CHK1i-induced breakdown in the separation between DNA replication and mitosis.

Activation of an MMB-FOXM1 complex-CDK1 positive feedback loop is required for CHK1i-induced replication catastrophe

CDK1 activity may be necessary for sensitivity to ATR-CHK1 inhibition (Aarts et al., 2012; Ruiz et al., 2016). CDK1 activity was restricted in CHK1i-resistant FAM122A KO cells via WEE1 stabilization (Li et al., 2020), suggesting that CDK1 activities during the S/G2 transition influences CHK1i sensitivity. However, it remains unclear however what activities of CDK1 are required for replication catastrophe. To identify CDK1 activities that trigger replication catastrophe, the levels of CDK1 activity required for specific CHK1i-associated phenotypes was

Figure 3.12. MMB-FOXM1 complex components are required for CHK1i-induced premature mitosis in Late S phase

A-C) Flow cytometry analysis of pH3 levels by cell cycle phase in NSCLC cells. Cells were stained for pH3 and cell cycle populations were identified by EdU incorporation and DAPI stain. A) Dot plot of pH3 levels vs DAPI levels with cell cycle phases overlaid in the colors denoted. Box denotes the pH3+ gate drawn from negative controls. Percent pH3 positive cells in B) Early and Late S phase and C) G2/M. N=3.

D-E) Flow cytometry analysis of pH3 levels by cell cycle phase in A549 cells after treatment with 100 nM CHK1i, 100 nM ATRi, or 1 μM ATMi. Samples were treated with inhibitors for 2 h and pulsed with EdU for the last hour.

F-H) Flow cytometry analysis of pH3 levels by phase of the cell cycle in LIN54 KO or FOXM1 KO A549 cells after CHK1i. Sample treatment regimen is the same as Fig. 6D-E. F) pH3 levels vs DAPI levels with cell cycle phases overlaid in the colors denoted. Box denotes the pH3+ gate drawn from negative controls. Percent pH3 positive cells in G) Early and Late S phase and H) G2/M. N=3.

I-J) Flow cytometry analysis of pH3 levels by phase of the cell cycle in A549 cells following LIN54, CCNA2, or MYBL2 siRNA knockdown. Percent pH3 positive cells in I) Early and Late S phase and J) G2/M. N=4.

Mean ± SEM; ANOVA with Tukey correction; *, $p<0.05$; **, $p<0.01$; ***, $p<0.001$.

Figure 3.12. (cont.)

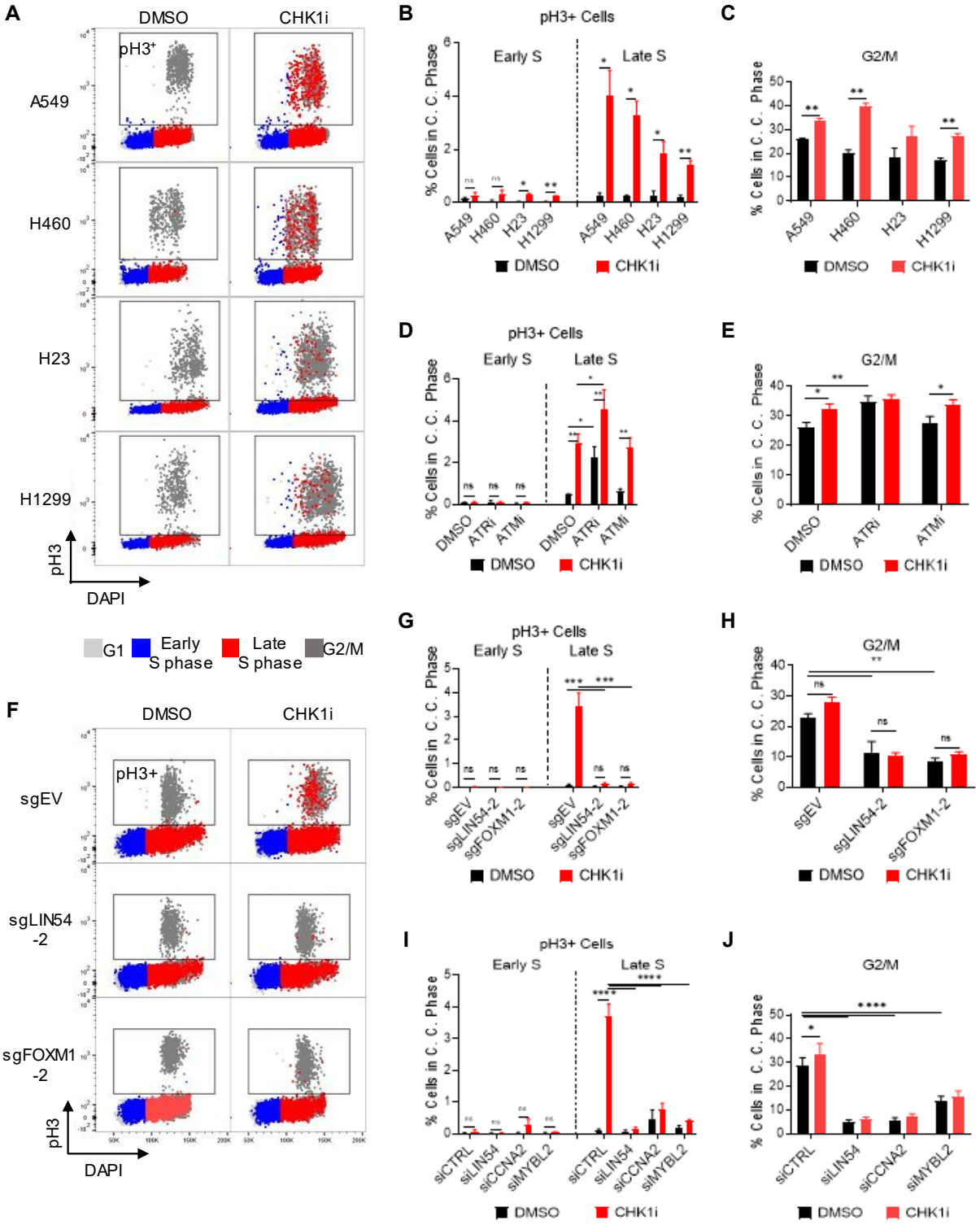

determined by treating A549 cells with CHK1i and increasing concentrations of the CDK1 inhibitor RO3306 (CDK1i). Levels of EdU incorporation, pFOXM1, pH3, and pKAP1 were assessed by flow cytometry after CHK1 inhibition to determine how inhibition of CDK1 activity impacted DNA replication, MMB-FOXM1 activity, mitosis, and DNA replication stress respectively. As levels of CDK1i increased, the fraction of G2/M cells increased independently of CHK1 inhibition (**Fig. 3.13D**) and the fraction of G1 and Early S phase cells decreased correspondingly (**Fig. 3.13A and 3.13B**). In contrast, the fraction cells in Late S phase cells did not change (**Fig. 3.135C**). Increased DNA synthesis in response to CHK1i was not diminished by less than 5 μM CDK1i (**Fig. 3.13E and 3.13F**).

In contrast to DNA replication, significant induction of pFOXM1-High cells by CHK1i in Late S phase was prevented by 2.5 μM CDK1i (**Fig. 3.13G**). While 1 μM CDK1i also significantly reduced the fraction of pFOXM1-High cells in Late S phase after CHK1i, pFOXM1-High cells were still significantly induced by CHK1i compared to the DMSO control for 1 μM CDK1i. A small but significant increase in pFOXM1 after CHK1i treatment was observed at 2.5 μM CDK1i **(Fig. 3.13H)** suggesting that, while FOXM1 can still be phosphorylated, the level of CDK1 activity blocked by 2.5 μM CDK1i was necessary for significant accumulation of pFOXM1. Increasing doses of CDK1i did not affect the fraction of pFOXM1-High cells in G2/M but led to a decrease in pT600 FOXM1 levels in a dose-dependent manner with a significant drop as the concentration of CDK1i increased from 1 μM to 2.5 μM (**Fig. 3.13I and 3.13J**). 2.5 μM CDK1i reduced the accumulation of pFOXM1 in S-phase synchronized A549 and H460 cells (**Fig. 3.14A**). CDK1 inhibition did not alter pT487-MYBL2 levels but caused a shift in the gel migration of the pMYBL2 band suggesting that other MYBL2 phosphorylation sites may be CDK1 dependent. The degradation of cyclin E in S phase is dependent on CDK2 activity (Clurman et al., 1996). Doses up to 10 μM of RO-3306 did not affect cyclin E degradation after CHK1

Figure 3.13. Distinct Levels of CDK1 activity are required for different CHK1i-associated phenotypes

Characterization of cell cycle and CHK1i-associated and cell cycle markers by flow cytometry after CHK1 and CDK1 inhibition. A549 cells were inhibited with the denoted concentrations of CDK1i ± 100 nM CHK1i for 2 h and pulsed with EdU for the last hour.

A-D) Cell cycle distribution. % of single cells in the G1 (A), Early S (B), Late S (C) and G2/M (D) phases determined by EdU vs DAPI staining.; N=5;

E and F) Relative EdU levels in Early (E) and Late (F) S phase. EdU levels were normalized to the 0 μM CDK1i-DMSO sample in each phase. N=5.

G-J) Quantification of pFOXM1 Levels during Late S phase and G2. G) % pFOXM1-High cells and H) pFOXM1 MFI in Late S phase. I) % of cells in G2/M with High pT600 FOXM1 J) MFI of pFOXM1 in G2/M. N=4.

K and L) Quantification of pH3+ cells during (K) Late S phase and (L) G2/M. N=5.

M-O) Quantification of pKAP1+ cells during (M) Early and (N) Late S phase as well as (O) G2/M. N=5; ANOVA-mixed effects analysis with Tukey correction.

P) Percent Annexin V^+ PI^- apoptotic cells after 24 h of treatment with 100 nM CHK1i and denoted CDK1i concentrations. N=3.

Mean ± SEM. *, ANOVA with Tukey correction; $p<0.05$; **, $p<0.01$; ***, $p<0.001$; ****, $p<0.0001$. Grey boxes denote concentrations of CDK1i that showed a significant increase in pH3 levels with CHK1i in (K).

Figure 3.13. (cont.)

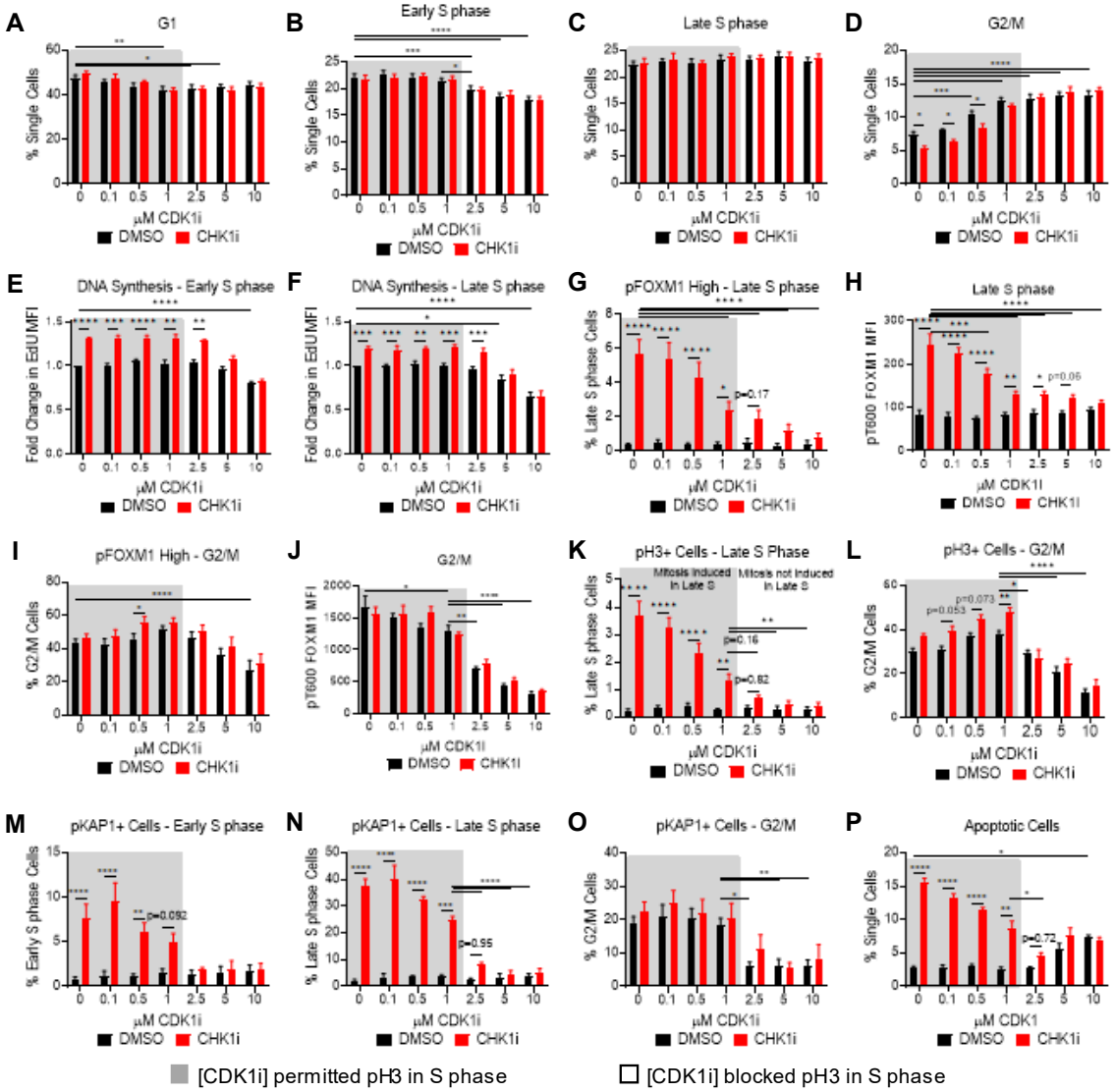

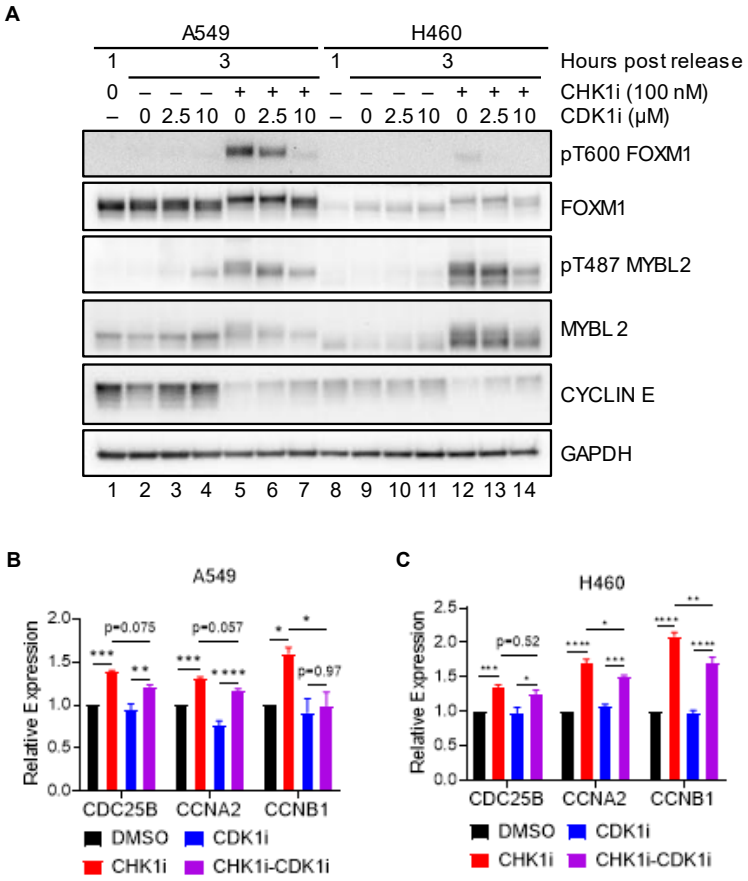

Figure 3.14. 2.5 μM CDK1i blocks MMB-FOXM1 activity during S phase

A) Immunoblot of MMB-FOXM1 complex phosphorylation after CHK1i and CDK1i. A549 and NCI-H460 cells were synchronized by a single thymidine block and released. Samples were treated at 1 post-release with combinations of 100 nM CHK1i and 2.5 or 10 μM CDK1i and samples were collected at the indicated times.

B and C) RT-qPCR for MMB-FOXM1 target genes CDC25B, CCNA2, and CCNB1, in S-phase A549 and H460 cells. A549 cells (B) and H460 cells (C) were synchronized by single thymidine block, released for 1 h and treated with 100 nM CHK1i and/or 2.5 μM CDK1i for 2 h. N=3. Mean ± SEM. *, ANOVA with Tukey correction; p<0.05; **, p<0.01; ***, p<0.001; ****, p<0.0001.

inhibition in either A549 or H460 cells, suggesting that the CDK1i treatment did not impair CDK2 activity.

To determine if 2.5 μM CDK1i also blocked the induction of G2/M genes by CHK1i, the expression of MMB-FOXM1 target genes was assessed by RT-qPCR in S phase A549 and H460 cells. 2.5 μM of CDK1i blocked the induction of CCNB1 but not CDC25B or CCNA2 in A549 cells (**Fig. 3.14B**) and significantly reduced the induction of CCNB1 and CCNA2 but not CDC25B in the more sensitive H460 cells (**Fig. 3.14C**). The differential effect of CDK1i on these MMB-FOXM1 targets genes could reflect the differing number of CHR motifs in the gene promoters (Fischer et al., 2016) or the recently identified regulation of epigenetic factors by CDK1 (Michowski et al., 2020). This data demonstrates that 2.5 μM CDK1i was sufficient to block CHK1i-induced MMB-FOXM1 activity and increased expression of CCNB1, the mitotic activator of CDK1, during S phase.

Similarly, 2.5 μM and higher doses of CDK1i reduced the appearance of the mitotic marker pH3 in response to CHK1i during Late S phase and, in general, during G2/M (**Fig. 3.13K and 3.13L**). Both the fraction of pKAP1-positive G2/M cells as well as CHK1i-induced pKAP1-positive S phase cells was dependent on CDK1 activity (**Fig. 3.13M-O**). Increasing levels of CDK1i reduced the appearance of pKAP1 in Early S, Late S, and G2. 2.5 μM CDK1i was sufficient to reduce pKAP1 levels in G2/M and block CHK1i-induced pKAP1 in Late S phase (**Fig. 3.13M-O**). Further, the same concentration of CDK1i, 2.5 μM, prevented pH3 induction suggesting that the breakdown in the separation of DNA synthesis and mitosis is a required step for DNA replication stress after CHK1 inhibition.

At 2.5 μM, CDK1i appears to block a critical threshold of CDK1 activity. While lower concentrations of CDK1i reduced the impact of CHK1 inhibition in Late S phase, 2.5 μM and higher concentrations of CDK1i prevented CHK1i-induced pH3, pKAP1, pFOXM1, and *CCNB1* expression but did not prevent increased DNA replication in Late S phase. This indicates that

2.5 μM CDK1i keeps CDK1 activity below the threshold necessary to trigger mitotic events while allowing for increased DNA replication.

To establish if activation of the MMB-FOXM1-CDK1 feedback loop is required for CHK1i-induced replication catastrophe, the amount of CDK1 activity required for apoptosis 24 h after CHK1 inhibition was assessed by dual Annexin V and PI staining. CHK1i induced an apoptotic population that was dependent on CDK1 activity (**Fig. 3.13P**). At 2.5 μM, CDK1i blocked CHK1i-induced apoptosis while 10 μM CDK1i significantly induced apoptosis by itself. The induction of replication stress markers was also examined at 24 h post-CHK1i treatment (**Fig. 3.15A**). pKAP1, as well as pRPA and pCHK1, were induced 24 h after CHK1 inhibition in the presence of 2.5 μM CDK1i but not 10 μM CDK1i. 10 μM CDK1i also induced low levels of γ-H2AX on its own but 2.5 μM or higher CDK1i reduced CHK1i-induced γ-H2AX. This data suggests that while replication stress may be induced lower levels of CDK1 activity, CHK1i-induced DNA damage and cell death require sufficient CDK1 activity to trigger the MMB-FOXM1-CDK1 feedback loop and premature mitosis.

Replication catastrophe occurs when replication factors such as RPA become exhausted leading to unrepairable DNA damage (Toledo et al., 2017). Prolonged CHK1i treatment induced a pS4/S8 RPA -positive population that was also γ-H2AX-High **(Fig. 3.15B-D)** indicating the accumulation of DNA damage in replication stressed cells. A pS4/S8 RPA positive population was observed with 2.5 μM CDK1i, consistent with a mitotic arrest where RPA is hyperphosphorylated (Liu et al., 2012; Oakley et al., 2003). Treatment with CHK1i and 2.5 μM or higher CDK1i reduced levels of pS4/S8 RPA-positive/γ-H2AX-High cells. Notably,10 μM CDK1i was required to completely block the induction of pS4/S8 RPA in response to CHK1i. This indicates that blocking sufficient CDK1 activity to induce mitosis during DNA replication prevented the accumulation of DNA damage but not replication stress. Chromatin-bound RPA and γ-H2AX

Figure 3.15. Blocking CDK1 activity limits replication catastrophe but not replication stress

A) Immunoblot of A549 and NCI-H460 lysates 24 h after treatment with 100 nM CHK1i and/or the denoted concentrations of CDK1i.

B-D) Chromatin-bound γ-H2AX and RPA S4/S8 phosphorylation assessing DNA damage in cells undergoing replication stress in cells after 24 hours of treatment with CHK1i ± CDKi. B) Percent pS4/S8 RPA+ cells. C) Percent pS4/S8 RPA and γ-H2AX double positive cells.

D) Density dot plot of γ-H2AX and pS4/S8 RPA cells after treatment with CHK1i ± CDKi. N=3.

E-G) Chromatin-bound γ-H2AX and RPA assessing replication catastrophe in cells after 24 hours of treatment with CHK1i ± CDKi. E) Percent cells showing high chromatin-associated RPA. F) Percent cells showing increasing levels of chromatin-associated RPA, in γ-H2AX high cells based on gates shown in G, following treatment with CDK1i and CHK1i as above. G) Density dot plot of γ-H2AX and RPA in cells after treatment with CHK1i ± CDKi. N=3.

Mean ± SEM. *, ANOVA with Tukey correction; $p<0.05$; **, $p<0.01$; ***, $p<0.001$; ****, $p<0.0001$.

Figure 3.15. (cont.)

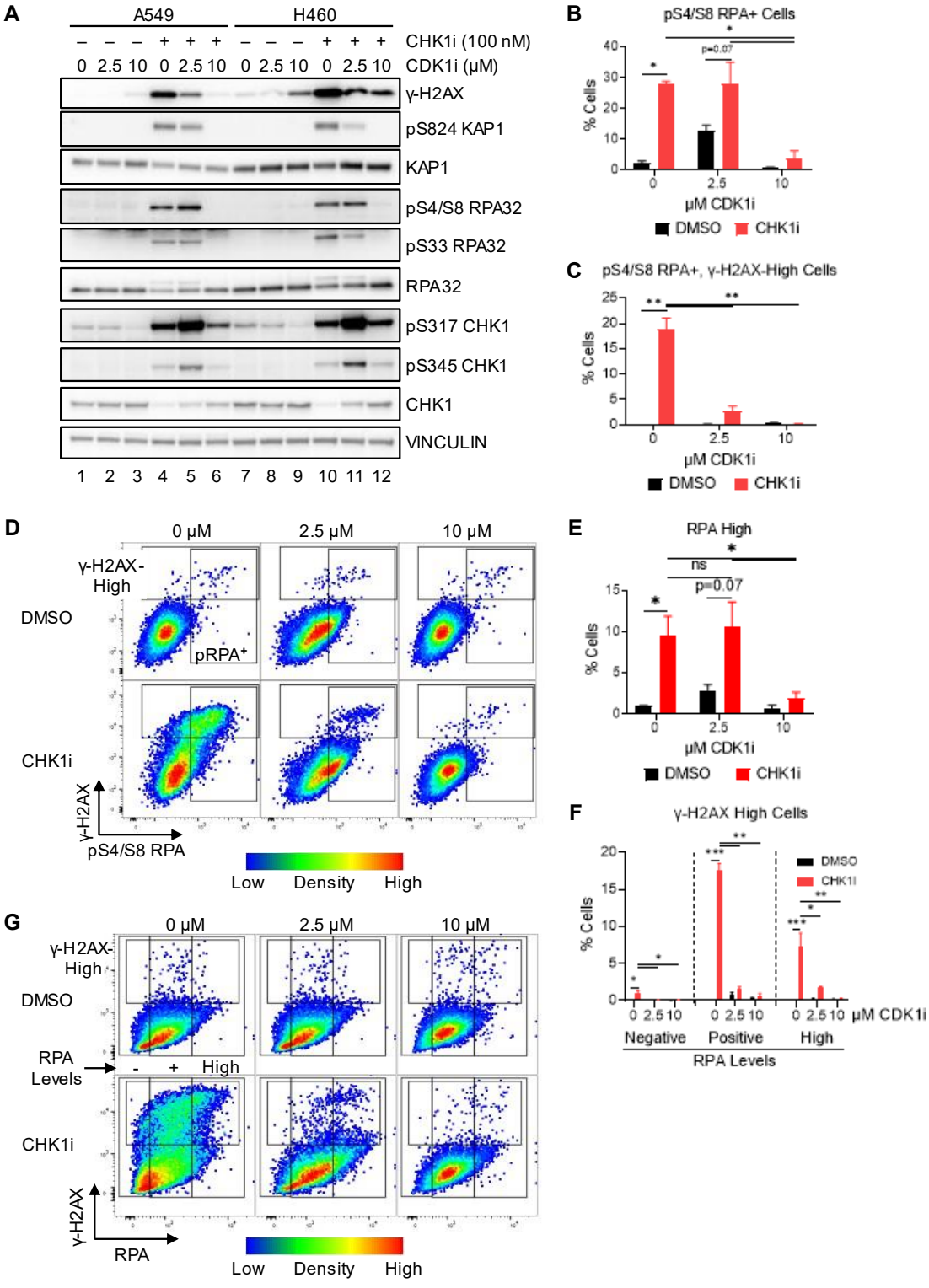

were also examined to determine if this DNA damage was due to RPA exhaustion. CHK1i induced an RPA-High population that was γ-H2AX-High (**Fig. 3.15 E-G**) consistent with replication catastrophe. An RPA-positive/γ-H2AX-High population was also induced suggesting a low RPA exhaustion threshold or exhaustion of an alternative replication factor. Similar to pS4/S8 RPA, 2.5 μM CDK1i blocked the induction of the RPA-High, γ-H2AX-High population indicating that premature activation of the mitotic program is required for the accumulation of DNA damage in RPA exhausted cells.

An MMB-FOXM1-CDK1 feedback loop is required for synergy between CHK1i and WEE1i

The requirement for mitotic levels of CDK1 activity in CHK1i-induced replication catastrophe raised the possibility that replication catastrophe could be induced in LIN54 or FOXM1 KO cells by aberrantly activating CDK activity by targeting an alternative negative regulator. Levels of *WEE1*, which phosphorylates an inhibitory site on CDK1 (McGowan and Russell, 1993a), were induced by CHK1 inhibition during S phase in EV, LIN54 KO, and FOXM1 KO cells (**Fig 3.16A**). An inhibitor of WEE1, adavosertib (WEE1i), has shown synergy in combination with CHK1 inhibitors *in vivo* (Carrassa et al., 2012; Chila et al., 2015; Russell et al., 2013). Treatment of EV and LIN54 KO cells with WEE1i resulted in the appearance of a slower migrating FOXM1 species consistent with phosphorylation resulting from increased CDK activity (**Fig. 3.16B**). The ATR-CHK1 pathway was activated after WEE1i treatment in EV, LIN54 KO, and FOXM1 KO cells as denoted by induction of pCHK1 in the WEE1i-treated samples. Thus, WEE1 and the ATR-CHK1 pathway work to oppose CDK activation when the other is inhibited. In EV cells, dual inhibition of CHK1 and WEE1 induced higher levels of γ-H2AX than either CHK1i or WEE1i alone while γ-H2AX was induced in the LIN54 or FOXM1 KO cells only in the presence of WEE1i or dual CHK1i/WEE1i treatment (**Fig. 3.16B**) suggesting LIN54 and FOXM1

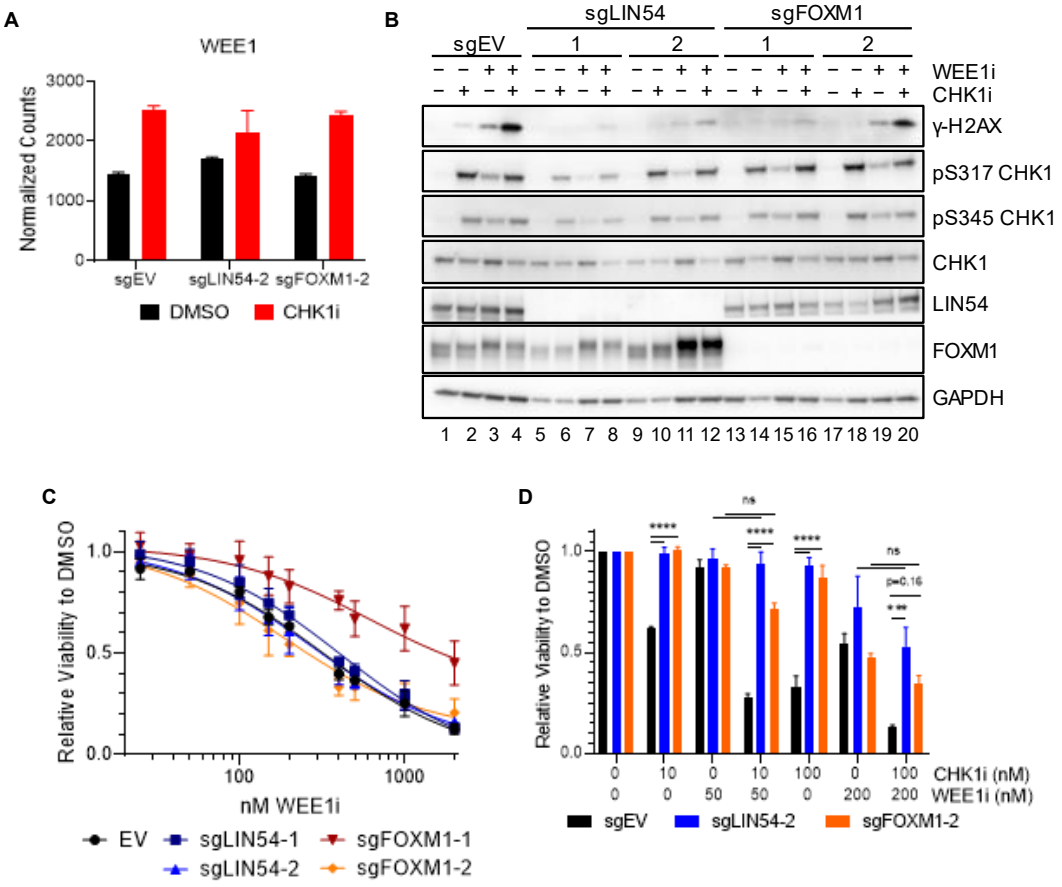

Figure 3.16. LIN54 and FOXM1 KOs retain sensitivity to WEE1 inhibition

A) Mean counts of WEE1 in EV, LIN54 KO and FOXM1 KO synchronized S phase cells after 2 h of CHK1i treatment. Data from the experiment collected in **Fig. 5D-G**.

B) Immunoblot of γ-H2AX levels in EV, LIN54 KO, and FOXM1 KO cells with 100 nM CHK1i and 200 nM WEE1i dual treatment for 8 h.

C) Viability curves of A549 EV, LIN54 KO, and FOXM1 KO cells in the presence of increasing WEE1i concentrations for 72 h. N=3. Mean ± SD.

D) Viability of A549 EV, LIN54 KO, and FOXM1 KO cells after treatment with the denoted CHK1i and WEE1i concentrations for 72 h. N=3. Mean ± SEM. *, ANOVA with Tukey correction; p<0.05; **, p<0.01; ***, p<0.001; ****, p<0.0001.

may still be sensitive to perturbation of WEE1 activity. Consistent with this observation, EV cells and three out of four LIN54 or FOXM1 KO cell lines had similar sensitivities to WEE1i (**Fig. 3.16C**). Viability in LIN54 KO and FOXM1 KO cells however was not further reduced by the addition of a CHK1i to a WEE1i in contrast to EV cells (**Fig. 3.16D)** implicating the premature mitosis induced by the MMB-FOXM1-CDK1 feedback loop after CHK1i in the synergy between CHK1i and WEE1 inhibition.

Discussion

The results in this study describe a positive feedback loop between the MMB-FOXM1 complex, the G2/M mitotic transcriptional program, and CDK1 activity that is restrained during S phase by ATR and CHK1 (**Fig S7E**). The ATR-CHK1 pathway has previously been observed to regulate FOXM1 via CDK1 activity (Saldivar et al., 2018) while cyclin A or B complexes, typically expressed as part of the mitotic transcription program, also promote MMB-FOXM1 activity (Fu et al., 2008; Lane et al., 1997; Laoukili et al., 2008b; Ziebold et al., 1997). In addition, loss of cyclin F, a negative regulator of CDK phosphorylation of MYBL2, sensitizes cells to inhibitors of the ATR-CHK1 pathway (Burdova et al., 2019; Klein et al., 2015; Mavrommati et al., 2018) underscoring that interplay between cyclin/CDK and MMB-FOXM1 activities in ATR/CHK1 inhibitor sensitivity. This study builds on these prior observations by demonstrating the interdependent nature of increased MMB-FOXM1 complex activity, G2/M gene expression, and CDK1 activity required for CHK1i sensitivity.

Positive feedback loops can promote the transition from one distinct state to another when a sufficient level of activating signal is achieved (Mitrophanov and Groisman, 2008). Such bimodal behavior was observed as levels of pH3 and pKAP1 significantly decreased when MMB-FOXM1 was disrupted or when CDK1 activity was decreased with increasing concentrations of CDK1i from 1 μM to 2.5 μM in Late S phase and G2/M after CHK1 inhibition. CDK1 is involved in multiple feedback loops critical for mitotic progression (Gavet and Pines, 2010; Pomerening et al., 2003) and our data identifies a positive feedback loop that links CDK1 activity to the MMB-FOXM1-dependent wave of G2/M gene expression required for mitosis.

The CHK1i-induced phosphorylation of KAP1 at S824 is an ATR- and CDK1-dependent event that reflects dysregulation of the S/G2/M transition. A CHK1i-independent population of pS824 KAP1-positive cells was observed basally in G2/M. The presence of this G2/M population and its dependency on CDK1 activity indicate that KAP1 S824 phosphorylation is a

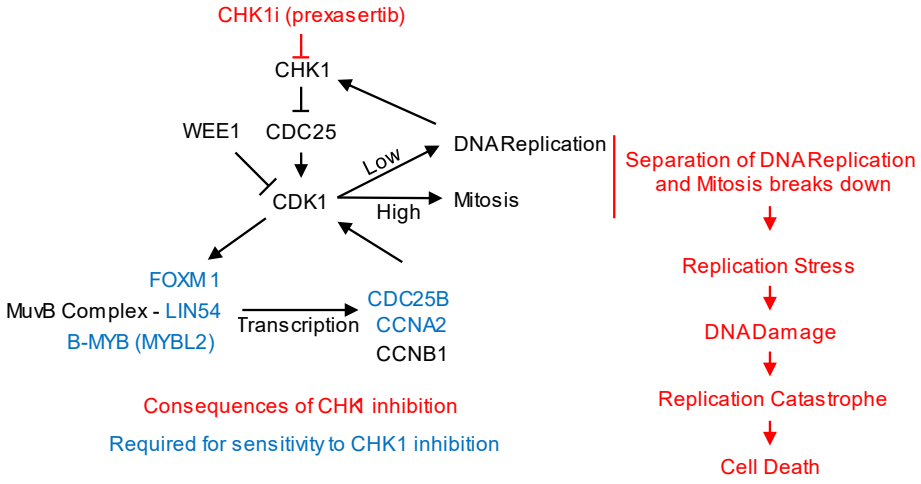

Figure 3.17. CHK1 prevents replication catastrophe by limiting an MMB-FOXM1-CDK1 feedback loop to keep DNA synthesis and mitosis separate

Model for regulation of S/G2/M transition by an MMB-FOXM1-CDK1 positive feedback loop that is restrained by the ATR-CHK1 pathway. CHK1 antagonizes the activation of an MMB-FOXM1-CDK1 positive feedback loop to allow for the completion of DNA replication without activating the mitotic program in Late S phase. Inhibition of CHK1 results in this feedback loop activating the mitotic program in Late S phase leading to replication catastrophe.

cell cycle-dependent event. KAP1 phosphorylation promotes chromatin relaxation to facilitate DNA damage repair and coincides with the loss of HP1 foci on chromatin (White et al., 2012; Ziv et al., 2006). HP1 chromatin dynamics are altered during mitosis to facilitate chromosome segregation (Abe et al., 2016; Chu et al., 2014) so the observed pKAP1 in G2/M could result from the regulation of heterochromatin during G2/M. Surprisingly, the induction of pKAP1 in Late S by CHK1i was ATR- but not ATM- or DNA-PK dependent. Increased pKAP1 after CHK1 inhibition could reflect altered heterochromatin dynamics, given that pKAP1 promotes chromatin relaxation, as the cell attempts to complete DNA replication prior to mitosis. Further study of KAP1 phosphorylation will be needed to understand the role of KAP1 phosphorylation in the S/G2 transition and in response to CHK1 inhibition.

Premature mitosis during DNA replication is necessary for replication catastrophe and stress after CHK1 inhibition. Loss of MMB-FOXM1 components reduced the induction of the mitotic marker pH3 during Late S phase after CHK1 inhibition. CDK1 inhibition restored the separation of DNA replication and mitosis with 2.5 μM of CDK1i blocking the induction of a pH3 positive population in Late S phase. The induction of pKAP1, pRPA-High/γ-H2AX positive cells, and apoptosis by CHK1i treatment was also blocked by 2.5 μM of CDK1i demonstrating that premature mitosis was necessary for DNA replication stress and subsequent replication catastrophe. 2.5 μM CDK1i was previously shown to partially rescue cell death after depletion of ATR by an inducible degron (Eykelenboom et al., 2013) suggesting that this threshold of CDK1 activity also may be relevant for ATR inhibition as well. The MMB-FOXM1 target gene *CCNB1* appears to be a key gene for CHK1 inhibitor resistance, as it was identified as a significant hit in H460 cells and depletion of CCNB1 reduced CHK1i sensitivity in recently published work in ovarian cancer cells (Nair et al., 2020). Expression of CCNB1 in interphase Xenopus extracts was recently shown to cause replisome disassembly suggesting a possible means by which activation of the mitotic program could lead to slowed replication forks and DNA synthesis

(Deng et al., 2019). Cyclin B1 levels however were not predictive of CHK1i sensitivity in a panel of head and neck squamous cell lines (van Harten et al., 2019) indicating that other components of the mitotic program may be involved in CHK1i sensitivity. Further investigation will be needed to identify the key components of the mitotic program that promote CHK1i-induced replication catastrophe.

Taken together, the results of this study add to the understanding of the factors that play a role in the S-M checkpoint, which delays entry into mitosis until after DNA synthesis is complete and was first described in fission yeast (Enoch and Nurse, 1990), Subsequently, vertebrate cells including DT40 B-lymphoma cells lacking Chk1 were shown to enter mitosis with incompletely replicated DNA when DNA synthesis is blocked (Zachos et al., 2005). Similar to this study, these prior studies highlighted the crucial role of regulation of CDK1 activity. Here, we demonstrated the impact of differences in CDK1 activity regulated by an MMB-FOXM1-dependent feedback loop in triggering replication catastrophe after CHK1 inhibition. LIN54 and FOXM1 were separately shown to modulate CHK1i sensitivity in ovarian and pancreatic cancer respectively (Blosser et al., 2020; Chung et al., 2019), during the preparation of this work. This indicates that the insights derived from this study could inform the use of CHK1 inhibitors in multiple cancer types.

Synergism of CHK1 or ATR with WEE1 inhibition has been observed in several preclinical studies (Bukhari et al., 2019; Busch et al., 2017; Carrassa et al., 2012; Chaudhuri et al., 2014; Chila et al., 2015; Chung et al., 2019; Davies et al., 2011; Ghelli Luserna Di Rora et al., 2019; Hauge et al., 2017; Magnussen et al., 2015; Mak et al., 2015; Russell et al., 2013), albeit with incomplete understanding as to why. Aberrant activation of CDK1 and CDK2, via inhibition of WEE1, may bypass the attenuation of CDK1 activation due to the loss of the MMB-FOXM1 complex. The addition of CHK1i to WEE1i may not be beneficial in cells that become resistant to CHK1i due to this mechanism. Other approaches, such as the addition of a DNA

damaging agent such as gemcitabine, may be more effective (Chung et al., 2019; Kausar et al., 2015).

Several CHK1 and ATR inhibitors as well as WEE1 inhibitors have been the subject of ongoing and completed clinical trials. In at least one trial (NCT02873975), patients were selected based on markers of replication stress, which stems from the idea that tumors prone to replication stress due to genetic abnormalities would be overwhelmed by additional DNA replication stress induced by CHK1 inhibition. Rather, it appears that premature activation of the mitotic program, which requires an intact MMB-FOXM1-CDK1 axis, triggers cell death via replication catastrophe. This work suggests further examination of cell cycle-associated biomarkers may inform our understanding of patients with responding tumors vs. those with intrinsic resistance.

Materials and Methods

Cancer Cell Lines and Cell Culture

Human NSCLC cell lines A549 and NCI-H460 cells stably transfected with pXPR_311 for constitutive expression of the Cas9 endonuclease (A549-Cas9 and NCI-H460-Cas9) were obtained from the Genetic Perturbation Platform at the Broad Institute, Cambridge, MA (Broad GPP). Cell lines listed in **Table 3.1** were propagated in RPMI 1640 medium (Life Technologies, Grand Island, NY) supplemented with 10% fetal bovine serum (Sigma-Aldrich, St. Louis, MO) and 1% Pen/Strep (Gibco) at 37ºC in 5% CO_2. KO populations of sgLIN54 and sgFOXM1 cell lines were generated by serial dilution using the sgRNAs in **Table 3.2** and confirmed by immunoblot. Inhibitors used in the study are listed in **Table 3.3**.

For single thymidine blocks, 500,000 (60 mm plate) or 1,200,000 (100 mm plate) cells were plated into 2 mM thymidine-containing RPMI media for 16 h. To release cells, cells were washed twice with prewarmed PBS and grown in prewarmed RPMI media to which inhibitors were added at the times denoted. For siRNA experiments, siRNAs listed in **Table 3.2** were reverse transfected at a final concentration of 20 nM into ~10^6 A549 cells using Lipofectamine RNAiMAX (Invitrogen, 13778030) in 100 mm dish. The next day cells were plate into 2 100 mm dishes for drug treatment the following day.

CRISPR positive selection screens for drug resistance

A549-Cas9 and NCI-H460-Cas9 cells were infected with the Brunello human genome-wide lentiviral gRNA pooled library (Broad Institute, Cambridge, MA). The library consists of 76,441 sgRNAs targeting 19,114 different genes (Doench et al., 2016). A minimum of 135 million cells of each cell line was cultured in 12-well tissue culture plates containing 3 million cells per well to ensure adequate representation of each sgRNA, e.g., an average of 500 cells per sgRNA, when infected at a multiplicity of infection of 0.3 in media supplemented with 8

μg/ml polybrene. Plates were centrifuged at 2000 rpm at 37ºC for 2 h, and then the media was replaced with fresh media without polybrene for incubation overnight. The cells were then transferred to 15 cm tissue culture dishes and infected cells were selected with 2 μg/mL puromycin for 4 days. After selection, 40 million cells were cultured for each of three replicates in 15 cm dishes containing 5 million cells per dish. An additional 40 million cells per replicate were harvested and frozen for subsequent genomic DNA extraction. Cultured cells were then treated with either 100 nM (A549) or 50 nM (NCI-H460) prexasertib for 19 days. These concentrations were selected to achieve roughly no net increase or decrease in the total number of cells during the 19 days. Cells were re-plated every 3–4 days and maintained in prexasertib-containing media, each time plating a minimum of 40 million cells per replicate. At the end of the screen, the cells were harvested and frozen from genomic DNA extraction.

Genomic DNA isolation, sgRNA sequencing and identification of top hits

Genomic DNA was isolated using QIAamp DNA blood midi and maxi kits (Qiagen, Hilden, Germany) per manufacturer's instructions. PCR was performed to attach sequencing adaptors and barcodes for multiplexed sgRNA sequencing, as previously described (Doench et al., 2016). Samples were sequenced on an Illumina HiSeq2000. Reads per million + 1 were $\log_2$ transformed, and then the $\log_2$-fold change of each sgRNA after 19 days of prexasertib treatment was determined by comparing its abundance to that in Brunello human genome-wide lentiviral sgRNA pooled library plasmid DNA. The average (mean) values of three replicates were used for subsequent analyses. The STARS gene-ranking algorithm was used to determine the top 10% of genes for which 2 or more sgRNAs became enriched in cells treated with prexasertib (Doench et al., 2016). Top gene hits were identified as those whose false discovery rates were < 10% in both NSCLC cell lines. Additionally, the normalized data were also analyzed with the hypergeometric distribution method

Table 3.1. Cell Lines

A549	ATCC	CCL-185
A549-Cas9 (pXPR_311)	Broad Institute	N/A
NCI-H460	ATCC	HTB-177
NCI-H460-Cas9 (pXPR_311)	Broad Institute	N/A
NCI-H23	ATCC	CRL-5800
NCI-H1299	ATCC	CRL-5803

Table 3.2. Oligonucleotides: sgRNA sequences and siRNAs

sgFOXM1-1	5’-ACCAGGTATGAGCTGACCCG-3’	
sgFOXM1-2	5’-CCTGGTCCAATGTCAAGTAG-3’	
sgLIN54-1	5’-CCTGGTCCAATGTCAAGTAG-3’	
sgLIN54-2	5’-AAGTAGTTACCATTGGAGGG-3’	
siCTRL	Dharmacon	D-001810-10
siLIN54	Dharmacon	L-019325-01
siCCNA2	Dharmacon	L-003205-00
siMYBL2	Dharmacon	L-010444-01

Table 3.3. Inhibitors

Prexasertib (LY2606368, CHK1i)	Eli Lilly & Co.	S7178
AZ20 (ATRi-2)	Santa Cruz Biotechnology	sc-503186
VE-822 (ATRi-1)	MedChem Express	HY-13902
KU-55933 (ATMi)	Selleck	S1092
Nedisertib (DNA-PKi)	MedChem Express	HY-10570
RO-3306 (CDK1i)	Santa Cruz Biotechnology	sc-358700
Adavosertib (AZD1775, WEE1i)	Selleck	S1525
Doxorubicin (DOXO)	Cell Signaling Technologies	5927S

(https://github.com/mhegde/volcano_plots). The volcano plots of these results were created using R (https://www.r-project.org).

Growth Curves

A549 cells were seeded at 30,000 cells in 60 mm dishes and harvested and fixed with cold ethanol (70%) every two days for ten days. The media was refreshed on days 4, 8, and 10, and cells were re-plated into 150 mm dishes on day 6 to prevent contact arrest. Cell count was determined using Countbright Beads (Life Technologies, C36950) and flow cytometry (BD FACS Canto II).

Viability Assays

1000 cells in 100 μl media were placed in each well of a 96 well plate the day before drug treatment. 100 μl of media with 2X drug concentration was added to achieve the final concentrations shown. 72 h post-treatment, cells were incubated at room temperature for 30 mins before quantification of viability using CellTiter-Glo (Promega) on an M200 Infinite plate reader (Tecan).

Immunoblotting

Whole-cell extracts were generated by incubating cell pellets in EBC buffer (50 mM Tris pH 8.0, 150 mM NaCl, 0.5 mM EDTA, 10% Glycerol, 0.5% NP-40, Protease Cocktail Set I (Millipore, 539131) and Phosphatase Cocktail Set I) and cleared by centrifugation. Relative protein levels in lysates were normalized by Bradford assay and samples were boiled in 6x SDS buffer. Samples were then loaded on 4-20% TGX gels (Bio-Rad) for electrophoresis which were then transferred to a nitrocellulose membrane (Bio-Rad) by wet transfer. Membranes were blocked in 5% nonfat milk (Boston Biochem) for 1 h at room temperature and incubated in primary antibody

overnight at 4C. Primary antibodies, listed in **Table 3.4**, were diluted as follows: CDK1 and cyclin E were diluted 1:200 in 3% nonfat milk in TBST; pS1981 ATM was diluted 1:500 in 3% nonfat milk in TBST; γ-H2AX, pS317 CHK1, CHK1, ATM, DNA-PKcs and MYBL2 were diluted 1:1000 in 3% nonfat milk in TBST; pS824 KAP1, KAP1, pS4/S8 RPA, pS33 RPA, RPA, cyclin B1, and GAPDH were diluted 1:2000 in 3% nonfat milk TBST; pT487 MYBL2 was diluted 1:5000 in 3% nonfat milk; LIN54 was diluted 1:1000 in 5% nonfat milk in TBST; FOXM1 was diluted 1:2000 in 5% nonfat milk TBST; vinculin was diluted 1:30000 in 5% nonfat milk in TBST; pS345 CHK1, pT161 CDK1, pY15 CDK1/2 and pS10 histone H3 were diluted 1:1000 in 5% BSA in TBST; pS2056 DNA-PKcs was diluted 1:2000 in 5% BSA in TBST. Membranes were incubated in secondary antibodies, diluted 1:5000 in 5% nonfat milk, for 1 h at room temperature. Bands were visualized using Super Signal West Pico (Thermo Scientific) or Immobilon Western Chemiluminescent (Millipore) HRP substrate on the G-box imaging system (Syngene).

Flow cytometry

Trypsinized cells were washed with PBS and fixed in 4% formalin in PBS for 15 min at room temperature. Cells were then washed three times with 1% BSA in PBS and permeabilized in 70% ethanol at -20ºC for 30 min to overnight. After three washes with 1% BSA in PBS, incorporated EdU was labeled using the reagents in **Table 3.5** with a CLICK reaction (2 mM CuSO4, 100 μM THPTA, 100 mM sodium ascorbate, and 2 μM Alexa 647 Azide or Calfluor 647 Azide in PBS) by rotating for 30 min at room temperature. In the case of pATM, instead of the CLICK reaction, samples were incubated in 200 ug/ml DNaseI in DPBS for 1 hour at 37ºC. Samples were then washed thrice with 1% BSA in PBS and incubated with the primary antibody in 1% BSA in PBS overnight at 4ºC. Primary antibodies were diluted, listed in **Table 3.4** as follows: 1:250, pT600 FOXM1; 1:500, pS824 KAP1; 1: 500, pS1981 ATM; and 1:50, pS10

Table 3.4. Antibodies

pS1981 ATM	Biolegend	651201
ATM	Cell Signaling Technologies	2873T
MYBL2	Millipore	MABE866
pT487 MYBL2	Abcam	Ab76009
CDC45	Cell Signaling Technologies	11881S
CDK1	Santa Cruz Biotechnology	sc-17
pT161 CDK1	Cell Signaling Technologies	9114S
pY15 CDK1/2	Cell Signaling Technologies	9111S
CHK1	Santa Cruz Biotechnology	sc-8408
pS317 CHK1	Cell Signaling Technologies	2344S
pS345 CHK1	Cell Signaling Technologies	2341S
Cyclin E (CCNE)	Santa Cruz Biotechnology	sc-247
Cyclin B1	Santa Cruz Biotechnology	sc-752
pS2056 DNA-PKcs	Cell Signaling Technologies	68716S
DNA-PKcs	Cell Signaling Technologies	38168S
FOXM1	Santa Cruz Biotechnology	sc-520
pT600 FOXM1	Cell Signaling Technologies	14655S
GAPDH	Santa Cruz Biotechnology	sc-47724
γ-H2AX	Millipore	05-636-I
pS10 histone H3	Cell Signaling Technologies	3377T
pS10 histone H3 - Alexa 488 conjugate	Cell Signaling Technologies	3465S
KAP1	Bethyl Laboratories	A300-274A-M

Table 3.4. (cont.) Antibodies

pS824 KAP1	Bethyl Laboratories	A300-767A-M
LIN54	Bethyl Laboratories	A300-799A-M
PCNA	Cell Signaling Technologies	2586S
RPA32	Bethyl Laboratories	A300-244A-M
pS4/S8 RPA32	Bethyl Laboratories	A300-245A-M
pS33 RPA32	Bethyl Laboratories	A300-246A-M
VINCULIN	Sigma-Aldrich	V9131
anti-BrdU-APC conjugate	Biolegend	339808
anti-mouse IgG - HRP	Bethyl Laboratories	A90-116P
anti-rabbit IgG - HRP	Bethyl Laboratories	A120-101P
anti-mouse IgG - Alexa 488 conjugate	Cell Signaling Technologies	4408S
Rabbit IgG Alexa 488 isotype control	Cell Signaling Technologies	4340S
anti-Rabbit IgG - Alexa 488 conjugate	Life Technologies	A11008
anti-Rabbit IgG - PE conjugate	Cell Signaling Technologies	4340S
anti-Rabbit IgG - Alexa 647 conjugate	Life Technologies	A21245

Table 3. 5. Flow Cytometry Reagents for Label DNA Synthesis

5-ethynyl-2'-deoxyuridine (EdU)	Life Technologies	A10044
THPTA	Click Chemistry Tools	1010
Alexa 647 Azide	Life Technologies	A10277
CalFluor 647 Azide	Click Chemistry Tools	1372
AFDye 546 Azide	Click Chemistry Tools	1283
5-bromo-2'-deoxyuridine (BrdU)	Sigma-Aldrich	B5002
DNaseI	Sigma Aldrich	D4513-1VL
4′,6-diamidino-2-phenylindole (DAPI)	Invitrogen	D3571

histone H3-Alexa Fluor 488 conjugate. After 3 washes with 1% BSA in PBS, samples were incubated with secondary antibodies, which were diluted 1:250 in 1% BSA in PBS, for 1 h at room temperature in darkness. pATM samples was incubated with mouse-Alexa Fluor 488 conjugate, pT600 FOXM1 was incubated with a rabbit-Alexa Fluor 488 conjugate and pS824 KAP1 was incubated with a rabbit-PE conjugate. After three more 1%BSA in PBS washes, DNA staining was then conducted by incubating samples in darkness and at room temperature for 1 h in a 1 μg/ml DAPI, 100 ng/ml RNase A staining solution. pATM samples were incubated with anti-BrdU-APC (1:50 in 1% BSA in PBS) for 1 hour at room temperature followed by three washes between secondary and DAPI staining. Samples were analyzed on Canto II or Fortessa analyzers (BD Biosciences) and 50,000 total events were captured for each sample. A negative control where an EdU pulse and primary antibodies were omitted but otherwise normally processed was used to establish negative populations and perform background subtraction on MFIs. A rabbit-Alexa 488 isotype control was used for the negative control for experiments with pH3-Alexa 488 staining. The Early and Late S phase gates were determined by dividing the EdU positive population of the EV or DMSO control in half based on DAPI signal.

The chromatin flow cytometry protocol was based upon approached used in previous studies (Hauge et al., 2017; Matson et al., 2016). Briefly, trypsinized cells were incubated on ice in 750 μl of Buffer A (300 mM sucrose, 100 mM NaCl, 3 mM $MgCl_2$,10 mM PIPES pH 7.0, 0.5% Triton x-100, Protease Cocktail Set I, and Phosphatase Cocktail Set I) for 5 min. 250 μl of Buffer B (300 mM sucrose,100 mM NaCl, 3 mM $MgCl_2$,10 mM PIPES pH 7.0, 0.5% Triton x-100, 10% Formalin, Phosphatase Cocktail Set I, and Phosphatase Cocktail Set I) was immediately added, and samples were incubated for an additional 15 min on ice. Cells were then pelleted (1000×g, 5 min, 4ºC) and washed with 1% BSA in PBS 3 times before proceeding onto EdU staining as with other samples. Primary antibodies for chromatin flow cytometry were diluted as follows: CDC45, 1:50; PCNA, 1:500; RPA32, 1:500; pS4/S8 RPA32, 1:1000; and H2AX, 1:1000.

For CDC45 samples, AFDye 546 Azide and anti-rabbit Alexa 647 secondary were used. An anti-mouse Alexa 488 secondary antibody and Calfluor 647 Azide was used with PCNA samples. For RPA32/pRPA32 and γ-H2AX samples, anti-rabbit Alexa 647 secondary and anti-mouse Alexa 488 secondary were used for RPA32/pRPA32 and γ-H2AX respectively. Otherwise, the CLICK reaction, primary and secondary as well as DAPI staining were conducted as described above.

For Annexin V/PI staining, cells were dissociated with StemPro Accutase (Gibco) and stained using the FITC Annexin V Apoptosis Detect Kit II (BD Biosciences, 556570).

RNA Expression

Total RNA was extracted from cell pellets using the RNeasy Plus kit (Qiagen). RNA was checked for quality using TapeStation and Qubit before library preparation using Kappa stranded mRNA Hyper Prep and sequencing using Illumina NS500. Reads were mapped to Hg19 using *STAR* alignment (Dobin et al., 2013) and counts were generated using *HTseq* (Anders et al., 2015). Differential gene expression analysis was perform using *DESeq2* (Love et al., 2014) and heatmaps were generated using R package *pheatmap.* Mean counts were generated using *DESeq2* mean-ratio normalization method. Gene set enrichment analysis was conducted using GSEA software ([http://www.broad.mit.edu/gsea/downloads.jsp) (Mootha et al., 2003; Subramanian et al., 2005). RNA-seq data sets have been deposited in the GEO database (accession number GSE154545). RT-qPCR to validate RNA expression data was done using cDNA generated from total RNA isolated by the RNeasy Plus kit and the High-Capacity cDNA Reverse Transcription Kit (Applied Biosystems). qPCR was performed on the cDNA using the primers listed in **Table 3.6** and Brilliant III Ultra-Fast qPCR Master Mix (Agilent) using a MxAria (Agilent). Relative RNA expression was calculated using the ΔΔCq method and GAPDH as reference gene.

Table 3.6. Oligonucleotides: qPCR Primers

CCNA2-qPCR-Forward Primer:	5’-TTCCTGTCTTCCATGTCAGTGC-3’
CCNA2-qPCR-Reverse Primer:	5’-ACACAAACTCTGCTACTTCTGGG-3’
CCNB1-qPCR-Forward Primer:	5’-GATGGAGCTGATCCAAACC-3’
CCNB1-qPCR-Reverse Primer:	5’-GGATGGCTCTCATGTTTCC-3’
CDC25B-qPCR-Forward Primer:	5’-GGAACCGTGGTATGTCTGC-3’
CDC25B-qPCR-Reverse Primer:	5’-GGACCGAGTGGGTAACTG-3’
GAPDH-qPCR-Forward Primer:	5' CGCCCAATACGACCAAAT-3'
GAPDH-qPCR-Reverse Primer:	5' CGCCCAATACGACCAAAT-3'

Data Analysis

Flow cytometry data was analyzed using FlowJo. GraphPad Prism was used to generate graphs and conduct statistical analyses for flow cytometry, viability, growth curves and RT-qPCR.

Data and Software Availability

RNA-seq data have been deposited in the NCI Gene Expression Omnibus database (https://www.ncbi.nlm.nih.gov/geo/) and are accessible through the following accession number: GSE154545, https://www.ncbi.nlm.nih.gov/geo/query/acc.cgi?acc=GSE154545

Chapter 4. APC/C dysregulation as a shared mechanistic step for CHK1i-induced replication and mitotic catastrophe

Author Contributions

All the experiments and preparations in this chapter were conceptualized and performed by me.

This research was supported by the US Public Health Service grants F31CA189328 to T.B. and R35CA232128, R01CA63113, R01CA173023, and P01CA203655 to J.A.D.

Abstract

CHK1 inhibition has been reported to trigger cell death through two mechanisms: DNA replication catastrophe and mitotic catastrophe. While treated as distinct phenomenon, it is unclear whether DNA replication catastrophe and mitotic catastrophe are triggered by shared or separate mechanisms, potentially limiting the effective targeting of these inhibitors in the clinic. To determine if there is a shared mechanistic step between CHK1i-induced DNA replication and mitotic catastrophe, CHK1i-induced cell cycle phenotypes were studied in parallel. DNA replication catastrophe, loss of S phase and G2/M cell cycle identities, and disruption of the spindle assembly checkpoint were triggered by a common threshold of CHK1 inhibition. This level of CHK1 inhibition impaired Aurora B activity in mitosis and triggered premature FBXO5 loss during S phase leading to the premature activation of the APC/C. While DNA polyploidy was induced at CHK1i concentrations that triggered premature APC/C activity, overall levels of DNA synthesis was impaired, likely due to the APC/C-dependent loss of DNA origin licensing factors, offering a potential link between to the mitotic program and impaired DNA synthesis. Consistent with this hypothesis, disruption of the MMB-FOXM1 complex, which drives expression of the mitotic program, reduced the impairment of DNA synthesis and the loss of these DNA replication factors. FBXO5 and Aurora B protein levels were stabilized or increased after CHK1i treatment in LIN54 or FOXM1 KOs and the protein levels of FBXO5 and Aurora B correlated with sensitivity to multiple CHK1 inhibitors in a cancer type-dependent manner. Thus, this study identifies a mechanistic step after CHK1i that links DNA replication catastrophe and mitotic catastrophe that has potential biomarkers for CHK1i sensitivity.

Introduction

The ATR-CHK1 pathway functions in a critical role during cell division by coordinating DNA replication with progression through the cell cycle. Oncogenic mutations that accelerate cell cycle progression are dependent on the ATR-CHK1 pathway to limit DNA replication stress, which can be generated by increased DNA replication (Gilad et al., 2010; Kotsantis et al., 2018; Murga et al., 2011; Vendetti et al., 2015). Consequently, CHK1 inhibition or depletion has been reported to induce cell death in cancer cells through two mechanisms: DNA replication catastrophe, where exhaustion of replication factors particularly RPA, triggers irreparable DNA damage, and mitotic catastrophe, where the dysregulation of mitosis, such as premature entry into mitosis, leads to cell death (King et al., 2015; Lam et al., 2004; Toledo et al., 2013; Zuazua-Villar et al., 2014). Replication catastrophe is typically assessed by comparing chromatin-bound RPA levels with DNA damage markers like γ-H2AX (Toledo et al., 2013), while mitotic catastrophe is measured by examining mitotic markers such as phosphorylated S10 Histone H3 (pH3) (Aarts et al., 2012). Replication and mitotic catastrophe after CHK1 inhibition however are rarely studied in parallel. Thus, it is unclear however if DNA replication and mitotic catastrophe result from a shared or distinct mechanisms of action. Understanding how CHK1 inhibition triggers DNA replication and mitotic catastrophe will provide mechanistic insights that could inform the use of CHK1 inhibitors in the clinic.

Emerging evidence has implicated the ATR-CHK1 pathway in the regulation of the spindle assembly checkpoint (SAC) during mitosis in addition to its role in DNA replication and the DNA damage response. During mitosis, ATR relocates to centrosomes where it is activated by R-loops leading to CHK1 activation (Kabeche et al., 2018). CHK1 phosphorylation of Aurora B on S331 promotes formation of the chromosome passenger complex, which fully activates Aurora B (Carmena et al., 2012; Petsalaki et al., 2011). Subsequently, Aurora B phosphorylates BUBR1 to facilitate formation of the mitotic checkpoint complex, which binds and sequesters CDC20 to limit APC/C activity as part of the SAC (Ditchfield et al., 2003; Izawa and Pines, 2015;

Petsalaki et al., 2011; Sudakin et al., 2001). Similar to coordinating the activation of the mitotic program with the completion of DNA replication, the ATR-CHK1 pathway also coordinates the activation of the APC/C with the onset of chromosome segregation.

The APC/C is a mitotic regulatory complex with an underappreciated role in regulating DNA synthesis. The APC/C facilitates the exit from M into the G1 phase of the cell cycle by degrading a number of drivers of mitosis, such as cyclin B1, PLK1, and Aurora B, to erase the mitotic program and allow for the resetting of origins of DNA replication (Alfieri et al., 2017; Irniger and Nasmyth, 1997; King et al., 1995; Norton and Diffley, 2000; Zhou et al., 2016). As APC/C substrates, geminin is degraded by APC/C-CDC20 complexes during the M/G1 transition while CDC6 is degraded as APC/C-FZR1 complexes form in the subsequent G1 (Clijsters et al., 2014; McGarry and Kirshcner, 1998; Peterson et al., 2000). During G1, CDC6 and CDT1 interact with origin of replication (ORC) complex to license for the loading of MCM helicases onto DNA (Coleman et al., 1996; Cook et al., 2004; Nishitani et al., 2000). To limit the cell to one round of genome replication, geminin binds to CDT1, during S phase/G2, blocking the interaction with CDC6 (Wohlschlegel et al., 2000). Thus, the temporal separation of the degradation of geminin and CDC6 by APC/C results in high levels of CDC6 and CDT1 that can interact in G1 to facilitate DNA origin licensing for S phase in actively dividing cells.

In addition to promoting formation of the spindle assembly complex in mitosis, the ATR-CHK1 pathway regulates the APC/C during S phase and the subsequent transition to G2/M. E2F-dependent expression of FBXO5 (EMI1) inhibits the APC/C by blocking the binding of substrates to the APC/C coactivators, FZR1 and CDC20, thereby allowing for entry into S phase (Cappell et al., 2016; Cappell et al., 2018; Di Fiore and Pines, 2007; Hsu et al., 2002). FBXO5 however needs to be subsequently degraded to allow for mitotic progression (Di Fiore and Pines, 2007; Reimann et al., 2001a). Although PLK1 targets FBXO5 for degradation during G2 and mitosis (Hansen et al., 2004; Moshe et al., 2004), the ATR-CHK1 pathway limits PLK1 activity in S phase during DNA replication (Lemmens et al., 2018), potentially impacting the

timing of FBXO5 degradation. CHK1 also promotes FZR1 degradation to limit APC/C-FZR1 activity during S phase when CDK activity is limited by the ATR-CHK1 pathway (Pal et al., 2020). Thus, the ATR-CHK1 pathway coordinate APC/C inhibition with cell cycle progression by limiting FZR1 levels and PLK1 activity during S phase to maintain FBXO5 levels and promoting spindle assembly complex formation in G2/M. However, whether APC/C activity is altered during the S/G2 transition after inhibition of the ATR-CHK1 pathway has yet to be explored.

Recently, the mitotic transcriptional program, which is driven by the MMB-FOXM1 complex was implicated in replication catastrophe induced by CHK1 inhibition (Branigan et al., 2021). Previously, CHK1 inhibition was thought to trigger replication stress and subsequent catastrophe through unscheduled origin firing (Petermann et al., 2010; Syljuasen et al., 2005). The increased demand for replication components results in the exhaustion of the replication machinery leading to the impaired DNA replication at late time points during S phase. Exhaustion of RPA, in particular, has been strongly implicated in triggering the DNA damage response (Toledo et al., 2017; Toledo et al., 2013). In contrast, we recently reported that CDK1 activity sufficient for premature MMB-FOXM1 activation and mitosis was required for replication catastrophe while increased DNA synthesis was not sufficient to induce replication catastrophe (Branigan et al., 2021). These results indicated that dysregulation of the mitotic program was required for DNA replication catastrophe after CHK1 inhibition similar to mitotic catastrophe.

Results

S phase and G2/M cell cycle identity is lost at CHK1i concentrations that trigger DNA replication catastrophe

To determine the level of CHK1 inhibition required to induce replication catastrophe, A549 cells were treated with increasing concentrations of the CHK1 inhibitor prexasertib (CHK1i) for 24 hours and chromatin bound levels of RPA and γ-H2AX were assessed (**Fig. 4.1A**). Cells were gated into three RPA populations: (i) Negative, non-detectable RPA levels; (ii) Positive, detectable levels of RPA below 99th percentile of the DMSO control; and (iii) High, where levels of RPA exceed the 99th percentile of the control and indicative of RPA exhaustion. CHK1i concentrations at 50 nM and higher significantly induced a γ-H2AX-High population, where γ-H2AX levels exceeded the 99th percentile of the DMSO control, in the RPA-Positive and RPA-High cells (**Fig 4.1B**) indicating that replication catastrophe was induced at ≥ 50 nM CHK1i. Induction of the RPA-High population however appeared to have a slightly lower threshold as 10 nM CHK1i induced an intermediate level of RPA-High cells compared to 5 nM and 50 nM CHK1i (**4.1C**).

This 10 to 50 nM CHK1i dose transition was also apparent in cell cycle populations at 24 hours post treatment. The S phase population decreased and G2/M population increased as the concentration of CHK1i increased from 10 nM to 50 nM (**Fig. 4.2A and 4.2B**). Similarly, DNA synthesis significantly decreased as the concentration of CHK1i increased above 10 nM (**Fig. 4.2C**). This increase in the G2/M population suggested a G2/M arrest so levels of the G2/M markers, pH3 and cyclin B1, were assessed. Distinct pH3-Low and pH3-High populations were observed (**Fig 4.2D**). The pH3-Low population was present in late S phase and G2/M population while the pH3-High population was restricted to G2/M (**Fig. 4.2E**) suggesting that the pH3-Low population represented a pre-mitotic population while pH3-High population was the mitotic

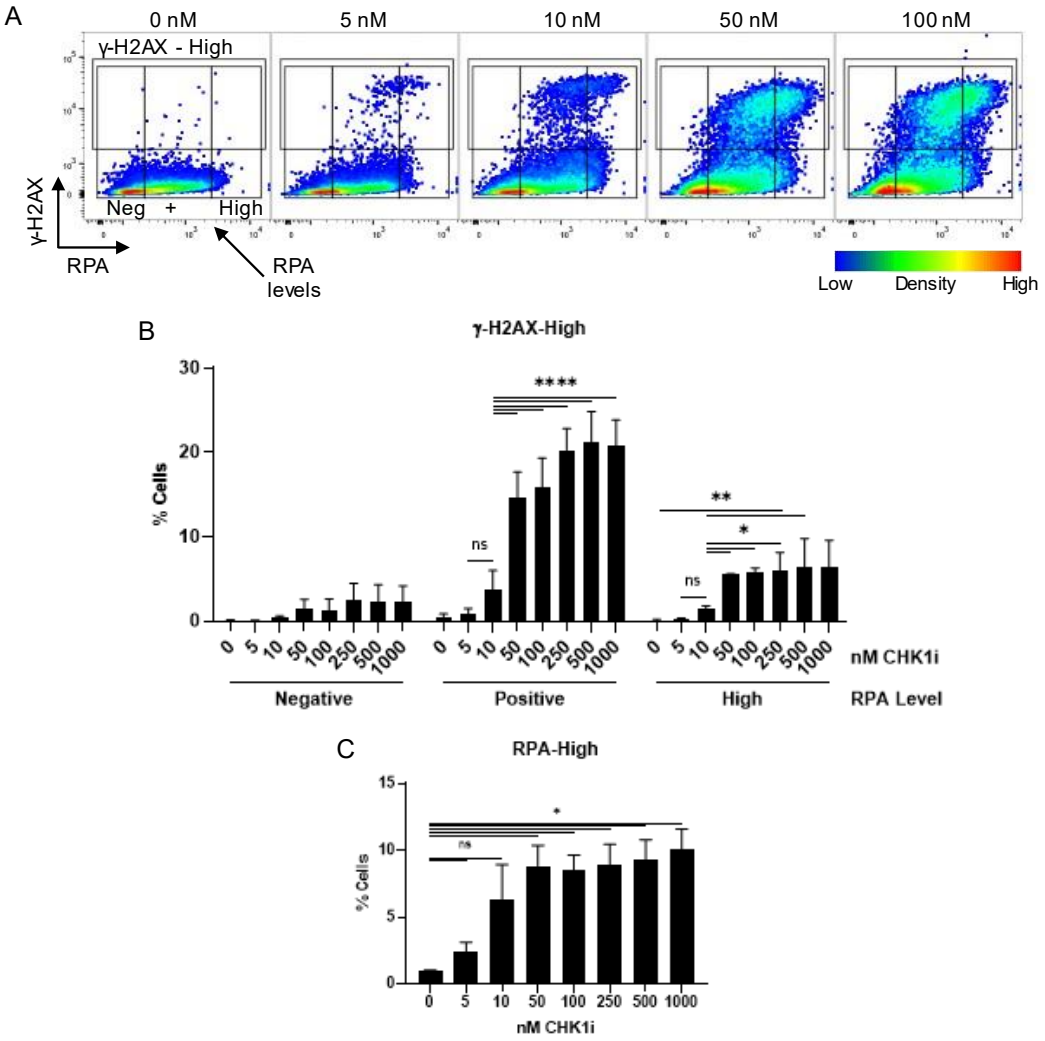

Figure 4.1. CHK1i induces replication catastrophe in a concentration-dependent manner

A-C) Induction of RPA exhaustion by CHK1i. A549 cells were treated with the denoted concentrations of CHK1i for 24h and chromatin-bound RPA and γ-H2AX levels were assessed by chromatin flow cytometry. A) Density dot plots comparing chromatin levels of γ-H2AX vs RPA for increasing concentrations of CHK1i. B) % Cells γ-H2AX-High in each RPA population. C) % cells in RPA-High population.

N=3. Mean ± SEM. ANOVA with Tukey correction; *, $p<0.05$; **, $p<0.01$; ***, $p<0.001$; ****, $p<0.0001$.

Figure 4.2. S phase and G2/M population identities are lost at CHK1i concentrations that trigger replication stress

A549 cells were treated with the denoted concentrations of CHK1i for 24 hours and then assessed for cell cycle phenotypes in the following assays.

A-C) Cell cycle distribution and DNA synthesis after CHK1i treatment. A) Pseudocolored density dot plots of the cell cycle population for increasing concentrations of CHK1i B) % cells in cell cycle populations from A) and C) Relative EdU incorporation for the denoted concentrations of CHK1i. For C) EdU incorporation normalized to 0 nM.

D-G) Levels of pH3 after CHK1 inhibition. D) Pseudocolored density dot plot showing the pH3 population in 0 nM CHK1i. E) Pseudocolored density dot plots showing the cell cycle distribution of the different pH3 populations. F) % cells of denoted cell phase that are pH3-Low G) % cells of denoted cell phase that are pH3-High.

H and I) cyclin B1 levels during the cell cycle phases after CHK1i treatment. H) Dot plot cyclin B1 levels vs EdU incorporation overlaid with cell cycle populations. I) Relative cyclin B1 levels in the denoted cell cycle phases at the listed CHK1i concentrations. Cyclin B1 levels were normalized to the S phase levels in 0 nM.

N=3. Mean ± SEM. ANOVA with Tukey correction; *, $p<0.05$; **, $p<0.01$; ***, $p<0.001$; ****, $p<0.0001$.

Figure 4.2. (cont.)

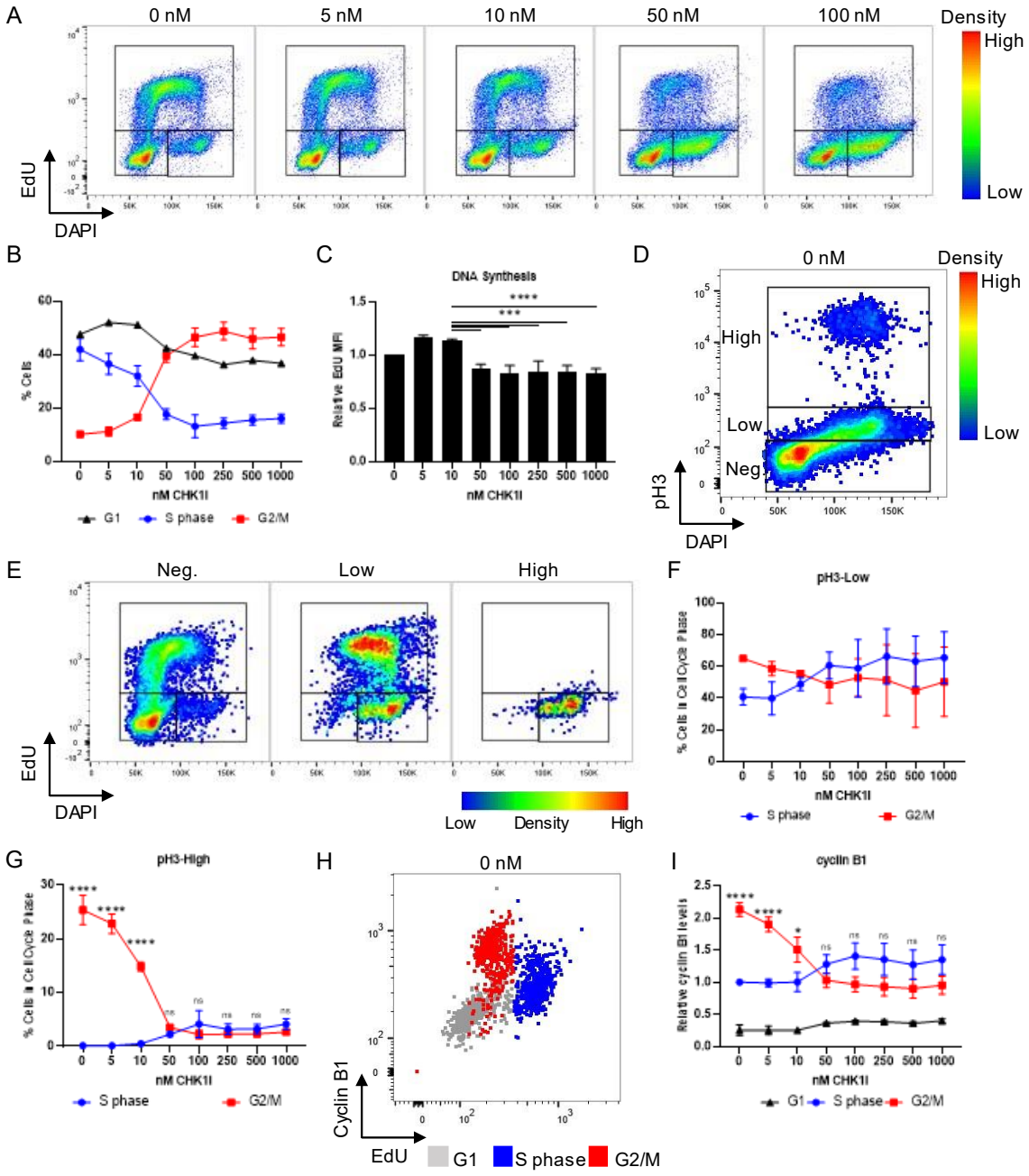

population of interest. The fraction of S phase and G2/M cells that were pH3-Low were similar and didn't change with CHK1i treatment (**Fig. 4.2F**). In contrast, the fraction of pH3-High cells that were in G2/M was significantly higher than in S phase in the absence of CHK1i but converged as CHK1i concentration increased and were not significantly different at concentrations 50 nM and greater (**Fig 4.2.G**). Cyclin B1 levels in A549 cells were significantly higher in G2/M compared to S phase in the absence of CHK1 inhibition (**Fig. 4.2H and 4.2I**). Similar to pH3, the difference in cyclin B1 levels between S phase and G2/M disappear at 50 nM CHK1i or higher with cyclin B1 levels increasing in S phase and decreasing in G2/M. The loss of DNA replication and convergence of cyclin B1 and pH3 levels in S phase and G2/M indicated concentrations of CHK1i sufficient to trigger replication catastrophe also compromised distinctions between the S and G2/M phases of the cell cycle.

Sufficient CHK1i to trigger DNA replication also compromises spindle assembly checkpoint

CHK1 helps to maintain G2/M cell cycle identity late in the cell cycle by phosphorylating Aurora B, which in turn activates BUBR1 to facilitate MCC formation (Ditchfield et al., 2003; Petsalaki et al., 2011). To determine if the loss of G2/M identity triggered by CHK1i involved CHK1-dependent regulation of the SAC, Aurora B activity and APC/C levels were assessed by immunoblot in nocodazole synchronized cells treated with sufficient (100 nM) or insufficient (10 nM) concentrations of CHK1i to trigger replication catastrophe. Aurora B activity was inhibited by 100 nM, but not 10 nM, of CHK1i (**Fig. 4.3A**). Furthermore, levels of APC/C substrates, CDC20, FOXM1, cyclin B1, etc., were not decreased at 10 nM but were lost at 100 nM of CHK1i. Thus, sufficient CHK1 inhibition to trigger DNA replication catastrophe was required to block Aurora B activation and trigger the loss of APC/C substrates.

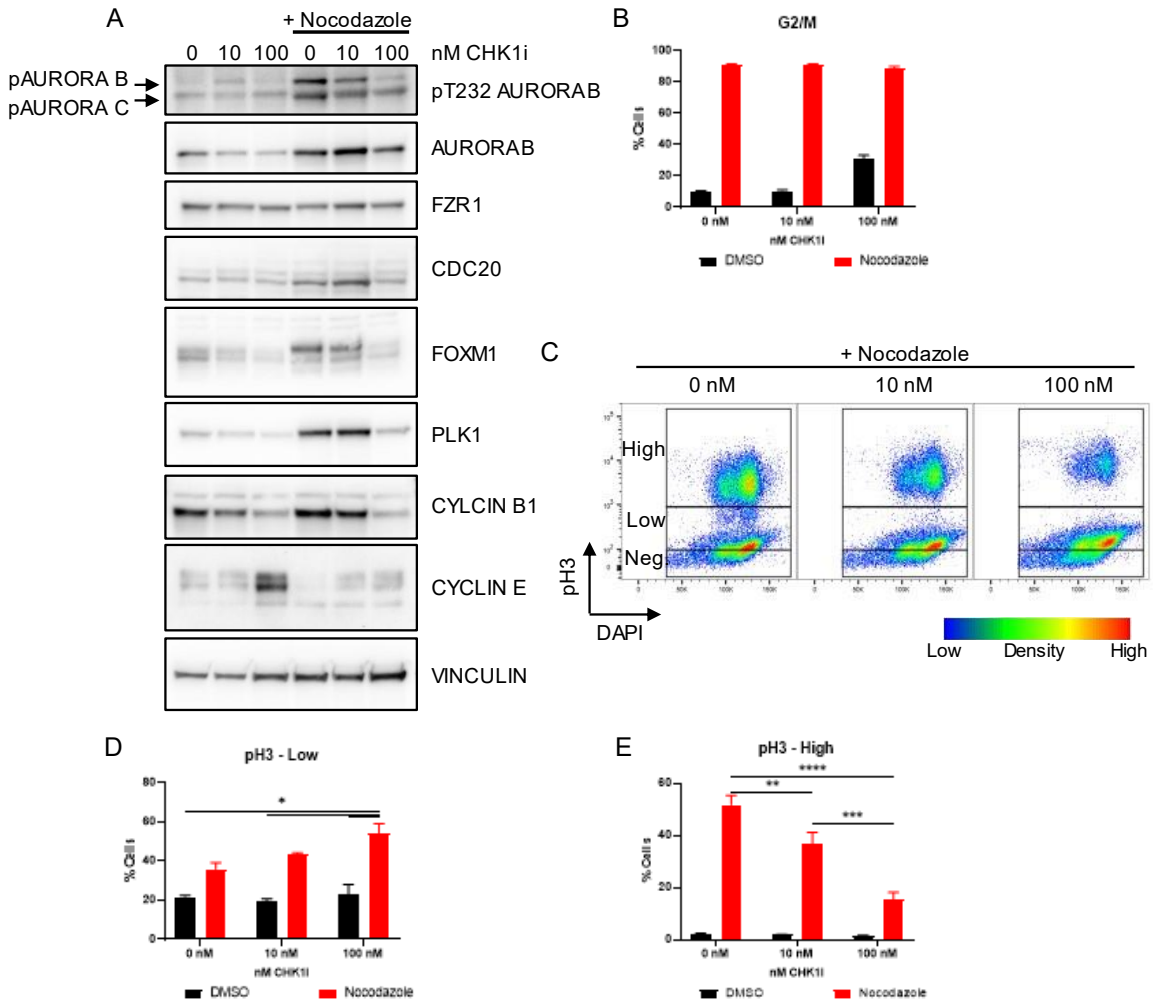

Figure 4.3. CHK1i inhibits Aurora Kinase B activity and compromises the SAC checkpoint at concentrations that trigger replication catastrophe

A549 cells were treated with the denoted concentrations of CHK1i in the presence or absence of nocodazole for 24 hours.

A) Immunoblot of lysates for Aurora B activity and APC/C substrates.

B-E) Analysis of pH3 staining in synchronized cells. B) % cells in G2/M as determined from EdU vs. DAPI plot. C) Pseudocolored density dot plots of pH3 vs DAPI denoting the pH3 populations. D) % cells pH3 - Low at the denoted CHK1i concentrations ± nocodazole. E) % cells pH3 - High at the denoted CHK1i concentrations ± nocodazole.

N=3. Mean ± SEM. ANOVA with Tukey correction; *, $p<0.05$; **, $p<0.01$; ***, $p<0.001$; ****, $p<0.0001$.

The loss of APC/C substrates at 100 nM CHK1i suggested that the SAC was compromised after CHK1i. Compromising the SAC can lead to mitotic slippage, where the cell completes mitosis without undergoing cytokinesis, causing polyploidy or mitotic catastrophe (Castedo et al., 2004; Zeng et al., 2019). To determine if CHK1i triggered mitotic slippage, pH3 levels were assessed in nocodazole-synchronized cells treated with 10 nM and 100 nM CHK1i. Similar levels of G2/M synchronization was achieved by nocodazole synchronization at all CHK1i concentrations (**Fig. 4.3B**). While pH3-Low levels slightly increased with 100 nM CHK1i in the nocodazole-synchronized samples, there was a dose dependent effect of CHK1i on the pH3-High population with 100 nM CHK1i being significantly lower than 0 or 10 nM CHK1i (**Fig. 4.3 C-E**). Although pH3-High levels significantly decreased with 10 nM CHK1i, the presence of cyclin B1, FOXM1, and other APC/C substrates indicates that the SAC is still intact. These results show that replication and mitotic catastrophe are induced by a similar level of CHK1 inhibition, which compromises the G2/M identity via CHK1-dependent regulation of the APC/C.

APC/C substrates are degraded in S phase after CHK1i as FBXO5 is prematurely lost

To determine if CHK1i prematurely activated the APC/C during S phase, APC/C substrates levels were assessed in synchronized A549 treated with 10 nM or 100 nM CHK1i. Cells were synchronized by thymidine block overnight then released for one hour followed by addition of CHK1i. In untreated synchronized cells, entry into mitosis and activation of the APC/C is expected to occur about 10 hours after release from a thymidine block. We observed that 100 nM but not 10 nM CHK1i was sufficient to trigger the loss of APC/C substrates, cyclin B1, cyclin A2, Aurora B, PLK1, and FOXM1, at 6 hours post treatment in S phase (**Fig 4.4**). Loss of cyclin B1 could be observed as early as 4 post hours treatment of 100 nM CHK1i. Although protein levels were decreased, 100 nM CHK1i treatment led to increased levels of *CCNB1* and *CCNA2* transcripts at 4 hours post treatment (**Fig 4.5A and 4.5B**). In addition, proteasome inhibition blocked the decrease in APC/C substrate protein levels (**Fig 4.5C**)

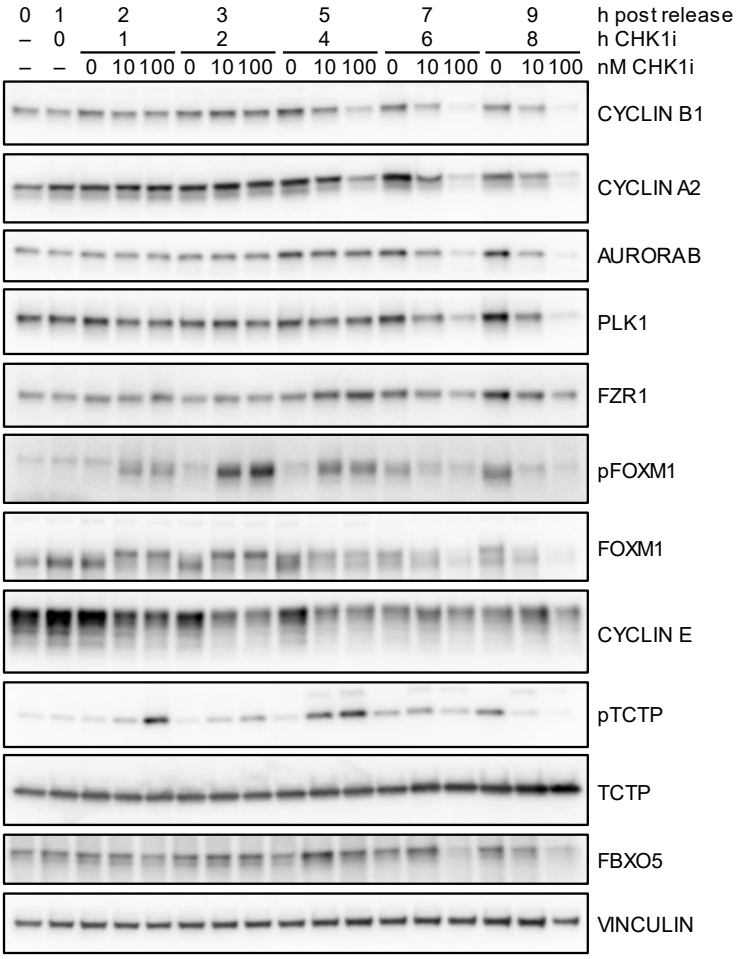

Figure 4.4. APC/C substrates and EMI1 protein levels decrease after CHK1i treatment in a concentration-dependent manner

Immunoblot of A549 lysates synchronized via a single thymidine block and treated 1 hour post release with the denoted concentrations of CHK1i. Whole cell lysates were generated and blotted with antibodies for the listed proteins.

Figure 4.5. CHK1 inhibition leads to premature APC/C activation

A and B) RT-qPCR of A) CCNB1 and B) CCNA2 in A549 cells after treatment with 100 nM CHK1i starting 1 hour post release from a single thymidine block.

C) Immunoblot of APC/C substrate levels after proteasome inhibition. A549 cells were synchronized and were treated as in A) with combinations of 100 nM CHK1i or 100 nM bortezomib for the denoted time periods.

D) Immunoblot of APC/C substrates after knockdown of individual APC/C co-activators. A549 cells were transduced with siRNA then synchronized by single thymidine 24 hours post transfection. Synchronized samples were then released and treated as in A) with 100 nM CHK1i for times denoted.

Figure 4.5. (cont.)

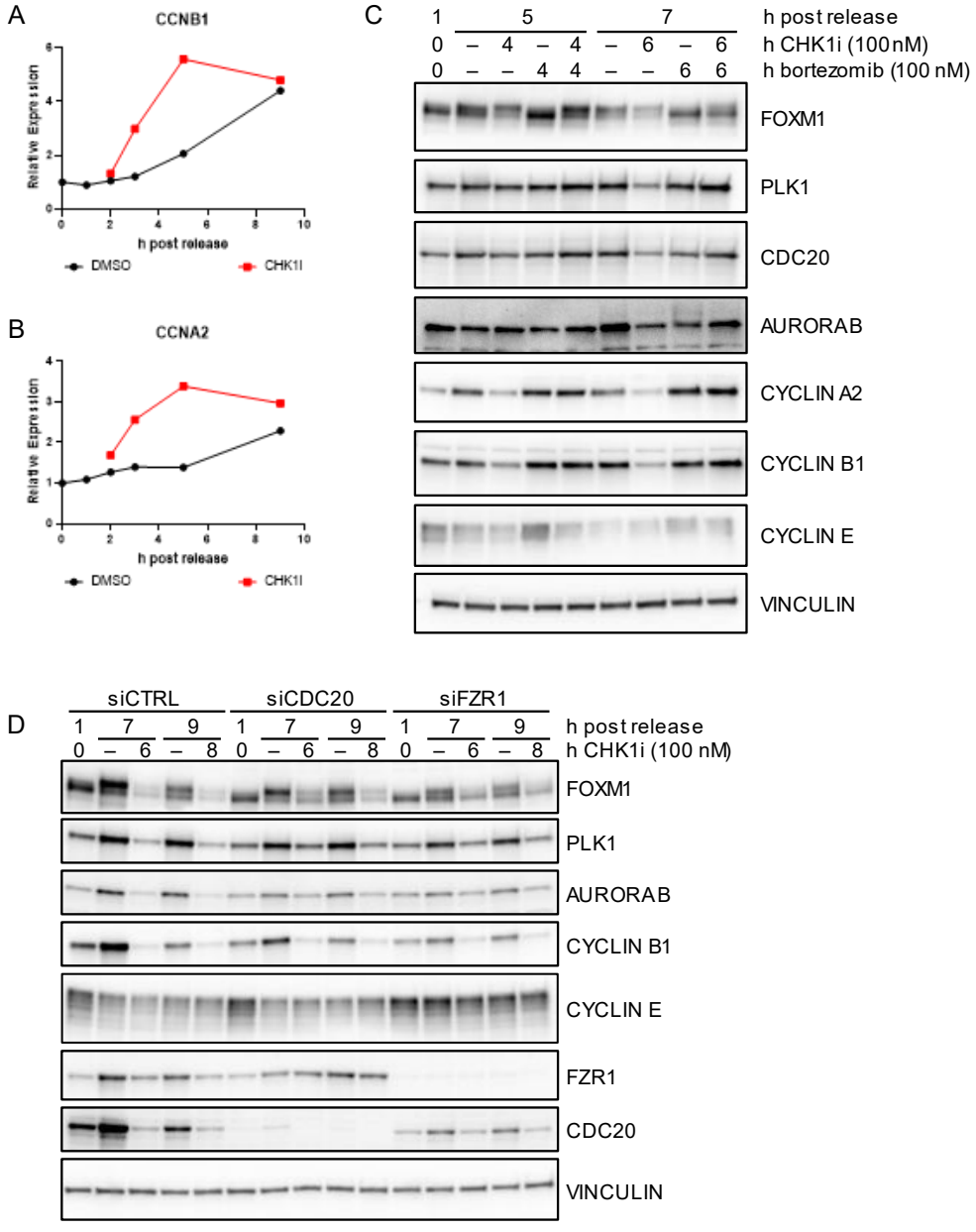

pointing to premature activation of the APC/C.

Knockdown of either APC/C co-activators FZR1 or CDC20 led to partial rescue of protein levels of the APC/C substrates AURKB and FOXM1 but was unable to rescue cyclin B1 (**Fig 4.5D**) suggesting the CHK1i activates both FZR1 and CDC20-containing APC/C complexes. Consistent with this hypothesis, FBXO5 was lost in the CHK1i 100 nM treated samples at 6 and 8 hours post treatment (**Fig. 4.4**). FBXO5 can inhibit either FZR1 or CDC20 containing complexes by blocking substrate binding (Reimann et al., 2001a; Reimann et al., 2001b). Of note, both 10 nM and 100 nM CHK1i were able to induce premature phosphorylation of pFOXM1 indicating that even low levels of CHK1 inhibition can induce CDK1 activity. A critical level of cyclin A/CDK1 activity triggers PLK1 activation during the S/G2 transition, which leads to phosphorylation of PLK1 substrate TCTP (Lemmens et al., 2018). 100 nM however induced pTCTP earlier than 0 nM or 10 nM CHK1i indicating that a higher level of CDK1 activity was induced by 100 nM CHK1i. PLK1 activity in G2 results in the degradation of APC/C-negative regulator, FBXO5 by an SCF complex (Hansen et al., 2004; Moshe et al., 2004). The induction of PLK1 activity by 100 nM CHK1i before 0 or 10 nM CHK1i would explain the loss of FBXO5 and subsequent degradation of APC/C substrates. The premature loss of FBXO5 and subsequent APC/C substrate loss in the only 100 nM CHK1i samples suggests that premature APC/C activity was also induced in S phase.

CHK1 inhibition sufficient for DNA replication catastrophe impairs DNA replication and triggers APC/C-dependent loss of replication factors

Premature loss of FBXO5 and APC/C activation during S phase has been previously implicated in genome rereplication (Di Fiore and Pines, 2007; Machida and Dutta, 2007). This effect could implicate premature APC/C activation in CHK1i-induced S phase identity loss and replication catastrophe. To determine if CHK1i induced DNA rereplication, DNA content was examined two days post CHK1i treatment. Reduplication in A549 cells however can be

restricted by p53 (Vaziri et al., 2003). To control for any p53-dependent effects, H23 cells, a NSCLC cell line with mutant p53, was included. Single cells were identified by comparing the FSC-A and FSC-H rather than DAPI stain to prevent any bias against >4N populations (**Fig. 4.6A**). An increase in the >4N population was induced by 50 and 100 nM CHK1i with little change at 10 nM or lower CHK1i in both cell types (**Fig 4.6B**). This indicates that DNA rereplication can be induced independent of p53 status at CHK1i concentrations sufficient to trigger DNA replication catastrophe and compromise the SAC.

EdU levels in the >4N population however were lower at higher concentration of CHK1i (**Fig. 4.6B**) indicating that DNA replication was impaired in rereplicating cells. It could be that fewer cells were undergoing DNA replication or that DNA replication was being impaired in cells that were replicating their genomes. To differentiate between these two models, DNA synthesis was measured in cells along with chromatin-bound PCNA, a marker for active replication forks (Sirbu et al., 2013). The percentage of cells with chromatin bound-PCNA decreased slightly in A549 cells with increasing CHK1i concentrations while remaining unchanged in H23 cells (**Fig. 4.7B**) indicating that a similar number of cells were undergoing DNA replication. The PCNA positive population can be divided into a High population, where robust DNA synthesis is occurring and a smaller low PCNA population that appear to be transition into and out of S phase (**Fig. 4.7A and 4.7G**). In both A549 and H23 cells the levels of PCNA-High cells decreased with at 100 nM CHK1i while there was a smaller but corresponding increase in the PCNA-Low population (**Fig. 4.7C and 4.7D**) suggesting that cells have fewer active replication forks at higher CHK1i concentrations that trigger APC/C activity. In addition to fewer replication forks, 100 nM CHK1 also impaired DNA synthesis as EdU incorporation in PCNA populations decreased significantly with 100 nM CHK1i (**Fig 4.7E and 4.7F**). Reflecting this decreased DNA synthesis, the PCNA- Low population shifted from early S phase to G2/M in both A549 and H23 (**Fig. 4.7 G-I**) indicating that the PCNA low population shifted from cells entering S phase to

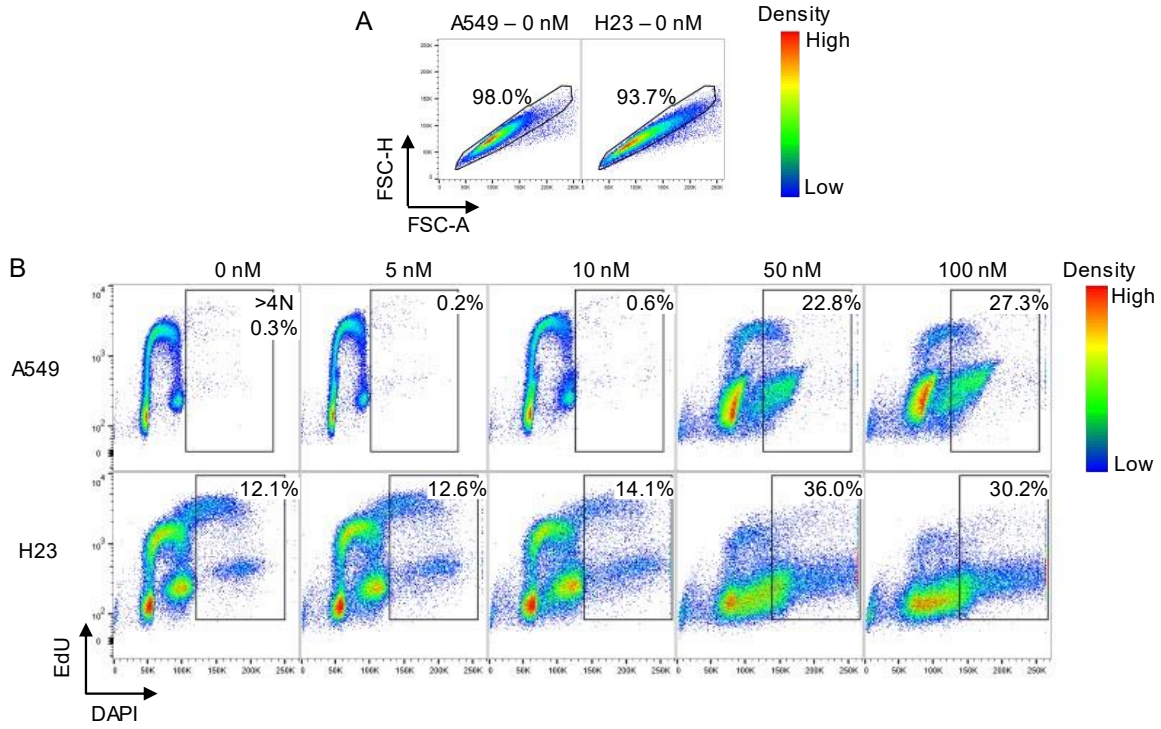

Figure 4.6. Genome reduplication is triggered by concentration of CHK1i sufficient for replication catastrophe

A549 or H23 cells were treated with the denoted concentration of CHK1i for 48 hours and pulsed with EdU for the last 30 min. Cell cycle distribution was determined using EdU and DAPI staining.

A) Pseudocolored density dot plots of FSC-H vs FSC-A used to identify single cells in this experiment.

B) Pseudocolored density dot plots of EdU vs DAPI displaying the >4N gate.

Figure 4.7. CHK1 disrupts DNA replication in a concentration-dependent manner

A549 and H23 cells were treated with the denoted concentrations of CHK1i for 24 hours and pulse with EdU for the last 30 min. Active DNA synthesis was examined using chromatin flow and staining for EdU, PCNA and DAPI.

A-D) Chromatin-bound PCNA levels after CHK1i treatment. A) Pseudocolored density dot plot showing chromatin-bound PCNA vs DAPI levels. Gates denote the particular PCNA populations. B) % cell positive for chromatin-bound PCNA, C and D) % cells with low or high levels of chromatin-bound PCNA in C) A549 cells and D) H23 cells.

E and F) DNA synthesis after CHK1i. Relative EdU incorporation in PCNA-Low and PCNA-High population in E) A549 cells and F) H23 cells.

G-I) Cell cycle distribution of cells with chromatin bound PCNA. G) Pseudocolored density dot plot showing cell cycle distribution of PCNA-Low and PCNA-High cells at the denoted CHK1i concentrations. Graphs showing the cell cycle populations at the denoted CHK1i concentrations in H) A549 cells and I) H23 cells for both PCNA-Low and PCNA-High cells.

N=3. Mean ± SEM. ANOVA with Tukey correction; *, $p<0.05$; **, $p<0.01$; ***, $p<0.001$; ****, $p<0.0001$.

Figure 4.7. (cont.)

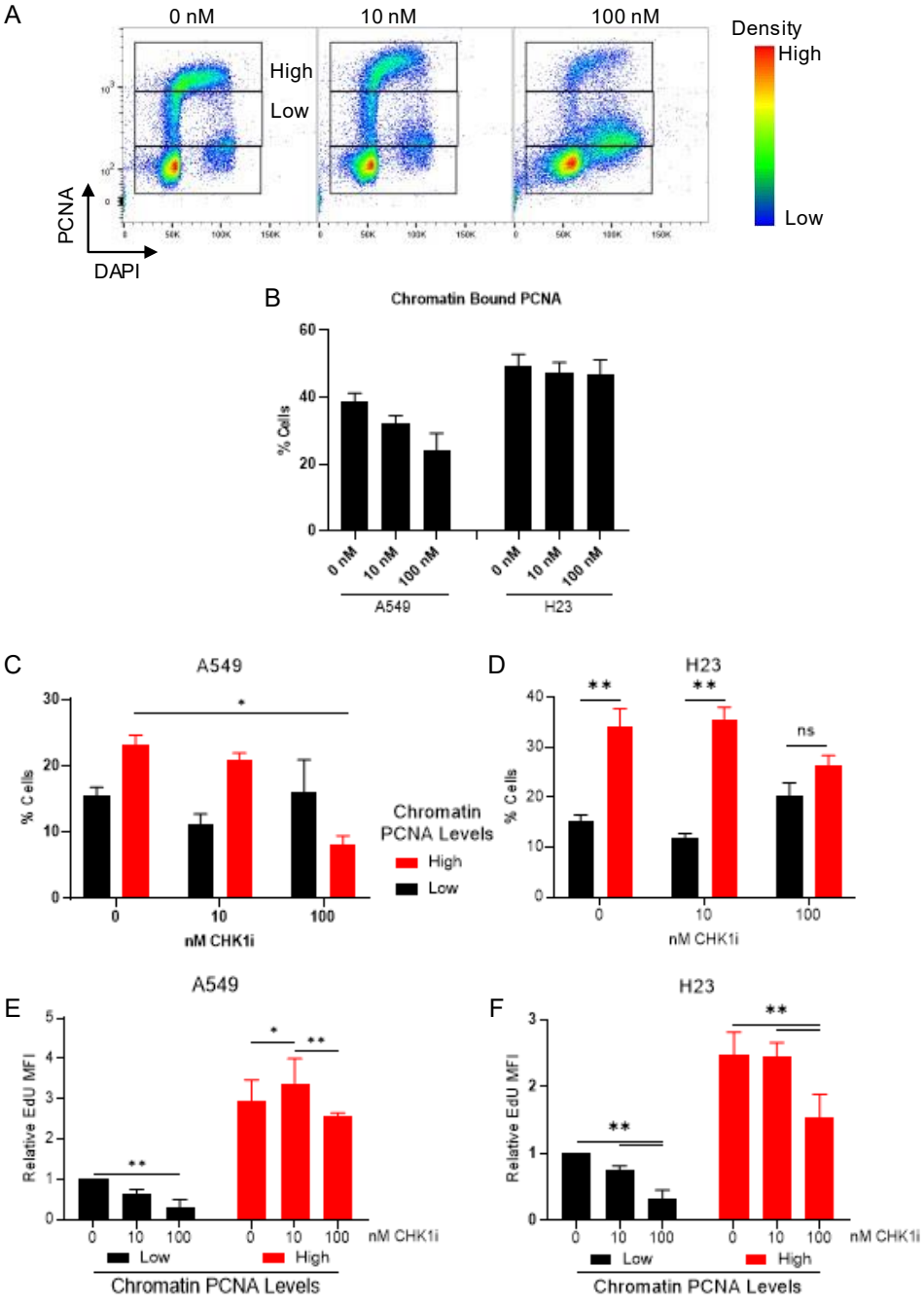

Figure 4.7. (cont.)

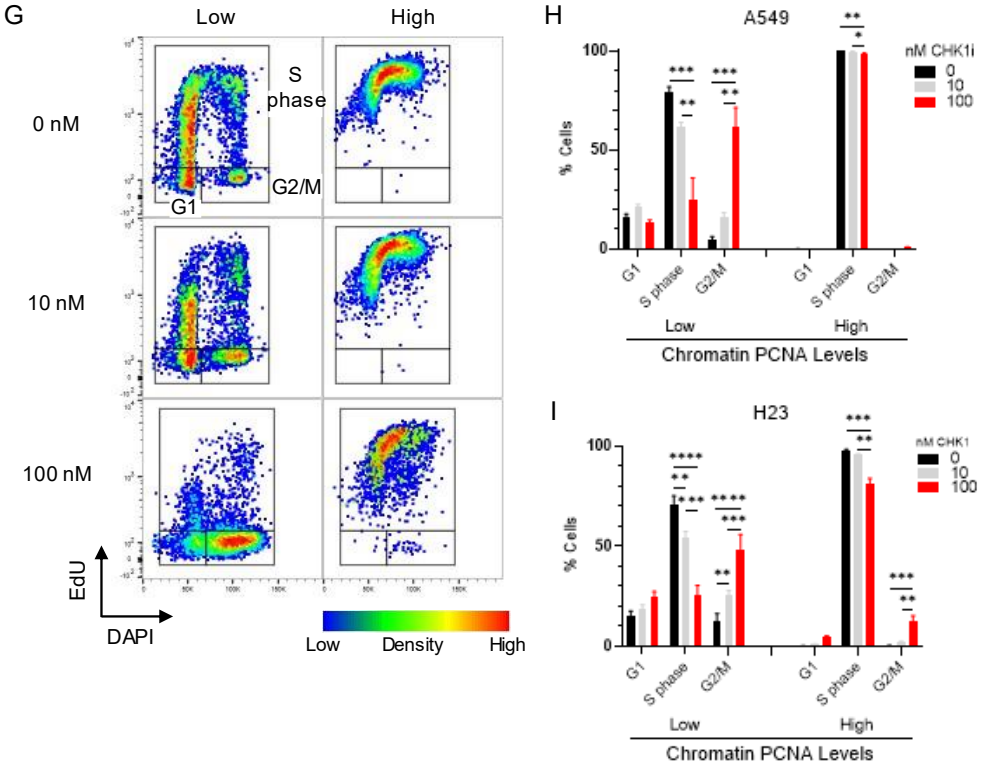

replicating cells with impaired DNA synthesis. While a small-but-significant shift to G2/M at 100 nM occurred in the PCNA-High cells H23 cells, the vast majority of PCNA-High regardless of CHK1i concentration were still in S phase showing that a smaller population of cells are still able to replicate their genome 24 hours after CHK1 inhibition. Together, this data indicates that DNA replication is impaired at concentrations of CHK1 sufficient to trigger APC/C activity in S phase.

The impairment of DNA synthesis at 100 nM but not 10 nM CHK1i raised the possibility that DNA synthesis was impaired after CHK1 inhibition due to premature activation of the APC/C. The APC/C has been previously implicated in the degradation of the DNA origin licensing factors CDC6, CDT1, geminin and ORC1 (Araki et al., 2003; Clijsters et al., 2014; McGarry and Kirshcner, 1998; Peterson et al., 2000; Sugimoto et al., 2008). Levels of CDC6, CDT1, and geminin, similar to cyclin B1, decreased at 50 nM or higher of CHK1i in both A549 and H23 cells (**Fig 4.8A**). Further, proTAME, an APC/C inhibitor that blocks APC/C co-activator binding (Zeng et al., 2010), prevented the loss of geminin, CDC6, and to a lesser extent CDT1 in addition to rescuing Aurora B, cyclin A2, and cyclin B1 levels (**Fig. 4.8B and 4.8C**) indicating that APC/C activity is required for CHK1i-induced loss of origin licensing factors.

Activation of the mitotic transcriptional program is required for impaired DNA synthesis after CHK1i treatment

Premature mitosis driven by an MMB-FOXM1-CDK1 positive feedback loop was recently implicated in CHK1i sensitivity (Branigan et al., 2021). Phosphorylation of APC1 and APC3 by CDK1 promotes APC/C complex formation (Fujimitsu et al., 2016) suggesting that premature APC/C activation was triggered by this MMB-FOXM1-CDK1 feedback loop after CHK1 inhibition. To determine if APC/C-dependent degradation of licensing factors required premature activation of the mitotic program, levels of CDC6, geminin and CDT1 were examined in LIN54 KO and FOXM1 KO cells after CHK1i treatment. In contrast to EV control cells, CDC6, CDT1, and geminin protein levels did not decrease with CHK1i in LIN54 or FOXM1 KO cells (**Fig. 4.9A**)

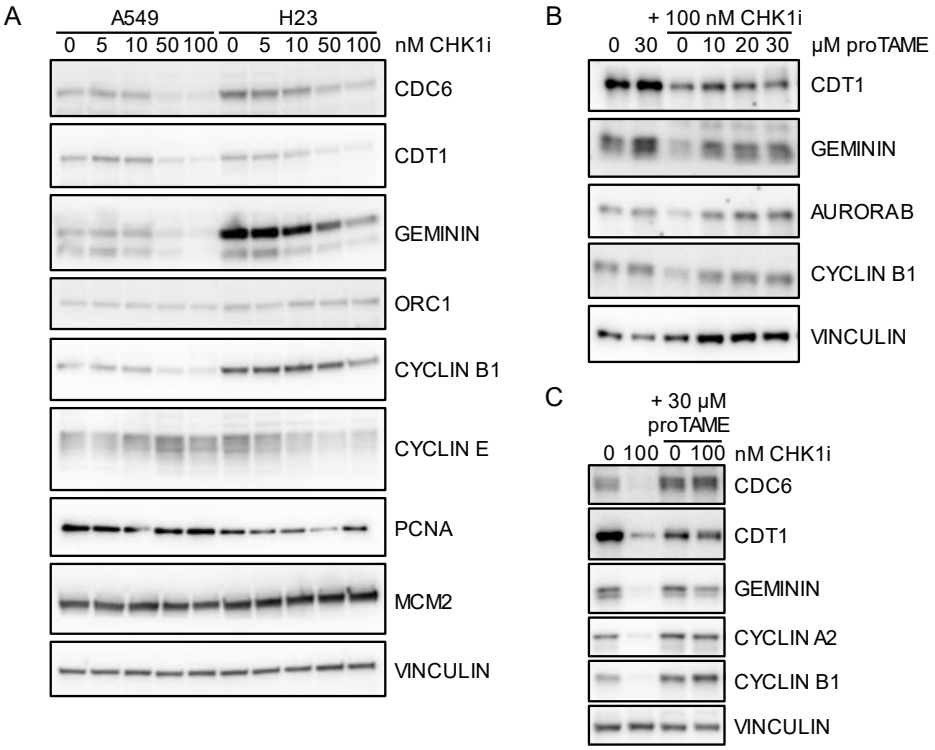

Figure 4.8. DNA Licensing Factors are degraded in APC/C dependent manner at concentrations of CHK1i that trigger replication catastrophe

A) Immunoblot of DNA origin licensing factors after CHK1i treatments. A549 or H23 cells were treated with the listed concentrations of CHK1i for 24 hours. Whole cell extracts were generated and probed by immunoblot with antibodies for the denoted proteins.

B and C) Immunoblot showing APC/C dependent-loss DNA origin licensing factors. A549 cells were treated for 24 hours with 100 nM CHK1i in concentrations with B) increasing dose of the APC/C inhibitor, proTAME or C) 30 µM proTAME.

Figure 4.9. Disruption of DNA replication by CHK1i requires activation of the mitotic transcriptional program

A) Immunoblot of DNA origin licensing factors in LIN54 KO and FOXM1 KO cells after CHK1i treatments. EV, LIN54 KO, and FOXM1 KO cells were treated with 100 nM CHK1i for 24 hours. Whole cell extracts were generated and probed by immunoblot with antibodies for the denoted proteins.

B-G) DNA replication in LIN54 KO and FOXM1 KO A549 cells. EV, LIN54 and FOXM1 cells were treated with 100 nM CHK1i for 24 hours and pulsed with EdU for the last 30 min. Chromatin flow cytometry for EdU, PCNA, MCM2, and DAPI was performed to assess DNA replication. B) % cells in S phase C) Relative EdU incorporation. Background subtracted EdU MFIs were normalized to sgEV-DMSO. D) Pseudocolored density dot plot showing chromatin-bound PCNA vs DAPI levels. Gates denote the particular PCNA populations. E) % cell positive for chromatin-bound PCNA F) % cells with low or high levels of chromatin-bound PCNA G) Pseudocolored density dot plot showing cell cycle distribution of PCNA-Low and PCNA-High cells at the denoted CHK1i concentrations. H) Cell cycle distribution of the PCNA-Low population I) Histograms of chromatin-bound MCM2 levels in the PCNA populations identified in D).

N=3. Mean ± SEM. ANOVA with Tukey correction and mixed effects analysis; *, $p<0.05$; **, $p<0.01$; ***, $p<0.001$; ****, $p<0.0001$.

Figure 4.9. (cont.)

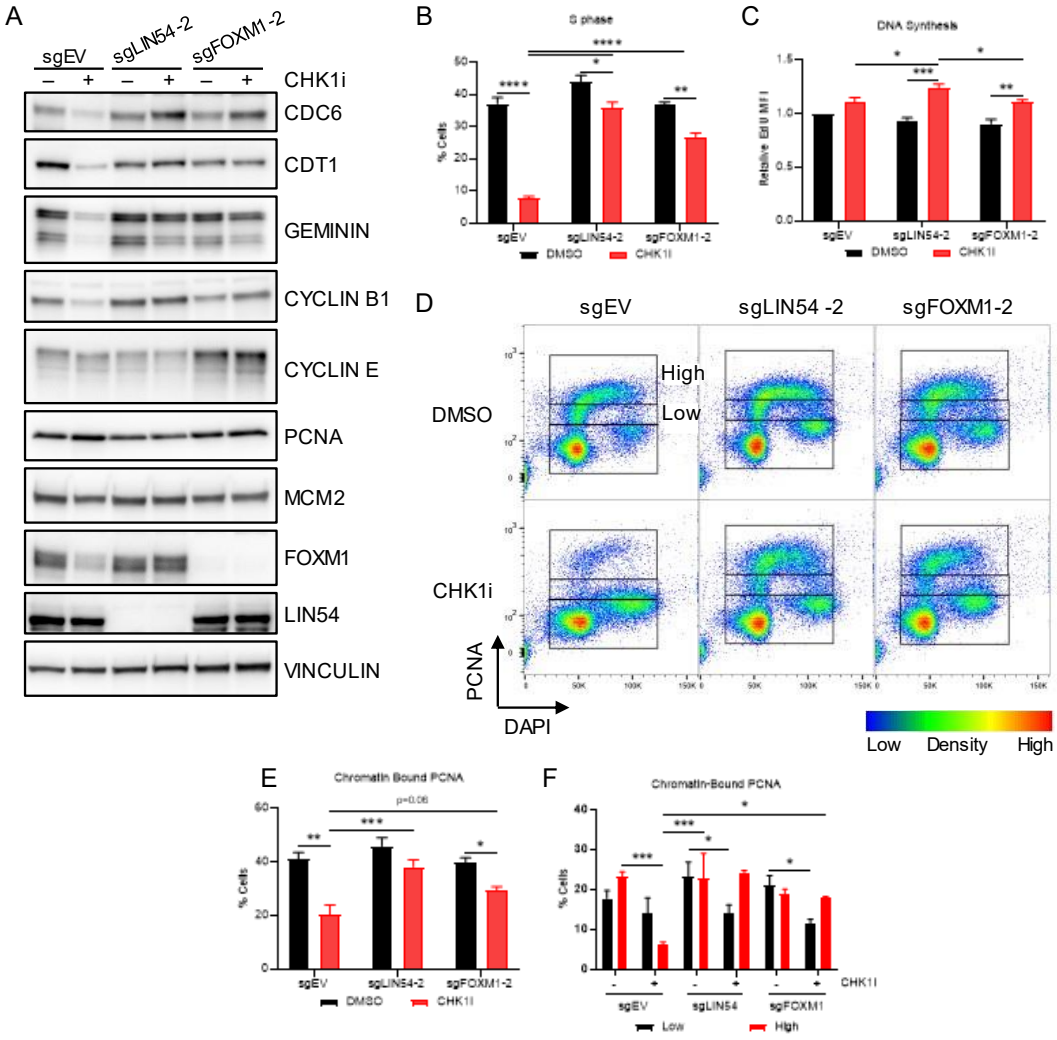

Figure 4.9. (cont.)

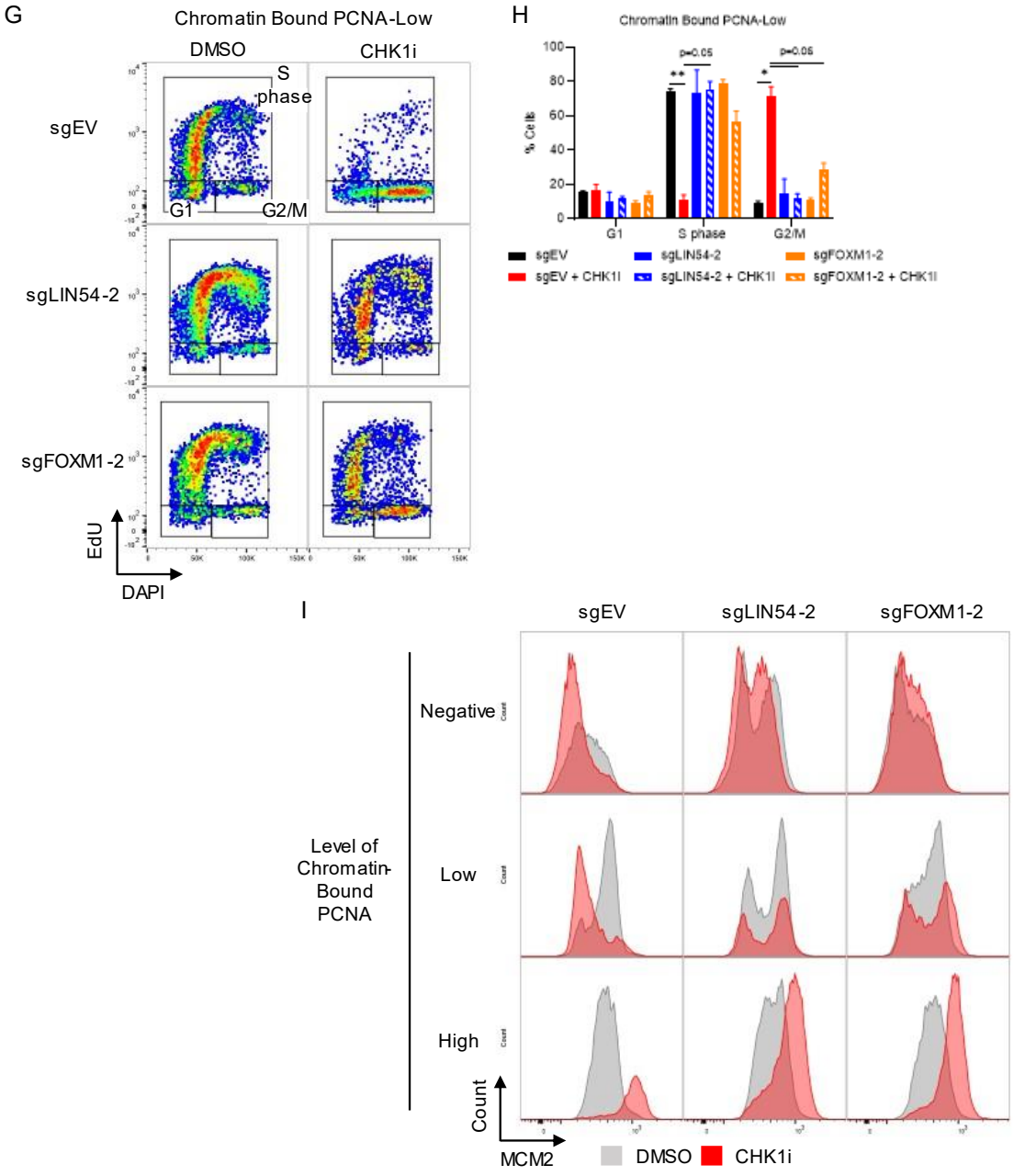

indicating that premature activation of the mitotic program is required for premature APC/C activation.

To determine if activation of the mitotic program was also required for impaired DNA synthesis after CHK1 inhibition, DNA synthesis via EdU incorporation was assessed in LIN54 KO and FOXM1 KO cells along with chromatin-bound PCNA, to measure active replication forks, and chromatin-bound MCM2, to assess loaded MCM helicase resulting from origin licensing (Matson et al., 2016). LIN54 and FOXM1 KO cells had a significantly higher S phase populations compared to EV after CHK1i treatment although these populations were significantly decreased compared to the respective DMSO samples. Strikingly, DNA synthesis was significantly higher in the LIN54 and FOXM1 KOs after CHK1i treatment. Active replication forks were also maintained in the LIN54 KO and FOXM1 KO cells after CHK1 inhibition (**Fig 4.9D-4.9F**). In particular, LIN54 and FOXM1 KO cells did not lose the PCNA-high population like the CHK1i treated EV cells. This was also reflected in the cell cycle distribution of the PCNA-Low population as perturbation of the MMB-FOXM1 complex prevented the shift from early S phase to G2/M triggered by CHK1i that was observed in the EV cells (**Fig 4.9G and 4.9H**). In EV cells, chromatin-bound levels of MCM2 decreased in the PCNA-Negative and PCNA-Low populations after CHK1 inhibition while PCNA-High cells actually had increased chromatin-bound MCM2 (**Fig 4.9I**). Perturbation of the MMB-FOXM1 complex prevented the loss of the MCM2 in the PCNA-Low and PCNA-Negative populations but did not block the increased MCM2 levels in the PCNA-High population after CHK1i treatment. Together, this data shows activation of the mitotic transcriptional program is required for impaired DNA synthesis induced by CHK1i. Furthermore, it demonstrates that origin licensing is impaired after CHK1 inhibition in an MMB-FOXM1-dependent manner, consistent with APC/C-dependent degradation of and subsequent dysregulation of origin licensing as a potential mechanism by which the mitotic program could trigger DNA replication catastrophe.

Negative regulators of APC/C activity as potential biomarker for CHK1i sensitivity

The absence of CHK1i-induced DNA synthesis defects in LIN54 or FOXM1 KO cells was consistent with altered regulation of APC/C activity in these KO cells. Levels of APC/C substrates and CHK1i-altered regulators were assessed in LIN54 KO and FOXM1 KO cells. Strikingly, cyclin B1, Aurora B and PLK1 protein levels were not lost after 6 hours of CHK1i treatment in both LIN54 and FOXM1 cells compared to EV control cells (**Fig 4.10A**). Cyclin B1 levels overall however were lower in both LIN54 and FOXM1 KO cells. FBXO5 levels were also maintained after CHK1i in the LIN54 KO cells while, in the FOXM1 KO cells, FBXO5 levels along with AURKB and PLK1 levels actually increased with CHK1i. The increase in PLK1 may explain the higher levels of pTCTP observed in the FOXM1 KOs which were down slightly in the LIN54 KOs. While Aurora B levels were not higher in the nocodazole synchronized FOXM1 cells, there were higher levels of pAurora B suggesting increased Aurora B activity (**Fig 4.10B**). There were slight decreases in APC/C substrates in the FOXM1 KO but not in the LIN54 KO cells suggest that some premature APC/C activation may occur in the FOXM1 KO cells. Thus, LIN54 KO cells appear to be impeding APC/C by preventing FBXO5 loss while FOXM1 KO cells stymied premature APC/C activation by upregulating negative regulators of FBXO5 and Aurora B activity.

Consequently, FBXO5 and Aurora B could be potential biomarkers for CHK1i sensitivity given the retention of FBXO5 and AURKB protein species in the LIN54 KO and FOXM1 KO cells. Proteomic data from *Nusinow et al.* and CHK1 inhibitor sensitivity data from *Corsello et al.* were integrated using DepMap Data Explorer to determine if FBXO5 or Aurora B protein levels correlated with CHK1i sensitivity in cancer cell lines. In NSCLC cells, there was a weak but significant negative correlation between FBXO5 protein levels and sensitivity to CHK1i (**Fig. 4.11A**). FBXO5 protein levels in NSCLC cell lines, also negatively correlated with the CHK1 inhibitor PF-477736 while there was a negative trend the CHK1 inhibitor AZD7762 (**Fig. 4.11B**). While Aurora B levels didn't significant correlate with CHK1i sensitivity in NSCLC (**Fig. 4.11A**), a

Figure 4.10. Perturbation of the MMB-FOXM1 complex leads to increased expression of APC/C negative regulators after CHK1i

A) Immunoblot of EV, LIN54 KO and FOXM1 KO A549 lysates after synchronization by a single thymidine block and treated with 100 nM CHK1i at 1 hour post release. Whole cell lysates were generated and blotted with antibodies for the listed proteins.

B) Immunoblot of lysates for Aurora B activity and APC/C substrates in LIN54 KOs and FOXM1 KO cells. A549 EV, LIN54 KO and FOXM1 KO cells were treated with combinations of 100 nM CHK1i and 100 ng/ml nocodazole for 24 hours.

Figure 4.10. (cont.)

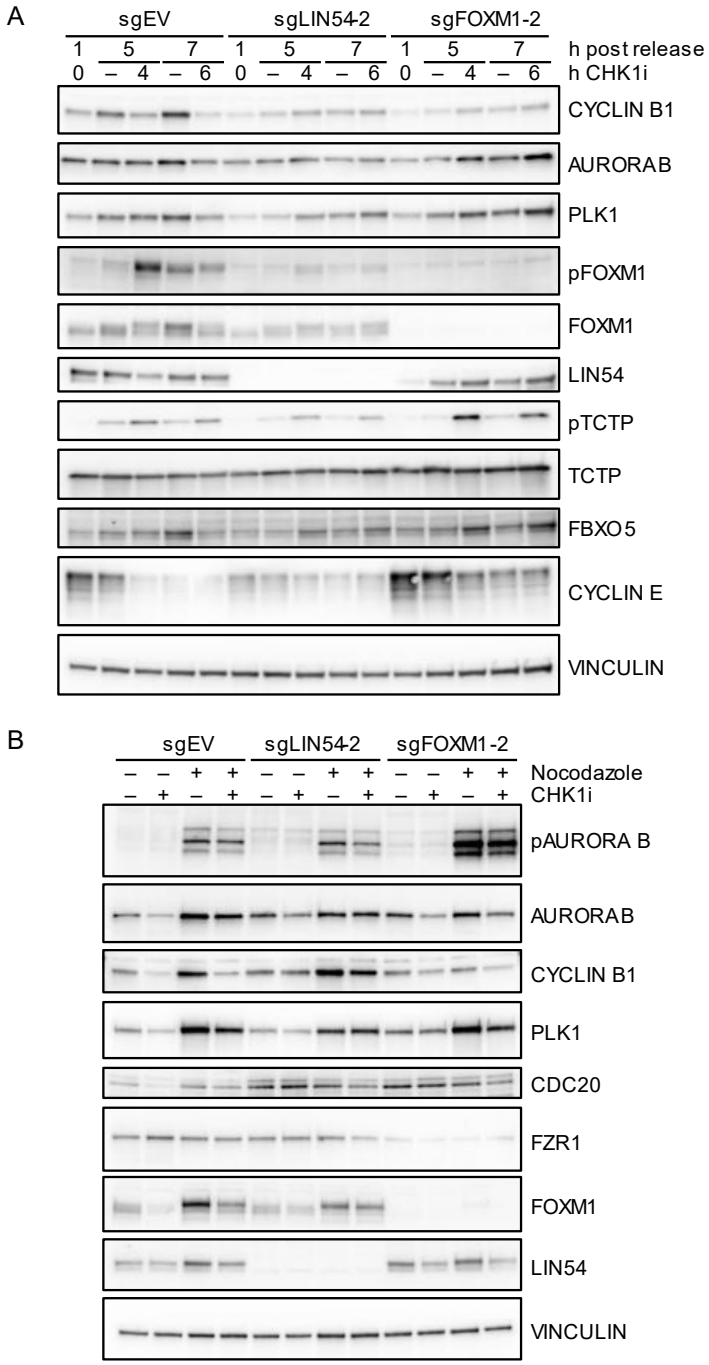

Figure 4.11. Levels of FBXO5 and Aurora B negatively correlate with CHK1i sensitivity

Comparison of FBXO5 and Aurora B protein levels from *Nusinow et al.* and CHK1 inhibitory sensitivity data from *Corsello et al.* using DepMap data explorer.

A) Dot plot comparing FBXO5 (left) and Aurora (right) protein levels and CHK1i sensitivity data in NSCLC cell lines.

B) Dot plot comparing FBXO5 protein levels and sensitivity data for CHK1 inhibitors PF-47736 (left) and AZD7762 (right) in NSCLC cell lines.

C and D) Dot plot comparing Aurora B protein levels and sensitivity data for CHK1 inhibitors prexasertib (left), PF-47736 (middle), and AZD7762 (right) in C) breast cancer cell lines and D) ovarian cancer cell lines.

Line of best fit, Pearson coefficient with p-value, number of cell lines (n) shown for each comparison.

Figure 4.11. (cont.)

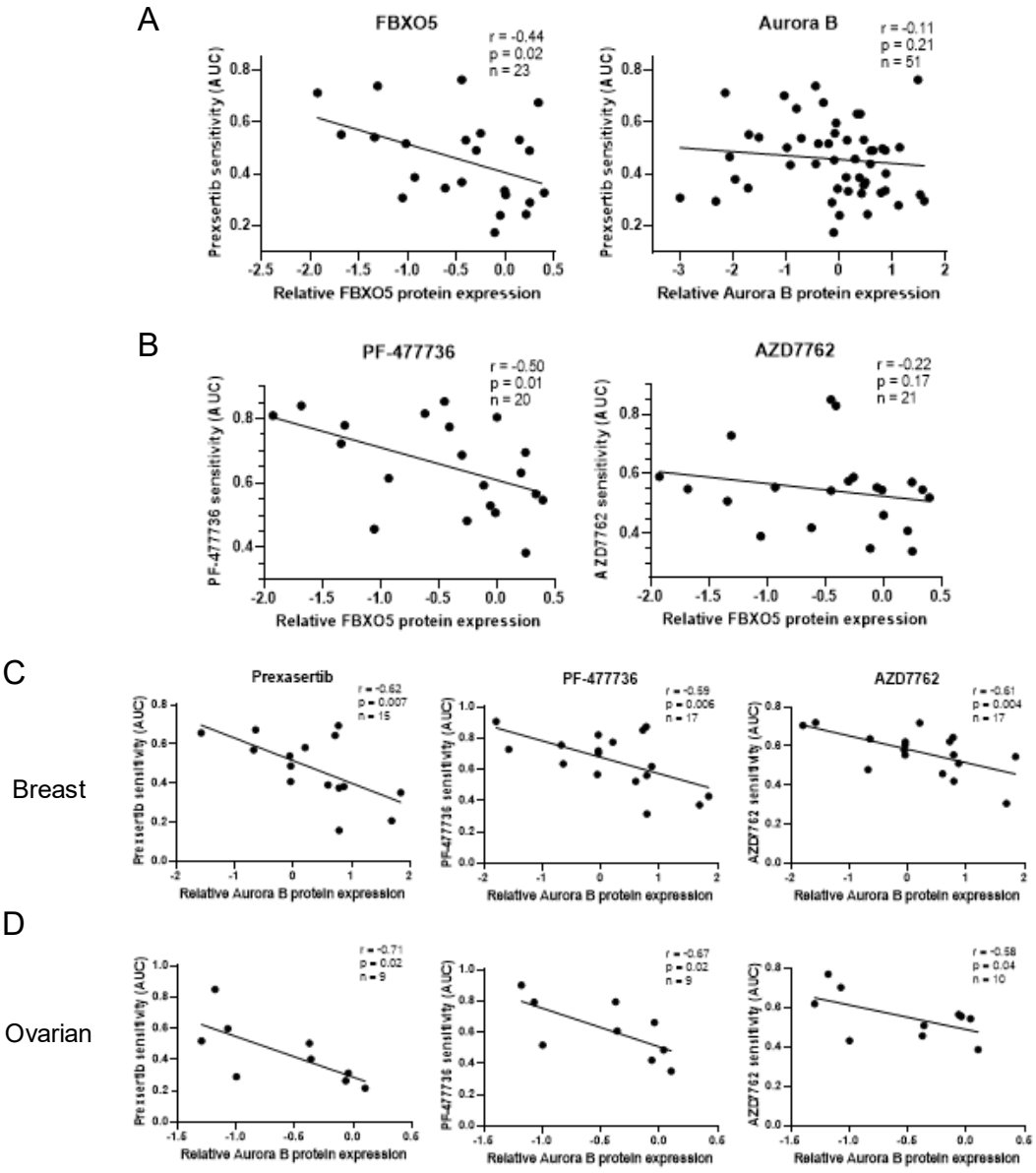

moderate to strong negative correlation between Aurora B protein levels and sensitivity to the CHK1 inhibitors prexasertib (CHK1i), PF477736, and AZD7762 in breast and ovarian cancer cell lines (**Fig. 4.11C and 4.11D**) indicating that negative regulators of APC/C activity could serve as potential biomarkers for CHK1i sensitivity in a cancer type-dependent manner.

Discussion

This study suggests a model in which CHK1i treatment induced both DNA replication catastrophe and mitotic catastrophe by premature activation of the APC/C (**Fig. 4.12**). CHK1i inhibition impairs APC/C inhibition during the S-M transition by promoting FBXO5 loss and reducing Aurora B activity in a manner dependent on activation of the MMB-FOXM1 complex and mitotic transcriptional program. This loss in APC/C inhibition leads to the premature degradation of mitotic factors such as cyclin B1 and DNA origin licensing factors such as CDC6, which impairs DNA synthesis in subsequent rounds of division. If the cell can complete DNA replication prior to APC/C dysregulation, it can undergo a flawed mitosis where it may be prone to DNA replication catastrophe in the subsequent S phase. If DNA synthesis is incomplete prior to APC/C dysregulation, then the cell likely will undergo mitotic catastrophe as these partially replicated structures impair chromosome segregation. Thus, these two different mechanisms of CHK1i-induced cell death appear to stem from a shared mechanistic event that requires activation of the mitotic program.

The current definition of replication catastrophe limits the cause of DNA replication catastrophe to RPA exhaustion (Toledo et al., 2017; Toledo et al., 2013). In contrast, this study suggests that dysregulation of additional replication factors may also be sufficient to trigger DNA replication catastrophe. DNA damage accumulated in a similar fashion in the RPA-positive and the RPA-exhausted RPA-High population suggesting that RPA might not be the limiting factor for replication-induced DNA damage after CHK1 inhibition. Cyclin A/CDK1 complexes promote late origin firing while excess MCM helicases on chromatin facilitate the utilization of back up origins when DNA replication is impeded (Ge et al., 2007; Katsuno et al., 2009). In agreement with these observations, cyclin A2 was degraded at levels of CHK1 inhibition sufficient to trigger impaired DNA replication and replication catastrophe while these concentration of CHK1i also resulted in lower levels of chromatin MCM2 in the PCNA-Low population. Notably, the PCNA-

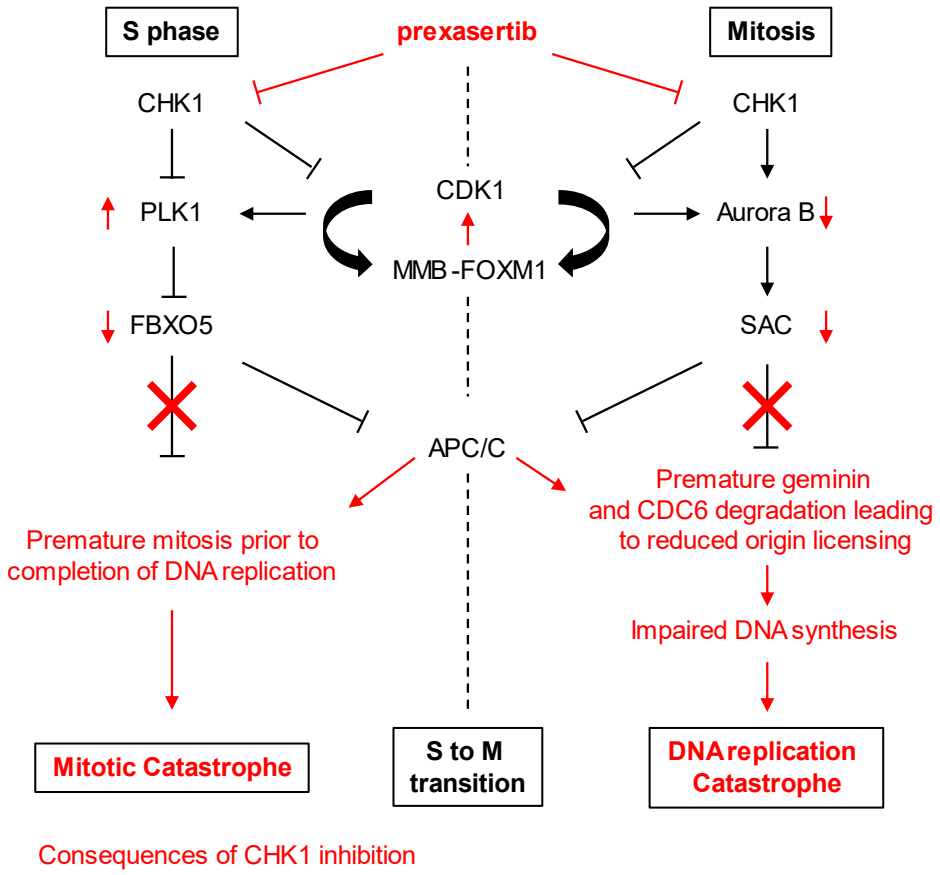

Figure 4.12. APC/C dysregulation as a shared mechanistic step for CHK1i-induced DNA replication and mitotic catastrophe

Model built upon observations in this study for how premature APC/C activity in either S phase or mitosis can lead to mitotic catastrophe or DNA replication catastrophe respectively.

High population, which sustained DNA replication after CHK1i, had increased chromatin-bound MCM2 levels highlighting the role of excess MCM complexes on chromatin during times of replication stress. Decreased levels of chromatin MCM2 in cells with impaired DNA replication after CHK1 inhibition can be attributed to the APC/C-dependent loss of origin licensing factors as the APC/C regulates CDC6 and geminin to facilitate origin licensing. To account for this data, the definition of DNA replication catastrophe should be extended to include DNA-damage triggered by the depletion of replication factors in addition to RPA such as CDC6.

The premature degradation of FBXO5 builds on the previous observation of CHK1 as a negative regulator of PLK1 while resolving a longstanding conflict in the field that had obscured the mitotic role of CHK1. CHK1 depletion in HeLa cells increased PLK1 activity and delayed mitotic progression, which was restored by depleting components of the mitotic checkpoint complex, (Tang et al., 2006) while knocking out CHK1 in DT40 cells impaired spindle assembly checkpoint due to decreased Aurora B activity and impaired mitotic checkpoint complex formation (Zachos et al., 2007). In this study, CHK1 inhibition led to premature loss of FBXO5, likely due to PLK1-mediated degradation. Importantly, FBXO5 protein levels are upregulated by HPV E7 leading to delays in mitosis (Yu and Munger, 2013). Consequently, APC/C activity in HeLa cells likely would also be impaired by FBXO5 for longer due to increased expression allowing the cells to enter mitosis. The higher levels of FBXO5 also would decrease the need for the mitotic checkpoint complex, partly compensating for any impairment of Aurora B activity. The Ying and Yang of FBXO5 and Aurora B inhibition was mirrored in LIN54 and FOXM1 KO cells as LIN54 KO cells stabilized FBXO5 while FOXM1 increased Aurora B expression. The overlapping abilities of FBXO5 and Aurora B to inhibit the APC/C demonstrates the interconnectedness of downstream events regulated by CHK1 and the need to understand the mechanism of CHK1 perturbations from the perspective of the cell cycle system rather than phenotypic outcomes.

FBXO5 and Aurora B protein levels are potential biomarkers for CHK1 inhibitor sensitivity in cancer type dependent manner. FBXO5 is an E2F-dependent gene that is degraded in G2 (Hansen et al., 2004; Hsu et al., 2002; Moshe et al., 2004) indicating that levels of FBXO5 in G1 may reflect activation of E2F dependent gene expression and progression through the restriction point. In tumors where E2F gene expression is repressed in G1, FBXO5 levels may correlate with CHK1i sensitivity since it would indicate that the tumor more readily expresses E2F genes and progresses into S phase. FBXO5 levels may have their prognostic value in tumors with oncogenic mutations that basally derepress E2F gene expression, as in these tumors, higher FBXO5 level would reflect a higher barrier to APC/C activation during S phase. Aurora B may be the stronger biomarker of the two as it is a mitotic kinase that is degraded by the APC/C in G1 (Stewart and Fang, 2005). Thus, high levels of Aurora B may indicate low basal levels of APC/C activity in addition to the robustness of the spindle assembly checkpoint. A major limitation of our analysis is the lack of proteomic data for cancer cell lines and tumors. Data on FBXO5, in particular, was limited outside of NSCLC cell lines. Further work to characterize the protein levels in cancer cells will facilitate the identification of additional biomarkers and allow for further analysis of the ones identified here.

Nonetheless, Aurora B and FBXO5 protein levels may be able to inform CHK1 inhibitor use in the clinic as multiple cancer types have elevated protein levels of Aurora B and FBXO5 (Chen et al., 2009; Guan et al., 2016; Lehman et al., 2007; Lin et al., 2010; Takeshita et al., 2013; Vaidyanathan et al., 2016; Vischioni et al., 2006). Elevated levels of Aurora B and FBXO5 have been found to correlate with poor prognosis and have been studied to understand tumor sensitivity to targeted- and chemo-therapies. FBXO5 levels were predictive of PARP inhibitor sensitivity in BRCA1-negative triple negative breast cancer (Marzio et al., 2019) while low Aurora B levels correlated with chemotherapy resistance in metastatic ovarian tumors (Hetland et al., 2013). To date, when molecular markers are being considered in clinical trials for CHK1 inhibitors, such as NCT02873975, markers of replication stress but not cell cycle regulator like

Aurora B and FBXO5 have been considered. Thus, the inclusion of Aurora B and FBXO5 protein levels as biomarkers may identify tumors sensitive to the DNA replication and mitotic catastrophe triggered by CHK1i-dependent APC/C dysregulation, improving identification of tumors that will respond to CHK1i.

Materials and Methods

Cancer Cell Lines and Cell Culture

Human NSCLC cell lines A549 and H23 cells were propagated in RPMI 1640 medium (Life Technologies, Grand Island, NY) supplemented with 10% fetal bovine serum (Sigma-Aldrich, St. Louis, MO) and 1% Pen/Strep (Gibco) at 37ºC in 5% CO_2. KO populations of sgLIN54 and sgFOXM1 cell lines were generated as described in **Chapter 3**. Inhibitors used in cell cultures experiments are listed in **Table 4.1**.

For single thymidine blocks, 500,000 (60 mm plate) or 1,200,000 (100 mm plate) cells were plated into 2 mM thymidine-containing RPMI media for 16 h. To release cells, cells were washed twice with prewarmed PBS and grown in prewarmed RPMI media to which inhibitors were added at the times denoted. For siRNA experiments, siRNA (listed in **Table 4.2**) were reverse transfected at a final concentration of 20 nM into ~10^6 A549 cells using Lipofectamine RNAiMAX in 100 mm dish. The next day cells were plated into 2 100 mm dishes for drug treatment the following day.

Immunoblotting

Whole-cell extracts were generated by incubating cell pellets in EBC buffer (50 mM Tris pH 8.0, 150 mM NaCl, 0.5 mM EDTA, 10% Glycerol, 0.5% NP-40, Protease Cocktail Set I and Phosphatase Cocktail Set I) and cleared by centrifugation. Relative protein levels in lysates were normalized by Bradford assay and samples were boiled in 6x SDS buffer. Samples were then loaded on 4-20% TGX gels (Bio-Rad) for electrophoresis which were then transferred to a nitrocellulose membrane (Bio-Rad) by wet transfer. Membranes were blocked in 5% nonfat milk (Boston Biochem) for 1 h at room temperature and incubated in primary antibody overnight at 4°C. Primary antibodies (listed in **Table 4.3**) were diluted as follows: FBXO5 was diluted 1:50 in 3% nonfat milk in TBST; FZR1 and cyclin E were diluted 1:200 in 3% nonfat milk in TBST

Table 4.1. Inhibitors and Chemicals

Prexasertib (LY2606368, CHK1i)	Eli Lilly & Co.	S7178
Bortezomib	Cell Signaling Technologies	2204S
Nocodazole	Sigma-Aldrich	M1404
Thymidine	Sigma-Aldrich	T1985
proTAME	R&D Systems	I-440-01M

Table 4.2. Oligonucleotides: siRNAs

siCTRL	Dharmacon	D-001810-10
siCDC20	Dharmacon	L-003225-00
siFZR1	Dharmacon	sc-44349

Table 4.3. Antibodies

Cyclin E (CCNE)	Santa Cruz Biotechnology	sc-247
Cyclin B1	Santa Cruz Biotechnology	sc-752
FOXM1	Santa Cruz Biotechnology	sc-520
pT600 FOXM1	Cell Signaling Technologies	14655S
γ-H2AX	Millipore	05-636-I
LIN54	Bethyl Laboratories	A300-799A-M
PCNA	Cell Signaling Technologies	2586S
RPA32	Bethyl Laboratories	A300-244A-M
VINCULIN	Sigma-Aldrich	V9131
PLK1	Cell Signaling Technologies	4535S
CDC20	Santa Cruz Biotechnology	
FZR1	Santa Cruz Biotechnology	sc-56312
AURORA B	Cell Signaling Technologies	3094S
pT232 AURORA B	Cell Signaling Technologies	2914T
CYCLIN A2	Sigma-Aldrich	C4710
FBXO5	Invitrogen	376600
pS46 TCTP	Cell Signaling Technologies	5251S
TCTP	Cell Signaling Technologies	8441S
ORC1	Cell Signaling Technologies	4731S
CDT1	Cell Signaling Technologies	8064S
CDC6	Cell Signaling Technologies	3387S
GEMININ	Cell Signaling Technologies	5208S
MCM2	Cell Signaling Technologies	3619S
Cyclin B1 conjugate	Cell Signaling Technologies	4118S

Table 4.3. Antibodies (cont.)

anti-rabbit IgG - PE conjugate	Cell Signaling Technologies	4340S
Rabbit-PE isotype control	Cell Signaling Technologies	5742S
Mouse-Alexa 647 isotype control	Cell Signaling Technologies	4843S
10 histone H3 - Alexa 488 conjugate	Cell Signaling Technologies	3465S
anti-mouse IgG - HRP	Bethyl Laboratories	A90-116P
anti-rabbit IgG - HRP	Bethyl Laboratories	A120-101P
anti-mouse IgG - Alexa 488 conjugate	Cell Signaling Technologies	4408S
Rabbit IgG isotype control	Cell Signaling Technologies	4340S
anti-mouse IgG - Alexa 488 conjugate	Life Technologies	A11008

pS1981 ATM was diluted 1:500 in 3% nonfat milk in TBST; pT600 FOXM1 and Geminin were diluted 1:1000 in 3% nonfat milk in TBST; PCNA, CDC20, cyclin B1, and GAPDH were diluted 1:2000 in 3% nonfat milk TBST; LIN54 was diluted 1:1000 in 5% nonfat milk in TBST; FOXM1 was diluted 1:2000 in 5% nonfat milk TBST; vinculin was diluted 1:30000 in 5% nonfat milk in TBST; cyclin A2 was diluted 1:50000 in 5% nonfat milk in TBST; MCM2, pS46 TCTP, TCTP, CDC6, CDT1, ORC1, PLK1, pT232 Aurora B and Aurora B were diluted 1:1000 in 5% BSA in TBST; pS2056 DNA-PKcs was diluted 1:2000 in 5% BSA in TBST. Membranes were incubated in secondary antibodies, diluted 1:5000 in 5% nonfat milk, for 1 h at room temperature. Bands were visualized using Super Signal West Pico (Thermo Scientific) or Immobilon Western Chemiluminescent (Millipore) HRP substrate on the G-box imaging system (Syngene).

Flow cytometry

Trypsinized cells were washed with PBS and fixed in 4% formalin in PBS for 15 min at room temperature. Cells were then washed three times with 1% BSA in PBS and permeabilized in 70% ethanol at -20ºC for 30 min to overnight. After three washes with 1% BSA in PBS, incorporated EdU was labeled with a CLICK reaction (2 mM CuSO4, 100 μM THPTA, 100 mM sodium ascorbate, and 2 μM Calfluor 647 Azide in PBS), using the reagents listed in **Table 4.4**, by rotating for 30 min at room temperature. Samples were then washed thrice with 1% BSA in PBS and incubated with the primary antibody (listed in **Table 4.3**) in 1% BSA in PBS overnight at 4ºC. Primary antibodies were diluted as follows: 1:50, pS10 histone H3-PE conjugate, 1:50, cyclin B1-Alexa Fluor 647 conjugate. After 3 washes with 1% BSA in PBS, samples were incubated with secondary antibodies, which were diluted 1:250 in 1% BSA in PBS, for 1 h at room temperature in darkness. After three more 1% BSA in PBS washes, DNA staining was then conducted by incubating samples in darkness and at room temperature for 1 h in a 1 μg/ml

Table 4.4. Flow Cytometry Reagents for Label DNA Synthesis

5-ethynyl-2'-deoxyuridine (EdU)	Life Technologies	A10044
THPTA	Click Chemistry Tools	1010
Alexa 647 Azide	Life Technologies	A10277
CalFluor 647 Azide	Click Chemistry Tools	1372
AFDye 546 Azide	Click Chemistry Tools	1283
5-bromo-2'-deoxyuridine (BrdU)	Sigma-Aldrich	B5002
DNaseI	Sigma Aldrich	D4513-1VL
4′,6-diamidino-2-phenylindole (DAPI)	Invitrogen	D3571

DAPI, 100 ng/ml RNase A staining solution. Samples were analyzed on a Fortessa analyzers (BD Biosciences) and 50,000 total events were captured for each sample. A negative control where an EdU pulse and primary antibodies were omitted but otherwise normally processed was used to establish negative populations and perform background subtraction on MFIs. Rabbit PE isotype and mouse Alexa Fluor 647 isotype controls were used for the negative control for experiments with pH3-PE and cyclin B-Alexa Fluor 647 staining respectively.

The chromatin flow cytometry protocol was based upon approached used in previous studies (Hauge et al., 2017; Matson et al., 2016). Briefly, trypsinized cells were incubated on ice in 750 μl of Buffer A (300 mM sucrose, 100 mM NaCl, 3 mM $MgCl_2$,10 mM PIPES pH 7.0, 0.5% Triton x-100, Protease Cocktail Set I, and Phosphatase Cocktail Set I) for 5 min. 250 μl of Buffer B (300 mM sucrose,100 mM NaCl, 3 mM $MgCl_2$,10 mM PIPES pH 7.0, 0.5% Triton x-100, 10% Formalin, Phosphatase Cocktail Set I, and Phosphatase Cocktail Set I) was immediately added, and samples were incubated for an additional 15 min on ice. Cells were then pelleted (1000×g, 5 min, 4ºC) and washed with 1% BSA in PBS 3 times before proceeding onto EdU staining as with other samples. Primary antibodies (listed in **Table 4.3**) for chromatin flow cytometry were diluted as follows: MCM2, 1:500 ; PCNA, 1:500; RPA32, 1:500; and H2AX, 1:1000. For RPA32 and γ-H2AX samples, anti-rabbit Alexa 647 secondary and anti-mouse Alexa 488 secondary were used for RPA32 and γ-H2AX respectively. For the PCNA and MCM2 staining, an Alexa Fluor 647-azide was used with mouse Alexa Fluor 488 and rabbit PE secondaries to stain for PCNA

and MCM2 respectively. Otherwise, the CLICK reaction, primary and secondary as well as DAPI staining were conducted as described above.

RT-qPCR

Total RNA was extracted from cell pellets using the RNeasy Plus kit (Qiagen). cDNA was generated from total RNA isolated using the High-Capacity cDNA Reverse Transcription Kit (Applied Biosystems). qPCR was performed on the cDNA using the primers listed in **Table 4.5** and Brilliant III Ultra-Fast qPCR Master Mix (Agilent) using a MxAria (Agilent). Relative RNA expression was calculated using the ΔΔCq method and GAPDH as reference gene.

Data Analysis

Proteomic data for cancer cell lines (Nusinow et al., 2020) and cell line drug sensitivity data (Corsello et al., 2020) were collated using DepMap Data Explorer (www.depmap.org) . Flow cytometry data was analyzed using FlowJo. GraphPad Prism was used to generate graphs and conduct statistical analyses for DepMap data, flow cytometry, viability, growth curves and RT-qPCR.

Table 4.5. Oligonucleotides: qPCR Primers

CCNA2-qPCR-Forward Primer:	5’-TTCCTGTCTTCCATGTCAGTGC-3’
CCNA2-qPCR-Reverse Primer:	5’-ACACAAACTCTGCTACTTCTGGG-3’
CCNB1-qPCR-Forward Primer:	5’-GATGGAGCTGATCCAAACC-3’
CCNB1-qPCR-Reverse Primer:	5’-GGATGGCTCTCATGTTTCC-3’
GAPDH-qPCR-Forward Primer:	5'-GTCAGCCGCATCTTCTTT-3'
GAPDH-qPCR-Reverse Primer:	5' CGCCCAATACGACCAAAT-3'

Chapter 5. Discussion

Summary of Results

In this dissertation, we sought to understand the mechanisms that regulate MMB-FOXM1 complex-dependent G2/M gene expression, the process by which the mitotic cellular identity is read from the genome. We identified how cyclin/CDK activity limited MMB-FOXM1 complex-dependent gene expression in G2/M. We determined how an MMB-FOXM1-CDK1 positive feedback loop was facilitating sensitivity to ATR and CHK1 inhibitors and found a shared mechanistic step between CHK1i-induced DNA replication and mitotic catastrophe.

In Chapter 2, we show that CDK-dependent degradation of MYBL2 by the $SCF^{cyclin\ F}$ complex turns off the MMB-FOXM1 complex and reduces levels of G2/M gene expression. MYBL2 degradation in G2 was cyclin A-dependent (**Fig. 2.1C**) and linked to MMB-FOXM1 activity as the 4N MYBL2-negative population had higher levels of pFOXM1, a marker of MMB-FOXM1 activity, than the MYBL2-positive population in S and G2(**Fig. 2.1F**). Depletion of $SCF^{cyclin\ F}$ complex components prevented MYBL2 degradation in G2/M (**Fig. 2.2D and 2.3E**) and loss of cyclin F reduced the 4N MYBL2-negative population but not the 2N MYBL2-negative population (**Fig. 2.4B**) indicating that cyclin F-dependent degradation of MYBL2 occurs later in the cell cycle.

The F-box domain of cyclin F was required to reduce mitotic levels of MYBL2 in CCNF KO cells (**Fig. 2.6B**) as demonstrated by the persistence of metabolically-labelled, pulse-chase, MYBL2 protein species in mitotic CCNF KO cells (**Fig. 2.7B**). Further, cyclin F overexpression promoted MYBL2 ubiquitination *in vivo* (**Fig. 2.7C**). Together, this data indicates that MYBL2 is a $SCF^{cyclin\ F}$ substrate for degradation.

Cyclin F interacted with MYBL2 through its cyclin fold (**Fig. 2.6C and 2.6D**) while an atypical RxH cyclin binding motif on MYBL2 was required for MYBL2 to interact with cyclin F (**Fig. 2.9B**). Mutation of CDK sites on MYBL2 reduced the MYBL2-cyclin F interaction (**Fig. 2.9A and 2.9E**) indicating that cyclin/CDK phosphorylation of MYBL2 is a secondary requirement for the MYBL2-cyclin F interaction and may facilitate access to the RxH motif. Expression and

accumulation of cyclin F during the S/G2 transition was found to be MMB-FOXM1-dependent as knockdown of MMB-FOXM1 components reduced *CCNF* transcript levels (**Fig. 2.11A**) and cyclin F was less stable than MYBL2 during the S/G2 transition in the presence of cycloheximide (**Fig. 2.11C and 2.11D**). Loss of cyclin F led to the MMB complex and G2/M gene expression persisting into mitosis (**Fig. 2.11C-E**) and the cell was able to better maintain the mitotic pH3 in the presence of an extended nocodazole block (**Fig. 2.12C**) indicating that cyclin F functions to turn off G2/M gene expression. Thus, cyclin F degrades MYBL2 as part of a negative feedback loop gated by cyclin/CDK activity to turn off MMB-FOXM1 activity and G2/M gene expression as cyclin/CDK1 activity accumulates in G2.

In Chapter 3, we demonstrate that an MMB-FOXM1-CDK1 positive feedback loop triggers premature mitosis after CHK1 inhibition leading to replication catastrophe. MMB-FOXM1 components, MYBL2, LIN54, and FOXM1, were identified in a genome-wide CRISPR screen as required for sensitivity to the CHK1 inhibitor (CHK1i) prexasertib (**Fig 3.1C-F**). Knock out of LIN54 and FOXM1 did not alter cellular growth (**Fig. 3.2B**) but did confer resistance to ATR and CHK1 inhibitors (**Fig. 3.2C-E**) as well as prevent the induction of replication stress markers (**Fig. 3.3**).

The replication stress marker pKAP1 was induced by CHK1i in late S phase in a panel of NSCLC cell lines (**Fig. 3.4D**). Perturbation of the MMB-FOXM1 complex prevented the induction of pKAP1 by CHK1i in late S (**Fig. 3.5D and 3.5E**). The induction of pKAP1 in Late S phase after CHK1i treatment was ATR-dependent (**Fig. 3.7C**) suggesting it was not part of a DNA damage response. Increased DNA synthesis and origin firing were still induced by CHK1i in the LIN54 KO and FOXM1 KO cells (**Fig 3.8A-C**) and the increased origin firing and DNA synthesis did not corelate with the induction of pKAP1 by CHK1i in EV control cells indicating that altered DNA replication was not sufficient for CHK1i-induced replication stress.

Levels of pFOXM1 and G2/M expression were increased during S phase after CHK1i treatment (**Fig. 3.9A-C, 3.10D, 3.10F and 3.10H**) . Loss of LIN54 or FOXM1 prevented the

induction of the mitotic cyclins, *CCNB1 and CCNA2*, by CHK1i (**Fig. 3.10K-P**). Loss of LIN54 or MYBL2 also prevented the induction of CDK1-dependent pFOXM1 after CHK1 inhibition (**Fig. 3.11A, 3.11B, and 3.11D**) indicating that the MMB-FOXM1 complex and CDK1 were in a positive feedback loop to promote G2/M gene expression that was being repressed by CHK1 in S phase.

Premature mitosis was induced by ATR or CHK1 inhibition (**Fig. 3.12D**) and the induction of premature mitosis by CHK1i required an intact MMB-FOXM1 complex (**Fig. 3.12F, 3.12G, and 3.12I**) indicating that, in the absence of CHK1 activity, the MMB-FOXM1-CDK1 positive feedback loop was triggering premature mitosis in S phase. Modulating CDK1 activity during CHK1 inhibition with a range of CDK1 inhibitor concentrations revealed that premature activation of the MMB-FOXM1 complex and the induction of mitosis in S phase was required for replication stress, DNA replication catastrophe, and apoptosis (**Fig. 3.13G, 3.13K, 3.13N, 3.14F, 3.14G and 3.13P**) . Together this data indicates that CHK1i depresses an MMB-FOXM1-CDK1 feedback look to triggers premature mitosis in S phase, eventually resulting in the induction of DNA replication catastrophe.

In Chapter 4, we identify premature APC/C activity as a shared mechanistic step for both CHK1i-induced DNA replication catastrophe and mitotic catastrophe. A threshold level of CHK1i was required (50-100 nM) to induce both DNA replication catastrophe and mitotic catastrophe (**Fig. 4.1A, 4.1B, and 4.3E**) suggesting a shared mechanism. 50 nM or greater of CHK1i also impaired DNA replication and triggered a loss of G2/M markers (**Fig. 4.2C, 4.2G and 4.2I**) including the APC/C substrate, cyclin B1, linking DNA replication and mitotic catastrophe to a loss of cell cycle identity. CHK1 inhibition sufficient to induce DNA replication and mitotic catastrophe also triggered premature APC/C activity as 100 nM CHK1i but not 10 nM CHK1i promoted the degradation of APC/C substrates, cyclin B1, cyclin A, Aurora B, PLK1, and FOXM1 in S phase and nocodazole synchronized cells (**Fig. 4.3A and 4.4**). This premature APC/C activity could be explained by 100 nM CHK1i impairing Aurora B activity and triggering

the premature loss of FBXO5 in S phase (**Fig. 4.3A and 4.4**). Consistent with DNA replication being impaired by higher levels of CHK1i, 100 nM CHK1i, but not 10 nM CHK1i, caused an accumulation of cells in G2/M with low levels of chromatin-bound PCNA at 24 hours post treatment in A549 and H23 cells (**Fig. 4.7G-I**). 50 nM or greater of CHK1i also induced the APC/C-dependent loss of DNA origin licensing factors at this timepoint (**Fig. 4.8**) suggesting that premature activation of the APC/C by CHK1i impaired DNA replication.

Knock out of the MMB-FOXM1 components, LIN54 or FOXM1, prevented the loss in DNA origin licensing factors and impaired DNA synthesis (**Fig. 4.9A and 4.9C**) implicating the mitotic cellular program in the premature activation of the APC/C and subsequent impairment of DNA synthesis by CHK1i. In support of DNA origin licensing being impaired by CHK1i, chromatin-bound MCM2 levels were lower in the PCNA-Low and PCNA-Negative populations of EV cells but not LIN54 KO or FOXM1 KO cells (**Fig. 4.9I**). FBXO5 loss in S phase was blocked in LIN54 KO cells while Aurora B and FBXO5 levels were upregulated in FOXM1 KOs (**Fig 4.10**) indicating that CHK1i-resistant LIN54 KO and FOXM1 KO cells stabilized or upregulated levels of APC/C negative regulators. Further, levels of FBXO5 or Aurora B negatively correlated with sensitivity to multiple CHK1 inhibitors in the cell lines of several cancer types (**Fig. 4.11**). Thus, this data implicates premature APC/C activity in CHK1i-induced DNA replication and mitotic catastrophe and suggests that negative regulators of APC/C activity, FBXO5 or Aurora B, could serve as potential biomarkers for CHK1 inhibitor sensitivity.

Cyclin F is the eraser or "off" switch for cell cycle gene expression

An $SCF^{cyclin\ F}$ complex was identified as the factor degrading MYBL2 in G2. Cyclin F had been previously reported to interact with MYBL2 but no evidence for cyclin F-mediated degradation was observed (Klein et al., 2015). This previous observation can be explained by the use of cycloheximide treatment to evaluate MYBL2 protein stability in the previous studies.

A key observation not previously noted was that MYBL2 levels did not decrease in the control cells after cycloheximide treatment (Klein et al., 2015) suggesting that MYBL2 was not being degraded under the experimental conditions. In contrast, cyclin F was rapidly degraded in the control cells after cycloheximide treatment. We observed a similar phenotype with cyclin F in our experiments as well. Levels of cyclin F but not MYBL2 were reduced after CHX treatment in HeLa cells at similar time points to *Klein et al.* in thymidine synchronized cells as well as every time point during S phase and G2 we tested. This means that cyclin F is less stable than MYBL2 in S/G2. Consequently, cycloheximide treatment is not an appropriate assay for interrogating the effect of cyclin F on MYBL2 protein stability. A key assumption of cycloheximide usage is that the degrader is more stable than the substrate that is being degraded but this was not the case with cyclin F and MYBL2. Cyclin F levels were depleted faster than MYBL2 can be degraded resulting in MYBL2 levels remaining stable after cycloheximide treatment.

A more appropriate assay would be to examine MYBL2 protein turnover in cyclin F KO cells using metabolic labeling, which wouldn't perturb cyclin F levels. In accordance with this thinking, AHA-labeled MYBL2 protein species were observed to persist in CCNF KO but not CTRL cells indicating the cyclin F promotes MYBL2 protein turnover. The AHA protein labeling experiment was supported by *in vivo* ubiquitination experiments where cyclin F overexpression promoted MYBL2 ubiquitination. Additionally, the failure of a cyclin F mutant deficient for ubiquitin ligase activity to restore MYBL2 loss in CCNF KO cells provides genetic evidence for cyclin F-mediated degradation of MYBL2. Thus, we have generated multiple lines of evidence supporting MYBL2 as a $SCF^{cyclin\ F}$ substrate for degradation in G2/M.

The identification of MYBL2 as a cyclin F substrate makes cyclin F the eraser or "off" switch for both the G1/S and G2/M waves of cell cycle gene expression as E2F1-3a had been previously identified as cyclin F substrates (Clijsters et al., 2019). Perturbation of cyclin F-mediated degradation of E2F1-3a or MYBL2 led to the respective waves of gene expression

occurring outside the appropriate phase of the cell cycle resulting in altered cell cycle progression. In the case of E2F-mediated degradation, cells expressing E2F degradation-resistant mutants licensed their origins of DNA replication faster and entered S phase faster in the next round of cell division leading to replication stress over time (Clijsters et al., 2019). For MYBL2 degradation, loss of cyclin F allowed the cell to more robustly maintain the spindle assembly checkpoint and mitotic cellular state in the presence of a mitotic block. Both cases illustrate that the role of erasers or protein degradation complexes in the cell cycle is to limit the DNA replication or mitotic cellular identity to the appropriate phase of the cell cycle.

A distinguishing feature between E2F and MYBL2 degradation by cyclin F is CDK activity. MYBL2 requires CDK phosphorylation for an optimal interaction with cyclin F while no CDK phosphorylation events were reported to regulate the E2F-cyclin F interaction (Clijsters et al., 2019). This allows for the temporal separation of E2F1-3a and MYBL2 degradation within the cell cycle as it adds an additional signal for MYBL2 degradation, delaying MYBL2 degradation until the cell is ready for mitosis. The interactions between cyclin F and substrates involved in G2/M and mitosis are likely gated by CDK phosphorylation based on whether the substrates are needed for establishing the mitotic cellular state. Substrates that primarily regulate G1/S and DNA replication do not need CDK phosphorylation to interact with cyclin F while the substrates that a have a role in G2/M required CDK phosphorylation to interact with cyclin F. Cyclin F substrates FZR1, CDC6, E2F1-3a and E2F7/8 regulate the establishment and maintenance of the DNA replication program and are reported to not require CDK phosphorylation to interact with cyclin F (Choudhury et al., 2016; Clijsters et al., 2019; Walter et al., 2016; Wasserman et al., 2020; Yuan et al., 2019). In contrast, RRM2 and SLBP, which regulate the G2/M DNA damage response among other roles, required CDK phosphorylation for their interaction with cyclin F (D'Angiolella et al., 2012; Dankert et al., 2016; Tanaka et al., 2000). While the CP110-cyclin F interaction was not reported to be dependent on CDK phosphorylation (D'Angiolella et al., 2010), CP110 is a cyclin/CDK1/2 substrate (Chen et al.,

2002), leaving open the possibility that cyclin/CDK phosphorylation could regulate the CP110-cyclin F interaction. Thus, cyclin/CDK phosphorylation may create early and late pools of cyclin F substrates that prioritizes cyclin F-mediated degradation. Factors involved in regulating the DNA replication program are degraded as cyclin F accumulates during the S/G2 transition while the degradation of substrates that regulate the establishment of the mitotic program is delayed until sufficient CDK1 activity is reached in G2/M.

CDC6 as a potential regulator of E2F degradation rather cyclin F substrate

CDC6 was reported to be a cyclin F substrate during G2/M (Walter et al., 2016). However, we did not observe any change in CDC6 stability in the cyclin F KOs during the M/G1 transition. The discrepancy might be explained by the experimental set up and interpretation in prior study. In the *Walter et al.* study, CDC6 protein stability was assessed in nocodazole-synchronized samples and two observation were made: (i) MG132 treatment increased CDC6 levels in siCTRL cells and (ii) CDC6 levels decreased with cycloheximide treatment. Depletion of cyclin F increased CDC6 protein levels in the nocodazole synchronized samples (Walter et al., 2016). The authors proposed that this is evidence for cyclin F-mediated degradation but this phenotype can also be understood through the regulation of cell cycle gene expression by cyclin F.

As an E2F transcriptional target, the higher levels of CDC6 could be explained by increased E2F transcriptional activity in the CCNF-depleted samples. Expression of degradation resistant E2F1, E2F2, or E2F3a leads to increased protein levels of CDC6 (Clijsters et al., 2019) similar to what was reported by *Walter et al*. The loss of CDC6 in nocodazole-synchronized control cells can be explained through the use of cycloheximide, which would block cyclin B1 translation in addition to CDC6 translation. Cyclin B1 is degraded by a $CUL2^{ZGY11}$ complex in mitosis in the absence of APC/C activity (Balachandran et al., 2016). Cycloheximide treatment would accelerate depletion of cyclin B1 levels via this complex below the threshold necessary to

inhibit FZR1, leading to APC/C activity. As CDC6 is an APC/C substrate, the APC/C activity induced by this cyclin B1 degradation would result in the decreased CDC6 levels observed. Cyclin B1 levels were not assessed in the experiment so this hypothesis cannot be excluded. We observed that cyclin B1 expression was higher during the M/G1 transition in cyclin F KO cells meaning it would take longer for $CUL2^{ZYG11}$ complexes to reduce cyclin B1 below a critical level in the absence of cyclin F, rendering the cyclin F-depleted samples more resistant to premature APC/C activity after cycloheximide treatment. In nocodazole-synchronized cyclin F KO cells released from nocodazole into cycloheximide in Chapter II, basal CDC6 levels were higher in cyclin F KOs than CTRL cells and CDC6 protein stability mirrored that of APC/C substrates, cyclin B1 and FOXM1, in both CCNF KO and CTRL cells suggesting that the APC/C, not cyclin F, is the main determinant of CDC6 protein stability. Thus, the higher protein levels of CDC6 observed in the cyclin F KO cells could be explained through indirect regulation of cyclin gene expression.

CDC6 interacts with cyclin F through an RxL-cyclin fold interaction, although it is unclear when they interact during the cell cycle. Binding studies conducted in this dissertation and in *Walter et al.*, were performed in asynchronous HEK293T cells. In G2/M, when cyclin F and CDC6 are proposed to be interacting to mediate CDC6 degradation, cyclin F and CDC6 are likely in different parts of the cell. During the late cell cycle, cyclin F localizes to the nucleus based on immunofluorescence experiments (D'Angiolella et al., 2012). CDC6 however gets exported from the nucleus by cyclin A/CDK2 phosphorylation and is largely cytoplasmic by G2/M (Petersen et al., 1999). This would suggest that the robust cyclin F-CDC6 interactions observed may be occurring early in the cell cycle during S phase. Additionally, minimal ubiquitination of CDC6 was observed in *in vitro* ubiquitination assays with co-immunoprecipitated cyclin F-CDC6 complexes (Walter et al., 2016). This lackluster ubiquitination could be due to technical or biological reasons but a positive control was not

included to demonstrate the robustness of the assay. Therefore, it is plausible that CDC6 is not target for degradation by $SCF^{cyclin\ F}$ complexes during G2/M.

Alternatively, the CDC6-cyclin F interaction could function as a sponge for $SCF^{cyclin\ F}$ complexes during S phase, preventing premature degradation of E2F until sufficient DNA replication has occurred. E2F reads the DNA replication program from the genome as it transactivates E2F target genes including MYBL2 as part of this wave, that subsequently leads to cyclin F expression (Fischer et al., 2016). Since CDK phosphorylation of E2F has not been implicated in the E2F-cyclin F interaction, cyclin F should be able to interact with the activating E2Fs and degrade them as cyclin F begins to be expressed in S phase. This would be problematic though as E2F-mediated expression of FBXO5 inhibits APC/C during S phase (Hsu et al., 2002). Active E2F gene expression may also be crucial for maintaining MYBL2 protein levels in S phase, as a PP2A-dependent phospho-degron (Morita et al., 2020) antagonizes MYBL2 accumulation. Consequently, piecemeal degradation of the E2Fs by cyclin F would not only impede DNA replication but could impair the transition to G2/M and establishment of the mitotic cellular state. Thus, the cell needs a way to prevent E2F degradation until sufficient DNA replication and MYBL2 accumulation has occurred.

One way to delay E2F degradation could be to limit MMB-FOXM1 activity via ATR-CHK1 and completely restrict cyclin F levels but this would prevent cyclin A expression necessary for late origin firing. A non-degratory interaction between CDC6 and cyclin F would allow block the E2F-cyclin F interaction on the protein level while allowing for the expression of cyclin A. CDC6 is expressed as part the E2F program after having licensed DNA and being degraded by APC/C in in G1 (Clijsters et al., 2013; Hateboer et al., 1998; Ohtani et al., 1998; Yan et al., 1998). CDC6 however has low affinity for licensed origins with bound MCM2 but regains its affinity for origins once they have been fired (Oehlmann et al., 2004). As a result, soluble levels of nuclear CDC6 accumulate during S phase until origins are fired or cyclin A/CDK2-dependent phosphorylation triggers nuclear export to the cytoplasm (Oehlmann et al., 2004; Petersen et

al., 1999). This would mean that as DNA replication progresses and cyclin A/CDK activity is permitted, CDC6 is titrated away from cyclin F resulting in free cyclin F to degrade the activating E2Fs once sufficient DNA replication has occurred. More study of the CDC6-cyclin F interaction in S phase is warranted as it may serve as an important timer to coordinate E2F degradation with DNA replication.

CDK-dependent degradation of MYBL2 is a negative regulatory event linked to MMB-FOXM1 activation

MYBL2 phosphorylation has been shown previously to promote MYBL2 degradation and MYBL2-mediated gene expression (Charrasse et al., 2000; Lane et al., 1997; Robinson et al., 1996; Saville and Watson, 1998; Ziebold et al., 1997). These apparently conflicting observations leads to the hypothesis that MYBL2 degradation could be required for the activation of the MMB-FOXM1 complex. However, perturbation of MYBL2 degradation by knockout of cyclin F led to persistent G2/M gene expression indicating the MYBL2 degradation is CDK-dependent negative regulatory event for the MMB-FOXM1 complex. Nonetheless, MYBL2 degradation appears to be linked to CDK-dependent activation of the MMB-FOXM1 complex in agreement with the previous studies linking MYBL2 phosphorylation and target gene expression. MYBL2 degradation in G2 is dependent on cyclin A, which also activates FOXM1 during the S/G2 transition. The 4N-MYBL2 negative population that was reduced in CCNF KO cells had higher levels of pFOXM1, a marker for MMB-FOXM1 activity, than the MYBL2-positive population in parental HeLa cells supporting cyclin A-mediated degradation coinciding with MMB-FOXM1 activation by cyclin/CDK complexes. Importantly, MYBL2-positive cells had intermediate levels of pFOXM1 indicating that activation of FOXM1 by CDKs slightly precedes MYBL2 degradation. Further, accumulation of cyclin F, which degrades MYBL2 during the S/G2 transition, is dependent on MMB-FOXM1 activity. This establishes a clear order of events: first cyclin/CDK phosphorylation activates the MMB-FOXM1 complex and then cyclin A/CDK activity

promotes MYBL2 degradation. MYBL2 activation and degradation by CDK phosphorylation is also linked to the regulation of the MYBL2 protein. Multiple phosphorylation sites mutated in the MYBL2ΔCDK mutant deficient for the cyclin F interaction have been implicated in facilitating an interaction between MYBL2 and PIN1 (Werwein et al., 2019). The conformational change in MYBL2 induced by PIN1 is reported to facilitate activating PLK1 phosphorylation but could also function as part of a restricted access degron that prevents an interaction with cyclin F in the absence of CDK activity. Thus, a conformational change reported to activate MYBL2 may also enable its own demise. Together, this work shows that CDK phosphorylation can antagonize MYBL2 and MMB-FOXM1 activity after initially promoting it.

Intriguingly, there appears to be a hierarchy of CDK phosphorylation sites on MYBL2. MYBL2 is phosphorylated early in S phase on S577 but phosphorylation of T487 does not appear until later in S phase (Werwein et al., 2019) suggesting that MYBL2 is phosphorylated in an ordered manner. In addition to the MYBL2-cyclin F interaction, the early S577 phosphorylation event has been implicated in the MYBL2-PIN1 interaction and conformational change that leads to activating PLK1 phosphorylation (Werwein et al., 2020; Werwein et al., 2019). However, it is unclear what molecular event late phosphorylation by PLK1 and CDK facilitates. Inhibition of CDK1 in A549 and H460 cells prevented phosphorylation of T600 on FOXM1 but failed to block phosphorylation of T487 indicating that pT487 is not CDK1-dependent, making it a likely cyclin A/CDK2 substrate. MYBL2 gel mobility increased despite CDK1 inhibition indicating that there are CDK1-dependent phosphorylation sites on MYBL2. However, it is unclear what determines the order of CDK phosphorylation events on MYBL2. Considering that the early phosphorylation sites on MYBL2 promote a conformational change in MYBL2 (Werwein et al., 2020), it is likely the structure of MYBL2 that determine the order of phosphorylation. Early phosphorylation sites may be more solvent exposed than late sites and the late phosphorylation sites become more exposed as the early sites get phosphorylated and MYBL2 becomes isomerized by PIN1. The progressive phosphorylation of MYBL2 points to

MYBL2 acting as sensor for CDK activity. Different thresholds of cyclin A/CDK activity would trigger particular events for MYBL2 with the threshold of sufficient CDK activity for mitosis likely triggering MYBL2 degradation. Such CDK phosphorylation codes are currently being worked out in yeast (Ord et al., 2019) and may be applied to MYBL2 as the ordered phosphorylation of MYBL2 is further described. Such work would help to incorporate MYBL2 phosphorylation in the mechanism of MMB-FOXM1 activity and provide insights into how cyclin/CDK activity triggers the switch from DNA replication to mitosis.

Another area for further study is the regulation of MYBL2 phosphorylation by phosphatases. Notably, when MYBL2 persists through the M/G1 transition in CCNF KO cells, there was a decrease in pT487 MYBL2 levels and an increase in MYBL2 gel mobility as the cell exited mitosis, indicative of dephosphorylation. During the M/G1 transitions, PP1 and PP2A complexes are activated to dephosphorylate CDK1 phosphorylation sites and erase the mitotic program to help establish G1 (Wurzenberger and Gerlich, 2011). Recently, PP2A-B56ε was shown to dephosphorylate S241 on MYBL2 in leukemia cells to promote degradation of MYBL2 by an unknown factor (Morita et al., 2020). S241 on MYBL2 is not a CDK phosphorylation site but fits the consensus phosphorylation sequence of S-X-X-E for CK2 kinase (Hornbeck et al., 2004; Meggio and Pinna, 2003). Substitution of S241 to alanine promotes MYBL2 degradation and prevented G2/M gene expression (Morita et al., 2020) indicating that S241 phosphorylation is likely preventing MMB-FOXM1 complex formation and modulates MYBL2 levels earlier in the cell cycle than cyclin F-mediated degradation. Given the diffuse nature of the MYBL2 signal on the nitrocellulose membrane, it was difficult to determine if total MYBL2 levels were decreasing during the M/G1 transition in CCNF KO cells but G1 cells were largely negative for MYBL2 in our flow cytometry experiments. If active in G1, the S241 degron would disfavor MYBL2 accumulation until sufficient E2F activity has been achieved. pS241 MYBL2 has been detected in IP-Mass Spec experiments of S phase-synchronized T98G cells (Litovchick et al., 2011) suggesting degradation through the S241 degron is inhibited by phosphorylation prior to or

during S phase. Interestingly, PP2A-B56 complexes have also been reported to dephosphorylate cyclin E to oppose the autocatalytic-mediated degradation of cyclin E (Davis et al., 2017) that occurs in S phase. Thus, PP2A-B56 activity promotes the establishment of the DNA replication cellular identity during G1/S by stabilizing cyclin E, part of the DNA replication program writer, and likely delaying the formation of the reader for the mitotic program, the MMB-FOXM1 complex, by promoting MYBL2 degradation. Further study of this degron during the cell cycle is warranted as it may provide insights into when the MMB complex forms during S phase and how the cell manages the transition from G1/S gene expression to G2/M gene expression.

The loss of pT487 MYBL2 signal during the M/G1 transition also indicates that CDK phosphorylation on MYBL2 can be removed by phosphatases. CDK phosphorylation of FOXM1 is antagonized by PP2A-B55α to limit its transcriptional activity (Alvarez-Fernandez et al., 2011). Similarly, CDK phosphorylation on MYBL2 could be regulated by PP2A complexes during S phase to delay MYBL2 degradation until FOXM1 is activated and recruited to the MMB-FOXM1 complex. While CHK1 inhibition activates cyclin/CDK complexes, it also antagonizes PP2A activity by blocking the CHK1-dependent sequestration of FAM122A/PABIR1, an inhibitor of PP2A, by 14-3-3 (Li et al., 2020). Thus, MYBL2 phosphorylation observed in S phase after CHK1 inhibition could reflect PP2A inhibition as much as it reflects cyclin/CDK activation. Regulation of MYBL2 phosphorylation by phosphatases, particularly in S phase, merits further study as understanding the negative regulation of MYBL2 phosphorylation will provide insights into the regulation of the MMB-FOXM1 complex.

Differential phenotypes caused by MYBL2, LIN54 and FOXM1 perturbations demonstrate how the MMB-FOXM1 complex spans the cell cycle from G1/S to mitosis.

A surprising outcome of this work was that depletion or knockout of MYBL2, LIN54 or FOXM1 led to distinct phenotypes even though all three proteins assemble to form the MMB-

FOXM1 transcription complex. Perturbations of MYBL2 and LIN54 led to an earlier arrest in the cell cycle then loss of FOXM1 while several G2/M genes could be induced by CHK1 inhibition in FOXM1 KO but not LIN54 KO cells. These differences in phenotypes may reflect how the MMB-FOXM1 complex spans the cell cycle from E2F-dependent gene expression of MYBL2 in G1 to recruitment of FOXM1 by the MMB complex that triggers G2/M gene expression in S/G2.

The enrichment of the G1 population after MYBL2 knockdown implicates the MMB complex in the G1/S transition. Consistent with previous studies (Saldivar et al., 2018), depletion of MYBL2 led to cells accumulating in G1. In contrast, LIN54 KO or depletion led to cells accumulating in late S phase and G2/M while only the G2/M population increased in FOXM1 KO cells. The accumulation of G1 cells after MYBL2 but not LIN54 depletion likely reflects the fact that DREAM complexes can still form in the absence of MYBL2 but are disrupted by LIN54 depletion (Litovchick et al., 2007a). Consequently, E2F genes can be expressed in the LIN54-depleted samples allowing for entry into S phase, but loss of LIN54 would impair progression through late S phase since the MMB complex could not form. But why would loss of MYBL2, a G2/M transcription factor, allow for the continued repression of G1/S genes? MYBL2 could disrupt MuvB-RBL1(p107) complex bound to CLE sites or titrate MuvB away from the DREAM complex. CLE sites, found at a subset of G1/S genes, are variant CHR sites that assist the E2F site in promoter repression and include such G1/S genes as CDC6, MCM5, CDC25A, and MYBL2 (Muller et al., 2017). MYBL2 has been reported to interact with RBL1, a member of the RB pocket protein family, and overcome RBL1-mediated G1 arrest in SAOS-2 cells (Joaquin et al., 2002). Recently, it was shown that RBL1 could form E2F4- or MuvB-containing complexes to limit cell cycle gene expression after DNA damage (Schade et al., 2019a), an environment, like G1, with low CDK1/2 activity. Thus, the absence of MYBL2 expression in G1 could allow MuvB-RBL1complexes to persist at G1/S promoters through MuvB that is still bound to the CLE site, preventing G1/S gene expression and entry into S phase.

About 50% of high confidence MMB-FOXM1 target genes were upregulated by 1.5-fold in S phase-synchronized FOXM1 KO cells after CHK1 inhibition indicating that the MMB complex is sufficient to promote expression of a large subset of G2/M genes. Supporting the sufficiency of the MMB complex was the upregulation of protein levels of Aurora B and FBXO5 in the FOXM1 KO cells after CHK1 inhibition. A few MMB-FOXM1 target genes, such as *TICRR* and *CCNA2*, regulate DNA replication (Katsuno et al., 2009; Kumagai et al., 2010) perhaps necessitating some MMB complex activity in S phase prior to FOXM1 recruitment. TICRR encodes the protein Treslin (human Sld3), an essential protein for origin firing (Kumagai et al., 2010; Pagliuca et al., 2011; Sansam et al., 2010). Treslin protein levels peak during M/G1 and decrease during G1/S phase as PP2A-B55-dependent dephosphorylation triggers protein degradation (Charrasse et al., 2017). Consequently, MMB-FOXM1 activity might sustain *TICRR*/Treslin levels to complete DNA replication during late S phase when Treslin protein levels reach a nadir. This could explain the delay in late S phase progression that was observed in our A549 LIN54 KO cells as well as in LIN54-depleted BJ-hTERT fibroblasts (Schmit et al., 2009a). Thus, the MMB complex may facilitate the completion of DNA replication by expression of low levels of MMB-FOXM1 target genes in S phase.

While the MMB complex could induce a subset of G2/M genes in FOXM1 KO cells after CHK1 inhibition, premature mitosis was not induced in FOXM1 KO cells by CHK1i indicating that the MMB complex is not sufficient to fully activate the G2/M program. Among the genes that were not be induced by the MMB complex after CHK1 inhibition include *CCNA2* and *CCNB1* highlighting the integral part FOXM1 plays within the MMB-FOXM1 complex promoting the transition to G2/M. The requirement of FOXM1 for *CCNA2* and *CCNB1* expression points to FOXM1 being the amplifier of the MMB-FOXM1 signal as cyclin A/CDK1 and cyclin B/CDK1 complexes are in positive feedback loops with the MMB-FOXM1 complex. FOXM1 is recruited to G2/M promoters during the S/G2 transition, likely due to activation by CDK phosphorylation of FOXM1 being restricted by the ATR-CHK1 pathway during S phase. FOXM1 acting as an

amplifier for G2/M gene expression would provide a rationale to limit its recruitment in S phase as FOXM1 recruitment would trigger mitotic positive feedback loops during DNA replication. Thus, MYBL2, MuvB, and FOXM1 each contribute to MMB-FOXM1 activity at different stages of the cell cycle that reflects their recruitment. MYBL2 may help MuvB transition away from repressive complexes in G1/S to the MMB complex, where the complex expresses G2/M genes that facilitate the completion of DNA replication. As DNA replication is finishing, FOXM1 is recruited to facilitate *CCNA2* and *CCNB1* expression, amplifying G2/M gene expression through positive feedback loops and driving the cell cycle from DNA replication into mitosis.

MYBL2 is the timer of MMB-FOXM1 activity while FOXM1 is the amplifier of MMB-FOXM1 activity

Prior to this work, it was known that the MMB complex formed in S phase and recruited FOXM1 to G2/M promoters and that perturbation of MYBL2, the MuvB complex, or FOXM1 impaired G2/M gene expression (Chen et al., 2013b; Down et al., 2012b; Sadasivam et al., 2012a). CDK dependent phosphorylation of MYBL2 and FOXM1 as well as MYBL2 degradation coincided with FOXM1 recruitment and G2/M gene expression (Sadasivam et al., 2012a) but it was unclear how these events facilitated MMB-FOXM1 activity. As discussed above, MYBL2 phosphorylation facilitates an interaction with cyclin F that leads to MYBL2 degradation indicating that MYBL2 phosphorylation functions to limit MMB-FOXM1 activity by MYBL2 degradation. But the question whether MYBL2 phosphorylation leads to MMB-FOXM1 activation remains. One possible explanation is that CDK phosphorylation does not activate but rather derepresses MYBL2. Cyclin A/CDK2 activity has been reported to disrupt an interaction between MYBL2 and the NCoR-SMRT corepressors (Li and McDonnell, 2002). Unfortunately, phospho-mutants for MYBL2 were not tested for the NCoR-SMRT interaction so it is unknown if cyclin A/CDK2 phosphorylation of MYBL2 or the NCoR-SMRT disrupts the interaction. The NCoR-SMRT complex interacts with MYBL2 C-terminal to the DNA binding domain raising the

possibility that MuvB and NCoR-SMRT compete for MYBL2 binding in G1/S. An interaction with the NCoR-SMRT complex could protect MYBL2 from degradation by the S241 degron, allowing MYBL2 to accumulate without initiating G2/M gene expression. Then, as cyclin A/CDK2 activity increases in late S phase, sufficient cyclin A/CDK activity is achieved to disrupt the MYBL2-NCoR-SMRT complex, but not activate FOXM1, allowing for the formation of the MMB complex. However, once cyclin/CDK1 activity has triggered G2/M gene expression by phosphorylation of FOXM1, sufficient to progress through mitosis, cyclin/CDK1 activity will promote MYBL2 degradation.

Phosphorylation of FOXM1 appears to be the rate limiting step for MMB-FOXM1 activation during the S/G2 transition. The ATR-CHK1 pathway is known to restrict phosphorylation of FOXM1 and G2/M gene expression during S phase and inhibition of this pathway leads to the induction of pT600 FOXM1 and G2/M gene expression (Saldivar et al., 2018) indicating that phosphorylation of FOXM1 is a key step for G2/M gene expression. However, it remained unclear how FOXM1 phosphorylation fits with activation of the MMB-FOXM1 complex considering MYBL2 phosphorylation had also been reported to be pro-transcriptional. In agreement with the previous studies, this work provides evidence that phosphorylation of FOXM1 may be the rate limiting step in MMB-FOXM1 activation. In our studies, the knocking out of LIN54 or treatment with CDK1i blocked CHK1i-induced pT600 FOXM1 phosphorylation and MMB-FOXM1-dependent gene expression but did not prevent CHK1-induced pT487 MYBL2. This indicates that MYBL2 phosphorylation likely accumulates prior to FOXM1 activation. Additionally, FOXM1 is likely the component of the MMB-FOXM1 complex participating in the MMB-FOXM1-CDK1 positive feedback loop as pT600 FOXM1 was LIN54- and CDK1-dependent while pMYBL2 was not. The phosphorylation of MYBL2 but not FOXM1 in the LIN54 KOs after CHK1 inhibition indicates that FOXM1 phosphorylation depends on an intact MMB complex while MYBL2 phosphorylation does not. Together, with the observation that a subset of MMB-FOXM1 target genes could be induced in FOXM1 KO cells,

these observations support the idea that FOXM1 acts an amplifier to fully active the G2/M transcriptional program.

It is important to note that FOXM1 gel mobility decreases with co-treatment of CHK1i and CDK1i indicating that FOXM1 is also phosphorylated by CDK2. Similar to MYBL2, FOXM1 may have early and late CDK phosphorylation sites that may be associated with different events with MMB-FOXM1 activation. The early and late CDK phosphorylation sites may mirror the two major events in which CDK phosphorylation of FOXM1 has been implicated, relieving an intramolecular interaction between the N-terminus (Laoukili et al., 2008b) and TAD and facilitating p300 recruitment by creating PLK1 binding sites (Fu et al., 2008; Marceau et al., 2019)suggesting a two-step mechanism. Moreover, There is some evidence to support this model as N-terminal cyclin D/CDK6 phosphorylation sites on FOXM1 were not sufficient to support gene transactivation but could stabilize FOXM1 in G1 (Anders et al., 2011).

A recent structural study of FOXM1 however questioned this two-step model by providing evidence that phosphorylation at consensus CDK sites in the N-terminus and the region just N-terminal to the TAD of FOXM1 were not sufficient to disrupt the interaction between the N-terminus and TAD by isothermal titration calorimetry. Rather, PLK1 phosphorylation at S715 was found to be necessary and sufficient to disrupt the interaction between the N-terminus and TAD, allowing for CBP to interact with the TAD (Marceau et al., 2019). A limitation of this study is that only purified domains of FOXM1 were used and the structural findings have yet to be validated with full length FOXM1 or in a cellular setting. Nonetheless, these finding suggest that FOXM1 activation occurs as a single step with CDK phosphorylation eventually leading to PLK1 phosphorylation which simultaneously relieves these intramolecular interaction and recruits p300. Thresholds of cyclin/CDK activity can be incorporated into either model. In the two-step model, there would be two distinct thresholds, a first threshold to relieve intramolecular interactions leading to a poised state and a second threshold of CDK activity that triggers p300 recruitment and MMB-FOXM1 activity, while, in the

one-step model, there would be just one threshold result in FOXM1 being opened up and activated once sufficient CDK phosphorylation had occurred at C-terminal CDK sites to generate PLK1 binding sites.

Finally, it remains to be determined if CDK phosphorylation is required for recruitment of FOXM1 to the MMB-FOXM1 complex. The N-terminus and forkhead binding domain of FOXM1 are required to interact with the MMB complex (Chen et al., 2013b) but it is unknown if the N-terminal-TAD interaction within FOXM1 inhibits its ability to interact with the MMB complex. If CDK phosphorylation of FOXM1 is not required to interact with the MMB complex, then this might suggest a poised model where unphosphorylated FOXM1 can associate with the MMB complex in late S phase and then be activated by CDK phosphorylation during the S/G2 transition. But considering that the FOXM1-LIN37 interaction increases at a similar rate as FOXM1 phosphorylation levels, when the cell transitions from S phase to G2 (Sadasivam et al., 2012a), it is more likely that CDK phosphorylation of FOXM1 promotes the association between FOXM1 and the MMB complex in some manner. This suggests that there could a separate CDK threshold for FOXM1 association with the MMB complex or a single CDK threshold for FOXM1 that triggers the confirmational change, MMB-FOXM1 association, and PLK1-dependent recruitment of p300, resulting in a flurry of gene expression once the CDK threshold is crossed.

Taken together, this work suggests a model where the MYBL2, MuvB, and FOXM1 components serve different roles. MuvB functions as the specifier/anchor of the complex by binding to the CHRs at G2/M promoters. MYBL2 serves as the timer for the MMB-FOXM1 complex with its accumulation in S phase allowing for MMB complex formation at G2/M promoters and then prevents continued MMB complex formation with CDK-dependent degradation after the G2/M transcriptional program is expressed. FOXM1 serves as the amplifying step with its recruitment to the complex and phosphorylation by cyclin A/B/CDK1 complexes triggering positives feedback loops that result in MMB-FOXM1 activation and G2/M gene expression.

The G1/S and G2/M waves of cell cycle gene expression are interconnected waves of transcription initiated by passing through the restriction point

The identification of cyclin F mediated MYBL2 degradation fills in a key missing piece in the puzzle of connections between the G1/S and G2/M waves of cell cycle gene expression. Cyclin F, expressed in the G2/M wave of gene expression, degrades key transcription factors for both G1/S and G2/M gene expression, E2F1-3a and MYBL2 respectively, expressed as part of the G1/S wave of gene expression (Clijsters et al., 2019; Fischer et al., 2016). Additionally, one of the binding partners of E2F transcription factors, DP1, as well as multiple MuvB components, LIN54, LIN52 and RBBP4, are G1/S genes while FOXM1 and the MuvB component, LIN9, are G2/M genes (Fischer et al., 2016). Thus, the components for G1/S gene expression are amplified in a positive feedback loop in G1 while components MuvB and MYBL2, necessary for initiating G2/M gene expression are expressed, creating a bridge from the G1/S wave to the G2/M wave. The inclusion of LIN52 in the G1/S wave is interesting as it is an essential component of the DREAM complex and phosphorylation of S28 on LIN52, a key factor for DREAM formation, promotes LIN52 protein turnover (Iness et al., 2019; Litovchick et al., 2011). This suggests a mechanism of LIN52 being replaced ahead of MMB-FOXM1 complex formation by G1/S gene expression as phosphorylated LIN52 remaining from the DREAM complex is degraded by a phospho-degron centered on S28 to enforce DREAM complex disassembly. A similar mechanism could exist for LIN54, the DNA binding protein of MuvB, as part of DREAM disassembly. In the G2/M program, there is another positive feedback with FOXM1 and LIN9 in the G2/M wave gene expression. The presence of LIN9 in the G2/M wave stands out as LIN9 functions as a scaffolding protein in the MMB-FOXM1 complex interacting with both MYBL2 and FOXM1 (Guiley et al., 2018; Wiseman et al., 2015). Little is known about the regulation of LIN9 so the significance of LIN9 being expressed in the G2/M wave of gene

expression is unclear. Finally, the expression of cyclin F in the G2/M wave of gene expression results in the termination of both waves of cell cycle gene expression.

This interconnectivity between the G1/S and G2/M waves of cell cycle gene expression underscores the concept of the G1/S checkpoint or restriction point first described by Arthur Pardee back in 1970s. Pardee showed that DNA synthesis could be blocked in cells emerging from quiescence if a deficiency or inhibitory agent in the media could pause cell division before a certain point in G1. Once the cell had passed that restriction point however the cell was committed to DNA synthesis (Pardee, 1974). While the molecular definition of the restriction point has evolved with new discoveries, activation of G1/S genes by the E2F transcription factors is a key step in the cell progressing past this restriction point (Bertoli et al., 2013; Cappell et al., 2018; Yao et al., 2008). Consequently, the interconnectivity between the G1/S and G2/M waves of cell cycle gene expression means that passing through the restriction point will result in the reading of the entire cell cycle transcriptional program.

There are secondary mechanisms to turn off or down regulate cell cycle gene expression in the absence of cyclin F. Given the instability of cyclin F, these alternative pathways may serve to modulate cell cycle gene expression when MMB-FOXM1 activity is low. For the activating E2Fs, phosphorylation of E2F1 by cyclin A/CDK2 inhibits the ability of E2F1/DP1 dimers to bind (Xu et al., 1994). The inhibition of E2F1 by cyclin A/CDK2 may also serve to limit E2F1 activity in late S phase prior to activation of the MMB-FOXM1 complex. E2F activity would reduce while preserving E2F1 level so, if DNA damage occurred or DNA replication was interrupted causing CDK activity to decrease, CDK phosphorylation can be removed by phosphatases and active E2F complexes can reform. As an alternative for MYBL2 degradation, FOXM1 degradation is part of the cell cycle reset driven by the APC/C (Laoukili et al., 2008a; Park et al., 2008) to allow the establishment of G1. APC/C-mediated degradation of E2F transcription factors has also be reported (Budhavarapu et al., 2012; Peart et al., 2010)

suggesting that APC/C may also limit E2F levels in its efforts to reset the cell cycle as the cell exits mitosis.

G2/M gene expression is part of the Intra-S ATR-CHK1 checkpoint that is critical for CHK1 inhibitors mechanism of action

The ATR-CHK1 pathway enforces a checkpoint in S phase to time the activation of the S/G2 transition with DNA replication. In an unperturbed cell cycle, this checkpoint functions to ensure completion of DNA replication of the genome prior to proceeding onto cytokinesis and, in the presence of DNA damage, the checkpoint arrests cell cycle progression and mobilizes the DNA damage response to resolve the offending DNA damage (Ciardo et al., 2019; Kotsantis et al., 2018; Sancar et al., 2004). Traditionally, the arrest of cell cycle progression by this checkpoint had focused on limiting the writing of the mitotic cellular state by restricting CDK1 activity through CHK1-dependent upregulation of WEE1 kinase activity and downregulation of CDC25 phosphatase activity (Ciardo et al., 2019; Furnari et al., 1997; Kotsantis et al., 2018; O'Connell et al., 1997). Consequently, the intra S checkpoint was typically investigated as a post-translational event. However, recent work identified a transcriptional component of the intra-S checkpoint by showing the ATR-CHK1 pathway to limit FOXM1-dependent G2/M gene expression, delaying mitotic entry (Saldivar et al., 2018). Thus, the intra-S checkpoint prevents the reading of the mitotic cellular program from the genome in addition to preventing the writing of the program by cyclin/CDK1 complexes.

Work in this dissertation builds upon the observation of a transcriptional component to the intra-S checkpoint by demonstrating how the ATR-CHK1-dependent restriction of G2/M gene expression during S phase is necessary for the ATR-CHK1 pathway to manage replication stress. ATR and CHK1 inhibitors are currently being considered for clinical use and the mechanism of action for these inhibitors has largely focused on the regulation of DNA replication and replication fork stability by the ATR-CHK1 pathway (Petermann et al., 2010; Qiu

et al., 2018; Syljuåsen et al., 2005). However, upregulation of origin firing and DNA replication during S phase did not correlate with the induction of replication stress and was still induced in CHK1i-resistant LIN54 KO and FOXM1 KO cells. Instead, the induction of premature mitosis in late S phase by CHK1 or ATR inhibition correlated with the induction of replication stress. Mechanistic experiments with LIN54 KO and FOXM1 KO cells as well as CDK1 inhibitors revealed that CHK1i-induced premature mitosis was necessary for replication stress and was being driven by the MMB-FOXM1-CDK1 feedback loop . An important feature of this feedback loop is that it links transcription of the mitotic cellular program with cyclin/CDK1 activity during the S/G2 transition, indicating that the cell coordinates the writing and reading of the mitotic cellular program through the intra-S checkpoint.

The requirement of MMB-FOXM1-driven premature mitosis for CHK1i sensitivity indicates that the rate limiting step for cell death following CHK1 inhibition lies within mitosis rather than DNA replication contrary to the current mechanism proposed for CHK1 inhibitors (Qiu et al., 2018). Sufficient CDK1 activity to induce premature mitosis was required to induce replication stress and apoptosis indicating that dysregulation of the mitotic cell program is necessary for cell death. DNA replication however was still upregulated at these levels of CDK1 activity, similar to the LIN54 KO and FOXM1 KO cells, highlighting that increased DNA replication after CHK1 inhibition was not sufficient to trigger cell death. Similarly, a concurrent study with CHK1i in ovarian cells showed that ovarian cancer cells with acquired resistance to CHK1i and parental cells had similar replication stability while the CHK1i-resistant cells had a lower cyclin B1 expression and a G2/M delay (Nair et al., 2020). These observations are in line with our model for CHK1i sensitivity in which dysregulation of the S/G2/M transition caused by MMB-FOXM1-CDK1-driven premature mitosis, rather than increased origin firing, triggers CHK1i-induced replication catastrophe.

Unifying DNA replication and mitotic catastrophe under cell cycle dysregulation

By studying CHK1i-induced DNA replication and mitotic catastrophe in parallel, premature APC/C activity was identified as a shared mechanistic step between DNA replication and mitotic catastrophe. While previous work on replication catastrophe has largely focused on dysregulation of the DNA replication machinery (Toledo et al., 2017; Toledo et al., 2013), the requirement of MMB-FOXM1 activity for the loss of replication factors, impaired DNA synthesis, and DNA replication catastrophe after CHK1 inhibition indicates a role for the mitotic cellular program in triggering DNA replication catastrophe. CHK1i-induced premature APC/C activation, due to loss of FBXO5 and impaired AURKB activity, leads to the degradation of G2/M regulators and DNA origin licensing factors. The loss of DNA origin firing factors leads to decreased chromatin-bound MCM complexes in cells with impaired DNA replication suggesting that, with each round of cell division in the presence of CHK1i, cells become less and less competent to replicate their genomes. Dormant origins are necessary for DNA replication under stressed conditions (Ge et al., 2007) and deregulation of origin licensing by FBXO5 depletion impairs DNA replication leading to the accumulation of ssDNA intermediates and replication stress during S phase (Neelsen et al., 2013) suggesting that origin exhaustion due to premature APC/C activity can trigger irreparable DNA damage during DNA replication similar to RPA exhaustion. For mitotic catastrophe, premature induction of the APC/C by CHK1i reduces the time that cells have to complete DNA replication, condense chromatin, and complete genome segregation before the cell is reset to G1 by the APC/C. This would result in an increasing number of cells undergoing failed genome segregation with a large amount of incomplete DNA replication structures, which is mitotic catastrophe.

Thus, DNA replication and mitotic catastrophe are fundamentally the same phenomena happening at different points in the cell cycle and consisting of two components: (i) accumulation of a DNA damage signal that can trigger cell death and (ii) altered APC/C activity that prevents cell cycle progression. The DNA damage signal could come from DSBs, ssDNA

replication intermediates, or mis-segregated chromosomes while the APC/C dysregulation locks the cell in a state where it cannot resolve these DNA damage signals allowing them to accumulate and cause cell death. If the APC/C dysregulation occurs in the presence of active DNA replication, it can present as DNA replication catastrophe, but if APC/C dysregulation occurs after completion of or in the absence of DNA replication, it will present as mitotic catastrophe due to the activation of the mitotic program.

This model can be extended to other DNA replication stress agents such as hydroxyurea and WEE1 inhibitors. Hydroxyurea alone and in combination with ATR inhibition triggers replication catastrophe (Toledo et al., 2013). Hydroxyurea inhibits ribonucleotide reductase, depleting the nucleotide pools necessary for DNA replication and resulting in the accumulation of stalled replication forks (Davis and Elledge, 1990; Sogo et al., 2002), generating a DNA damage signal. Studies of these conserved pathways in yeast provide clues as to how hydroxyurea treatment also creates APC/C dysfunction. In *S. pombe*, Flp1, the homologue of CDC14, is required for the replication stress response to hydroxyurea (Diaz-Cuervo and Bueno, 2008). ssDNA was identified as an activating ligand for CDC14 in studies of purified CDC14 from *S. cerevisiae* (Taylor et al., 1997) supporting the idea that CDC14 is activated by the ssDNA generated during hydroxyurea treatment. In humans, where there are three CDC14 homologues, CDC14B dephosphorylates FZR1 in G2 to activate the APC/C in response to DNA damage, leading to PLK1 degradation and cell cycle arrest to allow for repair of the DNA damage (Bassermann et al., 2008). Further, phosphorylation of CDC14 in yeast by CDC5, the homologue of PLK1, promotes CDC14 release from nucleoli facilitating its activation (Visintin et al., 2003). Thus, hydroxyurea could potentially trigger APC/C activity in S phase by ssDNA-dependent activation of CDC14. ATR/CHK1 would accelerate APC/C activation in this model by facilitating the release of CDC14 from nucleoli by upregulating CDC14 release from nuclei. While the LIN54 and FOXM1 KO cells were resistant to ATR/CHK1 inhibition, they retained sensitivity to WEE1 inhibition indicating that WEE1 inhibition can cause cell death through

activities other than restricting CDK1 activity. In addition to CDK1 and CDK2, WEE1 has been implicated as a negative regulator of APC/C activity through tyrosine phosphorylation of the complex (Vassilopoulos et al., 2015). Thus, WEE1 inhibitors may cause cell death in LIN54 and FOXM1 KOs by directing derepressing APC/C activity and upregulating DNA replication through increased CDK2 activity. Investigating whether these other replication stress agents activate the APC/C or another form of cell cycle dysregulation to cause replication catastrophe will provide insights that can potentially guide the use of this compound in the clinic.

Conclusion

In conclusion, this dissertation advances our understanding of how the MMB-FOXM1 complex promotes G2/M expression by identifying $SCF^{cyclin\ F}$-mediated degradation of MYBL2 as the “off” switch for G2/M gene expression that functions as part of a negative feedback loop to limit cyclin B/CDK1 activity. Additionally, this dissertation provides mechanistic insights into how CHK1 inhibition induces DNA replication catastrophe and mitotic catastrophe and the central role the MMB-FOXM1-CDK1 feedback loop plays in CHK1 inhibitor sensitivity. We demonstrate that CHK1i derepresses an MMB-FOXM1-CDK1 feedback loop to prematurely induce the mitotic cellular identity and that this premature mitosis in S phase is necessary for replication catastrophe and cell death. We provide evidence that CHK1i-induced DNA replication and mitotic catastrophe are linked by premature activation of the APC/C, which is triggered by MMB-FOXM1-dependent loss of FBXO5 and impaired Aurora B activity in mitosis. Our findings provide critical insights into the mechanism of action for CHK1 inhibitors, which are currently being developed for clinical use, while demonstrating the central role that the MMB-FOXM1 complex plays in transitioning between the two fundamental tasks of the cell division cycle, genome duplication and cellular division.

References

Aarts, M., Sharpe, R., Garcia-Murillas, I., Gevensleben, H., Hurd, M.S., Shumway, S.D., Toniatti, C., Ashworth, A., and Turner, N.C. (2012). Forced mitotic entry of S-phase cells as a therapeutic strategy induced by inhibition of WEE1. Cancer Discov *2*, 524-539.
Abate, F., Ambrosio, M.R., Mundo, L., Laginestra, M.A., Fuligni, F., Rossi, M., Zairis, S., Gazaneo, S., De Falco, G., Lazzi, S*., et al.* (2015). Distinct Viral and Mutational Spectrum of Endemic Burkitt Lymphoma. PLoS Pathog *11*, e1005158.
Abe, S., Nagasaka, K., Hirayama, Y., Kozuka-Hata, H., Oyama, M., Aoyagi, Y., Obuse, C., and Hirota, T. (2011). The initial phase of chromosome condensation requires Cdk1-mediated phosphorylation of the CAP-D3 subunit of condensin II. Genes Dev *25*, 863-874.
Abe, Y., Sako, K., Takagaki, K., Hirayama, Y., Uchida, K.S., Herman, J.A., DeLuca, J.G., and Hirota, T. (2016). HP1-Assisted Aurora B Kinase Activity Prevents Chromosome Segregation Errors. Dev Cell *36*, 487-497.
Abrieu, A., Brassac, T., Galas, S., Fisher, D., Labbé, J.C., and Dorée, M. (1998). The Polo-like kinase PLx1 is a component of the MPF amplication loop at the G2/M-phase transition of the cell cycle in *Xenopus* eggs. J Cell Sci *111*, 1751-1757.
Adam, K., Cartel, M., Lambert, M., David, L., Yuan, L., Besson, A., Mayeux, P., Manenti, S., and Didier, C. (2018). A PIM-CHK1 signaling pathway regulates PLK1 phosphorylation and function during mitosis. J Cell Sci *131*.
Adams, P.D., Li, X., Sellers, W.R., Baker, K.B., Leng, X., Harper, J.W., Taya, Y., and Kaelin, J., W. G. (1999). Retinoblastoma Protein Contains a C-terminal Motif That Targets It for Phosphorylation by Cyclin-cdk Complexes. Mol Cell Biol *19*, 1068-1080.
Aggarwal, P., Lessie, M.D., Lin, D.I., Pontano, L., Gladden, A.B., Nuskey, B., Goradia, A., Wasik, M.A., Klein-Szanto, A.J., Rustgi, A.K*., et al.* (2007). Nuclear accumulation of cyclin D1 during S phase inhibits Cul4-dependent Cdt1 proteolysis and triggers p53-dependent DNA rereplication. Genes Dev *21*, 2908-2922.
Akiyama, T., Ohuchi, T., Sumida, S., Matsumoto, M., and Toyoshima, K. (1992). Phosphorylation of the retinoblastoma protein by cdk2. *89*, 7900-7904.
Akopyan, K., Silva Cascales, H., Hukasova, E., Saurin, A.T., Mullers, E., Jaiswal, H., Hollman, D.A., Kops, G.J., Medema, R.H., and Lindqvist, A. (2014). Assessing kinetics from fixed cells reveals activation of the mitotic entry network at the S/G2 transition. Mol Cell *53*, 843-853.
Alfieri, C., Zhang, S., and Barford, D. (2017). Visualizing the complex functions and mechanisms of the anaphase promoting complex/cyclosome (APC/C). Open Biol *7*.
Alvarez-Fernandez, M., Halim, V.A., Aprelia, M., Laoukili, J., Mohammed, S., and Medema, R.H. (2011). Protein phosphatase 2A (B55alpha) prevents premature activation of forkhead transcription factor FoxM1 by antagonizing cyclin A/cyclin-dependent kinase-mediated phosphorylation. J Biol Chem *286*, 33029-33036.
Anders, L., Ke, N., Hydbring, P., Choi, Y.J., Widlund, H.R., Chick, J.M., Zhai, H., Vidal, M., Gygi, S.P., Braun, P*., et al.* (2011). A systematic screen for CDK4/6 substrates links FOXM1 phosphorylation to senescence suppression in cancer cells. Cancer Cell *20*, 620-634.
Anders, S., Pyl, P.T., and Huber, W. (2015). HTSeq--a Python framework to work with high-throughput sequencing data. Bioinformatics *31*, 166-169.
Andreassen, P.R., Lohez, O.D., Lacroix, F.B., and Margolis, R.L. (2001). Tetraploid State Induces p53-dependent Arrest of Nontransformed Mammalian Cells in G1. Mol Biol Cell *12*, 1315-1328.
Araki, M., Wharton, R.P., Tang, Z., Yu, H., and Asano, M. (2003). Degradation of origin recognition complex large subunit by the anaphase-promoting complex in Drosphila. The EMBO journal *22*, 6115-6126.
Ashley, A.K., Shrivastav, M., Nie, J., Amerin, C., Troksa, K., Glanzer, J.G., Liu, S., Opiyo, S.O., Dimitrova, D.D., Le, P*., et al.* (2014). DNA-PK phosphorylation of RPA32 Ser4/Ser8 regulates replication stress checkpoint activation, fork restart, homologous recombination and mitotic catastrophe. DNA Repair (Amst) *21*, 131-139.

Bai, C., Sen, P., Hofmann, K., Ma, L., Goebl, M., Harper, J.W., and Elledge, S.J. (1996). SKP1 connects cell cycle regulators to the ubiquitin proteolysis machinery through a novel motif, the F-box. Cell *86*, 263-274.
Bainor, A.J., Saini, S., Calderon, A., Casado-Polanco, R., Giner-Ramirez, B., Moncada, C., Cantor, D.J., Ernlund, A., Litovchick, L., and David, G. (2018). The HDAC-Associated Sin3B Protein Represses DREAM Complex Targets and Cooperates with APC/C to Promote Quiescence. Cell Rep *25*, 2797-2807 e2798.
Bakhoum, S.F., Kabeche, L., Murnane, J.P., Zaki, B.I., and Compton, D.A. (2014). DNA-damage response during mitosis induces whole-chromosome missegregation. Cancer Discov *4*, 1281-1289.
Balachandran, R.S., Heighington, C.S., Starostina, N.G., Anderson, J.W., Owen, D.L., Vasudevan, S., and Kipreos, E.T. (2016). The ubiquitin ligase CRL2ZYG11 targets cyclin B1 for degradation in a conserved pathway that facilitates mitotic slippage. J Cell Biol *215*, 151-166.
Barbash, O., Zamfirova, P., Lin, D.I., Chen, X., Yang, K., Nakagawa, H., Lu, F., Rustgi, A.K., and Diehl, J.A. (2008). Mutations in Fbx4 inhibit dimerization of the SCF(Fbx4) ligase and contribute to cyclin D1 overexpression in human cancer. Cancer Cell *14*, 68-78.
Barger, C.J., Branick, C., Chee, L., and Karpf, A.R. (2019). Pan-Cancer Analyses Reveal Genomic Features of FOXM1 Overexpression in Cancer. Cancers (Basel) *11*.
Barsotti, A.M., and Prives, C. (2009). Pro-proliferative FoxM1 is a target of p53-mediated repression. Oncogene *28*, 4295-4305.
Bartova, I., Otyepka, M., Kriz, Z., and Koca, J. (2004). Activation and inhibition of cyclin-dependent kinase-2 by phosphorylation; a molecular dynamics study reveals the functional importance of the glycine-rich loop. Protein Sci *13*, 1449-1457.
Bartsch, O., Horstmann, S., Toprak, K., Klempnauer, K.H., and Ferrari, S. (1999). Identification of cyclin A/Cdk2 phosphorylation sites in B-Myb. Eur J Biochem, 384-391.
Bashir, T., Dorrello, N.V., Amador, V., Guardavaccaro, D., and Pagano, M. (2004). Control of $SCF^{Skp2\text{-}Cks1}$ ubiquitin ligase by the APC/C^{Cdh1} ubiquitin ligase. Nature *428*, 190-193.
Bassermann, F., Frescas, D., Guardavaccaro, D., Busino, L., Peschiaroli, A., and Pagano, M. (2008). The Cdc14B-Cdh1-Plk1 axis controls the G2 DNA-damage-response checkpoint. Cell *134*, 256-267.
Bates, S., Bonetta, L., MacAllan, D., Parry, D., Holder, A., Dickson, C., and Peters, G. (1994). CDK6 (PLSTIRE) and CDK4 (PSK-J3) are a distinct subset of the cyclin-dependent kinases that associate with cyclin D1. Oncogene *9*, 71-79.
Bell, S.P., and Dutta, A. (2002). DNA replication in eukaryotic cells. Annu Rev Biochem *71*, 333-374.
Bergholtz, S., Andersen, T.Ø., Andersson, K.B., Borrebæk, J., Lüscher, B., and Gabrielsen, O.S. (2001). The highly conserved DNA-binding domains of A-, B-, and c-Myb differ with respect to DNA-binding, phosphorylation, and redox properties. Nucleic Acids Res *29*, 3546-3556.
Bertoli, C., Skotheim, J.M., and de Bruin, R.A. (2013). Control of cell cycle transcription during G1 and S phases. Nature reviews Molecular cell biology *14*, 518-528.
Bessa, M., Saville, M.K., and Watson, R.J. (2001). Inhibition of cyclin A/Cdk2 phosphorylation impairs B-Myb transactivation function without affecting interactions with DNA or the CBP coactivator. Oncogene *7*, 3376-3386.
Blosser, W.D., Dempsey, J.A., McNulty, A.M., Rao, X., Ebert, P.J., Lowery, C.D., Iversen, P.W., Webster, Y.W., Donoho, G.P., Gong, X.*, et al.* (2020). A pan-cancer transcriptome analysis identifies replication fork and innate immunity genes as modifiers of response to the CHK1 inhibitor prexasertib. Oncotarget *11*, 216-236.
Branigan, T.B., Kozono, D., Schade, A.E., Deraska, P., Rivas, H.G., Sambel, L., Reavis, H.D., Shapiro, G.I., D'Andrea, A.D., and DeCaprio, J.A. (2021). MMB-FOXM1-driven premature mitosis is required for CHK1 inhibitor sensitivity. Cell Rep *34*, 108808.

Brown, E.J., and Baltimore, D. (2000). ATR disruption leads to chromosomal fragmentation and early embryonic lethality. Genes Dev *14*, 397-402.
Brown, N.R., Lowe, E.D., Petri, E., Skamnaki, V., Antrobus, R., and Johnson, L.N. (2007). Cyclin B and cyclin A confer different substrate recognition properties on CDK2. Cell Cycle *6*, 1350-1359.
Brown, N.R., Noble, M.E.M., Endicott, J.A., and Johnson, L.N. (1999). The structural basis for specificity of substrate and recruitment peptides for cyclin-dependent kinases. Nat Cell Bio *1*, 438-443.
Budhavarapu, V.N., White, E.D., Mahanic, C.S., Chen, L., Lin, F.T., and Lin, W.C. (2012). Regulation of E2F1 by APC/C Cdh1 via K11 linkage-specific ubiquitin chain formation. Cell Cycle *11*, 2030-2038.
Buisson, R., Boisvert, J.L., Benes, C.H., and Zou, L. (2015). Distinct but Concerted Roles of ATR, DNA-PK, and Chk1 in Countering Replication Stress during S Phase. Mol Cell *59*, 1011-1024.
Bukhari, A.B., Lewis, C.W., Pearce, J.J., Luong, D., Chan, G.K., and Gamper, A.M. (2019). Inhibiting Wee1 and ATR kinases produces tumor-selective synthetic lethality and suppresses metastasis. J Clin Invest *129*, 1329-1344.
Burdova, K., Yang, H., Faedda, R., Hume, S., Chauhan, J., Ebner, D., Kessler, B.M., Vendrell, I., Drewry, D.H., Wells, C.I.*, et al.* (2019). E2F1 proteolysis via SCF-cyclin F underlies synthetic lethality between cyclin F loss and Chk1 inhibition. The EMBO Journal *38*.
Burke, J.R., Deshong, A.J., Pelton, J.G., and Rubin, S.M. (2010). Phosphorylation-induced conformational changes in the retinoblastoma protein inhibit E2F transactivation domain binding. J Biol Chem *285*, 16286-16293.
Busch, C.J., Kroger, M.S., Jensen, J., Kriegs, M., Gatzemeier, F., Petersen, C., Munscher, A., Rothkamm, K., and Rieckmann, T. (2017). G2-checkpoint targeting and radiosensitization of HPV/p16-positive HNSCC cells through the inhibition of Chk1 and Wee1. Radiother Oncol *122*, 260-266.
Calvisi, D.F., Simile, M.M., Ladu, S., Frau, M., Evert, M., Tomasi, M.L., Demartis, M.I., Daino, L., Seddaiu, M.A., Brozzetti, S.*, et al.* (2011). Activation of v-Myb avian myeloblastosis viral oncogene homolog-like2 (MYBL2)-LIN9 complex contributes to human hepatocarcinogenesis and identifies a subset of hepatocellular carcinoma with mutant p53. Hepatology *53*, 1226-1236.
Cappell, S.D., Chung, M., Jaimovich, A., Spencer, S.L., and Meyer, T. (2016). Irreversible APC(Cdh1) Inactivation Underlies the Point of No Return for Cell-Cycle Entry. Cell *166*, 167-180.
Cappell, S.D., Mark, K.G., Garbett, D., Pack, L.R., Rape, M., and Meyer, T. (2018). EMI1 switches from being a substrate to an inhibitor of APC/C(CDH1) to start the cell cycle. Nature *558*, 313-317.
Carmena, M., Wheelock, M., Funabiki, H., and Earnshaw, W.C. (2012). The chromosomal passenger complex (CPC): from easy rider to the godfather of mitosis. Nat Rev Mol Cell Biol *13*, 789-803.
Carr, J.R., Park, H.J., Wang, Z., Kiefer, M.M., and Raychaudhuri, P. (2010). FoxM1 mediates resistance to herceptin and paclitaxel. Cancer Res *70*, 5054-5063.
Carrassa, L., Chila, R., Lupi, M., Ricci, F., Celenza, C., Mazzoletti, M., Broggini, M., and Damia, G. (2012). Combined inhibition of Chk1 and Wee1: in vitro synergistic effect translates to tumor growth inhibition in vivo. Cell Cycle *11*, 2507-2517.
Castedo, M., Perfettini, J.L., Roumier, T., Andreau, K., Medema, R., and Kroemer, G. (2004). Cell death by mitotic catastrophe: a molecular definition. Oncogene *23*, 2825-2837.
Chang, D.C., Xu, N., and Luo, K.Q. (2003). Degradation of cyclin B is required for the onset of anaphase in Mammalian cells. J Biol Chem *278*, 37865-37873.

Charrasse, S., Carena, I., Brondani, V., Klempnauer, K.H., and Ferrari, S. (2000). Degradation of B-Myb by ubiquitin-mediated proteolysis: involvement of the Cdc34-SCF(p45Skp2) pathway. Oncogene *19*, 2986-2995.
Charrasse, S., Gharbi-Ayachi, A., Burgess, A., Vera, J., Hached, K., Raynaud, P., Schwob, E., Lorca, T., and Castro, A. (2017). Ensa controls S-phase length by modulating Treslin levels. Nat Commun *8*, 206.
Chaudhuri, L., Vincelette, N.D., Koh, B.D., Naylor, R.M., Flatten, K.S., Peterson, K.L., McNally, A., Gojo, I., Karp, J.E., Mesa, R.A.*, et al.* (2014). CHK1 and WEE1 inhibition combine synergistically to enhance therapeutic efficacy in acute myeloid leukemia ex vivo. Haematologica *99*, 688-696.
Chellappan, S.P., Hiebert, S., Mudryl, M., Horowitz, J.M., and Nevins, J.R. (1991). The E2F Transcription Factor Is a Cellular Target for the RB Protein. Cell *65*, 1053-1061.
Chen, J.Y., Lin, J.R., Tsai, F.C., and Meyer, T. (2013a). Dosage of Dyrk1a shifts cells within a p21-cyclin D1 signaling map to control the decision to enter the cell cycle. Mol Cell *52*, 87-100.
Chen, M.S., Ryan, C.E., and Piwnica-Worms, H. (2003). Chk1 kinase negatively regulates mitotic function of Cdc25A phosphatase through 14-3-3 binding. Mol Cell Biol *23*, 7488-7497.
Chen, R.-H., Waters, J.C., Salmon, E.D., and Murray, A.W. (1996). Association of Spindle Assembly Checkpoint Component XMAD2 with Unattached Kinetochores. Science *274*, 242-246.
Chen, X., Muller, G.A., Quaas, M., Fischer, M., Han, N., Stutchbury, B., Sharrocks, A.D., and Engeland, K. (2013b). The forkhead transcription factor FOXM1 controls cell cycle-dependent gene expression through an atypical chromatin binding mechanism. Mol Cell Biol *33*, 227-236.
Chen, Y.J., Chen, C.M., Twu, N.F., Yen, M.S., Lai, C.R., Wu, H.H., Wang, P.H., and Yuan, C.C. (2009). Overexpression of Aurora B is associated with poor prognosis in epithelial ovarian cancer patients. Virchows Arch *455*, 431-440.
Chen, Z., Indjeian, V.B., McManus, M., Wang, L., and Dynlacht, B.D. (2002). CP110, a Cell Cycle-Dependent CDK Substrate, Regulates Centrosome Duplication in Human Cells. Dev Cell *3*, 339-350.
Chila, R., Basana, A., Lupi, M., Guffanti, F., Gaudio, E., Rinaldi, A., Cascione, L., Restelli, V., Tarantelli, C., Bertoni, F.*, et al.* (2015). Combined inhibition of Chk1 and Wee1 as a new therapeutic strategy for mantle cell lymphoma. Oncotarget *6*, 3394-3408.
Choudhury, R., Bonacci, T., Arceci, A., Lahiri, D., Mills, C.A., Kernan, J.L., Branigan, T.B., DeCaprio, J.A., Burke, D.J., and Emanuele, M.J. (2016). APC/C and SCF(cyclin F) Constitute a Reciprocal Feedback Circuit Controlling S-Phase Entry. Cell reports *16*, 3359-3372.
Chu, L., Huo, Y., Liu, X., Yao, P., Thomas, K., Jiang, H., Zhu, T., Zhang, G., Chaudhry, M., Adams, G.*, et al.* (2014). The spatiotemporal dynamics of chromatin protein HP1alpha is essential for accurate chromosome segregation during cell division. J Biol Chem *289*, 26249-26262.
Chung, S., Vail, P., Witkiewicz, A.K., and Knudsen, E.S. (2019). Coordinately Targeting Cell-Cycle Checkpoint Functions in Integrated Models of Pancreatic Cancer. Clin Cancer Res *25*, 2290-2304.
Ciardo, D., Goldar, A., and Marheineke, K. (2019). On the Interplay of the DNA Replication Program and the Intra-S Phase Checkpoint Pathway. Genes (Basel) *10*.
Cimprich, K.A., Shin, T.B., Keith, C.T., and Schreiber, S.L. (1996). cDNA cloning and gene mapping of a candidate human cell cycle checkpoint protein. Proc Natl Acad Sci U S A *93*, 2850-2855.
Cleary, J.M., Aguirre, A.J., Shapiro, G.I., and D'Andrea, A.D. (2020). Biomarker-Guided Development of DNA Repair Inhibitors. Mol Cell *78*, 1070-1085.
Clijsters, L., Hoencamp, C., Calis, J.J.A., Marzio, A., Handgraaf, S.M., Cuitino, M.C., Rosenberg, B.R., Leone, G., and Pagano, M. (2019). Cyclin F Controls Cell-Cycle

Transcriptional Outputs by Directing the Degradation of the Three Activator E2Fs. Mol Cell *74*, 1264-1277 e1267.
Clijsters, L., Ogink, J., and Wolthuis, R. (2013). The spindle checkpoint, APC/C(Cdc20), and APC/C(Cdh1) play distinct roles in connecting mitosis to S phase. J Cell Biol *201*, 1013-1026.
Clijsters, L., van Zon, W., Riet, B.T., Voets, E., Boekhout, M., Ogink, J., Rumpf-Kienzl, C., and Wolthuis, R.M. (2014). Inefficient degradation of cyclin B1 re-activates the spindle checkpoint right after sister chromatid disjunction. Cell Cycle *13*, 2370-2378.
Clurman, B.E., Sheaff, R.J., Thress, K., Groudine, M., and Roberts, J.M. (1996). Turnover of cyclin E by the ubiquitin-proteasome pathway is regulated by cdk2 binding and cyclin phosphorylation. Genes Dev *10*, 1979-1990.
Cole, K.A., Huggins, J., Laquaglia, M., Hulderman, C.E., Russell, M.R., Bosse, K., Diskin, S.J., Attiyeh, E.F., Sennett, R., Norris, G.*, et al.* (2011). RNAi screen of the protein kinome identifies checkpoint kinase 1 (CHK1) as a therapeutic target in neuroblastoma. Proc Natl Acad Sci U S A *108*, 3336-3341.
Coleman, T.R., Carpernter, P.B., and Dunphy, W.G. (1996). The Xenopus Cdc6 Protein is Essential for the Initiation of a Single Round of DNA Replication in Cell-Free Extracts. Cell *67*, 53-63.
Collin, P., Nashchekina, O., Walker, R., and Pines, J. (2013). The spindle assembly checkpoint works like a rheostat rather than a toggle switch. Nat Cell Biol *15*, 1378-1385.
Consolaro, F., Basso, G., Ghaem-Magami, S., Lam, E.W., and Viola, G. (2015). FOXM1 is overexpressed in B-acute lymphoblastic leukemia (B-ALL) and its inhibition sensitizes B-ALL cells to chemotherapeutic drugs. Int J Oncol *47*, 1230-1240.
Cook, J.G., Chasse, D.A., and Nevins, J.R. (2004). The regulated association of Cdt1 with minichromosome maintenance proteins and Cdc6 in mammalian cells. J Biol Chem *279*, 9625-9633.
Corsello, S.M., Nagari, R.T., Spangler, R.D., Rossen, J., Kocak, M., Bryan, J.G., Humeidi, R., Peck, D., Wu, X., Tang, A.A.*, et al.* (2020). Discovering the anti-cancer potential of non-oncology drugs by systematic viability profiling. Nat Cancer *1*, 235-248.
Cortez, D., Glick, G., and Elledge, S.J. (2004). Minichromosome maintenance proteins are direct targets of the ATM and ATR checkpoint kinases. Proc Natl Acad Sci U S A *101*, 10078-10083.
Couch, F.B., Bansbach, C.E., Driscoll, R., Luzwick, J.W., Glick, G.G., Betous, R., Carroll, C.M., Jung, S.Y., Qin, J., Cimprich, K.A.*, et al.* (2013). ATR phosphorylates SMARCAL1 to prevent replication fork collapse. Genes Dev *27*, 1610-1623.
Coulonval, K., Kooken, H., and Roger, P.P. (2011). Coupling of T161 and T14 phopshorylations protects cyclin B-CDK1 from premature activation. Mol Biol Cell *22*, 3971-3985.
D'Angiolella, V., Donato, V., Forrester, F.M., Jeong, Y.-T.T., Pellacani, C., Kudo, Y., Saraf, A., Florens, L., Washburn, M.P., and Pagano, M. (2012). Cyclin F-mediated degradation of ribonucleotide reductase M2 controls genome integrity and DNA repair. Cell *149*, 1023-1034.
D'Angiolella, V., Donato, V., Vijayakumar, S., Saraf, A., Florens, L., Washburn, M.P., Dynlacht, B., and Pagano, M. (2010). SCF(Cyclin F) controls centrosome homeostasis and mitotic fidelity through CP110 degradation. Nature *466*, 138-142.
Dalal, S.N., Schweitzer, C.M., Gan, J., and DeCaprio, J.A. (1999). Cytoplasmic Localization of Human CDC25C during Interphase Requires an Intact 14-3-3 Binding Site. Mol Cell Biol *19*, 4465-4479.
Dankert, J.F., Rona, G., Clijsters, L., Geter, P., Skaar, J.R., Bermudez-Hernandez, K., Sassani, E., Fenyo, D., Ueberheide, B., Schneider, R.*, et al.* (2016). Cyclin F-Mediated Degradation of SLBP Limits H2A.X Accumulation and Apoptosis upon Genotoxic Stress in G2. Mol Cell *64*, 507-519.
Dart, D.A., Adams, K.E., Akerman, I., and Lakin, N.D. (2004). Recruitment of the cell cycle checkpoint kinase ATR to chromatin during S-phase. J Biol Chem *279*, 16433-16440.

Davidson, I.F., Li, A., and Blow, J.J. (2006). Deregulated replication licensing causes DNA fragmentation consistent with head-to-tail fork collision. Mol Cell *24*, 433-443.
Davies, K.D., Cable, P.L., Garrus, J.E., Sullivan, F.X., von Carlowitz, I., Huerou, Y.L., Wallace, E., Woessner, R.D., and Gross, S. (2011). Chk1 inhibition and Wee1 inhibition combine synergistically to impede cellular proliferation. Cancer Biol Ther *12*, 788-796.
Davis, R.J., Swanger, J., Hughes, B.T., and Clurmana, B.E. (2017). The PP2A-B56 Phosphatase Opposes Cyclin E Autocatalytic Degradation via Site-Specific Dephosphorylation. Mol Cell Biol *37*, e00657-00616.
Davis, R.W., and Elledge, S.J. (1990). Two genes differentially regulated in the cell cycle and by DNA-damaging agents encode alternative regulatory subunits of ribonucleotide reductase. Genes Dev *4*, 740-751.
De Antoni, A., Pearson, C.G., Cimini, D., Canman, J.C., Sala, V., Nezi, L., Mapelli, M., Sironi, L., Faretta, M., Salmon, E.D*., et al.* (2005). The Mad1/Mad2 complex as a template for Mad2 activation in the spindle assembly checkpoint. Curr Biol *15*, 214-225.
de Gooijer, M.C., van den Top, A., Bockaj, I., Beijnen, J.H., Wurdinger, T., and van Tellingen, O. (2017). The G2 checkpoint-a node-based molecular switch. FEBS Open Bio *7*, 439-455.
Deng, L., Wu, R.A., Sonneville, R., Kochenova, O.V., Labib, K., Pellman, D., and Walter, J.C. (2019). Mitotic CDK Promotes Replisome Disassembly, Fork Breakage, and Complex DNA Rearrangements. Mol Cell *73*, 915-929 e916.
Desai, D., Wessling, H.C., Fisher, R.P., and Morgan, D.O. (1995). Effects of Phosphorylation by CAK on Cyclin Binding by CDC2 and CDK2.

Mol Cell Biol *15*, 345-350.
Devoto, S.H., Mudryl, M., Pines, J., Hunter, T., and Nevins, J.R. (1992). A Cyclin A-Protein Kinase Complex Possesses Sequence-Specific DNA Binding Activity: $p33^{cdk2}$ Is a Component of the E2F-Cyclin A Complex. Cell *68*, 167-176.
Di Fiore, B., and Pines, J. (2007). Emi1 is needed to couple DNA replication with mitosis but does not regulate activation of the mitotic APC/C. J Cell Biol *177*, 425-437.
Di Micco, R., Fumagalli, M., Cicalese, A., Piccinin, S., Gasparini, P., Luise, C., Schurra, C., Garre, M., Nuciforo, P.G., Bensimon, A*., et al.* (2006). Oncogene-induced senescence is a DNA damage response triggered by DNA hyper-replication. Nature *444*, 638-642.
Diaz-Cuervo, H., and Bueno, A. (2008). Cds1 Controls the Release of CDC14-like Phosphatase Flp1 from the Nucleolus to Drive Full Activation of the Checkpoint Response to Replication Stress in Fission Yeast. Mol Biol Cell *19*, 2488-2499.
Dick, F.A., and Rubin, S.M. (2013). Molecular mechanisms underlying RB protein function. Nat Rev Mol Cell Biol *14*, 297-306.
Diehl, J.A., Cheng, M., Roussel, M.F., and Sherr, C.J. (1998). Glycogen synthase kinase-3β regulates cyclin D1 proteolysis and subcellular localization. Genes Dev *12*, 3499-3511.
Diehl, J.A., Zindy, F., and Sherr, C.J. (1997). Inhibition of cyclin D1 phosphorylation on threonine-286 prevents its rapid degradation via the ubiquitin-proteasome pathway. Genes Dev *11*, 957-972.
Dimova, D.K., and Dyson, N.J. (2005). The E2F transcriptional network: old acquaintances with new faces. Oncogene *24*, 2810-2826.
Ditchfield, C., Johnson, V.L., Tighe, A., Ellston, R., Haworth, C., Johnson, T., Mortlock, A., Keen, N., and Taylor, S.S. (2003). Aurora B couples chromosome alignment with anaphase by targeting BubR1, Mad2, and Cenp-E to kinetochores. J Cell Biol *161*, 267-280.
Dobin, A., Davis, C.A., Schlesinger, F., Drenkow, J., Zaleski, C., Jha, S., Batut, P., Chaisson, M., and Gingeras, T.R. (2013). STAR: ultrafast universal RNA-seq aligner. Bioinformatics *29*, 15-21.

Doench, J.G., Fusi, N., Sullender, M., Hegde, M., Vaimberg, E.W., Donovan, K.F., Smith, I., Tothova, Z., Wilen, C., Orchard, R.*, et al.* (2016). Optimized sgRNA design to maximize activity and minimize off-target effects of CRISPR-Cas9. Nat Biotechnol *34*, 184-191.
Dowdy, S.F., Hinds, P.W., Louie, K., Reed, S.I., Arnold, A., and Weinberg, R.A. (1993). Physical Interaction of the Reinoblastoma Protein with Human D Cyclins. Cell *73*, 499-511.
Down, C.F., Millour, J., Lam, E.W., and Watson, R.J. (2012a). Binding of FoxM1 to G2/M gene promoters is dependent upon B-Myb. Biochim Biophys Acta *1819*, 855-862.
Down, C.F., Millour, J., Lam, E.W., and Watson, R.J. (2012b). Binding of FoxM1 to G2/M gene promoters is dependent upon B-Myb. Biochimica et biophysica acta *1819*, 855-862.
Draetta, G., Luca, F., Westendof, J., Brizuela, L., Ruderman, J., and Beach, D. (1989). cdc2 Protein Kinase is Complexed with Both Cyclin A and B: Evidence for Proteolytic Inactivation of MPF. Cell *56*, 829-838.
Ducommun, B., Brambilla, P., Félix, M.-A., Franza, J., B. R., Karsenti, E., and Draetta, G. (1991). cdc2 phosphorylation is required for its interaction with cyclin. The EMBO Journal *11*, 3311-3319.
Dunlop, C.R., Wallez, Y., Johnson, T.I., Bernaldo de Quiros Fernandez, S., Durant, S.T., Cadogan, E.B., Lau, A., Richards, F.M., and Jodrell, D.I. (2020). Complete loss of ATM function augments replication catastrophe induced by ATR inhibition and gemcitabine in pancreatic cancer models. Br J Cancer *123*, 1424-1436.
Elledge, S.J., Richman, R., Hall, F.L., Williams, R.T., Lodgson, N., and Harper, J.W. (1992). CDK2 encodes a 33-kDa cyclin A-associated protein kinase and is expressed before CDC2 in the cell cycle. Proc Natl Acad Sci U S A *89*, 2907-2911.
Emptage, R.P., Schoenberger, M.J., Ferguson, K.M., and Marmorstein, R. (2017). Intramolecular autoinhibition of checkpoint kinase 1 is mediated by conserved basic motifs of the C-terminal kinase-associated 1 domain. J Biol Chem *292*, 19024-19033.
Enoch, T., and Nurse, P. (1990). Mutation of fission yeast cell cycle control genes abolishes dependence of mitosis on DNA replication. Cell *60*, 665-673.
Enomoto, M., Goto, H., Tomono, Y., Kasahara, K., Tsujimura, K., Kiyono, T., and Inagaki, M. (2009). Novel positive feedback loop between Cdk1 and Chk1 in the nucleus during G2/M transition. J Biol Chem *284*, 34223-34230.
Erlandsson, F., Linnman, C., Ekholm, S., Bengtsson, E., and Zetterberg, A. (2000). A detailed analysis of cyclin A accumulation at the G(1)/S border in normal and transformed cells. Exp Cell Res *259*, 86-95.
Errico, A., Deshmukh, K., Tanaka, Y., Pozniakovsky, A., and Hunt, T. (2010). Identification of substrates for cyclin dependent kinases. Adv Enzyme Regul *50*, 375-399.
Ewen, M.E., Sluss, H.K., Sherr, C.J., Matsushime, H., Kato, J., and Livingston, D.M. (1993). Functional Intersections of the Retinoblastoma Protein with Mammalian D-type cyclins. Cell *73*, 487-497.
Eykelenboom, J.K., Harte, E.C., Canavan, L., Pastor-Peidro, A., Calvo-Asensio, I., Llorens-Agost, M., and Lowndes, N.F. (2013). ATR activates the S-M checkpoint during unperturbed growth to ensure sufficient replication prior to mitotic onset. Cell Rep *5*, 1095-1107.
Eytan, E., Wang, K., Miniowitz-Shemtov, S., Sitry-Shevah, D., Kaisari, S., Yen, T.J., Liu, S.T., and Hershko, A. (2014). Disassembly of mitotic checkpoint complexes by the joint action of the AAA-ATPase TRIP13 and p31(comet). Proc Natl Acad Sci U S A *111*, 12019-12024.
Fan, X., Zhou, Y., and Chen, J.J. (2016). Role of Cdc6 in re-replication in cells expressing human papillomavirus E7 oncogene. Carcinogenesis *37*, 799-809.
Fang, G. (2002). Checkpoint protein BubR1 acts synergistically with Mad2 to inhibit anaphase-promoting complex. Mol Biol Cell *13*, 755-766.
Fang, G., Yu, H., and Kirschner, M.W. (1998). The checkpoint protein MAD2 and the mitotic regulator CDC20 form a ternary complex with the anaphase-promoting complex to control anaphase initiation. Genes Dev *12*, 1871-1883.

Feine, O., Hukasova, E., Bruinsma, W., Freire, R., Fainsod, A., Gannon, J., Mahbubani, H.M., Lindqvist, A., and Brandeis, M. (2014). Phosphorylation-mediated stabilization of Bora in mitosis coordinates Plx1/Plk1 and Cdk1 oscillations. Cell Cycle *13*, 1727-1736.
Fesquet, D., Labbe, J.C., Derancourt, J., Capony, J.-P., Galas, S., Girard, F., Lorca, T., Shuttleworth, J., Dorée, M., and Cavadore, J.-C. (1993). The MO15 gene ecodes the catalytic subunit of a protein kinase that activates cdc2 and other cyclin-dependent kinases (CDKs) through phosphorylation of Thr161 and it homologues. The EMBO Journal *12*, 3111-3121.
Fischer, M., Grossmann, P., Padi, M., and DeCaprio, J.A. (2016). Integration of TP53, DREAM, MMB-FOXM1 and RB-E2F target gene analyses identifies cell cycle gene regulatory networks. Nucleic Acids Research *44*, 6070-6086.
Fisher, R.P., and Morgan, D.O. (1994). A Novel Cyclin Associates with MO15/CDK7 to Form the CDK-Activating Kinase. Cell *78*, 713-724.
Fordham, S.E., Blair, H.J., Elstob, C.J., Plummer, R., Drew, Y., Curtin, N.J., Heidenreich, O., Pal, D., Jamieson, D., Park, C.*, et al.* (2018). Inhibition of ATR acutely sensitizes acute myeloid leukemia cells to nucleoside analogs that target ribonucleotide reductase. Blood Adv *2*, 1157-1169.
Forment, J.V., Blasius, M., Guerini, I., and Jackson, S.P. (2011). Structure-Specific DNA Endonuclease Mus81/Eme1 Generates DNA Damage Caused by Chk1 Inactivation. PLoS ONE *6*.
Fraschini, R., Beretta, A., Sironi, L., Musacchio, A., Lucchini, G., and Piatti, S. (2001). Bub3 interaction with Mad2, Mad3 and CDC20 is mediated by WD40 repeats and does not require intact kinetochores. The EMBO Journal *20*, 6648-6659.
Fu, Z., Malureanu, L., Huang, J., Wang, W., Li, H., van Deursen, J.M., Tindall, D.J., and Chen, J. (2008). Plk1-dependent phosphorylation of FoxM1 regulates a transcriptional programme required for mitotic progression. Nat Cell Biol *10*, 1076-1082.
Fujimitsu, K., Grimaldi, M., and Yamano, H. (2016). Cyclin-dependent kinase 1-dependent activation of APC/C ubiquitin ligase. Science *352*, 1121-1124.
Fung, T.K., Siu, W.Y., Yam, C.H., Lau, A., and Poon, R.Y. (2002). Cyclin F is degraded during G2-M by mechanisms fundamentally different from other cyclins. The Journal of biological chemistry *277*, 35140-35149.
Furnari, B., Rhind, N., and Russell, P. (1997). Cdc25 mitotic inducer targeted by chk1 DNA damage checkpoint kinase. Science *277*, 1495-1497.
Furuta, T., Takemura, H., Liao, Z.Y., Aune, G.J., Redon, C., Sedelnikova, O.A., Pilch, D.R., Rogakou, E.P., Celeste, A., Chen, H.T.*, et al.* (2003). Phosphorylation of histone H2AX and activation of Mre11, Rad50, and Nbs1 in response to replication-dependent DNA double-strand breaks induced by mammalian DNA topoisomerase I cleavage complexes. J Biol Chem *278*, 20303-20312.
Ganem, N.J., Cornils, H., Chiu, S.Y., O'Rourke, K.P., Arnaud, J., Yimlamai, D., Thery, M., Camargo, F.D., and Pellman, D. (2014). Cytokinesis failure triggers hippo tumor suppressor pathway activation. Cell *158*, 833-848.
García, P., and Frampton, J. (2006). The transcription factor B-Myb is essential for S-phase progression and genomic stability in diploid and polyploid megakaryocytes. J Cell Sci *119*, 1483-1493.
Gavet, O., and Pines, J. (2010). Progressive activation of CyclinB1-Cdk1 coordinates entry to mitosis. Dev Cell *18*, 533-543.
Ge, X.Q., and Blow, J.J. (2010). Chk1 inhibits replication factory activation but allows dormant origin firing in existing factories. J Cell Biol *191*, 1285-1297.
Ge, X.Q., Jackson, D.A., and Blow, J.J. (2007). Dormant origins licensed by excess Mcm2-7 are required for human cells to survive replicative stress. Genes Dev *21*, 3331-3341.
Geley, S., Kramer, E., Gieffers, C., Gannon, J., Peters, J.M., and Hunt, T. (2001). Anaphase-promoting Complex/Cyclosome-dependent Proteolysis of Human Cyclin A Starts at the

Beginning of Mitosis and Is Not Subject to the Spindle Assembly Checkpoint. J Cell Biol *153*, 137-147.
Gentles, A.J., Newman, A.M., Liu, C.L., Bratman, S.V., Feng, W., Kim, D., Nair, V.S., Xu, Y., Khuong, A., Hoang, C.D*., et al.* (2015). The prognostic landscape of genes and infiltrating immune cells across human cancers. Nat Med *21*, 938-945.
Gheghiani, L., Loew, D., Lombard, B., Mansfeld, J., and Gavet, O. (2017). PLK1 Activation in Late G2 Sets Up Commitment to Mitosis. Cell Rep *19*, 2060-2073.
Ghelli Luserna Di Rora, A., Bocconcelli, M., Ferrari, A., Terragna, C., Bruno, S., Imbrogno, E., Beeharry, N., Robustelli, V., Ghetti, M., Napolitano, R*., et al.* (2019). Synergism Through WEE1 and CHK1 Inhibition in Acute Lymphoblastic Leukemia. Cancers (Basel) *11*.
Gilad, O., Nabet, B.Y., Ragland, R.L., Schoppy, D.W., Smith, K.D., Durham, A.C., and Brown, E.J. (2010). Combining ATR suppression with oncogenic Ras synergistically increases genomic instability, causing synthetic lethality or tumorigenesis in a dosage-dependent manner. Cancer Res *70*, 9693-9702.
Godfrey, M., Touati, S.A., Kataria, M., Jones, A., Snijders, A.P., and Uhlmann, F. (2017). PP2A(Cdc55) Phosphatase Imposes Ordered Cell-Cycle Phosphorylation by Opposing Threonine Phosphorylation. Mol Cell *65*, 393-402 e393.
Grallert, A., Boke, E., Hagting, A., Hodgson, B., Connolly, Y., Griffiths, J.R., Smith, D.L., Pines, J., and Hagan, I.M. (2015). A PP1-PP2A phosphatase relay controls mitotic progression. Nature *517*, 94-98.
Gray-Bablin, J., Zalvide, J., Fox, M.P., Knickerbocker, C.J., DeCaprio, J.A., and Keyomarsi, K. (1996). Cyclin E, a redundant cyclin in breast cancer. Proc Natl Acad Sci U S A *93*, 15215-15220.
Gu, Y., Rosenblatt, J., and Morgan, D.O. (1992). Cell Cycle regulation of CDK2 activity by phosphorylation of Thr160 and Tyr15. The EMBO Journal *11*, 3995-4005.
Guan, C., Zhang, J., Zhang, J., Shi, H., and Ni, R. (2016). Enhanced expression of early mitotic inhibitor-1 predicts a poor prognosis in esophageal squamous cell carcinoma patients. Oncol Lett *12*, 114-120.
Guiley, K.Z., Iness, A.N., Saini, S., Tripathi, S., Lipsick, J.S., Litovchick, L., and Rubin, S.M. (2018). Structural mechanism of Myb-MuvB assembly. Proc Natl Acad Sci U S A *115*, 10016-10021.
Guiley, K.Z., Liban, T.J., Felthousen, J.G., Ramanan, P., Litovchick, L., and Rubin, S.M. (2015). Structural mechanisms of DREAM complex assembly and regulation. Genes Dev *29*, 961-974.
Guo, C., Kumagai, A., Schlacher, K., Shevchenko, A., Shevchenko, A., and Dunphy, W.G. (2015). Interaction of Chk1 with Treslin negatively regulates the initiation of chromosomal DNA replication. Mol Cell *57*, 492-505.
Guo, L., Mohd, K.S., Ren, H., Xin, G., Jiang, Q., Clarke, P.R., and Zhang, C. (2019). Phosphorylation of importin-alpha1 by CDK1-cyclin B1 controls mitotic spindle assembly. J Cell Sci *132*.
Haahr, P., Hoffmann, S., Tollenaere, M.A., Ho, T., Toledo, L.I., Mann, M., Bekker-Jensen, S., Raschle, M., and Mailand, N. (2016). Activation of the ATR kinase by the RPA-binding protein ETAA1. Nat Cell Biol *18*, 1196-1207.
Hamperl, S., Bocek, M.J., Saldivar, J.C., Swigut, T., and Cimprich, K.A. (2017). Transcription-Replication Conflict Orientation Modulates R-Loop Levels and Activates Distinct DNA Damage Responses. Cell *170*, 774-786 e719.
Hanna, R.E., and Doench, J.G. (2020). Design and analysis of CRISPR-Cas experiments. Nat Biotechnol.
Hansen, D.V., Loktev, A.V., Ban, K.H., and Jackson, P.K. (2004). Plk1 regulates activation of the anaphase promoting complex by phosphorylating and triggering SCFbetaTrCP-dependent destruction of the APC Inhibitor Emi1. Mol Biol Cell *15*, 5623-5634.

Harbour, J.W., Luo, R.X., Dei Santi, A., Postigo, A.A., and Dean, D.C. (1999). Cdk Phosphorylation Triggers Sequential Intramolecular Interactions that Progressively Block Rb Functions as Cells Move through G1. Cell *98*, 859-869.
Hateboer, G., Wobst, A., Petersen, B.O., Vigo, E., Sardet, C., and Helin, K. (1998). Cell Cycle-Regulated Expression of Mammalian CDC6 is Dependent on E2F. Mol Cell Biol *18*, 6679-6697.
Hauge, S., Naucke, C., Hasvold, G., Joel, M., Rodland, G.E., Juzenas, P., Stokke, T., and Syljuasen, R.G. (2017). Combined inhibition of Wee1 and Chk1 gives synergistic DNA damage in S-phase due to distinct regulation of CDK activity and CDC45 loading. Oncotarget *8*, 10966-10979.
Hein, J.B., Hertz, E.P.T., Garvanska, D.H., Kruse, T., and Nilsson, J. (2017). Distinct kinetics of serine and threonine dephosphorylation are essential for mitosis. Nat Cell Biol *19*, 1433-1440.
Hein, J.B., and Nilsson, J. (2016). Interphase APC/C-Cdc20 inhibition by cyclin A2-Cdk2 ensures efficient mitotic entry. Nat Commun *7*, 10975.
Helin, K., Harlow, E., and Fattaey, A. (1993). Inhibition of the E2F-1 Transactivation by Direct Binding of the Retinoblastoma Protein. Mol Cell Biol *13*, 6501-6508.
Hetland, T.E., Nymoen, D.A., Holth, A., Brusegard, K., Florenes, V.A., Kaern, J., Trope, C.G., and Davidson, B. (2013). Aurora B expression in metastatic effusions from advanced-stage ovarian serous carcinoma is predictive of intrinsic chemotherapy resistance. Hum Pathol *44*, 777-785.
Hewitt, L., Tighe, A., Santaguida, S., White, A.M., Jones, C.D., Musacchio, A., Green, S., and Taylor, S.S. (2010). Sustained Mps1 activity is required in mitosis to recruit O-Mad2 to the Mad1-C-Mad2 core complex. J Cell Biol *190*, 25-34.
Hibi, K., Liu, Q., Beaudry, G.A., Madden, S.L., Westra, W.H., Wehage, S.L., Yang, S.C., Heitmiller, R.F., Bertelsen, A.H., Sidransky, D.*, et al.* (1998). Serial Analysis of Gene Expression in Non-Small Cell Lung Cancer. Cancer Res *58*, 5690-5694.
Hinds, P.W., Mittnacht, S., Dulic, V., Arnold, A., Reed, S.I., and Weinberg, R.A. (1992). Regulation of Retinoblastoma Protein Functions by Ectopic Expression of Human Cyclins. Cell *70*, 993-1006.
Ho, G.P., Margossian, S., Taniguchi, T., and D'Andrea, A.D. (2006). Phosphorylation of FANCD2 on two novel sites is required for mitomycin C resistance. Mol Cell Biol *26*, 7005-7015.
Hong, D., Infante, J., Janku, F., Jones, S., Nguyen, L.M., Burris, H., Naing, A., Bauer, T.M., Piha-Paul, S., Johnson, F.M.*, et al.* (2016). Phase I Study of LY2606368, a Checkpoint Kinase 1 Inhibitor, in Patients With Advanced Cancer. J Clin Oncol *34*, 1764-1771.
Hong, D.S., Moore, K., Patel, M., Grant, S.C., Burris, H.A., 3rd, William, W.N., Jr., Jones, S., Meric-Bernstam, F., Infante, J., Golden, L.*, et al.* (2018). Evaluation of Prexasertib, a Checkpoint Kinase 1 Inhibitor, in a Phase Ib Study of Patients with Squamous Cell Carcinoma. Clin Cancer Res *24*, 3263-3272.
Hornbeck, P.V., Chabra, I., Kornhauser, J.M., Skrzypek, E., and Zhang, B. (2004). PhosphoSite: A bioinformatics resource dedicated to physiological protein phosphorylation. Proteomics *4*, 1551-1561.
Hsu, J.Y., Reimann, J.D., Sorensen, C.S., Lukas, J., and Jackson, P.K. (2002). E2F-dependent accumulation of hEmi1 regulates S phase entry by inhibiting APC(Cdh1). Nat Cell Biol *4*, 358-366.
Hutchins, J.R., Moore, W.J., Hood, F.E., Wilson, J.S., Andrews, P.D., Swedlow, J.R., and Clarke, P.R. (2004). Phosphorylation regulates the dynamic interaction of RCC1 with chromosomes during mitosis. Curr Biol *14*, 1099-1104.
Hutterer, A., Berdnik, D., Wirtz-Peitz, F., Zigman, M., Schleiffer, A., and Knoblich, J.A. (2006). Mitotic activation of the kinase Aurora-A requires its binding partner Bora. Dev Cell *11*, 147-157.
Hwang, S.G., Lee, D., Kim, J., Seo, T., and Choe, J. (2002). Human papillomavirus type 16 E7 binds to E2F1 and activates E2F1-driven transcription in a retinoblastoma protein-independent manner. J Biol Chem *277*, 2923-2930.

Iness, A.N., Felthousen, J., Ananthapadmanabhan, V., Sesay, F., Saini, S., Guiley, K.Z., Rubin, S.M., Dozmorov, M., and Litovchick, L. (2019). The cell cycle regulatory DREAM complex is disrupted by high expression of oncogenic B-Myb. Oncogene *38*, 1080-1092.
Inoue, K., and Fry, E.A. (2016). Novel Molecular Markers for Breast Cancer. Biomark Cancer *8*, 25-42.
Irniger, S., and Nasmyth, K. (1997). The anaphase-promoting complex is required in G1 arrested yeast cells to inhibit B-type cyclin accumulation and to prevent uncontrolled entry into S phase. J Cell Sci *110*, 1523-1531.
Irniger, S., Piatti, S., Michaelis, C., and Nasmyth, K. (1995). Genes Involved in Sister Chromatid Separation Are Needed for B-Type Cyclin Proteolyis in Budding Yeast. Cell *81*, 269-277.
Izawa, D., and Pines, J. (2015). The mitotic checkpoint complex binds a second CDC20 to inhibit active APC/C. Nature *517*, 631-634.
Jang, S.M., Redon, C.E., Thakur, B.L., Bahta, M.K., and Aladjem, M.I. (2020). Regulation of cell cycle drivers by Cullin-RING ubiquitin ligases. Exp Mol Med *52*, 1637-1651.
Janke, R., King, G.A., Kupiec, M., and Rine, J. (2018). Pivotal roles of PCNA loading and unloading in heterochromatin function. Proceedings of the National Academy of Sciences *115*, 201721573.
Jaspersen, S.L., Charles, J.F., and Morgan, D.O. (1999). Inhibitory phosphorylation of the APC regulator Hct1 is controlled by the kinase Cdc28 and the phosphatase Cdc14. Curr Biol *9*, 227-236.
Jeffery, P.D., Russo, A.A., Polyak, K., Gibbs, E., Hurwitz, J., Massagué, J., and Pavletich, N.P. (1995). Mechanism of CDK activation revealed by the structure of a cyclinA-CDK2 complex. Nature *376*, 313-320.
Jeon, Y., Lee, K.Y., Ko, M.J., Lee, Y.S., Kang, S., and Hwang, D.S. (2007). Human TopBP1 participates in cyclin E/CDK2 activation and preinitiation complex assembly during G1/S transition. J Biol Chem *282*, 14882-14890.
Jin, J., Fang, H., Yang, F., Ji, W., Guan, N., Sun, Z., Shi, Y., Zhou, G., and Guan, X. (2018). Combined Inhibition of ATR and WEE1 as a Novel Therapeutic Strategy in Triple-Negative Breast Cancer. Neoplasia *20*, 478-488.
Joaquin, M., Bessa, M., Saville, M., and Watson, R.J. (2002). B-Myb overcomes a p107-mediated cell proliferation block by interacting with an N-terminal domain of p107. Oncogene *21*, 7923-7932.
Johnson, D.G. (1995). Regulation of E2F-1 gene expression by p130 (RB2) and D-type cyclin kinase activity. Oncogene *11*, 1685-1692.
Johnson, L.R., Johnson, T.K., Desler, M., Luster, T.A., Nowling, T., Lewis, R.E., and Rizzino, A. (2002). Effects of B-Myb on gene transcription: phosphorylation-dependent activity ans acetylation by p300. J Biol Chem *277*, 4088-4097.
Johnson, T.K., Schweppe, R.E., Septer, J., and Lewis, R.E. (1999). Phosphorylation of B-Myb regulates its transactivation potential and DNA binding. J Biol Chem *274*, 36741-36749.
Jones, R.M., Mortusewicz, O., Afzal, I., Lorvellec, M., Garcia, P., Helleday, T., and Petermann, E. (2013). Increased replication initiation and conflicts with transcription underlie Cyclin E-induced replication stress. Oncogene *32*, 3744-3753.
Kabeche, L., Nguyen, H.D., Buisson, R., and Zou, L. (2018). A mitosis-specific and R loop–driven ATR pathway promotes faithful chromosome segregation. Science *359*, 108–114.
Kalaszczynska, I., Geng, Y., Iino, T., Mizuno, S., Choi, Y., Kondratiuk, I., Silver, D.P., Wolgemuth, D.J., Akashi, K., and Sicinski, P. (2009). Cyclin A is redundant in fibroblasts but essential in hematopoietic and embryonic stem cells. Cell *138*, 352-365.
Kasahara, K., Goto, H., Enomoto, M., Tomono, Y., and Inagaki, M. (2010). 14-3-3γ mediates Cdc25A proteolysis to block premature mitotic entry after DNA damage. The EMBO Journal *29*, 2802-2812.

Kato, J., Matsushime, H., Hiebert, S.W., Ewen, M.E., and Sherr, C.J. (1993). Direct binding of cyclin D to the retinoblastoma gene product (pRb) and pRb phosphorylation by the cyclin D-dependent kinase CDK4. Genes Dev *7*, 331-342.
Katsuno, Y., Suzuki, A., Sugimura, K., Okumura, K., Zineldeen, D.H., Shimada, M., Niida, H., Mizuno, T., Hanaoka, F., and Nakanishi, M. (2009). Cyclin A-Cdk1 regulates the origin firing program in mammalian cells. Proc Natl Acad Sci U S A *106*, 3184-3189.
Kausar, T., Schreiber, J.S., Karnak, D., Parsels, L.A., Parsels, J.D., Davis, M.A., Zhao, L., Maybaum, J., Lawrence, T.S., and Morgan, M.A. (2015). Sensitization of Pancreatic Cancers to Gemcitabine Chemoradiation by WEE1 Kinase Inhibition Depends on Homologous Recombination Repair. Neoplasia *17*, 757-766.
Kernan, J., Bonacci, T., and Emanuele, M.J. (2018). Who guards the guardian? Mechanisms that restrain APC/C during the cell cycle. Biochim Biophys Acta Mol Cell Res *1865*, 1924-1933.
Kim, D.H., Han, J.S., Ly, P., Ye, Q., McMahon, M.A., Myung, K., Corbett, K.D., and Cleveland, D.W. (2018). TRIP13 and APC15 drive mitotic exit by turnover of interphase- and unattached kinetochore-produced MCC. Nat Commun *9*, 4354.
Kim, S.T., Lim, D.S., Canman, C.E., and Kastan, M.B. (1999). Substrate specificities and identification of putative substrates of ATM kinase family members. J Biol Chem *274*, 37538-37543.
Kimura, T., Gotoh, M., Nakamura, Y., and Arakawa, H. (2003). hCDC4b, a regulator of cyclin E, as a direct transcriptional target of p53. Cancer Sci *94*, 431-436.
King, C., Diaz, H.B., McNeely, S., Barnard, D., Dempsey, J., Blosser, W., Beckmann, R., Barda, D., and Marshall, M.S. (2015). LY2606368 Causes Replication Catastrophe and Antitumor Effects through CHK1-Dependent Mechanisms. Mol Cancer Ther *14*, 2004-2013.
King, R.W., Glotzer, M., and Kirschner, M.W. (1996). Mutagenic Analysis of the Destruction Signal of Mitotic Cyclins and Structural Characterization of Ubiquitinated Intermediates. Mol Biol Cell *7*, 1343-1357.
King, R.W., Peters, J.M., Tugendreich, S., Rolfe, M., Hieter, P., and Kirshcner, M.W. (1995). A 20S Complex Containing CDC27 and CDC16 Catalyzes the Mitosis-Specific Conjugation of Ubiquitn to Cyclin B. Cell *81*, 279-288.
Klein, d., Muijtjens, M., van Os, R., Verhoeven, Y., Smit, B., Carr, A.M., Lehmann, A.R., and Hoeijmakers, J.H.J. (2000). Targeted disruption of the cell-cycle checkpoint gene ATR leads to early embryonic lethality in mice. Curr Biol *10*, 479-482.
Klein, D.K., Hoffmann, S., Ahlskog, J.K., O'Hanlon, K., Quaas, M., Larsen, B.D., Rolland, B., Rösner, H.I., Walter, D., Kousholt, A.N.*, et al.* (2015). Cyclin F suppresses B-Myb activity to promote cell cycle checkpoint control. Nature communications *6*, 5800.
Knight, A.S., Notaridou, M., and Watson, R.J. (2009). A Lin-9 complex is recruited by B-Myb to activate transcription of G2/M genes in undifferentiated embryonal carcinoma cells. Oncogene *28*, 1737-1747.
Koepp, D.M., Schaefer, L.K., Ye, X., Keyomarsi, K., Chu, C., Harper, J.W., and Elledge, S.J. (2001). Phosphorylation-Dependent Ubiquitination of Cyclin E by the SCFFbw7 Ubiquitin Ligase. Science *294*, 173-177.
Kohler, C., Koalick, D., Fabricius, A., Parplys, A.C., Borgmann, K., Pospiech, H., and Grosse, F. (2016). Cdc45 is limiting for replication initiation in humans. Cell Cycle *15*, 974-985.
Koppenhafer, S.L., Goss, K.L., Terry, W.W., and Gordon, D.J. (2018). mTORC1/2 and Protein Translation Regulate Levels of CHK1 and the Sensitivity to CHK1 Inhibitors in Ewing Sarcoma Cells. Mol Cancer Ther *17*, 2676-2688.
Kotsantis, P., Petermann, E., and Boulton, S.J. (2018). Mechanisms of Oncogene-Induced Replication Stress: Jigsaw Falling into Place. Cancer Discov *8*, 537-555.
Kotsantis, P., Silva, L.M., Irmscher, S., Jones, R.M., Folkes, L., Gromak, N., and Petermann, E. (2016). Increased global transcription activity as a mechanism of replication stress in cancer. Nat Commun *7*, 13087.

Kramer, E.R., Scheuringer, N., Podtelejnikov, A.V., Mann, M., and Peters, J.M. (2000). Mitotic Regulation of the APC Activator Proteins CDC20 and CDH1. Mol Biol Cell *11*, 1555-1569.
Kumagai, A., Lee, J., Yoo, H.Y., and Dunphy, W.G. (2006). TopBP1 activates the ATR-ATRIP complex. Cell *124*, 943-955.
Kumagai, A., Shevchenko, A., Shevchenko, A., and Dunphy, W.G. (2010). Treslin collaborates with TopBP1 in triggering the initiation of DNA replication. Cell *140*, 349-359.
Kumagai, A., Shevchenko, A., Shevchenko, A., and Dunphy, W.G. (2011). Direct regulation of Treslin by cyclin-dependent kinase is essential for the onset of DNA replication. J Cell Biol *193*, 995-1007.
Lam, E.W.-F., and Watson, R.J. (1993). An E2F-binding site mediates cell-cycle regulated repression of mouse B-Myb transcription. The EMBO Journal *12*, 2075-2713.
Lam, M.H., Liu, Q., Elledge, S.J., and Rosen, J.M. (2004). Chk1 is haploinsufficient for multiple functions critical to tumor suppression. Cancer Cell *6*, 45-59.
Lane, S., Farlie, P., and Watson, R. (1997). B-Myb function can be markedly enhanced by cyclin A-dependent kinase and protein truncation. Oncogene *14*, 2445-2453.
Lang, S.E., McMahon, S.B., Cole, M.D., and Hearing, P. (2001). E2F transcriptional activation requires TRRAP and GCN5 cofactors. J Biol Chem *276*, 32627-32634.
Laoukili, J., Alvarez-Fernandez, M., Stahl, M., and Medema, R.H. (2008a). FoxM1 is degraded at mitotic exit in a Cdh1-dependent manner. Cell Cycle *7*, 2720-2726.
Laoukili, J., Alvarez, M., Meijer, L.A., Stahl, M., Mohammed, S., Kleij, L., Heck, A.J., and Medema, R.H. (2008b). Activation of FoxM1 during G2 requires cyclin A/Cdk-dependent relief of autorepression by the FoxM1 N-terminal domain. Mol Cell Biol *28*, 3076-3087.
Laurell, E., Beck, K., Krupina, K., Theerthagiri, G., Bodenmiller, B., Horvath, P., Aebersold, R., Antonin, W., and Kutay, U. (2011). Phosphorylation of Nup98 by multiple kinases is crucial for NPC disassembly during mitotic entry. Cell *144*, 539-550.
Lee, H.J., Hwang, H.I., and Jang, Y.J. (2010). Mitotic DNA damage response: Polo-like kinase-1 is dephosphorylated through ATM-Chk1 pathway. Cell Cycle *9*, 2389-2398.
Lee, J., Kumagai, A., and Dunphy, W.G. (2001). Positivie Regulation of Wee1 by Chk1 and 14-3-3 Proteins. Mol Biol Cell *12*, 551-563.
Lee, Y., Dominy, J.E., Choi, Y.J., Jurczak, M., Tolliday, N., Camporez, J.P., Chim, H., Lim, J.H., Ruan, H.B., Yang, X.*, et al.* (2014). Cyclin D1-Cdk4 controls glucose metabolism independently of cell cycle progression. Nature *510*, 547-551.
Lee, Y.C., Zhou, Q., Chen, J., and Yuan, J. (2016). RPA-Binding Protein ETAA1 Is an ATR Activator Involved in DNA Replication Stress Response. Curr Biol *26*, 3257-3268.
Lehman, N.L., Tibshirani, R., Hsu, J.Y., Natkunam, Y., Harris, B.T., West, R.B., Masek, M.A., Montgomery, K., van de Rijn, M., and Jackson, P.K. (2007). Oncogenic regulators and substrates of the anaphase promoting complex/cyclosome are frequently overexpressed in malignant tumors. Am J Pathol *170*, 1793-1805.
Lemmens, B., Hegarat, N., Akopyan, K., Sala-Gaston, J., Bartek, J., Hochegger, H., and Lindqvist, A. (2018). DNA Replication Determines Timing of Mitosis by Restricting CDK1 and PLK1 Activation. Mol Cell *71*, 117-128 e113.
Leone, G., DeGregori, J., Sears, R., Jakol, L., and Nevins, J.R. (1997). Myc and Ras collaborate in inducing accumulation of active cyclin E/CDK2 and E2F. Nature, 422-426.
Li, F., Kozono, D., Deraska, P., Branigan, T., Dunn, C., Zheng, X.F., Parmar, K., Nguyen, H., DeCaprio, J., Shapiro, G.I.*, et al.* (2020). CHK1 Inhibitor Blocks Phosphorylation of FAM122A and Promotes Replication Stress. Mol Cell *80*, 410-422 e416.
Li, H.Y., and Zheng, Y. (2004). Phosphorylation of RCC1 in mitosis is essential for producing a high RanGTP concentration on chromosomes and for spindle assembly in mammalian cells. Genes Dev *18*, 512-527.
Li, L., Wu, D., Yu, Q., Li, L., and Wu, P. (2017). Prognostic value of FOXM1 in solid tumors: a systematic review and meta-analysis. Oncotarget *8*, 32298-32308.

Li, X., and McDonnell, D.P. (2002). The transcription factor B-Myb is maintained in an inhibited state in target cells through its interaction with the nuclear corepressors N-CoR and SMRT. Mol Cell Biol *22*, 3663-3673.
Li, X., Zhang, X., Wu, C.C., Li, P.P., Fu, Y.M., Xie, L.H., Sun, S.S., Zhou, Y.Y., and Zhu, B.L. (2021). The role of MYB proto-oncogene like 2 in tamoxifen resistance in breast cancer. J Mol Histol *52*, 21-30.
Lin, D.I., Barbash, O., Kumar, K.G., Weber, J.D., Harper, J.W., Klein-Szanto, A.J., Rustgi, A., Fuchs, S.Y., and Diehl, J.A. (2006). Phosphorylation-dependent ubiquitination of cyclin D1 by the SCF(FBX4-alphaB crystallin) complex. Mol Cell *24*, 355-366.
Lin, Z.Z., Jeng, Y.-M., Hu, F.-C., Pan, H.-W., Tsao, H.-W., Lai, P.-L., Lee, P.-H., and Cheng, A.-L. (2010). Significance of Aurora B overexpression in hepatocellular carcinoma. Aurora B Overexpression in HCC. BMC Cancer *10*, 461.
Linder, M.I., Kohler, M., Boersema, P., Weberruss, M., Wandke, C., Marino, J., Ashiono, C., Picotti, P., Antonin, W., and Kutay, U. (2017). Mitotic Disassembly of Nuclear Pore Complexes Involves CDK1- and PLK1-Mediated Phosphorylation of Key Interconnecting Nucleoporins. Dev Cell *43*, 141-156 e147.
Lindqvist, A., de Bruijn, M., Macurek, L., Brás, A., Mensinga, A., Bruinsma, W., Voets, O., Kranenburg, O., and Medema, R.H. (2009). Wip1 confers G2 checkpoint recovery competence by counteracting p53-dependent transcriptional repression. The EMBO journal *2009*, 3196-3206.
Litovchick, L., Florens, L.A., Swanson, S.K., Washburn, M.P., and DeCaprio, J.A. (2011). DYRK1A protein kinase promotes quiescence and senescence through DREAM complex assembly. Genes Dev *25*, 801-813.
Litovchick, L., Sadasivam, S., Florens, L., Zhu, X., Swanson, S.K., Velmurugan, S., Chen, R., Washburn, M.P., Liu, X.S., and DeCaprio, J.A. (2007a). Evolutionarily conserved multisubunit RBL2/p130 and E2F4 protein complex represses human cell cycle-dependent genes in quiescence. Molecular cell *26*, 539-551.
Litovchick, L., Sadasivam, S., Florens, L., Zhu, X., Swanson, S.K., Velmurugan, S., Chen, R., Washburn, M.P., Liu, X.S., and DeCaprio, J.A. (2007b). Evolutionarily conserved multisubunit RBL2/p130 and E2F4 protein complex represses human cell cycle-dependent genes in quiescence. Mol Cell *26*, 539-551.
Littler, D.R., Alvarez-Fernandez, M., Stein, A., Hibbert, R.G., Heidebrecht, T., Aloy, P., Medema, R.H., and Perrakis, A. (2010). Structure of the FoxM1 DNA-recognition domain bound to a promoter sequence. Nucleic Acids Res *38*, 4527-4538.
Liu, H., Takeda, S., Kumar, R., Westergard, T.D., Brown, E.J., Pandita, T.K., Cheng, E.H., and Hsieh, J.J. (2010). Phosphorylation of MLL by ATR is required for execution of mammalian S-phase checkpoint. Nature *467*, 343-346.
Liu, Q., Guntuku, S., Cui, X.-S., Matsuoka, S., Cortez, D., Tamai, K., Luo, G., Carattini-Rivera, S., DeMayo, F., Bradley, A*., et al.* (2000). Chk1 is an essential kinase that is regulaed by ATR and requried for the G2/M DNA damage checkpoint. Genes Dev *14*, 1488-1459.
Liu, S., Opiyo, S.O., Manthey, K., Glanzer, J.G., Ashley, A.K., Amerin, C., Troksa, K., Shrivastav, M., Nickoloff, J.A., and Oakley, G.G. (2012). Distinct roles for DNA-PK, ATM and ATR in RPA phosphorylation and checkpoint activation in response to replication stress. Nucleic Acids Res *40*, 10780-10794.
Liu, S.T., and Zhang, H. (2016). The mitotic checkpoint complex (MCC): looking back and forth after 15 years. AIMS Mol Sci *3*, 597-634.
Liu, X., Tesfai, J., Evrard, Y.A., Dent, S.Y., and Martinez, E. (2003). c-Myc transformation domain recruits the human STAGA complex and requires TRRAP and GCN5 acetylase activity for transcription activation. J Biol Chem *278*, 20405-20412.

Liu, Y., Li, Y., Wang, X., Liu, F., Gao, P., Quinn, M.M., Li, F., Merlino, A.A., Benes, C., Liu, Q.*, et al.* (2017). Gemcitabine and Chk1 Inhibitor AZD7762 Synergistically Suppress the Growth of Lkb1-Deficient Lung Adenocarcinoma. Cancer Res *77*, 5068-5076.
Lopez-Girona, A., Furnari, B., Mondesert, O., and Russell, P. (1999). Nuclear localization of Cdc25 is regulated by DNA damage and a 14-3-3 protein. Nature *397*, 172-175.
Love, M.I., Huber, W., and Anders, S. (2014). Moderated estimation of fold change and dispersion for RNA-seq data with DESeq2. Genome Biol *15*, 550.
Lundberg, A.S., and Weinberg, R.A. (1998). Functional Inactivation of the Retinoblastoma Protein Requires Sequential Modification by at Least Two Distinct Cyclin-cdk Complexes. Mol Cell Biol *18*, 753-761.
Luo, X., and Yu, H. (2008). Protein metamorphosis: the two-state behavior of Mad2. Structure *16*, 1616-1625.
Lupardus, P.J., Byun, T., Yee, M.C., Hekmat-Nejad, M., and Cimprich, K.A. (2002). A requirement for replication in activation of the ATR-dependent DNA damage checkpoint. Genes Dev *16*, 2327-2332.
Machida, Y.J., and Dutta, A. (2007). The APC/C inhibitor, Emi1, is essential for prevention of rereplication. Genes Dev *21*, 184-194.
Magnussen, G.I., Emilsen, E., Giller Fleten, K., Engesaeter, B., Nahse-Kumpf, V., Fjaer, R., Slipicevic, A., and Florenes, V.A. (2015). Combined inhibition of the cell cycle related proteins Wee1 and Chk1/2 induces synergistic anti-cancer effect in melanoma. BMC Cancer *15*, 462.
Mailand, N., and Diffley, J.F. (2005). CDKs promote DNA replication origin licensing in human cells by protecting Cdc6 from APC/C-dependent proteolysis. Cell *122*, 915-926.
Major, M.L., Lepe, R., and Costa, R.H. (2004). Forkhead Box M1B Transcriptional Activity Requires Binding of Cdk-Cyclin Complexes for Phosphorylation-Dependent Recruitment of p300/CBP Coactivators. Molecular and Cellular Biology *24*, 2649-2661.
Mak, J.P., Man, W.Y., Chow, J.P., Ma, H.T., and Poon, R.Y. (2015). Pharmacological inactivation of CHK1 and WEE1 induces mitotic catastrophe in nasopharyngeal carcinoma cells. Oncotarget *6*, 21074-21084.
Mäkelä, T.P., Tassan, J.-P., Nigg, E.A., Frutiger, S., Hughes, G.J., and Weinberg, R.A. (1994). A cyclin associated with CDK-activating kinase MO15.

Nature *371*, 254-257.
Malumbres, M. (2011). Physiological relevance of cell cycle kinases. Physiol Rev *91*, 973-1007.
Malumbres, M. (2014). Cyclin-dependent kinases. Genome Biol *15*, 122.
Malureanu, L.A., Jeganathan, K.B., Hamada, M., Wasilewski, L., Davenport, J., and van Deursen, J.M. (2009). BubR1 N terminus acts as a soluble inhibitor of cyclin B degradation by APC/C(Cdc20) in interphase. Dev Cell *16*, 118-131.
Mandal, S., Freije, W.A., Guptan, P., and Banerjee, U. (2010). Metabolic control of G1-S transition: cyclin E degradation by p53-induced activation of the ubiquitin-proteasome system. J Cell Biol *188*, 473-479.
Marceau, A.H., Brison, C.M., Nerli, S., Arsenault, H.E., McShan, A.C., Chen, E., Lee, H.W., Benanti, J.A., Sgourakis, N.G., and Rubin, S.M. (2019). An order-to-disorder structural switch activates the FoxM1 transcription factor. Elife *8*.
Marceau, A.H., Felthousen, J.G., Goetsch, P.D., Iness, A.N., Lee, H.W., Tripathi, S.M., Strome, S., Litovchick, L., and Rubin, S.M. (2016). Structural basis for LIN54 recognition of CHR elements in cell cycle-regulated promoters. Nat Commun *7*, 12301.
Marzio, A., Puccini, J., Kwon, Y., Maverakis, N.K., Arbini, A., Sung, P., Bar-Sagi, D., and Pagano, M. (2019). The F-Box Domain-Dependent Activity of EMI1 Regulates PARPi Sensitivity in Triple-Negative Breast Cancers. Mol Cell *73*, 224-237 e226.

Matos, D.A., Zhang, J.M., Ouyang, J., Nguyen, H.D., Genois, M.M., and Zou, L. (2020). ATR Protects the Genome against R Loops through a MUS81-Triggered Feedback Loop. Mol Cell *77*, 514-527 e514.
Matson, J.P., Dumitru, R., Coryell, P., Baxley, R.M., Chen, W., Twaroski, K., Weber, B.R., Tolar, J., Bielinksy, A.-K., Purvis, J.E.*, et al.* (2016). Rapid DNA replication origin licensing protects stem cell pluirpotency. eLife *6*, e30473.
Matsuoka, M., Kato, J., Fisher, R.P., Morgan, D.O., and Sherr, C.J. (1994). Activation of Cyclin-Dependent Kinase 4 (cdk4) by Mouse MO15-Associated Kinase. Mol Cell Biol *14*, 7265-7275.
Matsushime, H., Ewen, M.E., Strom, D.K., Kato, J., Hanks, S.K., Roussel, M.F., and Sherr, C.J. (1992). Identification and Properties of an Atypical Catalytic Subunit ($p34P^{SK-J3}$/Cdk4) for Mammalian D Type G1 Cyclins. Cell *71*, 323-334.
Mavrommati, I., Faedda, R., Galasso, G., Li, J., Burdova, K., Fischer, R., Kessler, B.M., Carrero, Z.I., Guardavaccaro, D., Pagano, M.*, et al.* (2018). beta-TrCP- and Casein Kinase II-Mediated Degradation of Cyclin F Controls Timely Mitotic Progression. Cell Rep *24*, 3404-3412.
McGarry, T.J., and Kirshcner, M.W. (1998). Geminin, an Inhibitor of DNA Replication Is Degraded during Mitosis. Cell *93*, 1043-1053.
McGowan, C.H., and Russell, P. (1993a). Human Wee1 kinase inhibits cell division by phosphorylating p34cdc2 exclusively on Tyr15. EMBO J *12*, 75-85.
McGowan, C.H., and Russell, P. (1993b). Human Wee1 kinase inhibits cell division by phosphorylating p34cdc2 exclusively on Tyr15. The EMBO journal *12*, 75-85.
Meggio, F., and Pinna, L.A. (2003). One-thousand-and-one substrates of protein kinase CK2? FASEB J *17*, 350-368.
Merrick, K.A., Larochelle, S., Zhang, C., Allen, J.J., Shokat, K.M., and Fisher, R.P. (2008). Distinct activation pathways confer cyclin-binding specificity on Cdk1 and Cdk2 in human cells. Mol Cell *32*, 662-672.
Meyerson, M., and Harlow, E. (1994). Identification of G_1 Kinase Activity for cdk6, a Novel Cyclin D Partner. Mol Cell Biol, 2077-2086.
Michowski, W., Chick, J.M., Chu, C., Kolodziejczyk, A., Wang, Y., Suski, J.M., Abraham, B., Anders, L., Day, D., Dunkl, L.M.*, et al.* (2020). Cdk1 Controls Global Epigenetic Landscape in Embryonic Stem Cells. Mol Cell *78*, 459-476 e413.
Mitrophanov, A.Y., and Groisman, E.A. (2008). Positive feedback in cellular control systems. Bioessays *30*, 542-555.
Moiseeva, T., Hood, B., Schamus, S., O'Connor, M.J., Conrads, T.P., and Bakkenist, C.J. (2017). ATR kinase inhibition induces unscheduled origin firing through a Cdc7-dependent association between GINS and And-1. Nat Commun *8*, 1392.
Moiseeva, T., Yin, Y., Calderon, M.J., Qian, C., Schamus-Haynes, S., Sugitani, N., Osmanbeyoglu, E., Watkins, S.C., and Bakkenist, C.J. (2019). An ATR and CHK1 kinase signaling mechanism that limits origin firing during unperturbed DNA replication. Proc Natl Acad Sci U S A *116*, 13374-13383.
Mootha, V.K., Lindgren, C.M., Eriksson, K.-F., Subramanian, A., Sihag, S., Lehar, J., Puigserver, P., Carlsson, E., Ridderstråle, M., Laurila, E.*, et al.* (2003). PGC-1α-responsive genes involved in oxidative phosphorylation are coordinately downregulated in human diabetes. Nat Genet *34*, 267-263.
Morita, K., He, S., Nowak, R.P., Wang, J., Zimmerman, M.W., Fu, C., Durbin, A.D., Martel, M.W., Prutsch, N., Gray, N.S.*, et al.* (2020). Allosteric Activators of Protein Phosphatase 2A Display Broad Antitumor Activity Mediated by Dephosphorylation of MYBL2. Cell *181*, 702-715 e720.
Morrow, C.J., Tighe, A., Johnson, V.L., Scott, M.I.F., Ditchfield, C., and Taylor, S.S. (2005). Bub1 and aurora B cooperate to maintain BubR1-mediated inhibition of APC/C^{CDC20}. J Cell Sci, 3639-3652.

Moshe, Y., Boulaire, J., Pagano, M., and Hershko, A. (2004). Role of Polo-like kinase in the degradation of early mitotic inhibitor 1, a regulator of the anaphase promoting complex/cyclosome. Proc Natl Acad Sci U S A *101*, 7937-7942.
Muller-Tidow, C., Wang, W., Idos, G.E., Diederichs, S., Yang, R., Readhead, C., Berdel, W.E., Serve, H., Saville, M., Watson, R.*, et al.* (2001). Cyclin A1 directly interacts with B-myb and cyclin A1/cdk2 phosphorylate B-myb at functionally important serine and threonine residues: tissue-specific regulation of B-myb function. Blood *97*, 2091-2097.
Muller, G.A., Quaas, M., Schumann, M., Krause, E., Padi, M., Fischer, M., Litovchick, L., DeCaprio, J.A., and Engeland, K. (2012). The CHR promoter element controls cell cycle-dependent gene transcription and binds the DREAM and MMB complexes. Nucleic Acids Res *40*, 1561-1578.
Muller, G.A., Stangner, K., Schmitt, T., Wintsche, A., and Engeland, K. (2017). Timing of transcription during the cell cycle: Protein complexes binding to E2F, E2F/CLE, CDE/CHR, or CHR promoter elements define early and late cell cycle gene expression. Oncotarget *8*, 97736-97748.
Muller, G.A., Wintsche, A., Stangner, K., Prohaska, S.J., Stadler, P.F., and Engeland, K. (2014). The CHR site: definition and genome-wide identification of a cell cycle transcriptional element. Nucleic Acids Res *42*, 10331-10350.
Munger, K., Werness, B.A., Dyson, N., Phelps, W.C., Harlow, E., and Howley, P.M. (1989). Complex formatiuon of human pappillomavirus E7 proteins with the retinoblastoma tumor suppressor gene product. The EMBO Journal *8*, 4099-4105.
Murga, M., Campaner, S., Lopez-Contreras, A.J., Toledo, L.I., Soria, R., Montana, M.F., Artista, L., Schleker, T., Guerra, C., Garcia, E.*, et al.* (2011). Exploiting oncogene-induced replicative stress for the selective killing of Myc-driven tumors. Nat Struct Mol Biol *18*, 1331-1335.
Musa, J., Cidre-Aranaz, F., Aynaud, M.M., Orth, M.F., Knott, M.M.L., Mirabeau, O., Mazor, G., Varon, M., Holting, T.L.B., Grossetete, S.*, et al.* (2019). Cooperation of cancer drivers with regulatory germline variants shapes clinical outcomes. Nat Commun *10*, 4128.
Nair, J., Huang, T.T., Murai, J., Haynes, B., Steeg, P.S., Pommier, Y., and Lee, J.M. (2020). Resistance to the CHK1 inhibitor prexasertib involves functionally distinct CHK1 activities in BRCA wild-type ovarian cancer. Oncogene.
Nakayama, K., Nagahama, H., Minamishima, Y.A., Matsumoto, M., Nakamichi, I., Kitagawa, K., Shirane, M., Tsunematsu, R., Tsukiyama, T., Ishida, N.*, et al.* (2000). Targeted disruption of Skp2 results in accumulation of cyclin E and p27(Kip1), polyploidy and centrosome overduplication. The EMBO journal *19*, 2069-2081.
Narasimha, A.M., Kaulich, M., Shapiro, G.S., Choi, Y.J., Sicinski, P., and Dowdy, S.F. (2014). Cyclin D activates the Rb tumor suppressor by mono-phosphorylation. Elife *3*.
Nass, S.J., and Dickson, R.B. (1998). Epidermal Growth Factor-dependent Cell Cycle Progression Is Altered in Mammery Epithelial Cells That Overexpress c-myc Clin Cancer Res *4*, 1813-1822.
Neelsen, K.J., Zanini, I.M., Mijic, S., Herrador, R., Zellweger, R., Ray Chaudhuri, A., Creavin, K.D., Blow, J.J., and Lopes, M. (2013). Deregulated origin licensing leads to chromosomal breaks by rereplication of a gapped DNA template. Genes Dev *27*, 2537-2542.
Nelson, D.A., Krucher, N.A., and Ludlow, J.W. (1997). High molecular weight protein phosphatase type 1 dephosphorylates the retinoblastoma protein. J Biol Chem *272*, 4528-4535.
Nestal de Moraes, G., Delbue, D., Silva, K.L., Robaina, M.C., Khongkow, P., Gomes, A.R., Zona, S., Crocamo, S., Mencalha, A.L., Magalhaes, L.M.*, et al.* (2015). FOXM1 targets XIAP and Survivin to modulate breast cancer survival and chemoresistance. Cell Signal *27*, 2496-2505.
Nevis, K.R., Cordeiro-Stone, M., and Cook, J.G. (2009). Origin licensing and p53 status regulate Cdk2 activity during G(1). Cell Cycle *8*, 1952-1963.

Nishitani, H., Lygerou, Z., Nishimoto, T., and Nurse, P. (2000). The Cdt1 protein is required to license DNA for replication in fission yeast. Nature *404*, 625-628.
Nitani, N., Yadani, C., Yabuuchi, H., Masukata, H., and Nakagawa, T. (2008). Mcm4 C-terminal domain of MCM helicase prevents excessive formation of single-stranded DNA at stalled replication forks. Proc Natl Acad Sci U S A *105*, 12973-12978.
Norton, E., and Diffley, J.F.X. (2000). CDK Inactivation is the Only Essential Function of the APC/C and the Mitotic Exit Nextwork Protein for Origin Resetting during Mitosis. Mol Cell *5*, 85-95.
Nusinow, D.P., Szpyt, J., Ghandi, M., Rose, C.M., McDonald, E.R., 3rd, Kalocsay, M., Jane-Valbuena, J., Gelfand, E., Schweppe, D.K., Jedrychowski, M.*, et al.* (2020). Quantitative Proteomics of the Cancer Cell Line Encyclopedia. Cell *180*, 387-402 e316.
O'Connell, M.J., Raleigh, J.M., Verkade, H.M., and Nurse, P. (1997). Chk1 is a wee1 kinase in the G2 DNA damage checkpoint inhibiting cdc2 by Y15 phosphorylation. EMBO J *16*, 545-554.
O'Connor, A., Maffini, S., Rainey, M.D., Kaczmarczyk, A., Gaboriau, D., Musacchio, A., and Santocanale, C. (2015). Requirement for PLK1 kinase activity in the maintenance of a robust spindle assembly checkpoint. Biol Open *5*, 11-19.
Oakley, G.G., Patrick, S.M., Yao, J., Carty, M.P., Turchi, J.J., and Dixon, K. (2003). RPA Phosphorylation in Mitosis Alters DNA Binding and Protein-Protein

Interactions. Biochemistry *42*, 3255-3264.
Oehlmann, M., Score, A.J., and Blow, J.J. (2004). The role of Cdc6 in ensuring complete genome licensing and S phase checkpoint activation. J Cell Biol *165*, 181-190.
Ohtani, K., DeGregori, J., and Nevins, J.R. (1995). Regulation of the cyclin E gene by transcription factor E2F1. Proc Natl Acad Sci U S A *92*, 12146-12150.
Ohtani, K., Tsujimoto, A., Ikeda, M., and Nakamura, M. (1998). Regulation of cell growth-dependent expression of mammalian CDC6 gene byt the cell cycle transcription factor E2F. Oncogene *17*, 1777-1785.
Oka, O., Waters, L.C., Strong, S.L., Dosanjh, N.S., Veverka, V., Muskett, F.W., Renshaw, P.S., Klempnauer, K.H., and Carr, M.D. (2012). Interaction of the transactivation domain of B-Myb with the TAZ2 domain of the coactivator p300: molecular features and properties of the complex. PLoS One *7*, e52906.
Okumura, F., Joo-Okumura, A., Nakatsukasa, K., and Kamura, T. (2017). Hypoxia-inducible factor-2alpha stabilizes the von Hippel-Lindau (VHL) disease suppressor, Myb-related protein 2. PLoS One *12*, e0175593.
Olson, E., Nievera, C.J., Klimovich, V., Fanning, E., and Wu, X. (2006). RPA2 is a direct downstream target for ATR to regulate the S-phase checkpoint. J Biol Chem *281*, 39517-39533.
Ord, M., Moll, K., Agerova, A., Kivi, R., Faustova, I., Venta, R., Valk, E., and Loog, M. (2019). Multisite phosphorylation code of CDK. Nat Struct Mol Biol *26*, 649-658.
Ord, M., Puss, K.K., Kivi, R., Moll, K., Ojala, T., Borovko, I., Faustova, I., Venta, R., Valk, E., Koivomagi, M.*, et al.* (2020). Proline-Rich Motifs Control G2-CDK Target Phosphorylation and Priming an Anchoring Protein for Polo Kinase Localization. Cell Rep *31*, 107757.
Paculova, H., Kramara, J., Simeckova, S., Fedr, R., Soucek, K., Hylse, O., Paruch, K., Svoboda, M., Mistrik, M., and Kohoutek, J. (2017). BRCA1 or CDK12 loss sensitizes cells to CHK1 inhibitors. Tumour Biol *39*, 1010428317727479.
Pagliuca, F.W., Collins, M.O., Lichawska, A., Zegerman, P., Choudhary, J.S., and Pines, J. (2011). Quantitative proteomics reveals the basis for the biochemical specificity of the cell-cycle machinery. Mol Cell *43*, 406-417.
Pal, D., Torres, A.E., Stromberg, B.R., Messina, A.L., Dickson, A.S., De, K., Willard, B., Venere, M., and Summers, M.K. (2020). Chk1-mediated phosphorylation of Cdh1 promotes the SCF(betaTRCP)-dependent degradation of Cdh1 during S-phase and efficient cell-cycle progression. Cell Death Dis *11*, 298.

Palazzo, L., Della Monica, R., Visconti, R., Costanzo, V., and Grieco, D. (2014). ATM controls proper mitotic spindle structure. Cell Cycle *13*, 1091-1100.
Pandit, B., Halasi, M., and Gartel, A.L. (2009). p53 negatively regulates expression of FoxM1. Cell Cycle *8*, 3425-3427.
Pardee, A.B. (1974). A Restriction Point for Control of Normal Animal Cell Proliferation. Proc Natl Acad Sci U S A *71*, 1286-1290.
Parikh, N., Hilsenbeck, S., Creighton, C.J., Dayaram, T., Shuck, R., Shinbrot, E., Xi, L., Gibbs, R.A., Wheeler, D.A., and Donehower, L.A. (2014). Effects of TP53 mutational status on gene expression patterns across 10 human cancer types. J Pathol *232*, 522-533.
Park, H.J., Costa, R.H., Lau, L.F., Tyner, A.L., and Raychaudhuri, P. (2008). Anaphase-promoting complex/cyclosome-CDH1-mediated proteolysis of the forkhead box M1 transcription factor is critical for regulated entry into S phase. Mol Cell Biol *28*, 5162-5171.
Peart, M.J., Poyurovsky, M.V., Kass, E.M., Urist, M., Verschuren, E.W., Summers, M.K., Jackson, P.K., and Prives, C. (2010). APC/C(Cdc20) targets E2F1 for degradation in prometaphase. Cell Cycle *9*, 3956-3964.
Peng, C.-Y., Graves, P.R., Thoma, R.S., Wu, Z., Shaw, A.S., and Piwnica-Worms, H. (1997). Mitotic and G2 Checkpoint Control: Regulation of 14-3-3 Protein Binding by Phosphorylation of CDC25C on Serine-216. Science *277*, 1501-1505.
Petermann, E., Woodcock, M., and Helleday, T. (2010). Chk1 promotes replication fork progression by controlling replication initiation. Proc Natl Acad Sci U S A *107*, 16090-16095.
Petersen, B.O., Lukas, J., Sørensen, C.S., Bartek, J., and Helin, K. (1999). Phosphorylation of mammalian CDC6 by Cyclin A/CDK2 regulates its subcellular localization. The EMBO Journal *18*, 396-410.
Peterson, B.O., Wagener, C., Marinomi, F., Kramer, E.R., Melixetian, M., Denchi, E.L., Gieffers, C., Matteucci, C., Peters, J.M., and Helin, K. (2000). Cell cycle- and cell growth-regulated proteolysis of mammalian CDC6 is dependent on APC-CDH1. Genes Dev *14*, 2330-2343.
Petsalaki, E., Akoumianaki, T., Black, E.J., Gillespie, D.A., and Zachos, G. (2011). Phosphorylation at serine 331 is required for Aurora B activation. J Cell Biol *195*, 449-466.
Pfister, K., Pipka, J.L., Chiang, C., Liu, Y., Clark, R.A., Keller, R., Skoglund, P., Guertin, M.J., Hall, I.M., and Stukenberg, P.T. (2018). Identification of Drivers of Aneuploidy in Breast Tumors. Cell Rep *23*, 2758-2769.
Pilkinton, M., Sandoval, R., Song, J., Ness, S.A., and Colamonici, O.R. (2007). Mip/LIN-9 regulates the expression of B-Myb and the induction of cyclin A, cyclin B, and CDK1. J Biol Chem *282*, 168-175.
Pomerening, J.R., Sontag, E.D., and Ferrell, J.E., Jr. (2003). Building a cell cycle oscillator: hysteresis and bistability in the activation of Cdc2. Nat Cell Biol *5*, 346-351.
Presolski, S.I., Hong, V.P., and Finn, M.G. (2011). Copper-Catalyzed Azide-Alkyne Click Chemistry for Bioconjugation. Curr Protoc Chem Biol *3*, 153-162.
Qin, H., Li, Y., Zhang, H., Wang, F., He, H., Bai, X., and Li, S. (2019). Prognostic implications and oncogenic roles of MYBL2 protein expression in esophageal squamous-cell carcinoma. Onco Targets Ther *12*, 1917-1927.
Qiu, Z., Oleinick, N.L., and Zhang, J. (2018). ATR/CHK1 inhibitors and cancer therapy. Radiother Oncol *126*, 450-464.
Ragland, R.L., Patel, S., Rivard, R.S., Smith, K., Peters, A.A., Bielinsky, A.K., and Brown, E.J. (2013). RNF4 and PLK1 are required for replication fork collapse in ATR-deficient cells. Genes Dev *27*, 2259-2273.
Rainey, M.D., Bennett, D., O'Dea, R., Zanchetta, M.E., Voisin, M., Seoighe, C., and Santocanale, C. (2020). ATR Restrains DNA Synthesis and Mitotic Catastrophe in Response to CDC7 Inhibition. Cell Rep *32*, 108096.

Raschellà, G., Cesi, V., Amendola, R., Negroni, A., Tanno, B., Altavista, P., Tonini, G.P., De Bernardi, B., and Calabretta, B. (1999). Expression of *B-myb* in Neuroblastoma Tumors Is a Poor Prognostic Factor Independent from MYCN Amplication. Cancer Res *59*, 3365-3368.
Reimann, J.D.R., Freed, E., Hsu, J.-Y., Kramer, E.R., Peters, J.M., and Jackson, P.K. (2001a). Emi1 Is a Mitotic Regulator that Interacts with Cdc20 and Inhibits the Anaphase Promoting Complex. Cell *105*, 645-655.
Reimann, J.D.R., Gardner, B.E., Margottin-Goguet, F., and Jackson, P.K. (2001b). Emi1 regulates the anaphase-promoting complex by a different mechanism than Mad2 proteins. Genes Dev *15*, 3278-3285.
Robinson, C., Light, Y., Groves, R., Mann, D., Marias, R., and Watson, R. (1996). Cell-cycle regulation of B-Myb protein expression: specific phosphorylation during the S phase of the cell cycle. Oncogene *12*, 1855-1864.
Rosenblatt, J., Gu, Y., and Morgan, D.O. (1992). Human cyclin-dependent kinase 2 is activated during the S and G2 phases of the cell cycle and associates with cyclin A. Proc Natl Acad Sci U S A *89*, 2824-2828.
Rubin, S.M., Gall, A.L., Zheng, N., and Pavletich, N.P. (2005). Structure of the Rb C-terminal domain bound to E2F1-DP1: a mechanism for phosphorylation-induced E2F release. Cell *123*, 1093-1106.
Ruiz, S., Mayor-Ruiz, C., Lafarga, V., Murga, M., Vega-Sendino, M., Ortega, S., and Fernandez-Capetillo, O. (2016). A Genome-wide CRISPR Screen Identifies CDC25A as a Determinant of Sensitivity to ATR Inhibitors. Mol Cell *62*, 307-313.
Russell, M.R., Levin, K., Rader, J., Belcastro, L., Li, Y., Martinez, D., Pawel, B., Shumway, S.D., Maris, J.M., and Cole, K.A. (2013). Combination therapy targeting the Chk1 and Wee1 kinases shows therapeutic efficacy in neuroblastoma. Cancer Res *73*, 776-784.
Sadasivam, S., and DeCaprio, J.A. (2013). The DREAM complex: master coordinator of cell cycle-dependent gene expression. Nature reviews Cancer *13*, 585-595.
Sadasivam, S., Duan, S., and DeCaprio, J.A. (2012a). The MuvB complex sequentially recruits B-Myb and FoxM1 to promote mitotic gene expression. Genes & development *26*, 474-489.
Sadasivam, S., Duan, S., and DeCaprio, J.A. (2012b). The MuvB complex sequentially recruits B-Myb and FoxM1 to promote mitotic gene expression. Genes Dev *26*, 474-489.
Sala, A., Kundu, M., Casella, I., Engelhard, A., Calabretta, B., Grasso, L., Paggi, M.G., Giordano, A., Watson, R.J., Khalili, K.*, et al.* (1997). Activation of human B-MYB by cyclins.
Saldivar, J.C., Cortez, D., and Cimprich, K.A. (2017). The essential kinase ATR: ensuring faithful duplication of a challenging genome. Nat Rev Mol Cell Biol *18*, 622-636.
Saldivar, J.C., Hamperl, S., Bocek, M.J., Chung, M., Bass, T.E., Cisneros-Soberanis, F., Samejima, K., Xie, L., Paulson, J.R., Earnshaw, W.C.*, et al.* (2018). An intrinsic S/G2 checkpoint enforced by ATR. Science *361*, 806-810.
Sancar, A., Lindsey-Boltz, L.A., Unsal-Kacmaz, K., and Linn, S. (2004). Molecular mechanisms of mammalian DNA repair and the DNA damage checkpoints. Annu Rev Biochem *73*, 39-85.
Sanidas, I., Morris, R., Fella, K.A., Rumde, P.H., Boukhali, M., Tai, E.C., Ting, D.T., Lawrence, M.S., Haas, W., and Dyson, N.J. (2019). A Code of Mono-phosphorylation Modulates the Function of RB. Mol Cell *73*, 985-1000 e1006.
Sanjana, N.E., Shalem, O., and Zhang, F. (2014). Improved vectors and genome-wide libraries for CRISPR screening. Nat Methods *11*, 783-784.
Sansam, C.L., Cruz, N.M., Danielian, P.S., Amsterdam, A., Lau, M.L., Hopkins, N., and Lees, J.A. (2010). A vertebrate gene, ticrr, is an essential checkpoint and replication regulator. Genes Dev *24*, 183-194.
Santamaria, D., Barriere, C., Cerqueira, A., Hunt, S., Tardy, C., Newton, K., Caceres, J.F., Dubus, P., Malumbres, M., and Barbacid, M. (2007). Cdk1 is sufficient to drive the mammalian cell cycle. Nature *448*, 811-815.

Santra, M.K., Wajapeyee, N., and Green, M.R. (2009). F-box protein FBXO31 mediates cyclin D1 degradation to induce G1 arrest after DNA damage. Nature *459*, 722-725.
Saville, M.K., and Watson, R.J. (1998). The cell-cycle regulated transcription factor B-Myb is phosphorylated by Cyclin A/Cdk2 at sites that enhance its transactivation properties. Oncogene *17*.
Schade, A.E., Fischer, M., and DeCaprio, J.A. (2019a). RB, p130 and p107 differentially repress G1/S and G2/M genes after p53 activation. Nucleic Acids Res *47*, 11197-11208.
Schade, A.E., Oser, M.G., Nicholson, H.E., and DeCaprio, J.A. (2019b). Cyclin D-CDK4 relieves cooperative repression of proliferation and cell cycle gene expression by DREAM and RB. Oncogene *38*, 4962-4976.
Schlacher, K., Wu, H., and Jasin, M. (2012). A distinct replication fork protection pathway connects Fanconi anemia tumor suppressors to RAD51-BRCA1/2. Cancer Cell *22*, 106-116.
Schmit, F., Cremer, S., and Gaubatz, S. (2009a). LIN54 is an essential core subunit of the DREAM/LINC complex that binds to the cdc2 promoter in a sequence-specific manner. The FEBS journal *276*, 5703-5716.
Schmit, F., Cremer, S., and Gaubatz, S. (2009b). LIN54 is an essential core subunit of the DREAM/LINC complex that binds to the cdc2 promoter in a sequence-specific manner. FEBS J *276*, 5703-5716.
Schmit, F., Korenjak, M., Mannefeld, M., Schmitt, K., Franke, C., von Eyss, B., Gagrica, S., Hanel, F., Brehm, A., and Gaubatz, S. (2007). LINC, a human complex that is related to pRB-containing complexes in invertebrates regulates the expression of G2/M genes. Cell Cycle *6*, 1903-1913.
Schulman, B.A., Lindstrom, D.L., and Harlow, E. (1998). Substrate recruitment to cyclin-dependent kinase 2 by a multipurpose docking site on cyclin A. Proc Natl Acad Sci U S A *95*, 10453-10458.
Schulze, A., Zerfass, K., Spitkovsky, D., Henglein, B., and Jansen-Dürr (1994). Activation of the E2F transcription factor by cyclin D1 is blocked by p16INK4, the product of the putative tumor suppressor gene MTS1. Oncogene *12*, 3475-3482.
Shalem, O., Sanjana, N.E., Hartenian, E., Shi, X., Scott, D.A., Mikkelsen, T.S., D., H., Ebert, B.L., Root, D.E., Doench, J.G.*, et al.* (2014). Genome-scale CRISPR-Cas9 Knockout Screening in Human Cells. Science *343*, 83-87.
Shiromizu, T., Goto, H., Tomono, Y., Bartek, J., Totsukawa, G., Inoko, A., Nakanishi, M., Matsumura, F., and Inagaki, M. (2006). Regulation of mitotic function of Chk1 through phosphorylation at novel sites by cyclin-dependent kinase 1 (Cdk1). Genes Cells *11*, 477-485.
Sirbu, B.M., McDonald, H.W., Dungrawala, H., Badu-Nkansah, A., Kavanaugh, G.M., Chen, Y., Tabb, D.L., and Cortez, D. (2013). Identification of Proteins at Active, Stalled, and Collapsed Replication Forks Using Isolation of Proteins on Nascent DNA (iPOND) Coupled with Mass Spectrometry. Journal of Biological Chemistry *288*, 31458-31467.
Sogo, J.M., Lopes, M., and Foiani, M. (2002). Fork Reversal and ssDNA Accumulation at Stalled Replication Forks Owing to Checkpoint Defects. Science *297*, 599-602.
Sokka, M., Koalick, D., Hemmerich, P., Syvaoja, J.E., and Pospiech, H. (2018). The ATR-Activation Domain of TopBP1 Is Required for the Suppression of Origin Firing during the S Phase. Int J Mol Sci *19*.
Sorensen, C.S., Lukas, C., Kramer, E.R., Peters, J.M., Bartek, J., and Lukas, J. (2001). A conserved cyclin-binding domain determines functional interplay between anaphase-promoting complex-Cdh1 and cyclin A-Cdk2 during cell cycle progression. Mol Cell Biol *21*, 3692-3703.
Sparano, J.A., and Paik, S. (2008). Development of the 21-gene assay and its application in clinical practice and clinical trials. J Clin Oncol *26*, 721-728.
Stewart, S., and Fang, G. (2005). Destruction box-dependent degradation of aurora B is mediated by the anaphase-promoting complex/cyclosome and Cdh1. Cancer Res *65*, 8730-8735.

Subramanian, A., Tamayo, P., Mootha, V.K., Mukherjee, S., Ebert, B.L., Gillette, M.A., Paulovich, A., Pomeroy, S.L., Golub, T.R., Lander, E.S*., et al.* (2005). Gene set enrichment analysis: a knowledge-based approach for interpreting genome-wide expression profiles. Proc Natl Acad Sci U S A *102*, 15545-15550.
Sudakin, V., Chan, G.K., and Yen, T.J. (2001). Checkpoint inhibition of the APC/C in HeLa cells is mediated by a complex of BUBR1, BUB3, CDC20, and MAD2. J Cell Biol *154*, 925-936.
Sudakin, V., Ganoth, D., Dahan, A., Heller, H., Hershko, J., Luca, F.C., Ruderman, J.V., and Hershko, A. (1995). The Cyclosome, a Large Complex Containing Cyclin-Selective Ubiquitin Ligase Activity, Targets Cyclins for Destruction at the End of Mitosis. Mol Biol Cell *6*, 185-198.
Sugimoto, N., Kitabayashi, I., Osano, S., Tatsumi, Y., Yugawa, T., Narisawa-Saito, M., Matsukage, A., Kiyono, T., and Fujita, M. (2008). Identification of Novel Human Cdt1-binding Proteins by a Proteomics Approach: Proteolytic Regulation by APC/C^{Cdh1}. Mol Biol Cell *19*, 1007-1021.
Sur, S., and Agrawal, D.K. (2016). Phosphatases and kinases regulating CDC25 activity in the cell cycle: clinical implications of CDC25 overexpression and potential treatment strategies. Mol Cell Biochem *416*, 33-46.
Suzuki, K., Sako, K., Akiyama, K., Isoda, M., Senoo, C., Nakajo, N., and Sagata, N. (2015). Identification of non-Ser/Thr-Pro consensus motifs for Cdk1 and their roles in mitotic regulation of C2H2 zinc finger proteins and Ect2. Sci Rep *5*, 7929.
Swaminathan, S., Kiendl, F., Korner, R., Lupetti, R., Hengst, L., and Melchior, F. (2004). RanGAP1*SUMO1 is phosphorylated at the onset of mitosis and remains associated with RanBP2 upon NPC disassembly. J Cell Biol *164*, 965-971.
Syljuåsen, R.G., Sørensen, C.S., and cellular biology, H.-L.T. (2005). Inhibition of human Chk1 causes increased initiation of DNA replication, phosphorylation of ATR targets, and DNA breakage. … and cellular biology.
Syljuasen, R.G., Sorensen, C.S., Hansen, L.T., Fugger, K., Lundin, C., Johansson, F., Helleday, T., Sehested, M., Lukas, J., and Bartek, J. (2005). Inhibition of human Chk1 causes increased initiation of DNA replication, phosphorylation of ATR targets, and DNA breakage. Mol Cell Biol *25*, 3553-3562.
Takahashi, Y., Rayman, J.B., and Dynlacht, B.D. (2000). Analysis of promoter binding by the E2F and pRB families in vivo: distinct E2F proteins mediate activation and repression. Genes Dev *14*, 804-816.
Takata, H., Madung, M., Katoh, K., and Fukui, K. (2018). Cdk1-dependent phosphorylation of KIF4A at S1186 triggers lateral chromosome compaction during early mitosis. PLoS One *13*, e0209614.
Takeda, D.Y., Wohlschlegel, J.A., and Dutta, A. (2001). A bipartite substrate recognition motif for cyclin-dependent kinases. J Biol Chem *276*, 1993-1997.
Takeshita, M., Koga, T., Takayama, K., Ijichi, K., Yano, T., Maehara, Y., Nakanishi, Y., and Sueishi, K. (2013). Aurora-B overexpression is correlated with aneuploidy and poor prognosis in non-small cell lung cancer. Lung Cancer *80*, 85-90.
Tan, W., van Twest, S., Murphy, V.J., and Deans, A.J. (2020). ATR-Mediated FANCI Phosphorylation Regulates Both Ubiquitination and Deubiquitination of FANCD2. Front Cell Dev Biol *8*, 2.
Tanaka, H., Arakawa, H., Yamaguchi, T., Shiraishi, K., Fukuda, S., Matsui, K., Takei, Y., and Nakamura, Y. (2000). A ribonucleotide reductase gene involved in a p53-dependent cell-cycle checkpoint for DNA damage. Nature *404*, 42-49.
Tang, J., Erikson, R.L., and Liu, X. (2006). Checkpoint kinase 1 (Chk1) is required for mitotic progression through negative regulation of polo-like kinase 1 (Plk1). Proc Natl Acad Sci U S A *103*, 11964-11969.
Tang, Z., Bharadwaj, R., Li, B., and Yu, H. (2001). Mad2-Independent Inhibition of APC^{Cdc20} by the Mitotic Checkpoint Protein BubR1. Dev Cell *1*, 227-237.

Taubert, S., Gorrini, C., Frank, S.R., Parisi, T., Fuchs, M., Chan, H.M., Livingston, D.M., and Amati, B. (2004). E2F-dependent histone acetylation and recruitment of the Tip60 acetyltransferase complex to chromatin in late G1. Mol Cell Biol *24*, 4546-4556.
Taylor, G.S., Liu, Y., Baskerville, C., and Charbonneau, H. (1997). The activity of Cdc14p, an oligomeric dual specificity protein phosphatase from Saccharomyces cerevisiae, is required for cell cycle progression. J Biol Chem *272*, 24054-24063.
Thompson, B.J., Bhansali, R., Diebold, L., Cook, D.E., Stolzenburg, L., Casagrande, A.S., Besson, T., Leblond, B., Desire, L., Malinge, S.*, et al.* (2015). DYRK1A controls the transition from proliferation to quiescence during lymphoid development by destabilizing Cyclin D3. J Exp Med *212*, 953-970.
Thomson, A.M., Gillespie, P.J., and Blow, J.J. (2010). Replication factory activation can be decoupled from the replication timing program by modulating Cdk levels. J Cell Biol *188*, 209-221.
Thorner, A.R., Hoadley, K.A., Parker, J.S., Winkel, S., Millikan, R.C., and Perou, C.M. (2009). In vitro and in vivo analysis of B-Myb in basal-like breast cancer. Oncogene *28*, 742-751.
Tien, J.F., Umbreit, N.T., Gestaut, D.R., Franck, A.D., Cooper, J., Wordeman, L., Gonen, T., Asbury, C.L., and Davis, T.N. (2010). Cooperation of the Dam1 and Ndc80 kinetochore complexes enhances microtubule coupling and is regulated by aurora B. J Cell Biol *189*, 713-723.
Tipton, A.R., Ji, W., Sturt-Gillespie, B., Bekier, M.E., 2nd, Wang, K., Taylor, W.R., and Liu, S.T. (2013). Monopolar spindle 1 (MPS1) kinase promotes production of closed MAD2 (C-MAD2) conformer and assembly of the mitotic checkpoint complex. J Biol Chem *288*, 35149-35158.
Tipton, A.R., Wang, K., Link, L., Bellizzi, J.J., Huang, H., Yen, T., and Liu, S.T. (2011). BUBR1 and closed MAD2 (C-MAD2) interact directly to assemble a functional mitotic checkpoint complex. J Biol Chem *286*, 21173-21179.
Toledo, L., Neelsen, K.J., and Lukas, J. (2017). Replication Catastrophe: When a Checkpoint Fails because of Exhaustion. Mol Cell *66*, 735-749.
Toledo, L.I., Altmeyer, M., Rask, M.B., Lukas, C., Larsen, D.H., Povlsen, L.K., Bekker-Jensen, S., Mailand, N., Bartek, J., and Lukas, J. (2013). ATR prohibits replication catastrophe by preventing global exhaustion of RPA. Cell *155*, 1088-1103.
Topacio, B.R., Zatulovskiy, E., Cristea, S., Xie, S., Tambo, C.S., Rubin, S.M., Sage, J., Koivomagi, M., and Skotheim, J.M. (2019). Cyclin D-Cdk4,6 Drives Cell-Cycle Progression via the Retinoblastoma Protein's C-Terminal Helix. Mol Cell *74*, 758-770 e754.
Trenz, K., Errico, A., and Costanzo, V. (2008). Plx1 is required for chromomal DNA replication under stressful conditions. The EMBO journal *27*, 876-885.
Trimarchi, J.M., and Lees, J.A. (2002). Sibling rivalry in the E2F family. Nat Rev Mol Cell Biol *3*, 11-20.
Vaidyanathan, S., Cato, K., Tang, L., Pavey, S., Haass, N.K., Gabrielli, B.G., and Duijf, P.H. (2016). In vivo overexpression of Emi1 promotes chromosome instability and tumorigenesis. Oncogene *35*, 5446-5455.
Valovka, T., Schonfeld, M., Raffeiner, P., Breuker, K., Dunzendorfer-Matt, T., Hartl, M., and Bister, K. (2013). Transcriptional control of DNA replication licensing by Myc. Sci Rep *3*, 3444.
van Harten, A.M., Buijze, M., van der Mast, R., Rooimans, M.A., Martens-de Kemp, S.R., Bachas, C., Brink, A., Stigter-van Walsum, M., Wolthuis, R.M.F., and Brakenhoff, R.H. (2019). Targeting the cell cycle in head and neck cancer by Chk1 inhibition: a novel concept of bimodal cell death. Oncogenesis *8*, 38.
Van Horn, R.D., Chu, S., Fan, L., Yin, T., Du, J., Beckmann, R., Mader, M., Zhu, G., Toth, J., Blanchard, K.*, et al.* (2010). Cdk1 activity is required for mitotic activation of aurora A during G2/M transition of human cells. J Biol Chem *285*, 21849-21857.

Vassilopoulos, A., Tominaga, Y., Kim, H.S., Lahusen, T., Li, B., Yu, H., Gius, D., and Deng, C.X. (2015). WEE1 murine deficiency induces hyper-activation of APC/C and results in genomic instability and carcinogenesis. Oncogene *34*, 3023-3035.
Vassin, V.M., Anantha, R.W., Sokolova, E., Kanner, S., and Borowiec, J.A. (2009). Human RPA phosphorylation by ATR stimulates DNA synthesis and prevents ssDNa accumulating during DNA-replication stress. J Cell Sci *122*, 4070-4080.
Vaziri, C., Saxena, S., Jeon, Y., Lee, C., Murata, K., Machida, Y.J., Wagle, N., Hwang, D.S., and Dutta, A. (2003). A p53-Dependent Checkpoint Pathway Prevents Rereplication. Mol Cell *11*, 997-1008.
Vendetti, F.P., Lau, A., Schamus, S., Conrads, T.P., O'Connor, M.J., and Bakkenist, C.J. (2015). The orally active and bioavailable ATR kinase inhbitor AZD6738 potentiates the anti-tumor effects of cisplatin to resolve ATM-deficient non-small cell lung cancer in vivo. Oncotarget *6*, 44289-44305.
Vigneron, S., Sundermann, L., Labbe, J.C., Pintard, L., Radulescu, O., Castro, A., and Lorca, T. (2018). Cyclin A-cdk1-Dependent Phosphorylation of Bora Is the Triggering Factor Promoting Mitotic Entry. Dev Cell *45*, 637-650 e637.
Vischioni, B., Oudejans, J.J., Vos, W., Rodriguez, J.A., and Giaccone, G. (2006). Frequent overexpression of aurora B kinase, a novel drug target, in non-small cell lung carcinoma patients. Mol Cancer Ther *5*, 2905-2913.
Visintin, R., Stegmeier, F., and Amon, A. (2003). The role of the polo kinase Cdc5 in controlling Cdc14 localization. Mol Biol Cell *14*, 4486-4498.
Walker, M., Black, E.J., Oehler, V., Gillespie, D.A., and Scott, M.T. (2009). Chk1 C-terminal regulatory phosphorylation mediates checkpoint activation by de-repression of Chk1 catalytic activity. Oncogene *28*, 2314-2323.
Wallez, Y., Dunlop, C.R., Johnson, T.I., Koh, S.B., Fornari, C., Yates, J.W.T., Bernaldo de Quiros Fernandez, S., Lau, A., Richards, F.M., and Jodrell, D.I. (2018). The ATR Inhibitor AZD6738 Synergizes with Gemcitabine In Vitro and In Vivo to Induce Pancreatic Ductal Adenocarcinoma Regression. Mol Cancer Ther *17*, 1670-1682.
Walter, D., Hoffmann, S., Komseli, E.-S.S., Rappsilber, J., Gorgoulis, V., and Sørensen, C.S. (2016). SCF(Cyclin F)-dependent degradation of CDC6 suppresses DNA re-replication. Nature communications *7*, 10530.
Wang, C., Wang, G., Feng, X., Shepherd, P., Zhang, J., Tang, M., Chen, Z., Srivastava, M., McLaughlin, M.E., Navone, N.M.*, et al.* (2019). Genome-wide CRISPR screens reveal synthetic lethality of RNASEH2 deficiency and ATR inhibition. Oncogene *38*, 2451-2463.
Wang, K., Sturt-Gillespie, B., Hittle, J.C., Macdonald, D., Chan, G.K., Yen, T.J., and Liu, S.T. (2014a). Thyroid hormone receptor interacting protein 13 (TRIP13) AAA-ATPase is a novel mitotic checkpoint-silencing protein. J Biol Chem *289*, 23928-23937.
Wang, L., Guo, Q., Fisher, L.A., Liu, D., and Peng, A. (2015). Regulation of polo-like kinase 1 by DNA damage and PP2A/B55alpha. Cell Cycle *14*, 157-166.
Wang, Z., Liu, P., Inuzuka, H., and Wei, W. (2014b). Roles of F-box proteins in cancer. Nat Rev Cancer *14*, 233-247.
Ward, I.M., and Chen, J. (2001). Histone H2AX is phosphorylated in an ATR-dependent manner in response to replicational stress. J Biol Chem *276*, 47759-47762.
Wasserman, D., Nachum, S., Cohen, M., Enrico, T.P., Meirav, N.-H., Parasol, J., Zomer-Polak, S., Auerbach, N., Sheinberger-Chorni, E., Nevenzal, H.*, et al.* (2020). Cell Cycle oscillators underlying orderly proteolysis of E2F8. Mol Biol Cell *31*, 725-740.
Wei, Q., Tang, Z., and Yu, H. (2006). Phosphorylation- and Polo-Box-dependent Binding of PLK1 to Bub1 is Required for the Kinetichore Localization of Plk1. Mol Biol Cell *17*, 3705-3716.
Welcker, M., Singer, J., Loeb, K.R., Grim, J., Bloecher, A., Gurien-West, M., Clurman, B.E., and Roberts, J.M. (2003). Multisite Phosphorylation by Cdk2 and GSK3 Controls Cyclin E Degradation. Molecular Cell *12*, 381-392.

Wells, J., Boyd, K.E., Fry, C.J., Bartley, S.M., and Farnham, P.J. (2000). Target Gene Specificity of E2F and Pocket Protein Family Members in Living Cells. Mol Cell Biol *20*, 5797-5807.
Werwein, E., Biyanee, A., and Klempnauer, K.H. (2020). Intramolecular interaction of B-MYB is regulated through Ser-577 phosphorylation. FEBS Lett *594*, 4266-4279.
Werwein, E., Cibis, H., Hess, D., and Klempnauer, K.H. (2019). Activation of the oncogenic transcription factor B-Myb via multisite phosphorylation and prolyl cis/trans isomerization. Nucleic Acids Res *47*, 103-121.
White, D., Rafalska-Metcalf, I.U., Ivanov, A.V., Corsinotti, A., Peng, H., Lee, S.C., Trono, D., Janicki, S.M., and Rauscher, F.J., 3rd (2012). The ATM substrate KAP1 controls DNA repair in heterochromatin: regulation by HP1 proteins and serine 473/824 phosphorylation. Mol Cancer Res *10*, 401-414.
White, D.E., Negorev, D., Peng, H., Ivanov, A.V., Maul, G.G., and Rauscher, F.J. (2006). KAP1, a novel substrate for PIKK family members, colocalizes with numerous damage response factors at DNA lesions. Cancer research *66*, 11594-11599.
Williams, K.L., Topp, S., Smith, B., Fifita, J.A., Warraich, S.T., Zhang, K.T., Farrawell, N., Vance, C., Hu, X., Chesi, A.*, et al.* (2016). CCNF mutations in amyotrophic lateral sclerosis and frontotemporal dementia. Nat Commun *7*, 11523.
Wiseman, E.F., Chen, X., Han, N., Webber, A., Ji, Z., Sharrocks, A.D., and Ang, Y.S. (2015). Deregulation of the FOXM1 target gene network and its coregulatory partners in oesophageal adenocarcinoma. Mol Cancer *14*, 69.
Wohlschlegel, J.A., Dwyer, B.T., Dhar, S.K., Cvetic, C., Walter, J.C., and Dutta, A. (2000). Inhibition of Eurkaryotic DNA Replication by Geminin Binding to Cdt1. Science *290*, 2309-2312.
Wu, C.X., Wang, X.Q., Chok, S.H., Man, K., Tsang, S.H.Y., Chan, A.C.Y., Ma, K.W., Xia, W., and Cheung, T.T. (2018). Blocking CDK1/PDK1/beta-Catenin signaling by CDK1 inhibitor RO3306 increased the efficacy of sorafenib treatment by targeting cancer stem cells in a preclinical model of hepatocellular carcinoma. Theranostics *8*, 3737-3750.
Wurzenberger, C., and Gerlich, D.W. (2011). Phosphatases: providing safe passage through mitotic exit. Nat Rev Mol Cell Biol *12*, 469-482.
Xu, M., Sheppard, K.-A., Peng, C.-Y., Yee, A.S., and Piwnica-Worms, H. (1994). Cyclin A/CDK2 Binds Directly to E2F-1 and Inhibits the DNA-binding Activity of E2F-1/DP-1 by phosphorylation. Mol Cell Biol *14*, 8420-8431.
Yajima, H., Lee, K.J., Zhang, S., Kobayashi, J., and Chen, B.P. (2009). DNA double-strand break formation upon UV-induced replication stress activates ATM and DNA-PKcs kinases. J Mol Biol *385*, 800-810.
Yan, Z., DeGregori, J., Shohet, R., Leone, G., Stillman, B., Nevins, J.R., and Williams, R.S. (1998). Cdc6 is regulated by E2F and is essential for DNA replication in mammalian cells. Mol Cell Biol *95*, 3603-3608.
Yang, C., Chen, H., Yu, L., Shan, L., Xie, L., Hu, J., Chen, T., and Tan, Y. (2013). Inhibition of FOXM1 transcription factor suppresses cell proliferation and tumor growth of breast cancer. Cancer Gene Ther *20*, 117-124.
Yang, Q., and Ferrell, J.E., Jr. (2013). The Cdk1-APC/C cell cycle oscillator circuit functions as a time-delayed, ultrasensitive switch. Nat Cell Biol *15*, 519-525.
Yao, G., Lee, T.J., Mori, S., Nevins, J.R., and You, L. (2008). A bistable Rb-E2F switch underlies the restriction point. Nat Cell Biol *10*, 476-482.
Ye, Q., Rosenberg, S.C., Moeller, A., Speir, J.A., Su, T.Y., and Corbett, K.D. (2015). TRIP13 is a protein-remodeling AAA+ ATPase that catalyzes MAD2 conformation switching. Elife *4*.
Yeh, K.H., Kondo, T., Zheng, J., Tsvetkov, L.M., Blair, J., and Zhang, H. (2001). The F-box protein SKP2 binds to the phosphorylated threonine 380 in cyclin E and regulates ubiquitin-dependent degradation of cyclin E. Biochem Biophys Res Commun *281*, 884-890.

Yoo, H.Y., Shevchenko, A., Shevchenko, A., and Dunphy, W.G. (2004). Mcm2 is a direct substrate of ATM and ATR during DNA damage and DNA replication checkpoint responses. J Biol Chem *279*, 53353-53364.
Yu, Y., and Munger, K. (2013). Human papillomavirus type 16 E7 oncoprotein inhibits the anaphase promoting complex/cyclosome activity by dysregulating EMI1 expression in mitosis. Virology *446*, 251-259.
Yuan, R., Liu, Q., Segeren, H.A., Yuniati, L., Guardavaccaro, D., Lebbink, R.J., Westendorp, B., and de Bruin, A. (2019). Cyclin F-dependent degradation of E2F7 is critical for DNA repair and G2-phase progression. EMBO J *38*, e101430.
Yudkovsky, Y., Shteinberg, M., Listovsky, T., Brandeis, M., and Hershko, A. (2000). Phosphorylation of Cdc20/fizzy negatively regulates the mammalian cyclosome/APC in the mitotic checkpoint. Biochem Biophys Res Commun *271*, 299-304.
Zachariae, W., Schwab, M., Nasmyth, K., and Seufert, W. (1998). Control of Cyclin Ubiquitination by CDK-Regulated Binding of Hct1 to the Anaphase Promoting Complex. Science *282*, 1721-1724.
Zachos, G., Black, E.J., Walker, M., Scott, M.T., Vagnarelli, P., Earnshaw, W.C., and Gillespie, D.A. (2007). Chk1 is required for spindle checkpoint function. Dev Cell *12*, 247-260.
Zachos, G., Rainey, M.D., and Gillespie, D.A. (2005). Chk1-dependent S-M checkpoint delay in vertebrate cells is linked to maintenance of viable replication structures. Mol Cell Biol *25*, 563-574.
Zeng, X., Sigoillot, F., Gaur, S., Choi, S., Pfaff, K.L., Oh, D.C., Hathaway, N., Dimova, N., Cuny, G.D., and King, R.W. (2010). Pharmacologic inhibition of the anaphase-promoting complex induces a spindle checkpoint-dependent mitotic arrest in the absence of spindle damage. Cancer Cell *18*, 382-395.
Zeng, X., Xu, W.K., Lok, T.M., Ma, H.T., and Poon, R.Y.C. (2019). Imbalance of the spindle-assembly checkpoint promotes spindle poison-mediated cytotoxicity with distinct kinetics. Cell Death Dis *10*, 314.
Zhang, L., and Wang, C. (2006). F-box protein Skp2: a novel transcriptional target of E2F. Oncogene *25*, 2615-2627.
Zhang, S., Chang, L., Alfieri, C., Zhang, Z., Yang, J., Maslen, S., Skehel, M., and Barford, D. (2016). Molecular mechanism of APC/C activation by mitotic phosphorylation. Nature *533*, 260-264.
Zhang, S., Tischer, T., and Barford, D. (2019). Cyclin A2 degradation during the spindle assembly checkpoint requires multiple binding modes to the APC/C. Nat Commun *10*, 3863.
Zhang, Y.W., Otterness, D.M., Chiang, G.G., Xie, W., Liu, Y.C., Mercurio, F., and Abraham, R.T. (2005). Genotoxic stress targets human Chk1 for degradation by the ubiquitin-proteasome pathway. Mol Cell *19*, 607-618.
Zhao, F., Siu, M.K., Jiang, L., Tam, K.F., Ngan, H.Y., Le, X.F., Wong, O.G., Wong, E.S., Gomes, A.R., Bella, L.*, et al.* (2014). Overexpression of forkhead box protein M1 (FOXM1) in ovarian cancer correlates with poor patient survival and contributes to paclitaxel resistance. PLoS One *9*, e113478.
Zhao, H., and Piwnica-Worms, H. (2001). ATR-mediated checkpoint pathways regulate phosphorylation and activation of human Chk1. Mol Cell Biol *21*, 4129-4139.
Zhong, Y., Nellimoottil, T., Peace, J.M., Knott, S.R., Villwock, S.K., Yee, J.M., Jancuska, J.M., Rege, S., Tecklenburg, M., Sclafani, R.A.*, et al.* (2013). The level of origin firing inversely affects the rate of replication fork progression. J Cell Biol *201*, 373-383.
Zhou, Z., He, M., Shah, A.A., and Wan, Y. (2016). Insights into APC/C: from cellular function to diseases and therapeutics. Cell Div *11*, 9.
Ziebold, U., Bartsch, O., Marais, R., Ferrari, S., and Klempnauer, K.H. (1997). Phosphorylation and activation of B-Myb by cyclin A-Cdk2. Curr Biol *7*, 253-260.

Ziv, Y., Bielopolski, D., Galanty, Y., Lukas, C., Taya, Y., Schultz, D.C., Lukas, J., Bekker-Jensen, S., Bartek, J., and Shiloh, Y. (2006). Chromatin relaxation in response to DNA double-strand breaks is modulated by a novel ATM- and KAP-1 dependent pathway. Nature Cell Biology *8*, 870-876.
Zou, L., and Elledge, S.J. (2003). Sensing DNA damage through ATRIP recognition of RPA-ssDNA complexes. Science *300*, 1542-1548.
Zuazua-Villar, P., Rodriguez, R., Gagou, M.E., Eyers, P.A., and Meuth, M. (2014). DNA replication stress in CHK1-depleted tumour cells triggers premature (S-phase) mitosis through inappropriate activation of Aurora kinase B. Cell Death & Disease *5*.
Zur, A., and Brandeis, M. (2002). Timing of AP/C substrate degradation is determined by fzy/fzr specificity of destruction boxes. The EMBO Journal *21*, 4500-4510.